



**HAL**  
open science

# Photochemical and photocatalytic degradation of pharmaceutical and personal care products (PPCPS) in aqueous solution: a case study of atenolol and 2-phenylbenzimidazole-5-sulfonic acid

Yuefei Ji

► **To cite this version:**

Yuefei Ji. Photochemical and photocatalytic degradation of pharmaceutical and personal care products (PPCPS) in aqueous solution: a case study of atenolol and 2-phenylbenzimidazole-5-sulfonic acid. Other. Université Claude Bernard - Lyon I; Nanjing University (Chine), 2014. English. NNT : 2014LYO10073 . tel-01058226

**HAL Id: tel-01058226**

**<https://theses.hal.science/tel-01058226>**

Submitted on 26 Aug 2014

**HAL** is a multi-disciplinary open access archive for the deposit and dissemination of scientific research documents, whether they are published or not. The documents may come from teaching and research institutions in France or abroad, or from public or private research centers.

L'archive ouverte pluridisciplinaire **HAL**, est destinée au dépôt et à la diffusion de documents scientifiques de niveau recherche, publiés ou non, émanant des établissements d'enseignement et de recherche français ou étrangers, des laboratoires publics ou privés.

**THESE DE L'UNIVERSITE DE LYON**

délivrée par

**L'UNIVERSITE CLAUDE BERNARD LYON 1**

et préparée en cotutelle avec

**L'UNIVERSITE DE NANJING**

ECOLE DOCTORALE DE CHIMIE de LYON

**DIPLOME DE DOCTORAT**

(arrêté du 7 août 2006 / arrêté du 6 janvier 2005)

**Spécialité chimie de l'environnement**

soutenue publiquement le 19 mai 2014

par

**Mr Yuefei Ji**

-----  
PHOTOCHEMICAL AND PHOTOCATALYTIC DEGRADATION OF PHARMACEUTICAL  
AND PERSONAL CARE PRODUCTS (PPCPs) IN AQUEOUS SOLUTION : A CASE STUDY  
OF ATENOLOL AND 2-PHENYLBENZIMIDAZOLE-5-SULFONIC ACID.  
-----

Directeurs de thèse : Pr Jean-Marc CHOVELON  
Pr Shixiang. GAO

**Membres du jury**

Dr Gilles MAILHOT	Rapporteur
Prof. Juhne LU	Rapporteur et Président
Prof. Khalil Hanna	Examineur
Pr. Jean-Marc CHOVELON	Directeur de thèse
Dr Corinne FERRONATO	Co-directeur de thèse
Pr Shixiang. GAO	Directeur de thèse
Pr. Yang Xi	Co-directeur de thèse

# UNIVERSITE CLAUDE BERNARD - LYON 1

Président de l'Université	M. François-Noël GILLY
Vice-président du Conseil d'Administration	M. le Professeur Hamda BEN HADID
Vice-président du Conseil des Etudes et de la Vie Universitaire	M. le Professeur Philippe LALLE
Vice-président du Conseil Scientifique	M. le Professeur Germain GILLET
Directeur Général des Services	M. Alain HELLEU

## *COMPOSANTES SANTE*

Faculté de Médecine Lyon Est – Claude Bernard	Directeur : M. le Professeur J. ETIENNE
Faculté de Médecine et de Maïeutique Lyon Sud – Charles Mérieux	Directeur : Mme la Professeure C. BURILLON
Faculté d'Odontologie	Directeur : M. le Professeur D. BOURGEOIS
Institut des Sciences Pharmaceutiques et Biologiques	Directeur : Mme la Professeure C. VINCIGUERRA
Institut des Sciences et Techniques de la Réadaptation	Directeur : M. le Professeur Y. MATILLON
Département de formation et Centre de Recherche en Biologie Humaine	Directeur : Mme. la Professeure A-M. SCHOTT

## *COMPOSANTES ET DEPARTEMENTS DE SCIENCES ET TECHNOLOGIE*

Faculté des Sciences et Technologies	Directeur : M. le Professeur F. De MARCHI
Département Biologie	Directeur : M. le Professeur F. FLEURY
Département Chimie Biochimie	Directeur : Mme le Professeur H. PARROT
Département GEP	Directeur : M. N. SIAUVE
Département Informatique	Directeur : M. le Professeur S. AKKOUCHE
Département Mathématiques	Directeur : M. le Professeur A. GOLDMAN
Département Mécanique	Directeur : M. le Professeur H. BEN HADID
Département Physique	Directeur : Mme S. FLECK
Département Sciences de la Terre	Directeur : Mme la Professeure I. DANIEL
UFR Sciences et Techniques des Activités Physiques et Sportives	Directeur : M. Y. VANPOULLE
Observatoire des Sciences de l'Univers de Lyon	Directeur : M. B. GUIDERDONI
Polytech Lyon	Directeur : M. P. FOURNIER
Ecole Supérieure de Chimie Physique Electronique	Directeur : M. G. PIGNAULT
Institut Universitaire de Technologie de Lyon 1	Directeur : M. C. VITON
Ecole Supérieure du Professorat et de l'Education	Directeur : M. A. MOUGNIOTTE
Institut de Science Financière et d'Assurances	Directeur : M. N. LEBOISNE

## Abstract

The wide occurrence of pharmaceutical and personal care products (PPCPs) in natural aquatic environment received extensive scientific interest as well as public awareness recently due to their potential hazardous effect on human beings and ecological system. The environmental fate of these PPCPs, including transportation and transformation, is still largely unknown up to date. Photochemical degradation is known to be an important abiotic transformation pathway for organic compounds depletion in natural environment. Photochemical reactions can fall into two categories, namely direct photolysis and indirect photolysis. Direct photolysis occurs when the absorption spectrum of one compound overlap with the solar emitting spectrum. Indirect photolysis takes place by reaction with reactive oxygen species (ROS) and/or excited triplet state generated from photosensitizers such as nitrate and dissolved organic matter (DOM). For those organic compounds unable to undergo direct photolysis, indirect photolysis may play a critical role in limiting their occurrence in natural environment. On the other hand, the extensive and frequent detection of PPCPs in aquatic environment requires the development of high efficient, economic and environment-friendly advanced oxidation processes (AOPs) for their elimination. Heterogeneous semi-conductor photocatalysis using  $\text{TiO}_2$  as the photocatalyst has recently been found to be a promising treatment technology for destructing organic pollutants, including PPCPs. Valence band holes ( $h_{\text{vb}}^+$ ) and reductive conduction band electrons ( $e_{\text{cb}}^-$ ) are generated after the photocatalyst excited by the photons with energy equal to or exceeding the band gap energy. The photogenerated holes can directly oxidize the adsorbed chemical substance or produce adsorbed hydroxyl radical ( $\text{HO}\cdot$ ) via the surface-bound  $\text{OH}^-$  and/or the adsorbed water molecules.  $h_{\text{vb}}^+$  and  $\text{HO}\cdot$  have been known to be highly reactive species capable of destructing a variety of organic compounds.

In the present study, the photochemical and photocatalytic degradation of atenolol (ATL) and 2-phenylbenzimidazole-5-sulfonic acid (PBSA) have been systematically investigated in aqueous solutions with the purpose of evaluating the photofate as a potential loss process and photocatalysis as a promising treatment technology for degradation these two compounds. ATL and PBSA have been chosen as two model compounds of PPCPs in the current work due to their wide occurrence and relatively high level in natural aquatic environment. The main conclusions

are as follows:

(1) nitrate-induced photodegradation of ATL followed pseudo-first-order kinetics upon simulated solar irradiation. The photodegradation was found to be dependent on nitrate concentration and increasing the nitrate from 0.5 mmol L<sup>-1</sup> to 10 mmol L<sup>-1</sup> led to the enhancement of rate constant from 0.00101 min<sup>-1</sup> to 0.00716 min<sup>-1</sup>. Hydroxyl radical was determined to play a key role in the photolysis process by using isopropanol as molecular probe. Increasing the solution pH from 4.8 to 10.4, the photodegradation rate slightly decreased from 0.00246 min<sup>-1</sup> to 0.00195 min<sup>-1</sup>, probably due to pH-dependent effect of nitrate-induced ·OH formation. Bicarbonate decreased the photodegradation of ATL in the presence of nitrate ions mainly through pH effect, while humic substance inhibited the photodegradation via both attenuating light and competing radicals. Upon irradiation for 240 min, only 10% reduction of total organic carbon (TOC) can be achieved in spite of 72% transformation rate of ATL, implying a majority of ATL transformed into intermediate products rather than complete mineralization. The main photoproducts of ATL were identified by using solid phase extraction-liquid chromatography-mass spectrometry (SPE-LC-MS) techniques and possible nitrate-induced photodegradation pathways were proposed. The toxicity of the phototransformation products was evaluated using aquatic species *Daphnia magna*, and the results revealed that photodegradation was an effective mechanism for ATL toxicity reduction in natural waters.

(2) Photocatalytic degradation of atenolol (ATL) was investigated in aqueous suspensions using TiO<sub>2</sub> as photocatalyst. Complete degradation of 37.6 μM ATL was obtained after 60 min irradiation in pH 6.8 Milli-Q water in the presence of 2.0 g L<sup>-1</sup> Degussa P25 TiO<sub>2</sub>. Degradation of ATL followed pseudo-first-order reaction kinetics. Hydroxyl radical (HO·) was determined to be the predominant reactive species during photocatalysis by means of radical probes. Major transformation products were elucidated by high performance liquid chromatograph-mass spectrometry (HPLC-MS/MS) technique. ATL photodegradation pathways included generation of 3-(isopropylamino)propane-1,2-diol and *p*-hydroxyphenylacetamide through ether chain cleavage, hydroxylation and the formation of 4-[2-hydroxy-3-(isopropylamino)propoxy] benzaldehyde. Frontier electron densities calculation verified the formation of mono-hydroxylation products with HO· primarily attacking on benzene ring, which is in agreement with LC-MS/MS analysis. Five carboxylic acids, i.e., oxalic, glyoxylic, malonic, oxamic and formic acids were identified by ion

exchange chromatography by comparison with authentic standards. Photocatalytic degradation efficiency of ATL was highly dependent on the properties of the water matrix, such as pH, the presence of organic and inorganic species (e.g., humic substance,  $\text{HCO}_3^-$ ). River water matrix was found to play a detrimental effect on ATL photocatalytic degradation with a longer irradiation time required for complete elimination of mother compound and intermediate products. Degussa P25 exhibited the highest photocatalytic activity for oxidizing ATL as well as intermediates compared to Aldrich rutile, Millennium PC500 and Hombikat UV100.

(3) Photochemical degradation mechanism and pathways of PBSA were investigated under artificial solar irradiation with the goal of assessing the potential of photolysis as a transformation mechanism in aquatic environments. The quantum yield of PBSA direct photolysis in pH 6.8 buffer solution under filtered mercury lamp irradiation was determined as  $2.70 \times 10^{-4}$ . Laser flash photolysis (LFP) experiments confirmed the involvement of PBSA radical cation ( $\text{PBSA}^{*\cdot}$ ) during direct photolysis. Acidic or basic condition facilitated PBSA direct photolysis in aqueous solution. Indirect photolysis out-competes direct photolysis as a major process for PBSA attenuation only at higher level of photosensitizers (e.g.,  $\text{NO}_3^- > 2 \text{ mM}$ ). Thus, direct photolysis is likely to be the major loss pathway responsible for the elimination of PBSA in natural sunlit surface waters, while indirect photolysis (e.g., mediated by  $\text{HO}\cdot$ ) appeared to be less important due to a general low level of steady-state concentration of  $\text{HO}\cdot$  ( $[\text{HO}\cdot]_{\text{ss}}$ ) in natural surface waters. Direct photolysis pathways of PBSA includes desulfonation and benzimidazole ring cleavage, which are probably initiated by the excited triplet state ( $^3\text{PBSA}^*$ ) and radical cation ( $\text{PBSA}^{*\cdot}$ ). Conversely, hydroxylation products of PBSA and 2-phenyl-1H-benzimidazole as well as their ring opening intermediates were found in nitrate-induced PBSA photolysis, suggesting the indirect photodegradation was primarily mediated by  $\text{HO}\cdot$  and followed a different mechanism.

(4) The kinetics and mechanism of photocatalytic degradation of PBSA were studied in illuminated  $\text{TiO}_2$  suspensions. Photocatalysis of PBSA were systematically investigated under different process conditions and water matrices. Experimental results demonstrated that PBSA photocatalytic reactions followed pseudo-first-order kinetics. Radical scavenging experiments indicated that hydroxyl radical ( $\text{HO}\cdot$ ) is the predominant reactive species responsible for an appreciable degradation of PBSA. Secondary order rate constant of PBSA- $\text{HO}\cdot$  reaction was determined to be  $5.8 \times 10^9 \text{ M}^{-1} \text{ s}^{-1}$  by competition kinetics method. Major intermediates included

hydroxylated products, benzamide, hydroxylated benzamidine, hydroxylated 2-phenyl-1H-benzimidazole as well as phenylimidazolecarboxylic derivatives which were elucidated by means of high performance liquid chromatography-mass spectrometry (HPLC-MS) technique. Four carboxylic acids, oxalic, malonic, acetic and maleic acids were detected during PBSA photocatalysis by HPLC-UV analysis. Ion chromatography (IC) results revealed that the sulfonic group of PBSA was primarily converted to sulfate ion while nitrogen atoms were released predominantly as ammonium and a less extent as nitrate. The reduction of TOC processed much more slowly compared to PBSA degradation, however, approximately 80% TOC was removed after 720 min irradiation. A comparison of photocatalytic degradation of PBSA and structurally related compounds revealed that the 5-sulfonic moiety in PBSA had negligible effect on the photocatalysis of 2-phenyl-1H-benzimidazole while 2-phenyl substituent stabilized the benzimidazole ring system to photocatalytic degradation.

Keywords: Atenolol; 2-Phenylbenzimidazole-5-sulfonic acid; Photochemistry; Photocatalysis; Degradation

# Contents

Chapter 1 Introduction.....	1
1.1. The occurrence of PPCPs in natural aquatic environment.....	3
1.2. Effect of PPCPs in the aquatic environment.....	5
1.3. Sources, pathways and fate of PPCPs in the aquatic environment.....	5
1.3.1. The sources for PPCPs releasing into the aquatic environment.....	5
1.3.2. Pathways for PPCPs depletion in the aquatic environment.....	6
1.4. Photodegradation of PPCPs in the aquatic environment.....	10
1.4.1. Direct photolysis of PPCPs.....	10
1.4.2. Indirect photolysis of PPCPs.....	12
1.5. Photocatalytic degradation of PPCPs.....	16
1.6. Objectives and outlines of the thesis.....	19
1.7. Reference.....	20
Chapter 2 Experimental Section.....	31
2.1. Chemicals and Materials.....	32
2.2. Photolysis experiments.....	33
2.2.1. Steady-state photolysis experiments.....	34
2.2.2. Laser flash photolysis experiments.....	34
2.3. Photocatalysis experiments.....	34
2.4. Analytical procedures.....	35
2.4.1. High performance liquid chromatography (HPLC) .....	35
2.4.2. Solid phase extraction-liquid chromatography-mass spectrometry (SPE-LC-MS) .....	36
2.4.3. HPLC-UV analysis for measuring carboxylic acids.....	37
2.4.4. Ion chromatography for measuring inorganic ions.....	37
2.4.5. TOC measurement.....	38
2.4.6. UV-vis absorption spectra.....	38
2.4.7. pH measurement.....	38
2.5. Calculation.....	38
2.5.1. Determination of the quantum yields.....	38

2.5.2. Calculation of light-screening factor.....	39
2.5.3. Determination of second-order rate constant for reaction of PPCPs with HO•.....	39
2.5.4. Calculation of frontier electron density.....	40
2.6. Toxicity test.....	40
<b>Chapter 3 Direct and indirect photolysis of atenolol in aqueous</b>	
<b>solution.....</b>	<b>41</b>
3.1. Results and discussion.....	42
3.1.1. Direct photolysis of ATL.....	42
3.1.1.1. Speciation and UV-vis absorption spectrum of ATL.....	43
3.1.1.2. Direct photolysis of ATL under different irradiation source.....	44
3.1.1.3. Intermediates and degradation pathways of ATL direct photolysis under xenon lamp irradiation.....	47
3.1.2. NO <sub>3</sub> <sup>-</sup> induced indirect photolysis of ATL.....	47
3.1.2.1. Photolysis kinetics.....	47
3.1.2.1.1. Effect of nitrate concentration.....	47
3.1.2.1.2. Effect of solution pH.....	48
3.1.2.1.3. Effect of bicarbonate concentration.....	48
3.1.2.1.4. Effect of humic substance.....	50
3.1.2.2. Identification of photoproducts and possible photodegradation pathways.....	51
3.1.2.3. Mineralization and toxicity.....	52
3.2. Conclusions.....	54
3.3. Reference.....	54
3.4. Supplementary Material.....	58
<b>Chapter 4 Photocatalytic degradation of atenolol in aqueous titanium</b>	
<b>dioxide suspensions.....</b>	<b>63</b>
4.1. Results and discussion.....	64
4.1.1. Preliminary experiment.....	64
4.1.2. Determination of HO• as major reactive species.....	65

4.1.3. Effect of solution pH.....	67
4.1.4. Effect of typical natural water constituents and river water matrix.....	67
4.1.5. Effect of different type of photocatalyst.....	68
4.1.6. Identification of organic intermediates.....	73
4.1.7. Elucidation of photocatalytic degradation pathways.....	74
4.1.8. Identification of carboxylic acids.....	76
4.1.9. Mineralization.....	77
4.2. Conclusions.....	78
4.3. Reference.....	79
4.4. Supplementary Material.....	84

## Chapter 5 Photochemical degradation of sunscreen agent

2-phenylbenzimidazole-5-sulfonic acid in different water matrices.....	89
5.1. Results and discussion.....	90
5.1.1. Protonation states of PBSA and UV-vis absorption spectra.....	90
5.1.2. LFP experiments to measure transient species of PBSA.....	91
5.1.3. Direct photolysis of PBSA at various pH values.....	92
5.1.4. Indirect photolysis of PBSA in the presence of nitrate.....	96
5.1.5. Photolysis of PBSA in different water matrices.....	99
5.1.6. Photodegradation products and pathways.....	100
5.2. Conclusions.....	103
5.3. Reference.....	103
5.4. Supplementary Material.....	107

## Chapter 6 Degradation of sunscreen agent

2-phenylbenzimidazole-5-sulfonic acid by TiO <sub>2</sub> photocatalysis.....	111
6.1. Results and discussion.....	113
6.1.1. Preliminary experiments of PBSA photocatalytic degradation.....	113
6.1.2. Determination of major reactive species.....	114
6.1.3. Effect of process conditions and water matrices on PBSA photocatalytic	

degradation.....	116
6.1.4. Identification of photodegradation intermediates and products.....	122
6.1.4.1. Evolution of organic intermediates.....	122
6.1.4.2. Evolution of carboxylic acids.....	124
6.1.4.3. Evolution of inorganic ions.....	125
6.1.4.4. Mineralization.....	126
6.1.5. Elucidation of photocatalytic degradation pathways.....	126
6.1.6. Comparison to structurally related compounds.....	128
6.2. Conclusions.....	130
6.3. Reference.....	131
6.4. Supplementary Material.....	137
Chapter 7 General conclusions and respects.....	143
Acknowledgement.....	145
Appendix.....	146
Résumé étendu de la these en Français	148



---

## Chapter 1 Introduction

### 1.1. The occurrence of PPCPs in natural aquatic environment

Pharmaceutical and personal care products (PPCPs) comprise a larger group of chemicals with substantial variability in structures, function, behavior and activity. The PPCPs include prescribed and non-prescribed drugs such as antibiotics, steroid, anti-inflammatory, analgesic, anti-epileptic, lipid regulator, anti-hypertensive, anti-depressant, antiseptic, X-ray contrast, nitro musks and sunscreens.<sup>1</sup> In recent years, PPCPs have been frequently detected in various aquatic environment, such as river water,<sup>2</sup> wastewater treatment plant effluents,<sup>3,4</sup> ground water<sup>5,6</sup> as well as drinking water<sup>7-9</sup> due to the advance in more sensitive, reliable and cost-effective analytical apparatus. For example, Kolpin et al. carried out the first nationwide reconnaissance of the occurrence of pharmaceuticals, hormones, and other organic wastewater contaminants (OWCs) in water samples from a network of 139 streams across 30 states during 1999 and 2000 in USA<sup>2</sup>. It was found that OWCs were prevalent during this study, being found in 80% of the streams sampled. The compounds detected represent a wide range of residential, industrial, and agricultural origins and uses with 82 of the 95 OWCs being found during this study. The detection of multiple OWCs was common for this study, with a median of seven and as many as 38 OWCs being found in a given water sample. In German, the occurrence of 32 drug residues belonging to different medicinal classes as well as five metabolites has been investigated in municipal sewage treatment plant (STP) discharges, river and stream waters. 80% of the selected drugs were detectable in at least one municipal STP effluent with concentration levels up to 6.3  $\mu\text{g L}^{-1}$  (carbamazepine). 20 different drugs and 4 corresponding metabolites were measured in river and stream waters, mainly acidic drugs, their metabolites, as well as neutral or weak basic drugs, mostly in the  $\text{ng L}^{-1}$  range.<sup>3</sup> Vieno et al. investigated the occurrence of pharmaceuticals in river water and their elimination in a pilot-scale drinking water treatment plant in Finland. The processes applied by the plant consisted of ferric salt coagulation, rapid sand filtration (GAC), and UV disinfection. Following the coagulation, sedimentation, and rapid sand filtration, the studied pharmaceuticals were found to be eliminated only by an average of 13%. An efficient elimination was found to take place during ozonation at ozone dose of about 1  $\text{mg L}^{-1}$ . Following this treatments, the concentrations of the pharmaceuticals dropped to below the quantification limits

---

with the exception of ciprofloxacin<sup>9</sup>. In China, the occurrence and transport of 12 antibiotics (from the tetracycline, sulfonamide, quinolone, and macrolide families) was studied in a 72 km stretch of the Haihe River, and in six of its tributaries. The sulfonamides were detected at the highest concentrations (24 – 385 ng L<sup>-1</sup>) and highest frequencies (76 – 100 %). Eight of the 12 antibiotics likely originated from veterinary applications in swine farms and fishponds, and concentrations at these source (0.12 - 47µg L<sup>-1</sup>) were 1 – 2 orders of magnitude higher than in the effluent of local wastewater treatment plants.<sup>10</sup> The occurrence of steroid estrogens, endocrine-disrupting phenols, and acid pharmaceutical residues in urban riverine water of the Pearl River Delta, South China, has been conducted by Peng et al.<sup>11</sup> Estrone was detected in > 60% water samples with a maximum concentration of 65 ng L<sup>-1</sup>. Endocrine disrupting phenols (nonylphenol, bisphenol A, triclosan, 2-phenylphenol, methyparaben and propylparaben) were found to be widely present at rather high concentrations in the urban riverine water of Guangzhou. Salicylic acid, clofibrac acid and ibuprofen were detected in most water samples with maximum concentrations of 2098, 248 and 1417 ng L<sup>-1</sup> respectively, whereas naproxen was less frequently detected and also at lower concentration. In Taiwan, Lin et al. and investigated the occurrence and distribution of pharmaceuticals (including antibiotics, estrogens, non-steroidal anti-inflammatory drugs (NSAIDs), beta-blockers, and lipid regulators) in three rivers and in the waste streams of six hospitals and four pharmaceutical production facilities.<sup>12,13</sup> The most frequently detected pharmaceuticals were acetaminophen, erythromycin-H<sub>2</sub>O, sulfamethoxazole, and gemfibrozil. NSAIDs were the next most-often detected compounds, with a detection frequency > 60%. The other analytes were not detected or were seen in only a few samples at trace concentrations.

Compared with the natural surface water, the groundwater is generally received less consideration. However, the groundwater can also be contaminated by PPCPs. Barber et al. measured OWCs in samples collected from monitoring wells located along a 4.5 km transect of a plume of groundwater contaminated by 60 years of continuous rapid infiltration disposal of wastewater treatment plant effluent.<sup>5</sup> Fifteen percent of the 212 OWCs analyzed were detected, including the antibiotic sulfamethoxazole (SMX), the nonionic surfactant degradation product 4-nonylphenol (4-NP), the solvent tetrachloroethene (PCE), and the disinfectant 1,4-dichlorobenzene (DCB). A recent review by Lapworth et al. highlighted the widespread contamination of groundwaters by a range of PPCPs, industrial compounds and life-style

---

compounds, with carbamazepine, sulfamethoxazole, ibuprofen, bisphenol A and caffeine being the most widely reported compounds.<sup>6</sup>

## 1.2. Effect of PPCPs in the aquatic environment

The presence of PPCPs in the aquatic environment may have potential hazardous effect on aquatic and terrestrial organisms. Once the PPCPs are released into the environment there is also the risk of exposure to humans via potable water supplied. Among the PPCPs, antibiotics are of particular interest because we currently do not know whether their presence in natural waters contributes to the spread of antibiotic resistance in microorganisms. Antibiotics are among the most widely used pharmaceutical compounds in animals. These drugs are used in animal husbandry for veterinary purpose, or as growth promoters (particularly in large-scale animal farming and intensive livestock treatment). Antibiotics also have the potential to affect the microbial population in sewage treatment system, and the inhibition of wastewater bacteria has the potential to seriously affect organic matter degradation as well as nitrification and denitrification.<sup>14</sup>

Numerous toxicity tests, including ecotoxicity, genotoxicity, cytotoxicity, and phytotoxicity, have been carried out to investigate the potential hazardous effect caused by the presence of PPCPs in aquatic system.<sup>15,16</sup> For instance, Isidori et al. investigated the ecotoxicity of six antibiotics (erythromycin, oxytetracyclin, sulfamethoxazole, ofloxacin, lincomycin and clarithromycin) on aquatic organisms.<sup>16</sup> Bioassays were performed on bacteria, algae, rotifers, microcrustaceans and fish to assess acute and chronic toxicity, while SOS Chromotest and Ames test were used to detect the genotoxic potential of the investigated drugs. The results showed that acute toxicity was in the order of  $\text{mg L}^{-1}$ , while for the chronic data the antibiotics were bioactive at concentrations in the order of  $\mu\text{g L}^{-1}$ , mainly for the algae. Drugs investigated were one or two order of magnitude less active against rotifers and crustaceans. Ofloxacin was the only genotoxic compound and sulfamethoxazole, ofloxacin and lincomycin were mutagenic. Macrolides were showed to be the most harmful for the aquatic environment. Kim et al. investigated the acute toxicity of the four most abundantly used pharmaceuticals in Korea, namely acetaminophen, carbamazepine, cimetidine, and diltiazem, and six sulfonamide related antibiotics, including sulfamethoxazole, sulfachlorpyridazine, sulfathiazole, sulfamethazine, sulfadimethoxine, and trimethoprim by using a marine bacterium (*Vibrio fischeri*) a freshwater invertebrate (*Daphnia*

---

*magna*), and the Japanese medaka fish (*Oryzias latipes*).<sup>15</sup> It was found that, in general, *Daphnia* was the most susceptible among the test organisms. The most acutely toxic among the chemicals tested in this study was diltiazem, with a median lethal concentration of 8.2 mg L<sup>-1</sup> for *D. magna*.

The toxicity of other kinds of pharmaceuticals were also studied by various authors using different approaches. For example, Hernando et al. carried out the environmental risk assessment of pharmaceutical residues in wastewater effluents, surface waters and sediments.<sup>17</sup> High risk is suspected to be induced in STP effluents as well as in surface waters for the following drugs: antibiotics (erythromycin), anti-inflammatories (ibuprofen, naproxen, diclofenac, ketoprofen), lipid regulators agents (gemfibrozil, clofibrate),  $\beta$ -blockers (propranolol, metoprolol) and antiepileptics (carbamazepine). Schwaiger et al. studied the toxic effects of the non-steroidal anti-inflammatory drug diclofenac on rainbow trout (*Oncorhynchus mykiss*).<sup>18</sup> The histopathological examinations of diclofenac-exposed fish revealed alterations of the kidney such as an hyaline droplet degeneration of the tubular epithelial cells and the occurrence of an interstitial nephritis. In the gills, the predominant finding consisted in a necrosis of pillar cells leading to damage of the capillary wall within the secondary lamellae. This finding assumed that prolonged exposure in environmentally relevant concentrations of diclofenac leads to an impairment of the general health condition of fish. Bonninaer et al.<sup>19</sup> used fluvial biofilms, as a pertinent tool, to assess  $\beta$ -blockers toxicity. It was found that propranolol was the most toxic  $\beta$ -blocker, mostly affecting the algal photosynthetic process. However, metoprolol was particularly toxic for bacteria. Atenolol was the least toxic of the three tested  $\beta$ -blockers. The higher toxicity of metoprolol and propranolol was proposed to be due to better absorption within biofilms of these two chemicals. The implication of this study is that since  $\beta$ -blockers are mainly found in mixtures in rivers, their differential toxicity could have potential relevant consequences on the interactions between algae and bacteria within river biofilms.

It should be noted that, most of the PPCPs presented in aquatic environment are under ng L<sup>-1</sup> level as a mixture, therefore, the long-term, subtle and chronic toxic effect should be taken into consideration rather than acute toxicity.<sup>20-22</sup> For example, a mixture of drugs at ng L<sup>-1</sup> levels can inhibit cells proliferation by affecting their physiology and morphology<sup>23</sup>. In addition, since different researchers usually used different methods to assess the toxicity effect of PPCPs such as algae, microbes, daphnids and fish, a large variability in the toxicity, or even opposite conclusion

---

can be obtained for the same compounds. However, the potential toxicity effect on the ecosystem and humans due to the presence of PPCPs in aquatic environment cannot be ruled out.

### **1.3. Sources, pathways and fate of PPCPs in the aquatic environment**

#### 1.3.1. The sources for PPCPs releasing into the aquatic environment

PPCPs can be more or less extensively metabolized by humans and animals. After consumption, PPCPs for human use or their metabolites are excreted into the effluent and reach the wastewater treatment plant (WWTP).<sup>1,3,4</sup> It has been reported that approximately 70% of the total amount of antibiotics consumed in German was excreted unchanged.<sup>14</sup> Also the household disposal of unused or expired pharmaceuticals resulted in the releasing into WWTP. Since most of the PPCPs is polarized, water soluble and persist organic compounds, the conventional WWTP with coagulation, flocculation and sedimentation, was found to be less efficient for elimination of large groups and various PPCPs. Since the majority of the PPCPs and their metabolites have microbial activities such as antibiotics and hormones, the conventional WWTP using biological process of active sludge appears to be insufficient for depletion of such kinds of PPCPs.<sup>3,4</sup> For example, antibiotics are only partially eliminated in sewage treatment plants. If they are not eliminated during the purification process, they pass through the sewage system and may end up in the environment, mainly in the water compartment. Residual amounts can reach surface waters, groundwater or sediments.<sup>14</sup> Thus, the urban wastewater treatment plants was regarded as hotspots for the release of antibiotics in the environment according to a recent review by Michael et al.<sup>24</sup> From a critical review by Jones et al., pharmaceutical are used in large amounts in human (and veterinary) medicine and reach the aquatic environment mainly through sewage treatment systems, where their concentration can reach micrograms per liter levels.<sup>25</sup>

The leakage of the landfill, manure storage tanks or septic tanks is another important source for PPCPs introducing into the aquatic environment. From a recent study by Eggen et al., PPCPs such as the non-steroidal anti-inflammatory drug ibuprofen and polycyclic musk compounds have been identified in municipal landfill leachates.<sup>26</sup> This study has shown that municipal landfill leachates may represent a significant source of concern for legacy, new and emerging chemicals in groundwater. In addition, the application of biosolids as a fertilizer/soil conditioner is other possible routes of entry for PPCPS into groundwater.

---

The livestock and poultry breeding and aquaculture are also important sources for PPCPs releasing into environment.<sup>6,14</sup> PPCPs, especially antibiotics, used in huge amount as anti-microbiological agents and promoter in livestock and poultry farm. Active substances discharged with liquid manure can be washed off from the top soil after rain. Waste lagoons are also potential sources of hormones and steroids. In intensive fish farming, infections are treated by feeding antimicrobial agents directly into the water. The substances used in fish farming can enter the surface waters directly without undergoing any kind of attenuation process. This results in high local concentrations in the water compartment and in the adjoining sediments.

For some personal care products, direct recreational water activities (e.g., bathing and swimming) are considered as the dominant pathway responsible for their wide occurrence in aquatic environment.<sup>27</sup> Rodil et al applied the SPE-LC-MS/MS method to determine the UV filters in three sets of (raw and treated) wastewater, three river water, and two seawater samples.<sup>28</sup> 2-phenylbenzimidazole-5-sulfonic acid (PBSA) and benzophenone-4 (BP-4) were the two compounds detected in higher concentration in wastewater samples (109 – 2679 ng L<sup>-1</sup> and 237 – 1481 ng L<sup>-1</sup> for PBSA and BP-4, respectively) and the only detected compounds in seawater (38 – 138 ng L<sup>-1</sup>). It is noteworthy that, this is the first data available in the literature on the occurrence of BP-4 in the environment, with very high concentrations found in the river sample taken in the summer (849 ng L<sup>-1</sup>).

### 1.3.2. Pathways for PPCPs depletion in the aquatic environment

There are a great variety of processes responsible for the fate of PPCPs in the aquatic environment. These processes include biotic ones (i.e., biodegradation by bacteria and fungi) and non-biotic ones (e.g., sorption, photolysis).

Sorption onto matrix surface (soil and mineral) is an important process able to attenuate PPCPs in the aquatic environment and is the key factor in terms of PPCPs accumulation, bioavailability and degradation.<sup>29</sup> The sorption of PPCPs is closely related to their physical-chemical properties (e.g.,  $pK_a$ ,  $\log K_{ow}$ ,  $\log K_{oc}$  and  $K_{DOM}$ ) as well as the characteristics of the target particles. Compounds with high  $\log K_{ow}$  values are known to sorb to sludge, while substances with lower values are more likely to stay in the aquatic phase. Likewise, the higher the  $\log K_{oc}$ , the higher is the likelihood that a compound will sorb to matter containing organic carbon.

---

Sorption coefficients, expressed as  $\log K_d$ , were usually calculated from fits using the Freundlich isothermic model. In a critical review, Toll reported the sorption behavior of antibiotics in soil.<sup>29</sup> In some cases, the mechanism other than hydrophobic partitioning may play a significant role in sorption of veterinary pharmaceuticals. A number of hydrophobicity-independent mechanisms, such as cation exchange, cation bridging at clay surfaces, surface complexation, and hydrogen bonding appear to be involved. Gu et al. studied the sorption of the antimicrobial ciprofloxacin to hydrous oxides of Al (HAO) and Fe (HFO).<sup>30</sup> Sorption to both HAO and HFO showed a strong pH-dependent behavior. Increasing the ionic strength had insignificant effect on the extent of ciprofloxacin sorption. Ligand-promoted dissolution of hydrous oxides, more pronounced for HAO, was observed in the presence of ciprofloxacin by using macroscopic and spectroscopic analyses. Different types of surface complexes between ciprofloxacin and HAO or HFO are formed. It was indicated that a monodentate mononuclear complex (with  $-\text{COO}^-$ ) appeared likely between ciprofloxacin and HAO, while keto O and one O from  $\text{COO}^-$  seem to be involved in the formation of a six membered ring with Fe on the HFO surface. This study increased our understanding of the environmental reactivity of fluoroquinolones. In another study, the same authors observed the same ligand-promoted dissolution during tetracycline sorption to these hydrous oxides.<sup>31</sup> The ability of tetracycline to form strong complexes with Al and Fe will increase the solubility of these minerals. Spectroscopic result suggests that tricarbonylamide and carbonyl functional groups of tetracycline could be responsible for sorption to mineral surfaces. Gao et al. investigated the adsorption of three sulfonamide to clay minerals as a function of pH, ionic strength, and type of exchangeable cation.<sup>32</sup> The sulfonamide adsorption exhibited pronounced pH dependence, which was consistent with sorbate speciation and clay properties. Cation exchange appeared to contribute to sorption of cationic sulfonamide species to montmorillonite. Anionic sulfamethazine adsorption was negligible. The heterocyclic R group influenced the degree of adsorption of cationic and neutral species. These results highlights the importance of speciation and clay surface charge density in determining the transport of sulfonamides. In another studies, humic substances were found to alter the surface properties and sites available for sorption and reactions.<sup>33</sup> They can either suppress or promote sorption of organic compounds to mineral surfaces. Haham et al. gave a further insight into the role of dissolved organic matter in sorption of sulfapyridine by soils.<sup>33</sup> DOM could decrease the sorption

---

of sulfapyridine to soils probably due to the blockage of sorption sites by DOM. Competition between preferentially sorbed DOM moieties (e.g., carboxyl, phenol) and sulfapyridine for sorption sites is proposed. This study suggests that the chemical nature of DOM can significantly affect the fate of sulfonamide compounds in soils. Note that, the sorption may also occurred with accompany of slow degradation. A study on adsorption and transformation of macrolide clarithromycin and roxithromycin on the surface of three environmental subsurface sorbents (clay, iron(III) and manganese(IV) oxy-hydroxides) showed that adsorption probably occurred through a surface complexation mechanism and was accompanied by slow transformation, such as hydrolysis and *N*-dealkylation.<sup>34</sup> However, the disappearance of a substance by sorption does not necessarily indicate biological or photochemical degradation.

Biodegradation (aerobic/anaerobic by micro-organism) is another pathway for PPCPs transformation in aquatic environment, especially in the secondary stage of treatment in WWTP where these compounds are exposed to large concentrations of micro-organisms. Aerobic and anaerobic biodegradation have been reported to be the most important processes for removal of pharmaceutical products from the aqueous phase in WWTP. The removal rate increased with increasing hydraulic retention time and with the age of the sludge in the activated sludge treatment. For example, diclofenac has been shown to be significantly biodegraded only when the sludge retention time was at least 8 days, whereas carbamazepine is less than 10% biodegraded.<sup>35</sup> Biological degradation of PPCPs leads to the formation of a series of transformation products (TPs). It has been proposed that more than 90% ibuprofen was biologically transformed into hydroxyl and carboxyl derivatives. Schulz et al. studied the biotransformation of iodinated contrast medium iopromide in water/soil system and found twelve TPs.<sup>36</sup> All TPs exhibited transformations at the side chain containing either carboxylic moieties and/or primary and secondary amide moieties, while the triiodoisophthalic acid structure remained unaltered. It should be noted that, the conjugates of pharmaceuticals can be cleaved during biodegradation, resulting in the release of the active parent compound, which provides an additional indirect source for release of the PPCPs into the environment. For the sunscreen agent sulisobenzone (BP-4), the biological degradation with active sludge in aerobic bath experiments formed at least nine TPs. At the beginning of the biotransformation of BP-4, a benzhydrol analogue was formed due to the reduction of the keto moiety. Further reactions (e.g., oxidation, demethylation, decarboxylation)

---

led to the formation of extremely polar TPs.<sup>37</sup>

The biodegradation ability may differ significantly from different PPCPs. For example, ibuprofen was found to be readily degraded under most studied conditions, whereas carbamazepine appeared to be recalcitrant by biodegradation.<sup>38</sup>

Both of caffeine and paracetamol are more biodegradable during wastewater treatment and transport in the subsurface and as such are generally detected less frequently compared to other PPCPs such as carbamazepine and sulfamethoxazole which are more resistant to biodegradation.<sup>39</sup> This result is not surprising since antibiotics are designed to be active against bacterial and this point is of particular importance for biodegradability testing of antibiotics. However, even among the antibiotics, biodegradability varies from case to case. For example, at environmental relevant concentration, cefalexin and the two sulfonamides (sulfamethoxazole and sulfadiazine) were predominantly removed by biodegradation in both freshwater and saline sewage systems.<sup>40</sup> The three fluoroquinolones also exhibited certain biodegradability in the saline activated sludge reactor. However, anhydro-erythromycin was persistent in both saline and freshwater systems under the experimental conditions and could not be removed at all. Similar result has been observed elsewhere. In a laboratory testing at realistic concentration, approximately 25% of benzylpenicillin was mineralized within 21 d, while ceftriaxone and trimethoprim were not mineralized at all.<sup>41</sup> These results are not unexpected since some kinds of PPCPs have shown to be unbiodegradable under aerobic conditions. Kim et al. studied the fate of tetracycline in the activated sludge process in wastewater treatment and reported no evidence of biodegradation for tetracycline during a biodegradability test, and sorption was found to be the principal removal mechanism for tetracycline in activated sludge.<sup>42</sup>

It can be assumed that microbial degradation will be slower in surface water than in the sewage system due to its lower bacterial density and lower diversity. Unlike in active sludge system, biodegradation may play a less important role in depletion PPCPs in groundwater. The anaerobic groundwater conditions are thought to contribute to the persistence of PPCPs, especially antibiotics, in groundwater after they have been leached from the base of the lagoon.<sup>43</sup> On the other hand, microbial degradation of PPCPs occurred relatively slowly in estuarine and coastal surface waters. Antipyrine, carbamazepine, cotinine, sulfamethoxazole, and trimethoprim were the most refractory (half-lives,  $t_{1/2} = 35$  to  $> 100$  days). Nicotine, acetaminophen, and fluoxetine

---

were labile across all treatments ( $t_{1/2} = 0.68$  to 11 days). Caffeine, diltiazem, and nifedipine were relatively labile. The slower rates of microbial degradation help explain the observed ubiquity of many of these pharmaceuticals in these and other receiving waters. Factors which control the relative persistence of organic substrates in estuarine and coastal waters are not well understood, but are likely to be attributed to the many factor, such as the concentrations and mixtures of PPCPs and other organic substrates, bacterial abundances and species compositions, temperature and environmental conditions.<sup>39</sup>

#### 1.4. Photodegradation of PPCPs in the aquatic environment

Photolysis is believed to be one of the most important abiotic pathways responsible for the depletion of organic pollutants, including PPCPs, in natural environment.<sup>44,45</sup> The photolysis can be categorized into two different types, namely direct photolysis and indirect photolysis. Direct photolysis occurs when the UV-visible absorption spectrum of one molecule overlaps with the solar emission spectrum, or one molecule absorbs solar light which reaches to the surface of the earth ( $\lambda > 290$  nm). Unlike direct photolysis, the indirect photolysis is initiated by reactions with reactive species (e.g.,  $^1\text{O}_2$ ,  $\text{HO}\cdot$  and  $^3\text{DOM}^*$ ) generated by photosensitizers (e.g., nitrate ( $\text{NO}_3^-$ ), dissolved organic matter (DOM), ferric ion ( $\text{Fe}^{3+}$ ) after solar light absorption.<sup>46</sup> A critical review about the photodegradation of pharmaceuticals in the aquatic environment was reported by Boreen. et al. in 2003.<sup>46</sup>

##### 1.4.1. Direct photolysis of PPCPs

Direct photolytic degradation of PPCPs, such as diclofenac and triclosan, has been well-documented in literature.<sup>47-57</sup> The direct photolysis is closely related with the chemical structure of compounds. This is because the light absorbance properties of PPCPs is associated with the delocalizing  $\pi$  electronic system in their molecules. Such molecules can be easily subject to  $\pi-\pi^*$  transition. If the  $\pi$  electronic system contains non-binding heteroatom,  $n-\pi^*$  transition are also likely to take place. For those molecules bearing strong chromophoric groups such as naphthalene, benzophenone and nitro, direct degradation appears to be important for eliminating these compounds in natural sunlit surface waters. A typical illustration was the direct photolysis of  $\beta$ -blockers, atenolol, metoprolol, and propranolol in waters.<sup>58</sup> It was found that propranolol

---

underwent relatively fast direct photolysis relative to atenolol or metoprolol. This result can be attributed to the naphthalene structure in propranolol, whose absorption spectrum has a significant overlap with solar spectrum. Whereas, atenolol and metoprolol possess benzyl ring in their molecular structure, thus has less absorbance at wavelength with  $\lambda > 290$  nm, which in turn limited their direct photolysis. Similarly, the rapid direct photolysis of ketoprofen under xenon lamp irradiation ( $765\text{W/m}^2$ ,  $290\text{ nm} < \lambda < 700\text{ nm}$ ) can be explained by the fact that the carbonyl moiety is in conjugation with two aromatic rings. When the carbonyl is highly conjugated, the energy of the  $n-\pi^*$  transition is lowered, resulting in a very reactive triplet state.<sup>59</sup> Fig. 1.1. Shows the direct photolytic degradation pathway of ketoprofen.

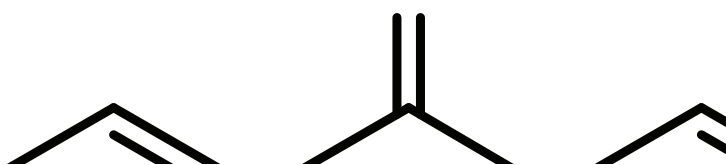


Fig. 1.1. Direct photolytic pathway of ketoprofen and fluoxetine.<sup>59,66</sup>

Edhlund and coauthors studied the aquatic photochemistry of nitrofuran antibiotic and found that direct photolysis is the dominant photodegradation pathways for these compounds.<sup>60</sup> The nitro group is the chromophore of the nitrofurans that has its  $\lambda_{\text{max}}$  near 365 nm and is responsible for the photochemistry of these compounds. Ranitidine was also degraded in direct photolysis and the nitroacetamide portion of ranitidine has been shown to be the moiety active in direct

---

photolysis.<sup>61</sup> It is worth noting that direct photolysis of PPCPs is also highly pH-dependent. This is because a wide range of PPCPs have ionizable functional groups which can undergo protonation or deprotonation process and solution pH alters the speciation of these compounds. Thus, the absorption spectra of different existing species of organic compounds usually varies under different pH value, which consequently influence the photolysis behavior of PPCPs. Boreen et al. investigated the photochemical fate of five sulfa drugs with varying five-membered heterocyclic substituents and observed that the rate of direct photolysis of these compounds is dependent upon the identity of the heterocyclic R group as well as the pH of the solution.<sup>62</sup> The quantum yields calculated rang from  $< 0.005$  for the neutral state of sulfamethizole to  $0.7 \pm 0.3$  for the protonated state of sulfisoxazole. Wei et al. differentiated and confirmed that the five dissociation species of ciprofloxacin have different photodegradation pathways, products and kinetics.<sup>63</sup> In the normal pH range (6 - 9) of surface waters,  $H_2CIP^+$  is the predominant dissociation species of CIP, which can photodegrade fast by defluorination. Similar result has been report by Sturini et al. on photochemical degradation of marbofloxacin and enrofloxacin in natural waters.<sup>64</sup> Jiao et al. observed pronounced photodegradation of tetracycline with increasing pH.<sup>65</sup> However, the influence of pH on photodegradation of PPCPs could be complex. For example, the photodegradation of the nitrofurantoin antibiotics was found to be acid-catalyzed.<sup>60</sup> The rate constant for photodegradation of fluoxetine at pH 9 was approximately double the rate constants in pH 4 and pH 7 buffer solutions and in DI water.<sup>66</sup> Since the comparison of the UV-vis spectra taken at neutral and basic pH illustrated that a shift in the UV-vis absorption spectrum to longer wavelengths did not occur with increase in pH. Thus, a more likely explanation is that the mechanism for direct photolysis is base-catalyzed. Defluorination of the trifluoromethyl group and products resulting from O-dealkylation of FLX were both observed in direct photolysis of fluoxetine (see Fig. 1.1.).<sup>66</sup>

#### 1.4.2. Indirect photolysis of PPCPs

Under solar irradiation, various reactive oxygen species (ROS) and photoreactive transients can be generated in natural surface waters by photosensitizers. These reactive species played an important role in depletion of PPCPs in aquatic system, especially when there compounds undergo weak or negligible direct photolysis. Previous studies have demonstrated that  $NO_3^-$  is the key

---

source of HO• in natural surface waters upon solar irradiation.<sup>67,68</sup> NO<sub>3</sub><sup>-</sup> is known to be ubiquitous in natural aquatic environment with a concentration ranging from 10<sup>-5</sup> to 10<sup>-3</sup> M, which is highly related to the geographic location and human agriculture activity. NO<sub>3</sub><sup>-</sup> could mediated degradation of pollutants by reaction with photogenerated reactive HO• and NO<sub>2</sub>•. Nélieu et al. studied the nitrate-induced photodegradation of chlorotoluron in natural water through two series of experiments in outdoor aquatic mesocosms.<sup>69</sup> It was shown that the pesticide degradation kinetics was clearly dependent on nitrate concentration. Photodegradation products included *N*-terminus oxidation products, oxidation of the methyl attached to the phenyl, Cl substitution by OH, hydroxylation and nitration of the phenyl ring. Similar result has been observed by Shankar et al. in a study on photo-induced degradation of diuron in aqueous solution by nitrites and nitrates (see Fig. 1.2.).<sup>70</sup> However, in the case of fluometuron, hydroxylation of the aromatic ring with or without hydrolysis of CF<sub>3</sub> into CO<sub>2</sub>H and oxidation of the urea chain leading to demethylation were observed.<sup>71</sup> The oxidations of the aromatic ring and of the urea chain were also observed in phototransformation of methabenthiazuron in the presence of nitrate and nitrite ions.<sup>72</sup> It was suggested that HO• generated by irradiated nitrate at concentrations present in wastewater effluent plays an important role as a photosensitizer even in the presence of fulvic acid.<sup>73</sup> However, it should be emphasized that NO<sub>3</sub><sup>-</sup>-induced phototransformation of organic pollutants in some case lead to nitration or nitrosation, thus, raises the concern about generating carcinogenic or mutagenic compounds.<sup>74,75</sup>

Fig. 1.2. Degradation pathways of diuron photo-induced by NO<sub>3</sub><sup>-</sup> and NO<sub>2</sub><sup>-</sup>.<sup>70</sup>

---

Dissolved organic matter (DOM) is another well-known photosensitizer widely presented in natural surface waters. DOM-mediated indirect photodegradation of organic pollutants through photogenerated reaction oxygen species (e.g.,  $^1\text{O}_2$  and  $\text{HO}\cdot$ ) as well as excited triplet state  $^3\text{DOM}^*$  has been well documented.<sup>76,77</sup>  $^1\text{O}_2$  is an electrophilic species and react with electron-rich compounds at higher rate. In the environment,  $^1\text{O}_2$  is responsible for oxidative transformations of certain classes of organic contaminants, particularly those containing phenolic, heterocyclic, olefinic, and sulfidic moieties, and may be involved in the weathering of dissolved organic matter itself.<sup>78,79</sup> For example, photooxidation mediated by  $^1\text{O}_2$  is the likely degradation pathway for cimetidine in most natural waters because  $^1\text{O}_2$  is reactive toward reaction with imidazole model compound.<sup>61</sup> On the other hand,  $^3\text{DOM}^*$  could mediate organic compounds degradation through energy transfer, electron transfer as well as hydrogen atom abstraction. Boreen et al., have shown that indirect photolysis of sulfa drugs containing six-membered heterocyclic substituents was attributable to interaction with triplet excited-state DOM.<sup>80</sup> The interaction of the sulfa drugs with triplet excited-states is perhaps due to electron-transfer or hydrogen atom abstraction reactions. A recent study on indirect photodegradation of amine drugs in aqueous solution under simulated sunlight has demonstrated that the electron transfer from the nonbonding electrons on nitrogen of the amine drugs to the excited ketone of the humic substrate occurred.<sup>81</sup> However, DOM could also inhibit organic compounds destruction by severing as inner filter to attenuate light, radical quencher to compete for reactive photooxidants, and reduce intermediates of mother compounds. Wenk and coauthors have suggested that DOM could reduce the transformation rate of various aqueous organic contaminants by inhibiting the transformation of oxidation intermediates.<sup>82,83</sup> Therefore, it can be concluded that the role of DOM in photo-induced transformation of PPCPs should be complex in natural sunlit surface waters. It also should be noted that the composition of DOM significantly influenced the photodegradation of PPCPs because DOM plays an important role in the type and amount of reactive transients formed when irradiated.<sup>77</sup> For example, microbially-derived DOM showed to be much more photoreactive than terrestrially-derived DOM for ibuprofen transformation.<sup>84</sup> It was proposed that  $\text{HO}\cdot$  pathway is more important for terrestrially derived-DOM, while  $^3\text{DOM}^*$  is the dominant mechanism for DOM derived from microbial precursors.

Another photoreactive species is  $\text{Fe}^{3+}$ , which is found out to be one of the most abundant

---

transient metal ions ubiquitously present in natural waters. The photochemical reaction of Fe(III) in the aquatic system is believed to play an important role in chemical and biological processes.<sup>85</sup> In most natural waters, Fe(III) is probably complexed with hydroxide ion and organic ligands. The photochemical process of Fe(III) species gives rise to Fe(II) through ligand-metal charge transfer (LMCT) mechanism which is highly-species dependent. Therefore, two types of photochemical reactions may occur: (I) the organic matter or the pollutant is able to complex Fe(III) and the resulting complex absorbs solar radiation and undergoes a direct photolysis; (II) Fe(III) is only complexed by hydroxide ion and the degradation is achieved by HO• radicals formed by irradiation of Fe(III) aquo complexes.<sup>86</sup> For example, in the presence of DOM, Fe(III) could complex with DOM. The photochemical reaction of Fe(III)-DOM complex was believed to be one important pathway for generating HO• in natural surface waters upon solar irradiation via photo-Fenton like reaction. Among various Fe(III) aquo complexes, FeOH<sup>2+</sup>, the species present at 3 < pH < 5, is the most photoreactive species of Fe<sup>3+</sup>. At near neutral pH, dimeric form Fe<sub>2</sub>(OH)<sub>2</sub><sup>4+</sup> is the dominant species, however, this species is much less photoreactive as compared to FeOH<sup>2+</sup> and therefore contributed negligibly to the degradation of aquatic pollutants. The photodegradation rate of carbamazepine decreased with increasing pH.<sup>87</sup> This is because at most acidic pH values, Fe(III) is mainly in the dissolved form and FeOH<sup>2+</sup> is the most photoactive Fe(III) species. Upon pH increase, dimeric and oligomeric Fe(III) compounds up to Fe(III) colloids tend to prevail over mononuclear species. The main difference between monomeric and dimeric/oligomeric species or colloids is that the irradiation of the former yields HO• with reasonable to elevated quantum yield, while HO• production by dimeric /oligomeric colloids is quite low.

It is noteworthy that the various water constituents usually behave in a complicated way for influence PPCPs photodegradation as well as the irradiation source. For example, the aqueous speciation of tetracycline over a range of natural pH and water hardness values is dominated by association with Ca<sup>2+</sup> and Mg<sup>2+</sup>, which consequently strongly influenced the environmental photochemical kinetics of the antibiotic compound.<sup>88</sup> Ge et al. have reported a light-source-dependent effect of main water constituents on photodegradation of phenolic antibiotics.<sup>89</sup> Also, Vione et al. observed that HCO<sub>3</sub><sup>-</sup> could promote the production of nitration of phenolic compounds in the presence of nitrate.<sup>90,91</sup>

---

A important issue which should be taken into consideration is that phototransformation of PPCPs in aqueous environment sometimes results in higher toxic intermediates or byproducts.<sup>92</sup> A well known example is the phototransformation of triclosan in river water can resulted in the formation of much more harmful 2,8-dichlorodibenzo-*p*-dioxin.<sup>53,54</sup> Other examples included antibiotics cephalosporin and sulfamethoxazole.<sup>93,94</sup>

### 1.5. Photocatalytic degradation of PPCPs

Numerous PPCPs in the aquatic system such as surface water, ground water, wastewater treatment plant effluents and even drink water raised great scientific concerns as well as public awareness for developing efficient clean-up technology. Photocatalysis using semiconductor as sensitizers for photo-induced decomposition of pollutants in waters has being studied for more than 30 years. Among them, heterogeneous semiconductor photocatalysis using TiO<sub>2</sub> as the photocatalyst has been found to be a promising treatment technology for eliminating organic pollutants in waters, including PPCPs, because TiO<sub>2</sub> is non-toxic, inexpensive, and relatively biologically and chemically stable.<sup>95-98</sup> When irradiating with photons of energy equal to or exceeding the band gap energy of TiO<sub>2</sub> (for anatase, 3.2 eV band gap), valence band holes (h<sub>vb</sub><sup>+</sup>) and reductive conduction band electrons (e<sub>cb</sub><sup>-</sup>) are generated. The photogenerated holes can: (i) directly oxidize the adsorbed chemical substance; or (ii) produce adsorbed hydroxyl radical (HO•) via the surface-bound OH<sup>-</sup> and/or the adsorbed water molecules. As a highly reactive oxidant, HO• is capable of unselectively reacting with most recalcitrant organic contaminants at near-diffusion-controlled rates in water (10<sup>8</sup> - 10<sup>10</sup> M<sup>-1</sup> s<sup>-1</sup>). Therefore, TiO<sub>2</sub> is considered to be the most suitable semiconductor for widespread environmental photocatalytic applications.<sup>95-98</sup>

There are numerous published papers about degradation of PPCPs in waters by TiO<sub>2</sub> photocatalyst. Research activities focused on investigating the influence factors (operational parameters) such as the TiO<sub>2</sub> types and dosages, the initial substrate concentration, the effect of solution pH and coexisting water constituents. For instance, Hapeshi et al. investigated the effect of catalyst type and loading, initial substrate concentration, initial pH and H<sub>2</sub>O<sub>2</sub> as an additional oxidant on substrate conversion and mineralization in photocatalytically degradation of drugs ofloxacin and atenolol.<sup>99</sup> However, no detail degradation pathways of ofloxacin and atenolol were provided by these researchers. Zhang et al. investigated the photocatalytic degradation of

---

acetaminophen in TiO<sub>2</sub> suspended solution under a 250 W metal halide lamp.<sup>100</sup> The influence of some parameters on the degradation APAP was studied and described in details, such as initial APAP concentration, initial pH value and TiO<sub>2</sub> dosage. Hu et al studied the oxidation of sulfamethoxazole and related antimicrobial agents by TiO<sub>2</sub> photocatalysis under ultraviolet-A light (UVA: 324 ≤ λ ≤ 400 nm) and found the rates of UVA-TiO<sub>2</sub> photocatalyzed SMX degradation are dependent upon several variables, including the initial SMX concentration, catalyst phase identity and concentration, electron acceptor identity and concentration, catalyst phase identity and concentration, and the presence of non-target water constituents.<sup>101</sup> It should be noted that the water constituents played an important role in photocatalysis process since some constituents which are ubiquitous in natural waters (e.g., bicarbonate ions, dissolved organic matter (DOM)) may serve as HO• scavengers. Hu et al. also reported that the presence of natural organic matter (NOM) inhibits photocatalytic degradation of SMX to a much greater extent at pH 5 than pH 9. In addition, the presence of bicarbonate leads to enhanced SMX photocatalysis at pH 9.<sup>101</sup> Direct photolysis and solar TiO<sub>2</sub> photocatalysis of Trimethoprim (TMP) in different water matrices have been studied by Sirtori et al.<sup>102</sup> It was found that during TiO<sub>2</sub> photocatalysis, TMP was completely eliminated in both water matrices at a similar rate, however, the mineralization rate was appreciably reduced in seawater, which can be explained by the presence of inorganic species acting as HO• scavengers, and directly affecting photocatalytic efficiency.<sup>102</sup>

Some researchers also studies the underlying mechanism, the degradation pathways and the toxicity assessment of the degradation intermediates and products. For example, Calza et al. studied the photocatalytic transformation of non-steroidal anti-inflammatory drug diclofenac, under simulated solar irradiation using TiO<sub>2</sub> as catalyst, to assess the decomposition of the pharmaceutical compound, to identify intermediates, as well as to elucidate some mechanistic details of the degradation.<sup>103</sup> In addition Microtox bioassay (*Vibrio fischeri*) was employed in evaluating the ecotoxicity of solutions treated by photocatalysis. They observed several hydroxyl- and bihydroxy diclofenac derivatives, which were further transformed into chloro or hydroxyl-phenol derivatives. The formation of carboxylic acids was achieved through the ring opening and complete mineralization was obtained after 2 h irradiation as assessed by TOC measurement. Ecotoxicity measurements on the treated solutions emphasized the efficiency of the photocatalytic treatment in the detoxification process. Ohko and coauthors studied the degradation

---

of 17 $\beta$ -estradiol (E2) in water by TiO<sub>2</sub> photocatalysis and evaluated the estrogenic activity of the treated water during the photocatalytic reactions by an estrogen screening assay.<sup>104</sup> The cited authors found that the estrogenic activities of the intermediate products were negligible. It was concluded that the phenol moiety of the E2 molecule, one of essential functional groups to interact with the estrogen receptor, should be the starting point of the photocatalytic oxidation of E2. A detailed study on identification of photocatalytic degradation products of bezafibrate (BZF), a lipid regulator, in TiO<sub>2</sub> aqueous suspensions under simulated solar light has been carried out by Lambropoulou et al. using powerful analytical techniques such as LC-TOF-MS, GC-MS and HPLC-DAD.<sup>105</sup> The degradation pathways include single or multiple hydroxylation of BZF with subsequent phenoxy ring opening and the cleavage of the amide and ether bonds. However, no data about the toxicity of the photoproducts had been provided by these authors.

Recent studies have also provided evidence that the photodegradation behavior was highly substrate-specific with respect to certain kind of TiO<sub>2</sub>. For example, one study by Doll and Frimmel showed that P25 had a better photocatalytic activity for clofibrac acid and carbamazepine than Hombikat UV 100.<sup>106</sup> For photocatalytic degradation of iomeprol, Hombikat UV 100 was more suitable than P25. The authors attributed this result to the higher adsorption capacity of Hombikat UV 100. Ryu and Choi systematically investigated the multidimensional aspects of the photocatalytic activity.<sup>107</sup> The photocatalytic activities of eight commercial TiO<sub>2</sub> samples were quantified by employing 19 test substrates in terms of their degradation or conversion rates in water. They found that the measured activities exhibited a complex behavior that depends on the test substrate. This suggested that the highly substrate-specific activity of TiO<sub>2</sub> photocatalysts hinders the straightforward comparison of which catalyst is better than others. Finally, these authors proposed the multivalued photocatalytic activity test in relation with water treatment application.

Another attracting field in photocatalytic degradation of PPCPs was using the solar irradiation as new and sustainable energy. Photocatalytic degradation of pharmaceuticals acetaminophen, atenolol and ranitidine have been performed in a well-defined system of a pilot plant scale Compound Parabolic Collector (CPC) reactor by Radjenović et al.<sup>108,109</sup> Two types of heterogeneous photocatalytic experiments were performed: catalyzed by TiO<sub>2</sub> semiconductor and by Fenton reagent (Fe<sup>2+</sup>/H<sub>2</sub>O<sub>2</sub>), each one with distilled water and synthetic wastewater effluent

---

matrix. Complete disappearance of the parent compounds and discreet mineralization were attained in all experiments.

From the above analysis, it can be expected that photocatalytic degradation of organic contaminant is complex although research activities focused on this field have been carried out for more than a few decades. The photocatalytic reactivity is closely related with the physical-chemical properties of the catalyst, such as crystallinity, composite, BET surface area, impurities/defect and density of surface hydroxyl group etc, as well as the physical-chemical properties of the target molecule. The photocatalytic reactivity is also known to be strongly depended on the solution pH value or the coexist of the inorganic ions, especially fluoride, which could modify or even shift the photocatalytic mechanism. For example, Sun et al. studied the photocatalytic degradation of 2,4-dichlorophenoxyacetic acid (2,4-D) in UV-illuminated aqueous TiO<sub>2</sub> suspension.<sup>110</sup> At pH ~ 3, the initial step is chiefly direct hole (h<sup>+</sup>) oxidation, while below and especially above pH 3, it shifts progressively to hydroxyl radical like reaction following rate-limiting h<sup>+</sup> oxidation of surface hydroxyls. The formation of surface fluorides on TiO<sub>2</sub> by replacing >Ti-OH<sub>2</sub><sup>+</sup> by >Ti-F species, uniquely affects both photocatalytic reactions and photoelectrochemical behaviors.<sup>111</sup> For example, when the hydroxyl groups on the surface of TiO<sub>2</sub> were replaced by F<sup>-</sup>, there were little adsorbed Acid orange 7 molecules to be trapped by hole, so the initial process could shift progressively from hole-dominated surface reaction to homogeneous radical reaction in bulk solution.<sup>112</sup> Thus, photocatalytic degradation/transformation efficiency usually varies from case to case, and extrapolation of one result to another usually cannot be obtained.

## 1.6. Objectives and outlines of the thesis

The main objective of this thesis is studying the photochemical and photocatalytic degradation of atenolol and 2-phenylbenzimidazole-5-sulfonic acid, as representatives of pharmaceuticals and personal care products, respectively. ATL and PBSA have been chosen as two model compounds of PPCPs in the current work due to their wide occurrence and relatively high level in natural aquatic environment.<sup>28,113</sup> Atenolol (ATL), 4-[2-hydroxy-3-[(1-methyl)amino]propoxyl]benzeacetamide, is a selective β<sub>1</sub> receptor antagonist and has been used primarily for the treatment of cardiovascular diseases for more than thirty years.

---

Previous studies have provided evidence that ATL could inhibit the growth of human embryonic cells and was ecotoxic to freshwater species.<sup>114</sup> A more recent study has shown that atenolol was toxic to fluvial biofilms in freshwater ecosystems.<sup>115</sup> On the other hand, 2-phenylbenzimidazole-5-sulfonic acid (PBSA) is known to photo-generate reactive species such as  $^1\text{O}_2$  and  $\text{O}_2^-$ , thus can cause DNA damage. For example, Johnson and Inbaraj studied the photo-physical and photochemical properties of PBSA and demonstrated that UV irradiation of PBSA generates a variety of free radicals and active oxygen species that may be involved in the photodamage of DNA.<sup>116</sup> The photochemical reaction of these compounds, as a potential loss process in natural environment, should be clarified and photocatalytic oxidation, as a promising treatment technology, should be evaluated.

This thesis included investigation of the kinetics, identification of the transformation intermediates and products, exploring the degradation mechanisms and the reactive species involved in the photodegradation, proposing the degradation pathways and evaluation of the reduction in TOC and decrease in toxicity, etc. Thus, the thesis is subsequently organized as follows:

Chapter 1 is the background of the research work and literatures survey.

Chapter 2 introduces the materials and experimental methodologies used in this work.

Chapter 3 studies the photolysis of atenolol in aqueous solution, especially the indirect photolysis of atenolol induced by nitrate ions.

Chapter 4 studies the photocatalytic oxidation of atenolol in aqueous  $\text{TiO}_2$  suspensions.

Chapter 5 studies the photochemical degradation of PBSA in different water matrices.

Chapter 6 studies the photocatalytic degradation of PBSA in aqueous  $\text{TiO}_2$  suspensions.

Chapter 7 provide the general conclusions and prospects.

## 1.7. Reference

- (1) Daughton, C. G.; Ternes, T. A. Pharmaceuticals and personal products in the environment: agents of subtle change? *Environ. Health Perspect.* **1999**, 107, 907-938.
- (2) Kolpin, D. W.; Furlong, E. T.; Meyer, M. T.; Thurman, E. M.; Zaugg, S. T.; Barber, L. B.; Buxton, H. T. Pharmaceuticals, hormones, and other organic wastewater contaminants in U.S. streams, 1999-2000: a national reconnaissance. *Environ. Sci. Technol.* **2002**, 36, 1202-1211.

- 
- (3) Ternes, T. A. Occurrence of drugs in German sewage treatment plants and rivers. *Water Res.* **1998**, 32, 3245-3260.
- (4) Vieno, N. M.; Tuhkanen, T.; Kronberg, L. Seasonal variation in the occurrence of pharmaceuticals in effluents from a sewage treatment plant and in the recipient water. *Environ. Sci. Technol.* **2005**, 39, 8220-8226.
- (5) Barber, L. B.; Keefe, S. H.; Leblanc, D. R.; Bradley, P. M.; Chapelle, F. H.; Meyer, M. T.; Loftin, K. A.; Kolpin, D. W.; Rubio, F. Fate of sulfamethoxazole, 4-nonylphenol, and 17 $\beta$ -estradiol in groundwater contaminated by wastewater treatment plant effluent. *Environ. Sci. Technol.* **2009**, 43, 4843-4580.
- (6) Lapworth, D. J.; Baran, N.; Stuart, M. E.; Ward, R. S. Emerging organic contaminants in groundwater: a review of sources, fate and occurrence. *Environ. Pollut.* **2012**, 163, 287-303.
- (7) Westerhoff, P.; Yoon, Y.; Snyder, S.; Wert, E. Fate of endocrine-disruptor, pharmaceutical, and personal care product chemicals during simulated drinking water treatment process. *Environ. Sci. Technol.* **2005**, 39, 6649-6663.
- (8) Loraine, G. A.; Pettigrove, M. E. Seasonal variations in concentrations of pharmaceuticals and personal care products in drinking water and reclaimed wastewater in southern California. *Environ. Sci. Technol.* **2006**, 40, 687-695.
- (9) Vieno, N. M.; Härkki, H.; Tuhkanen, T.; Kronberg, L. Occurrence of pharmaceuticals in river water and their elimination in a pilot-scale drinking water treatment plant. *Environ. Sci. Technol.* **2007**, 41, 5077-5084.
- (10) Luo, Y.; Xu, L.; Rysz, M.; Wang, Y.; Zhang, H.; Alvarez, P. J. J. Occurrence and transport of tetracycline, sulfonamide, quinolone, and macrolide antibiotics in the Haihe river basin, China. *Environ. Sci. Technol.* **2011**, 45, 1827-1823.
- (11) Peng, W.; Yu, Y.; Tang, C.; Tan, J.; Huang, Q.; Wang, Z. Occurrence of steroid estrogens, endocrine-disrupting phenols, and acid pharmaceutical residues in urban riverine water of the Pearl River Delta, South China. *Sci. Total Environ.* **2008**, 397, 158-166.
- (12) Lin, A. Y. C.; Tsai, Y. T. Occurrence of pharmaceuticals in Taiwan's surface waters: impact of waste streams from hospitals and pharmaceutical production facilities. *Sci. Total Environ.* **2009**, 407, 3793-3802.
- (13) Lin, A. Y. C.; Yu, T. H.; Lin, C. F. Pharmaceutical contamination in residential, industrial, and

- 
- agricultural waste streams: risk to aqueous environments in Taiwan. *Chemosphere* **2008**, 74, 131-141.
- (14) Kümmerer, K. Antibiotics in the aquatic environment-A review-Part I. *Chemosphere* **2009**, 75, 417-434.
- (15) Kim, Y.; Choi, K.; Jung, J.; Park, S.; Kim, P.G.; Park, J. Aquatic toxicity of acetaminophen, carbamazepine, cimetidine, diltiazem and six major sulfonamides and their potential ecological risks in Korea. *Environ. Int.* **2007**, 33, 370-375.
- (16) Isidori, M.; Lavorgna, M.; Nardelli, A.; Pascarella, L.; Parrella, A. Toxic and genotoxic evaluation of six antibiotics on non-target organisms. *Sci. Total Environ.* **2005**, 346, 87-98.
- (17) Hernando, M. D.; Mezcuá, M.; Fernández-Alba, A. R.; Barceló, D. Environmental risk assessment of pharmaceutical residues in wastewater effluents, surface waters and sediments. *Talanta*, **2006**, 69, 334-342.
- (18) Schwaiger, J.; Ferling, H.; Mallow, U.; Wintermayr, H.; Negele, R. D. Toxic effects of the not-steroidal anti-inflammatory drug diclofenac Part I: histopathological alterations and bioaccumulation in rainbow trout. *Aquat. Toxicol.* **2004**, 68, 141-150.
- (19) Bonnineau, C.; Guasch, H.; Proia, L.; Ricart, M.; Geiszing, A.; Romani, A. M.; Sabater, S. Fluvial biofilms: a pertinent tool to assess  $\beta$ -blockers toxicity. *Aquat. Toxicol.* **2010**, 96, 225-233.
- (20) Cleuvers, M. Aquatic ecotoxicity of pharmaceuticals including the assessment of combination effects. *Toxicol. Lett.* **2003**, 142, 185-194.
- (21) Crane, M.; Watts, C.; Boucard, T. Chronic aquatic environmental risks from exposure to human pharmaceuticals. *Sci. Total Environ.* **2006**, 367, 23-41.
- (22) Fent, K.; Weston, A. A.; Caminada, D. Ecotoxicology of human pharmaceuticals. *Aquat. Toxicol.* **2006**, 76, 122-159.
- (23) Pomati, F.; Castiglioni, S.; Zuccato, E.; Fanelli, R.; Vigetti, D.; Rossetti, C.; Calamari, D. Effects of a complex mixture of therapeutic drugs at environmental levels on human embryonic cells. *Environ. Sci. Technol.* **2006**, 40, 2442-2447.
- (24) Michael, I.; Rizzo, L.; McArdell, C. S.; Manaia, C. M.; Merlin, C.; Schwartz, T.; Dagot, C.; Fatta-Kassinos, D. Urban wastewater treatment plants as hotspots for the release of antibiotics in the environment: a review. *Water Res.* **2013**, 47, 957-995.
- (25) Jones, O. A. H.; Voulvoulis, N.; Lester, J. N. Human pharmaceuticals in wastewater treatment

- 
- process. *Crit. Rev. Environ. Sci. Technol.* **2005**, 35, 401-427.
- (26) Eggen, T.; Moeder, M.; Arukwe, A. Municipal landfill leachates: a significant source for new and emerging pollutant. *Sci. Total Environ.* **2010**, 408, 5147-5157.
- (27) Di'az-Cruz, S. M.; Llorca, M.; Barceló, D. Organic UV filters and their photodegradates, metabolites and disinfection by-products in the aquatic environment. *Trend. Anal. Chem.* **2008**, 27, 873-887.
- (28) Rodil, R.; Quintana, J. B.; López-Mahía, P.; Muniategui-Lorenzo, S.; Prada-Rodríguez, D. Multiclass determination of sunscreen chemicals in water samples by liquid chromatography-tandem mass spectrometry. *Anal. Chem.* **2008**, 80, 1307-1315.
- (29) Tolls, J. Sorption of veterinary pharmaceuticals in soils: a review. *Environ. Sci. Technol.* **2001**, 35, 3397-3406.
- (30) Gu, C.; Karthikeyan, K. G. Sorption of the antimicrobial ciprofloxacin to aluminum and iron hydrous oxides. *Environ. Sci. Technol.* **2005**, 39, 9166-9173.
- (31) Gu, C.; Karthikeyan, K. G. Interaction of tetracycline with aluminum and iron hydrous oxides. *Environ. Sci. Technol.* **2005**, 39, 2660-2667.
- (32) Gao, J.; Pedersen, J. A. Adsorption of sulfonamide antimicrobial agents to clay minerals. *Environ. Sci. Technol.* **2005**, 39, 9509-9516.
- (33) Haham, H.; Oren, A.; Chefetz, B. Insight into the role of dissolved organic matter in sorption of sulfapyridine by semiarid soils. *Environ. Sci. Technol.* **2012**, 46, 11870-11877.
- (34) Feitosa-Felizzola, J.; Hanna, K.; Chiron, S. Adsorption and transformation of selected human-used macrolide antibacterial agents with iron (III) and manganese (IV) oxides. *Environ. Pollut.* **2009**, 157, 1317-1322.
- (35) Nikolaou, A.; Meric, S.; Fatta, D. Occurrence patterns of pharmaceuticals in water and wastewater environments. *Anal. Bioanal. Chem.* **2007**, 387, 1225-1234.
- (36) Schulz, M.; Löffler, D.; Wagner, M.; Ternes, T. A. Transformation of the X-ray contrast medium iopromide in soil and biological wastewater treatment. *Environ. Sci. Technol.* **2008**, 42, 7207-7217.
- (37) Beel, R.; Lütke Eversloh, C.; Ternes, T. A. Biotransformation of the UV-Filter sulisobenzone: challenges for the identification of transformation products. *Environ. Sci. Technol.* **2013**, 47, 6819-6828.

- 
- (38) Onesios, K. M.; Yu, J.T.; Bouwer, E.J. Biodegradation and removal of pharmaceuticals and personal care products in treatment systems: a review. *Biodegradation*, **2009**, 20, 441-466.
- (39) Benotti, M. J.; Brownawell, B. J. Microbial degradation of pharmaceuticals in estuarine and coastal seawater. *Environ. Pollut.* **2009**, 157, 994-1002.
- (40) Li, B.; Zhang, T. Biodegradation and adsorption of antibiotics in the activated sludge process. *Environ. Sci. Technol.* **2010**, 44, 3468-3473.
- (41) Junker, T.; Alexy, R.; Knacker, T.; Kümmerer, K. Biodegradability of <sup>14</sup>C-labelled antibiotics in a modified laboratory scale sewage treatment plant at environmentally relevant concentrations. *Environ. Sci. Technol.* **2006**, 40, 318-326.
- (42) Kim, S.; Eichhorn, P.; Jensen, J. N.; Weber, A. S.; Aga, D.S. Removal of antibiotics in wastewater: effect of hydraulic and solid retention times on the fate of tetracycline in the activated sludge process. *Environ. Sci. Technol.* **2005**, 39, 5816-5823.
- (43) Watanabe, N.; Bergamaschi, B. A.; Loftin, K. A.; Meyer, M. T.; Harter, T. Use and Environmental occurrence of antibiotics in Freestall dairy farms with manured forage fields. *Environ. Sci. Technol.* **2010**, 44, 6591-6600.
- (44) Andreozzi, R.; Raffaele, M.; Nicklas, P. Pharmaceuticals in STP effluents and their solar photodegradation in aquatic environment. *Chemosphere* **2003**, 50, 1319-1330.
- (45) Lam, M. W.; Tantuco, K.; Mabury, S. A. Photofate: a new approach in accounting for the contribution of indirect photolysis of pesticides and pharmaceuticals in surface water. *Environ. Sci. Technol.* **2003**, 37, 899-907.
- (46) Boreen, A. L.; Arnold, W. A.; McNeill, K. Photodegradation of pharmaceuticals in the aquatic environment: a review. *Aquat. Sci.* **2003**, 65, 320-341.
- (47) Buser, H.-R.; Poiger, T.; Müller, M. Occurrence and fate of the pharmaceutical drug diclofenac in surface waters: rapid photodegradation in a lake. *Environ. Sci. Technol.* **1998**, 22, 3449-3456.
- (48) Poiger, T.; Buser, H.-R.; Müller, M. Photodegradation of the pharmaceutical drug diclofenac in a lake: pathway, field measurements, and mathematical modeling. *Environ. Toxicol. Chem.* **2001**, 20, 256-263.
- (49) Eriksson, J.; Svanfelt, J.; Kronberg, L. A photochemical study of diclofenac and its major transformation products. *Photochem. Photobiol.* **2010**, 86, 528-532.

- 
- (50) Agüera, A.; Pérez Estrada, L. A.; Ferrer, I.; Thurman, E. M.; Malato, S.; Fernández-Alba A. R. Application of time-of-flight mass spectrometry to the analysis of phototransformation products of diclofenac in water under natural sunlight. *J. Mass Spectrom.* **2005**, 40, 908-915.
- (51) Scheurell, M.; Franke, S.; Shah, R. M.; Hühnerfuss, H. Occurrence of diclofenac and its metabolites in surface water and effluent samples from Karachi, Pakistan. *Chemosphere* **2009**, 77, 870-876.
- (52) Tixier, C.; Singer, H. P.; Canonica, S.; Müller S. R. Phototransformation of triclosan in surface waters: a relevant elimination process for this widely used biocide-laboratory studies, field measurements, and modeling. *Environ. Sci. Technol.* **2002**, 36, 3482-3489.
- (53) Latch, D. E.; Packer, J. L.; Arnold, W. A.; McNeill, K. Photochemical conversion of triclosan to 2,8-dichlorodibenzo-*p*-dioxin in aqueous solution. *J. Photochem. Photobiol. A: Chem.* **2003**, 158, 63-66.
- (54) Latch, D. E.; Packer, J. L.; Stender, B. L.; Van Overbeke, J.; Arnold, W. A.; McNeill, K. Aqueous photochemistry of triclosan: formation of 2,4-dichlorophenol, 2,8-dichlorodibenzo-*p*-dioxin, and oligomerization products. *Environ. Toxicol. Chem.* **2005**, 24, 517-525.
- (55) Wong-Wah-Chung, P.; Rafqah, S.; Voyard, G.; Sarakha, M. Photochemical behavior of triclosan in aqueous solutions: kinetic and analytical studies. *J. Photochem. Photobiol. A: Chem.* **2007**, 191, 201-208.
- (56) Aranami, K.; Readman, J. W. Photolytic degradation of triclosan in freshwater and seawater. *Chemosphere* **2007**, 66, 1052-1056.
- (57) Sanchez-Prado, L.; Llompарт, M.; Lores, M.; García-Jares, C.; Bayona, J. M.; Cela, R. Monitoring the photochemical degradation of triclosan in wastewater by UV light and sunlight using solid-phase microextraction. *Chemosphere* **2006**, 65, 1338-1347.
- (58) Liu, Q.-T.; Williams, H. E. Kinetics and degradation products for direct photolysis of  $\beta$ -blockers in water. *Environ. Sci. Technol.* **2007**, 41, 803-810.
- (59) Lin, A. Y. C.; Reinhard, M. Photodegradation of common environmental pharmaceuticals and estrogens in river water. *Environ. Toxicol. Chem.* **2005**, 24, 1303-1309.
- (60) Edhlund, B. L.; Arnold, W. A.; McNeill, K. Aquatic photochemistry of nitrofurantoin antibiotics. *Environ. Sci. Technol.* **2006**, 40, 5422-5427.

- 
- (61) Latch, D. E.; Stender, B. L.; Packer, J. L.; Arnold, W. A.; McNeill, K. Photochemical fate of pharmaceuticals in the environment: cimetidine and ranitidine. *Environ. Sci. Technol.* **2003**, *37*, 3342-3350.
- (62) Boreen, A. L.; Arnold, W. A.; McNeill, K. Photochemical fate of sulfa drugs in the aquatic environment: sulfa drugs containing five-membered heterocyclic group. *Environ. Sci. Technol.* **2004**, *38*, 3933-3940.
- (63) Wei, X.; Chen, J.; Xie, Q.; Zhang, S.; Ge, L.; Qiao, X. Distinct photolytic mechanisms and products for different dissociation species of ciprofloxacin. *Environ. Sci. Technol.* **2013**, *47*, 4284-4290.
- (64) Sturini, M.; Speltini, A.; Maraschi, F.; Profumo, A.; Pretali, L.; Fasani, E.; Albini, A. Photochemical degradation of marbofloxacin and enrofloxacin in natural waters. *Environ. Sci. Technol.* **2010**, *44*, 4564-4569.
- (65) Jiao, S.; Zheng, S.; Yin, D.; Wang, L.; Chen, L. Aqueous photolysis of tetracycline and toxicity of photolytic products to luminescent bacteria. *Chemosphere* **2008**, *73*, 377-382.
- (66) Lam, M. W.; Young, C. J.; Mabury, S. A. Aqueous photochemical reaction kinetics and transformation of fluoxetine. *Environ. Sci. Technol.* **2005**, *39*, 513-522
- (67) Brezonik, P. L.; Fulkerson-Brekken, J. Nitrate-induced photolysis in natural waters: Controls on concentrations of hydroxyl radical photo-intermediates by natural scavenging agents. *Environ. Sci. Technol.* **1998**, *32*, 3004-3010.
- (68) Vione, D.; Falletti, G.; Maurino, V.; Minero, C.; Pelizzetti, E.; Malandrino, M.; Ajassa, R.; Olariu, R. L.; Arsene, C. Sources and sinks of hydroxyl radicals upon irradiation of natural water samples. *Environ. Sci. Technol.* **2006**, *40*, 3775-3781.
- (69) Nélieu, S.; Perreau, F.; Bonnemoy, F.; Ollitrault, M.; Azam, D.; Lagadic, L.; Bohatier, J.; Einhorn, J. Sunlight nitrate-induced photodegradation of chlorotoluron: evidence of the process in aquatic mesocosms. *Environ. Sci. Technol.* **2009**, *43*, 3148-3154.
- (70) Shankar, M. V.; Nélieu, S.; Kerhoas, L.; Einhorn, J. Photo-induced degradation of diuron in aqueous solution by nitrites and nitrates: kinetics and pathways. *Chemosphere* **2007**, *66*, 767-774.
- (71) Halladja, S.; Amine-Khodja, A.; ter Halle, A.; Boulkamh, A.; Richard, C. Photolysis of fluometuron in the presence of natural water constituents. *Chemosphere* **2007**, *69*, 1647-1654.
- (72) Malouki, M. A.; Lavédrine, B.; Richard, C. Phototransformation of methabenthiuron in the

- 
- presence of nitrate and nitrite ions. *Chemosphere* **2005**, 60, 1523-1529.
- (73) Jacobs, L. E.; Weavers, L. K.; Houtz, E. F.; Chin, Y.-P. Photosensitized degradation of caffeine: role of fulvic acids and nitrate. *Chemosphere* **2012**, 86, 124-129.
- (74) Suzuki, J.; Okazaki, H.; Sato, T.; Suzuki, S. Formation of mutagens by photochemical reaction of biphenyl in nitrate aqueous solution. *Chemosphere* **1982**, 11, 437-444.
- (75) Machado, F.; Boule, P. Photonitration and photonitrosation of phenolic derivatives induced in aqueous solution by excitation of nitrite and nitrate ions. *J. Photochem. Photobiol. A: Chem.* **1995**, 86, 73-80.
- (76) Chin, Y. P.; Miller, P. L.; Zeng, L.; Cawley, K.; Weavers, L. K. Photosensitized degradation of bisphenol A by dissolved organic matter. *Environ. Sci. Technol.* **2004**, 38, 5888-5894.
- (77) Guerard, J. J.; Miller, P. L.; Trouts, T. D.; Chin, Y. P. The role of fulvic acid composition in the photosensitized degradation of aquatic contaminants. *Aquat. Sci.* **2009**, 71, 160-169.
- (78) Vialaton, D.; Richard, C. Phototransformation of aromatic pollutants in solar light: photolysis versus photosensitized reactions under natural water conditions. *Aquat. Sci.* **2002**, 64, 207-215.
- (79) Boreen, A. L.; Edlund, B. L.; Cotney, J. B.; McNeill, K. Indirect photodegradation of dissolved free amino acids: the contribution of singlet oxygen and the differential reactivity of DOM from various sources. *Environ. Sci. Technol.* **2008**, 42, 5492-5498.
- (80) Boreen, A. L.; Arnold, W. A.; McNeill, K. Triplet –sensitized photodegradation of sulfa drug containing six-membered heterocyclic group: Identification of an SO<sub>2</sub> extrusion photoproducts. *Environ. Sci. Technol.* **2005**, 39, 3630-3638.
- (81) Chen, Y.; Hu, C.; Hu, X.; Qu, J. Indirect photodegradation of amine drugs in aqueous solution under simulated sunlight. *Environ. Sci. Technol.* **2009**, 43, 2760-2765.
- (82) Wenk, J.; von Gunten, U.; Canonica, S. Effect of dissolved organic matter on the transformation of contaminants induced by excited triplet states and the hydroxyl radical. *Environ. Sci. Technol.* **2011**, 45, 1334-1340.
- (83) Wenk, J.; Canonica, S. Phenolic antioxidants inhibit the triplet-induced transformation of anilines and sulfonamide antibiotics in aqueous solution. *Environ. Sci. Technol.* **2012**, 46, 5455-5462.
- (84) Jacobs, L. E.; Fimmen, R. L.; Chin, Y.-P.; Mash, H. E.; Weavers, L. K. fulvic acid mediated photolysis of ibuprofen in water. *Water Res.* **2011**, 45, 4449-4458.

- 
- (85) Southworth, B. A.; Voelker, B. M. Hydroxyl radical production via the photo-Fenton reaction in the presence of fulvic acid. *Environ. Sci. Technol.* **2003**, 37, 1130-1136.
- (86) Catastini, C.; Sarakha, M.; Mailhot, G.; Bolte, M. Iron(III) aquacomplexes as effective photocatalysts for the degradation of pesticides in homogeneous aqueous solutions. *Sci. Total Environ.* **2002**, 298, 219-228.
- (87) Chiron, S.; Minero, C.; Vione, D. Photodegradation processes of the antiepileptic drug carbamazepine, relevant to estuarine waters. *Environ. Sci. Technol.* **2006**, 40, 5977-5983.
- (88) Werner, J. J.; Arnold, W. A.; McNeill, K. Water hardness as a photochemical parameter: tetracycline photolysis as a function of calcium concentration, magnesium concentration, and pH. *Environ. Sci. Technol.* **2006**, 40, 7236-7241.
- (89) Ge, L.; Chen, J.; Qiao, X.; Lin, J.; Cai, X. Light-source-dependent effects of main water constituents on photodegradation of phenicol antibiotics: mechanism and kinetics. *Environ. Sci. Technol.* **2009**, 43, 3101-3107.
- (90) Vione, D.; Khanra, S.; Cucu Man, S.; Reddy Maddigapu, P.; Das, R.; Arsene, C.; Olariu, R.-I.; Maurino, V.; Minero, C. Inhibition vs. enhancement of the nitrate-induced phototransformation of organic substrates by the HO• scavengers bicarbonate and carbonate. *Water Res.* **2009**, 43, 4718-4728.
- (91) Chiron, S.; Barbati, S.; Khanra, S.; Dutta, B. K.; Minella, M.; Minero, C.; Maurino, V.; Pelizzetti, E.; Vione, D. Bicarbonate-enhanced transformation of phenol upon irradiation of hematite, nitrate, and nitrite. *Photochem. Photobiol. Sci.* **2009**, 8, 91-100.
- (92) Fatta-Kassinos, D.; Vasquez, M. I.; Kümmerer, K. Transformation products of pharmaceuticals in surface waters and wastewater formed during photolysis and advanced oxidation processes-Degradation, elucidation of byproducts and assessment of their biology potency. *Chemosphere* **2011**, 85, 693-709.
- (93) Wang, X. H.; Lin, A. Y. C. Phototransformation of cephalosporin antibiotics in an aqueous environment results in higher toxicity. *Environ. Sci. Technol.* **2012**, 46, 12417-12426.
- (94) Trovó, A. G.; Nogueira, R. F. P.; Agüera, A.; Sirtori, C.; Fernández-Alba, A. R. Photodegradation of sulfamethoxazole in various aqueous media: persistence, toxicity and photoproducts assessment. *Chemosphere* **2009**, 77, 1292-1298.
- (95) Dalrymple, O. K.; Yeh, D. H.; Trotz, M. A. Removing pharmaceuticals and

---

endocrine-disrupting compounds from wastewater by photocatalysis. *J. Chem. Technol. Biotechnol.* **2007**, 82, 121-134.

(96) Gaya, U. I.; Abdullah, A. H. Heterogeneous photocatalytic degradation of organic contaminants over titanium dioxide: a review of fundamentals, progress and problems. *J. Photochem. Photobiol. C: Photochem. Rev.* **2008**, 9, 1-12.

(97) Nan Chong, M.; Jin, B.; Chow, C. W. K.; Saint, C. Recent developments in photocatalytic water treatment technology: a review. *Water Res.* **2010**, 44, 2997-3027.

(98) Augugliaro, V.; Bellardita, M.; Loddo, V.; Palmisano, G.; Palmisano, L.; Yurdakal, S. Overview on oxidation mechanisms of organic compounds by TiO<sub>2</sub> in heterogeneous photocatalysis. *J. Photochem. Photobiol. C: Photochem. Rev.* **2012**, 13, 224-245.

(99) Hapeshi, E.; Achilleos, A.; Vasquez, M. I. Drugs degrading photocatalytically: kinetics and mechanisms of ofloxacin and atenolol removal on titania suspensions. *Water Res.* **2010**, 44, 1737-1746.

(100) Zhang, X.; Wu, F.; Wu, X.; Chen, P.; Deng, N. Photodegradation of acetaminophen in TiO<sub>2</sub> suspended solution. *J. Hazard. Mater.* **2008**, 157, 300-307.

(101) Hu, L.; Flanders, P. M.; Miller, P. L.; Strathmann, T. J. Oxidation of sulfamethoxazole and related antimicrobial agent by TiO<sub>2</sub> photocatalysis. *Water Res.* **2007**, 41, 2612-2626.

(102) Sirtori, C.; Agüera, A.; Gernjak, W. Effect of water-matrix composition on trimethoprim solar photodegradation kinetics and pathways. *Water Res.* **2010**, 44, 2735-2744.

(103) Calza, P.; Sakkas, V. A.; Medana, C.; Baiocchi, C.; Dimou, A.; Pelizzetti, E.; Albanis, T. Photocatalytic degradation study of diclofenac over aqueous TiO<sub>2</sub> suspensions. *Appl. Catal. B: Environ.* **2006**, 67, 197-205.

(104) Ohko, Y.; Iuchi, K.-I.; Niwa, C.; Tatsuma, T.; Nakashima, T.; Iguchi, T.; Kubota, Y.; Fujishima, A. 17 $\beta$ -estradiol degradation by TiO<sub>2</sub> photocatalysis as a means of reducing estrogenic activity. *Environ. Sci. Technol.* **2002**, 36, 4175-4181.

(105) Lambropoulou, D. A.; Hernando, M. D.; Konstantinou, I. K.; Thurman, E. M.; Ferrer, I.; Albanis, T. A.; Fernández-Alba, A. R. Identification of photocatalytic degradation products of bezafibrate in TiO<sub>2</sub> aqueous suspensions by liquid and gas chromatography. *J. Chromatogr. A* **2008**, 1183, 38-48.

(106) Doll, T. E.; Frimmel, F. H. Photocatalytic degradation of carbamazepine, clofibric acid and

---

omeprol with P25 and Hombikat UV 100 in the presence of natural organic matter (NOM) and other organic water constituents, *Water Res.* **2005**, 39, 403-411.

(107) Ryu, J.; Choi, W. Substrate-specific photocatalytic activities of TiO<sub>2</sub> and multiactivity test for water treatment application, *Environ. Sci. Technol.* 42 (2008) 294-300.

(108) Radjenović, J.; Sirtori, C.; Petrović, M.; Barceló, D.; Malato, S. Solar photocatalytic degradation of persistent pharmaceuticals at pilot-scale: kinetics and characterization of major intermediate products. *Appl. Catal. B: Environ.* **2009**, 89, 255-264.

(109) Radjenović, J.; Sirtori, C.; Petrović, M.; Barceló, D.; Malato, S. Characterization of intermediate products of solar photocatalytic degradation of ranitidine at pilot-scale. *Chemosphere* **2010**, 79, 368-376.

(110) Sun, Y.; Pignatello, J. J. Evidence for a surface dual hole-radical mechanism in the TiO<sub>2</sub> photocatalytic oxidant of 2,4-dichlorophenoxyacetic acid. *Environ. Sci. Technol.* **1995**, 29, 2065-2072.

(111) Park, H.; Choi, W. Effects of TiO<sub>2</sub> surface fluorination on photocatalytic reactions and photoelectrochemical behaviors. *J. Phys. Chem. B.* **2004**, 108, 4086-4093.

(112) Chen, Y.; Yang, S.; Wang, K.; Lou, L. Role of primary active species and TiO<sub>2</sub> surface characteristic in UV-illuminated photodegradation of Acid Orange 7. *J. Photochem. Photobiol. A: Chem.* **2005**, 172, 47-54.

(113) Alder, A.C.; Schaffner, C.; Majewsky, M.; Klasmeier, J.; Fenner, K. Fate of  $\beta$ -blocker human pharmaceuticals in surface water: comparison of measured and simulated concentrations in the Glatt Valley Watershed, Switzerland. *Water Res.* **2010**, 44, 936-948.

(114) Pomati, F.; Castiglioni, S.; Zuccato, E.; Fanelli, R.; Vigetti, D.; Rossetti, C.; Calamari, D. Effects of a complex mixture of therapeutic drugs at environmental levels on human embryonic cells. *Environ. Sci. Technol.* **2006**, 40, 2442-2447.

(115) Bonnineau, C.; Guasch, H.; Proia, L.; Ricart, M.; Geiszinger, A.; Romaní, A.M.; Sabater, S. Fluvial biofilms: A pertinent tool to assess  $\beta$ -blockers toxicity. *Aquat. Toxicol.* **2010**, 96, 225-233.

(116) Johnson Inbaraj, J.; Bilski, P.; Chignell, C. F. Photophysical and photochemical studies of 2-phenylbenzimidazole and UVB sunscreen 2-phenylbenzimidazole-5-sulfonic acid. *Photochem. Photobiol.* **2002**, 75, 107-116.

## Chapter 2 Experimental Section

### 2.1. Chemicals and Materials

The chemical reagents used in this study are listed in Table 2.1.

**Table 2.1 Main characteristics of the chemical reagents used in this study.**

Name	Formula	Purity	Supplier
Atenolol (ATL)	$C_{14}H_{22}N_2O_3$	98%	TOKYO Chemical Industry Co., Ltd
4-Hydroxyphenylacetamide	$C_8H_9NO_2$	99%	Sigma-Aldrich
2-Phenylbenzimidazole-5-sulfonic acid (PBSA)	$C_{13}H_{10}O_3N_2S$	96%	Sigma-Aldrich
2-Phenylbenzimidazole (PBI)	$C_{13}H_{10}N_2$	97%	Sigma-Aldrich
Benzimidazole (BI)	$C_7H_6N_2$	99%	Sigma-Aldrich
Benzamide	$C_7H_7NO$	99%	Sigma-Aldrich
Suwannee river fulvic acid (SRFA)			International Humic Substance Society (IHSS)
Nordic river fulvic acid (NOFA)			International Humic Substance Society (IHSS)
Nordic river humic acid (NOHA)			International Humic Substance Society (IHSS)
Aldrich humic acid (sodium salt)			Aldrich
Fluka humic acid			Fluka
Methanol (MeOH)	$CH_3OH$	HPLC or LC-MS grade	Fisher Scientific
Acetonitrile (ACN)	$CH_3CN$	HPLC or LC-MS grade	Fisher Scientific
Sodium nitrate	$NaNO_3$	99.9%	Sigma-Aldrich

Sodium bicarbonate	NaHCO <sub>3</sub>	99.9%	Sigma-Aldrich
Sodium dihydrogenphosphate	NaH <sub>2</sub> PO <sub>4</sub>	99%	Aldrich
Phosphoric acid	H <sub>3</sub> PO <sub>4</sub>	99%	Aldrich
<i>p</i> -Nitroanisole	C <sub>7</sub> H <sub>7</sub> NO <sub>3</sub>	97%	Sigma-Aldrich
Pyridine	C <sub>5</sub> H <sub>5</sub> N	99%	Sigma-Aldrich
Sorbic acid	C <sub>6</sub> H <sub>8</sub> O <sub>2</sub>	99%	Sigma-Aldrich

Milli-Q water (18 MΩ cm) was prepared from a Millipore Milli-Q System. All experimental solutions were prepared by dissolving the reagents directly in Milli-Q water without further purification. All stock solutions were stored in dark under 4 °C after preparation and used within one month. River water was sampled from the Rhône River nearby Parc de la Tête d'Or in Villeurbanne (France) using a Teflon bottle and transported to Institut de recherches sur la catalyse et l'environnement de Lyon (IRCELYON). River water samples were stored in dark at 4 °C. Before photolysis processing, the river water was vacuum filtered on cellulose acetate filters (0.45 μm pore diameter, Millipore).

**Table 2.2 Specification and characteristics of TiO<sub>2</sub> photocatalysts.**

Photocatalyst	Composition	Specific surface area BET (m <sup>2</sup> /g)	Particle size (nm)
Degussa P25	75% anatase + 25% rutile	50	21
Hombikat UV100	100% anatase	250	5
Millennium PC500	100% anatase	287	5-10
Aldrich rutile	100% rutile	3	750

For studies on photocatalytic degradation of PPCPs, titanium dioxide (TiO<sub>2</sub>) was used as photocatalyst. The specification and characteristics of photocatalysts are shown in Table 2.2.

---

## 2.2. Photolysis experiments

### 2.2.1. Steady-state photolysis experiments

Photolysis experiments were conducted in a XPA-II photochemical reactor (Nanjing Xujiang Motor Factory, China), equipped with a 290 nm filtered 1000 W Xenon arc lamp (Beijing Electric Light Source Institute, China) as the simulated solar irradiation source. The lamp was placed inside a water cooled borosilicate jacket to maintain the temperature. Incidence photo flux was monitored by an UV radiometer (Beijing Normal University Photoelectrical Company, China) to ensure that the photon flux did not vary significantly (>5%). The Xe lamp was turned on preliminarily for 10 min for stabilization, then 50 mL photo reaction solution was transferred to a capped cylindrical tube (22 mm i.d., 60 mL volume), which was vertically placed outside the jacket at a fixed distance. 1 mL sample of each reaction solution was withdraw at selected time intervals and the residual concentration of ATL was analyzed by high performance liquid chromatography (HPLC). Each photolysis experiment was carried out in triplicate.

In the case of PBSA, steady-state photolysis experiments were conducted in a home-made photochemical reactor equipped with a 125 W high pressure mercury lamp (HPK, Heraeus) housed in a borosilicate immersion well ( $\lambda > 290$  nm). The HPK lamp was turned on preliminarily for 10 min for stabilization, then 50 mL solution of PBSA (10  $\mu$ M) was pipetted into a Pyrex reactor (i.d. = 5 cm, H = 15 cm, V = 150 mL), and the reactor was placed in the photoreactor for irradiation. The light intensity (300-400 nm) in the center of the reaction solutions was measured at approximately 3.3 mW cm<sup>-2</sup> by actinometer, comparable to the midday sunlight in June, Lyon (France; 45°N latitude). A radiometer (VLX-3W) was used to ensure that no significant changes in irradiance occurred during photolysis. The temperature was maintained at 20  $\pm$  1 °C by cooling water circulation. Dark controls wrapped in aluminum foil were also carried out under identical condition. The effect of solution pH on direct photolysis was examined in buffered solutions with different pH values (10 mM phosphate buffer or 10 mM borate buffer). The deoxygenated and aerated conditions were achieved by purging Ar and O<sub>2</sub> into the solution for investigating the influence of dissolved oxygen on direct photolysis. The HO• radical scavenger, 2-propanol, was used to verify the involvement of HO• in PBSA photolysis at acidic pH. The triplet quencher, sorbic acid (2.5  $\mu$ M), was also used to confirm if triplet state of PBSA was involved in PBSA direct photolysis. The involvement of indirect photochemical processes was assessed by

---

photolyzing 10  $\mu$ M PBSA in Milli-Q water in the presence of nitrate. The nitrate-spiked reaction solutions were buffered (10 mM phosphate) to neutral pH (pH = 6.8). PBSA photolysis in different water matrices (e.g., in the presence of humic acid, NaCl or river water) were performed at environmentally relevant pH ( $\sim$ 8.0). Aliquots (1 mL) were withdrawn at predetermined time intervals and stored in amber vials prior to analysis by high performance liquid chromatography (HPLC). Sample aliquots of dark controls were taken at the same time points as those for irradiation experiments. All samples from time courses were quantitatively analyzed by HPLC for the amount of PBSA remaining in the solution after irradiation based on external calibration. Pseudo-first-order rate constants,  $k_{\text{obs}}$ , for the photolysis reaction were obtained by linear regression of logarithmic concentration values determined as a function of time.

### 2.2.2. Laser flash photolysis experiments

Laser flash photolysis (LFP) experiments were carried out using the fourth harmonic (266 nm) of a Quanta Ray GCR 130-01 Nd:YAG laser. This laser produces a pulse of 9 ns in duration and, during these experiments, operated with an output of 30 mJ per pulse. Transient species produced upon 266 nm irradiation of the samples inside a quartz cuvette (3 mL volume) were monitored by a detection system consisting of a pulsed xenon lamp (150 W), monochromator and a photomultiplier (1P28). A spectrometer control unit was used for synchronizing the pulsed light source and programmable shutters with the laser output. The signal from the photomultiplier was digitized by a programmable digital oscilloscope (HP54522A). A 32 bits RISC-processor kinetic spectrometer workstation was used to analyze the digitized signal. After each laser shot a peristaltic pump system was used in order to replace the solution before a new experiment. The absorbance and disappearance of the transient species were investigated in PBSA aqueous solution. LFP experiments were also performed in the presence of acrylamide (triplet quencher) and NaI (radical cation quencher).

### 2.3. Photocatalysis experiments

The photocatalytic experiments were performed in an open Pyrex glass cell with approximately 60 mL volume containing the aqueous suspension of TiO<sub>2</sub> powder and ATL or PBSA. The irradiation source was a high pressure mercury lamp (HPK 125W, Heraeus) with maximum emission wavelength mainly around 365 nm. Infrared radiation (IR) was well filtered

---

by water circulation in the reactor jacket which maintained the temperature at  $20 \pm 1^\circ\text{C}$ . Direct photolysis caused by UV irradiation was avoided by using a 340 nm cut-off filter (0-52 Corning). The radiant flux entering the reactor was measured directly by a VLX-3W radiometer with a CX-365 detector (UV-A) and was found to be approximately  $3.32 \text{ mW cm}^{-2}$ . A volume of 25 mL aqueous solution containing ATL or PBSA and  $\text{TiO}_2$  powder with required concentration was introduced in the reactor. Before irradiation, the suspension was magnetically stirred in the dark for 30 min to reach adsorption-desorption equilibrium. During irradiation, aliquots of samples ( $\sim 300 \mu\text{L}$ ) were withdrawn with the help of syringe at various intervals and filtered through syringe filters to remove  $\text{TiO}_2$  particles before analysis. The adsorption of ATL or PBSA on filters was found to be negligible based on a preliminary test. Total volume of the samples withdrawn from each experiment was less than 10% (by volume) of the reaction solution. The pH of the reaction solution was adjusted by adding 0.1 M  $\text{HClO}_4$  or 0.1 M NaOH.

## 2.4. Analytical procedures

### 2.4.1. High performance liquid chromatography (HPLC)

ATL concentration was measured by HPLC (1100, Agilent, USA) equipped with a  $5\text{-}\mu\text{m}$  Agilent TC-C18 reversed phase column (250 mm $\times$ 4.5 mm i.d., 170 Å pore size, 12% carbon loading and endcapped) at  $30^\circ\text{C}$ . The mobile phase was consisting of 70% ammonium acetate solution (pH 7, 10 mM) and 30% methanol at a flow rate of  $0.8 \text{ mL min}^{-1}$ . A  $10 \mu\text{L}$  injection of each sample was performed using an autosampler. Detection was performed with an UV detector (1100, Agilent, USA) at a wavelength of 224 nm. For analysis of nitrobenzene, the mobile phase was methanol-water (60/40, v/v) with a flow rate of  $1 \text{ mL min}^{-1}$ . Detection wavelength was at 270 nm.

PBSA was analyzed using a Shimadzu 10A series high performance liquid chromatography (HPLC, Shimadzu) system equipped with a Model 7725i injector with a  $20 \mu\text{L}$  sample loop and coupled with a LC-10AT binary pump and a SPD-M10A DAD. Samples were separated with an Yperspher BDS C18 column ( $5\mu\text{m}$ , 125mm $\times$ 4.0mm, i.d.) (Interchim, France) at  $25^\circ\text{C}$ . The mobile phase was a mixture of 10% acetonitrile and 90% acidified water (10 mM phosphate buffer, pH 3.0) with a flow rate of  $0.8 \text{ mL min}^{-1}$ . The detection wavelength was selected at 300 nm. For analyzing 2-phenyl-1H-benzimidazole (PBI), benzimidazole (BI) and benzoic acid (BA), the

HPLC analysis parameters are showed in Table 2.3.

**Table 2.3. HPLC analysis parameters for measuring 2-phenylbenzimidazole-5-sulfonic acid (PBSA), 2-phenyl-1H-benzimidazole (PBI), benzimidazole (BI) and benzoic acid (BA) .**

Compound	Separation column <sup>a</sup>	Flow rate (mL/min)	Mobile phase composition		Injection volume (μL)	Detective wavelength (nm)
			water <sup>b</sup>	acetonitrile		
PBSA	Yperspher BDS C18	0.8	90%	10%	20	300
PBI	Yperspher BDS C18	0.8	80%	20%	20	300
BI	Yperspher BDS C18	0.8	90%	10%	20	266
BA	Yperspher BDS C18	0.8	80%	20%	20	230

<sup>a</sup> The specification of the columns: 5 μm, 150 mm × 4.0 mm.

<sup>b</sup> The water phase was 10 mM phosphate buffer (pH 3.0).

#### 2.4.2. Solid phase extraction-liquid chromatography-mass spectrometry (SPE-LC-MS)

To determine and identify the main photodegradation products of ATL in the presence of nitrate, 100 mL solution samples with 40 μmol L<sup>-1</sup> ATL and 10 mmol L<sup>-1</sup> NO<sub>3</sub><sup>-</sup> were subjected to irradiation for 24 h. After irradiation, the reaction solution was concentrated by solid phase extraction (SPE) workstation (Supleco, USA) using Water Oasis HLB cartridges (6cc, 200mg L<sup>-1</sup>). Before extraction, the HLB cartridges were conditioned by 5 mL methanol and 5 mL purified water. Subsequently, 100 mL reaction solution was percolated through the cartridges at 5 mL min<sup>-1</sup>. After rinsing with 2 mL water, the final extracted phototransformation products were obtained by eluting with 2×2 mL of methanol.

A Thermo Finnigan Surveyor Modular HPLC system equipped with a Finnigan LCQ Advantage MAX ion trap mass spectrometer was employed to analysis the photoproducts. The LC separation was carried out on a 5-μm Agilent Zorbax SB-C18 column (150 mm×4.6 mm i.d., 80 Å pore size). The mobile phase was consisting of water (10 mM ammonium acetate as buffer) as

---

eluent A and methanol as eluent B. Elution was performed at a flow rate of 0.2 mL min<sup>-1</sup> with linear gradient from 5% B to 95% B in 25 min. The injection volume was 10 µL. An electrospray interface (ESI) was used for the MS and MS-MS measurement in positive ionization mode and full scan acquisition between m/z 100-350. The spray voltage was 4.5 kV and an ion-transfer capillary temperature was 200 °C. Nitrogen was used as sheath and auxiliary gas at a flow rate of 35 arbitrary unit and argon was used as a collision gas at 0.25 MPa.

Identification of PBSA photoproducts were carried out using the SPE-LC-MS method. A mixture solution composed of samples withdrawn at different irradiation time was concentrated by solid phase extraction (SPE) workstation using Waters Oasis HLB-C18 cartridges (WAT106202, 6 cc/200 mg). The cartridges were sequentially conditioned with 5 mL methanol and 5 mL Milli-Q water, loaded with 100 mL samples, washed with 5 mL Milli-Q water and dried with purified N<sub>2</sub> for 30 min. The final extracted photoproducts were obtained by eluting with 2 × 2 mL methanol and analyzed by LC-MS.

A Thermo Finnigan Surveyor Modular HPLC system equipped with a Finnigan LCQ Advantage MAX ion trap mass spectrometer was employed to analysis the photoproducts. The LC separation was carried out on an Agilent Zorbax SB-C18 column (5 µm, 150 mm × 4.6 mm i.d.). The mobile phase was consisting of water (10 mM ammonium acetate as buffer) as eluent A and methanol as eluent B. Elution was performed at a flow rate of 0.2 mL min<sup>-1</sup> with linear gradient from 5% B to 95% B in 25 min. The injection volume was 10 µL. An electrospray interface (ESI) was used for the MS and MS-MS measurement in positive ionization mode and full scan acquisition between m/z 100-350. The spray voltage was 4.5 kV and an ion-transfer capillary temperature was 200 °C. Nitrogen was used as sheath and auxiliary gas at a flow rate of 35 arbitrary unit and argon was used as a collision gas at 0.25 MPa.

#### 2.4.3. HPLC-UV analysis for measuring carboxylic acids

The detection of carboxylic acids was performed using a HPLC-UV system (Varian 9010 model) equipped with a ICSep-GOREGEL-87H3 cation exchange column (9 µm, 300 mm × 7.8 mm, i.d.) (Transgenomic, USA). The mobile phase was 5.5 mM H<sub>2</sub>SO<sub>4</sub> at a flow rate of 0.6 mL min<sup>-1</sup>. The injection volume was 100 µL and the wavelength for detection was 210 nm. Quantification of the carboxylic acids was performed by comparison with standards.

#### 2.4.4. Ion chromatography for measuring inorganic ions

---

The analyses of inorganic ions released during photocatalysis process were carried out by using a Metrohm ion chromatographic instrument (881 Compact IC Pro, Switzerland) coupled with an autosampler (863 Compact). Detection was performed with a Conductivity Detector (881 Compact IC Pro 1) equipped with a Metrohm Suppressor Module (MSM). For anion measurement, separation was carried out using a Metrosep A Supp 5-150/4.0 column under the following elution condition: 3.2 mM Na<sub>2</sub>CO<sub>3</sub> + 1.0 mM NaHCO<sub>3</sub> as mobile phase at a flow rate of 0.7 mL min<sup>-1</sup>. For cation measurement, separation was carried out using a Metrosep C4 column (150 mm × 4.0 mm, i.d.) by using 1.7 mM nitric acid + 0.7 mM dipicolinic acid as mobile phase at a flow rate of 0.9 mL min<sup>-1</sup>.

#### 2.4.5. TOC measurement

To determine the extent of mineralization during photolysis and photocatalysis, total organic carbon (TOC) of filtered suspension samples was measured using a TOC-5050A analyzer (Shimadzu). The concentration of dissolved SRFA, NOFA, NOHA, and HA were also determined by the TOC analyzer and expressed as mgC L<sup>-1</sup>. Calibration was achieved by injecting standards of succinic acid solution.

#### 2.4.6. UV-vis absorption spectra

The spectrum of the ATL, nitrate, SRFA, NOFA, and NOHA solution was scanned by a UV-vis spectrophotometer (UV2450, Shimadzu, Japan). The UV-visible absorption spectra of PBSA and humic acid aqueous solutions were recorded using a Lambda 950 UV-vis spectrophotometer (PerkinElmer, USA) equipped with quartz cuvettes (optical path length 1.0 cm).

#### 2.4.7. pH measurement

The pH of the solutions was measured with a combined glass electrode connected to a PHM 210 standard pH meter (Radiometer, Copenhagen, Denmark).

## 2.5. Calculation

### 2.5.1. Determination of the quantum yields

The quantum yields of PBSA direct photolysis in aqueous solution at different pH values were determined by using *p*-nitroanisole (PNA)/pyridine (pyr) as actinometer according to the following equation.

$$\Phi_p = \frac{k_p \sum(L_\lambda \varepsilon_\lambda)_a}{k_a \sum(L_\lambda \varepsilon_\lambda)_p} \Phi_a \quad (1)$$

Where the subscript “a” and “p” refer to actinometer and PPCPs, respectively;  $\varepsilon_\lambda$  and  $L_\lambda$  are the extinction coefficient and the lamp irradiance, respectively, at a specific wavelength  $\lambda$ ;  $\sum(L_\lambda \varepsilon_\lambda)_a$  and  $\sum(L_\lambda \varepsilon_\lambda)_p$  are the light absorption for actinometer and PBSA, respectively;  $\Phi_a$  is the quantum yield of the actinometer determined by the concentration of pyridine ( $\Phi_a = 0.44 [\text{pyr}] + 0.00028$ ).

### 2.5.2. Calculation of light-screening factor

The light attenuation effect of humic substance on nitrate-induced ATL photodegradation or nitrate on PBSA direct photolysis was evaluated by light-screening factor  $S_\lambda$ . Samples with different nitrate concentration were scanned by spectrophotometer from 200 to 600 nm. The collected absorbance was used to calculate attenuation coefficient and light-screening factor. Application of  $S_\lambda$  to rate constant measured in Milli-Q water,  $k_{\text{Milli-Q}}$ , can yield an *upper-limit* estimate of an expected direct photolysis rate constant in a given nitrate solution under identical irradiation conditions. The wavelength-specific light-screening factor can be calculated as follows.

$$S_\lambda = \frac{1 - 10^{-\alpha_\lambda l}}{2.303 \alpha_\lambda l} \quad (2)$$

Where  $l$  (cm) is the path length of the test tube used for the experiment,  $\alpha_\lambda$  ( $\text{cm}^{-1}$ ) is the wavelength specific attenuation coefficient. Since a polychromatic light source was used in the present photolysis experiment, an overall screening factor,  $S_{\sum\lambda}$  for all of the wavelengths that could be absorbed by nitrate (290-340 nm) was calculated.  $S_{\sum\lambda}$  were determined by taking the ratio of the integrated area of a plot of  $S_\lambda$  versus wavelength (nm) and normalizing by theoretical area of the plot if no inner filtering occurred (i.e.,  $S_\lambda = 1.0$  for all wavelengths).

### 2.5.3. Determination of second-order rate constant for reaction of PPCPs with HO•

The second-order rate constant for reaction of ATL/PBSA with HO• was determined by competition kinetics method (Eq. (3)) using Fenton’s reagent as HO• generation source as described below.

$$\ln \left( \frac{[\text{PPCPs}]_t}{[\text{PPCPs}]_0} \right) = \frac{k_{\text{HO}\cdot, \text{PPCPs}}}{k_{\text{HO}\cdot, \text{BA}}} \ln \left( \frac{[\text{BA}]_t}{[\text{BA}]_0} \right) \quad (3)$$

---

Benzoic acid (BA), with a known rate constant ( $k_{\text{HO}\cdot, \text{BA}} = 5.9 \times 10^9 \text{ M}^{-1} \text{ s}^{-1}$ ) was used as reference compound in this study. The initial solution contained 60  $\mu\text{M}$  BA, 60  $\mu\text{M}$  PBSA, 0.2 mM  $\text{Fe}^{2+}$  and 0.5 mM  $\text{H}_2\text{O}_2$  at pH 3.5 (adjusted by sulfuric acid). The reactor was wrapped in aluminum foil to exclude light and prevent photo-Fenton chemistry. Incubations were performed at room temperature ( $22 \pm 1^\circ\text{C}$ ). Samples (0.5 mL) were withdrawn at predetermined intervals, and the reactions were quenched with an equivalent volume of methanol. Samples were then analyzed via HPLC.

For measuring the second-order rate constant for ATL-  $\text{HO}\cdot$  reaction, nitrobenzene (NB) with a known rate constant ( $k_{\text{HO}\cdot, \text{NA}} = 3.9 \times 10^9 \text{ M}^{-1} \text{ s}^{-1}$ ) was used as reference compound. The experimental procedure was identical with that described above.

#### 2.5.4. Calculation of frontier electron density

Molecular orbital calculations were carried out at the single determinant (B3LYP/6-311+G\*) level with the optimal conformation having a minimum energy obtained at the same level in a Gaussian 09 program. The frontier electron densities (FEDs) of the highest occupied molecular orbital (HOMO) and the lowest unoccupied molecular orbital (LUMO) were determined. Values of  $\text{FED}_{\text{HOMO}}^2 + \text{FED}_{\text{LUMO}}^2$  were calculated to predict the reaction sites for hydroxyl addition.

## 2.6. Toxicity test

The toxicity test were performed using aquatic organism *daphnia magna straus* under the guideline from OECD (1981). Sample solutions with 40  $\mu\text{mol L}^{-1}$  ATL in the presence of 5  $\text{mmol L}^{-1}$  nitrate after irradiation 0, 30, 60 and 120 min were tested and a control using only freshwater was also tested. After 24 and 48 h of incubation, the number of dead and immobilized daphnids was calculated. The toxicity was expressed by immobilization rate of *D. magna*.

---

## Chapter 3 Direct and indirect photolysis of atenolol in aqueous solution

As an emerging class of environmental pollutant, pharmaceuticals and personal care products (PPCPs) received extensively consideration in recent years due to their potential risk to human beings and aquatic organism.<sup>1,2</sup> Effluents of wastewater treatment plants (WWTPs) were regarded as the major source for PPCPs introduce into aquatic environment due to incomplete removal during the treatment process.<sup>3</sup> Since PPCPs have been designed to have a specific physiological effect on humans or animals in trace concentration level, many of them showed quite resistance to biodegradation.<sup>4</sup> Consequently, a wide range of PPCPs are frequently detected in surface, ground and coastal waters with a concentration usually ranging from  $\text{ng L}^{-1}$  to  $\mu\text{g L}^{-1}$ .<sup>5-7</sup> Atenolol (ATL) belongs to the group of beta-blocker ( $\beta$ -adrenergic receptors), which is primarily used for the treatment of disorders such as hypertension, angina and arrhythmias.<sup>8</sup> As been used for a long history in Europe and North America, it was detected at considerably high level ranging from 83  $\text{ng L}^{-1}$  in river water and 2  $\mu\text{g L}^{-1}$  in sewage treatment plant effluent.<sup>9,10</sup> Furthermore, environmental behavior and ecological risk of ATL is of great concern due to its potential ecotoxicity posed to the environment as it can affect cardiac rhythm, generate abnormalities or reduce mobility of spermatozooids of fish.<sup>11</sup> Fig. S1 shows the chemical structure and UV-vis absorbance spectrum of protonated and neutral molecular state of atenolol (see Supplementary Material).

Direct and indirect photolysis are the primary pathways for abiotic transformation of PPCPs in surface waters.<sup>12,13</sup> While the direct photolysis of PPCPs is caused by direct absorption of solar light, the indirect photolysis is initiated via light absorption by photosensitizer, such as nitrate and

---

dissolved organic matter (DOM).<sup>14</sup> Excited photosensitizers can generate extremely reactive oxygenated species (ROS) (e.g.  $^1\text{O}_2$  and  $\cdot\text{OH}$ ) and other reactive photooxidant which influence the persistence and photofate of the PPCPs in natural waters.<sup>15,16</sup> Among them, nitrate has long being recognized as a main source of  $\cdot\text{OH}$  upon solar irradiation.<sup>14,17</sup>

Up to date, few reports stressed on the relationship of photo reactive natural water constituents (e.g.,  $\text{NO}_3^-$ , DOM,  $\text{Fe}^{3+}$ ) with the fate and photodegradation mechanism of ATL in natural environment. Meanwhile, literature data based on the potential toxicity of ATL phototransformation products posed to the environment is scarce. Therefore, the study on the photochemical reaction of ATL induced by natural water constituents is of great interest.

The main purpose of this study is (1) to study the photolysis kinetics of ATL in aqueous solution in the presence of nitrate under simulated solar irradiation and investigate the influences of several water constituents (bicarbonate, DOM); (2) to identify the main intermediates and propose the possible photodegradation pathway of ATL in aqueous solution containing nitrate; (3) to evaluate the toxicity of intermediate products photogenerated during the photolysis process.

### **3.1. Results and discussion**

#### 3.1.1. Direct photolysis of ATL

##### 3.1.1.1. Speciation and UV-vis absorption spectrum of ATL

The speciation and UV-vis absorption spectrum of ATL at different pH values are shown in Fig. 3.1. As seen, ATL has two maximum absorption peaks, corresponding to 224 and 274 nm, respectively, in Milli-Q water. Since pKa value of ATL was known to be 9.6, protonation occurs with respect to the secondary N in ether chain in  $5.8 < \text{pH} < 9.18$ .<sup>18,19</sup> Thus, no significant difference in UV-vis absorption spectrum was observed at pH 5.8, 9.2 and in Milli-Q water. Unlikely, in pH 10.3 solution, the absorbance of ATL at 224 and 274 nm disappeared while the absorbance at  $< 224$  nm markedly enhanced. This observation can be attributed to the molecular form of ATL, which is expected to be the dominant form at  $\text{pH} > 9.6$  in aqueous solutions. The

different species resulted in the changes in UV-vis absorption spectrum.

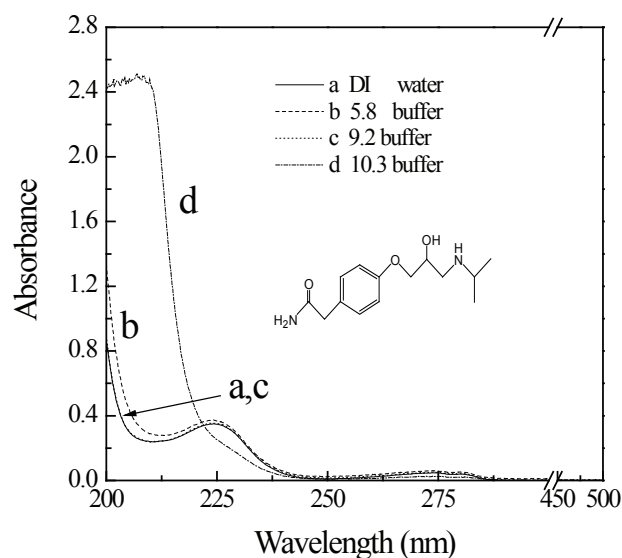


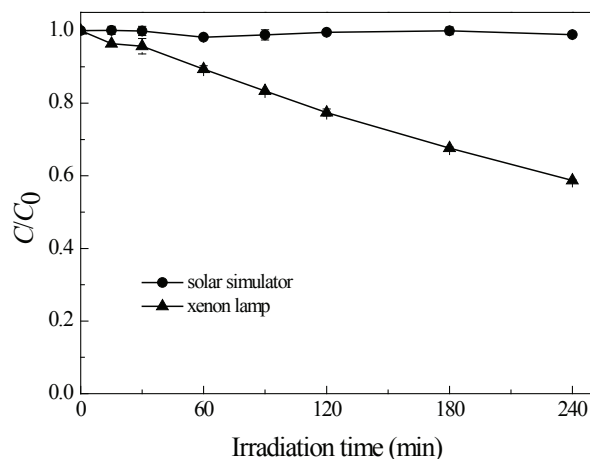
**Fig. 3.1. Speciation and UV-visible absorption spectrum of atenolol at different pH values.**

#### 3.1.1.2. Direct photolysis of ATL under different irradiation source

Fig. 3.2. shows the direct photolysis of 10  $\mu\text{M}$  ATL in Milli-Q water under different irradiation source. As it can be seen, the degradation rate of ATL could reach 42% under direct irradiation of xenon lamp after 4h reaction, whereas no degradation of ATL was observed upon simulated solar irradiation. These results suggest that the emission light from xenon lamp with wavelength lower than 290 nm contributed to the direct photolysis of ATL. These findings also corroborated with the UV-vis absorption spectrum of ATL, in which the absorbance of ATL at  $>$  290 nm was unappreciable. Similar result was also observed by Piram et al.<sup>20</sup> that ATL was stable by photodegradation under UV light cutting out wavelengths shorter than 280 nm. Considering that the wavelength of the solar radiation reached to the surface of earth mainly ranges from 290 to 600 nm, it can be expected that direct photolysis of ATL is unlikely to occur in natural surface sunlit surface waters. However, it is possible that ATL could undergo indirect photolysis through reactions with reactive oxygen or transients' species (e.g.,  $^1\text{O}_2$ ,  $\text{HO}\cdot$  and  $^3\text{DOM}^*$ ) produced by photosensitizers which are widely presented in natural waters (e.g.,  $\text{NO}_3^-$ , DOM and  $\text{Fe}^{3+}$ ).

Dark control experiments were also carried out in the present study. No degradation of ATL was found in the absence of light, indicating that the contribution of hydrolysis was negligible to ATL degradation. In addition, it was also found that no degradation of ATL occurred in pH 5.8, 6.8,

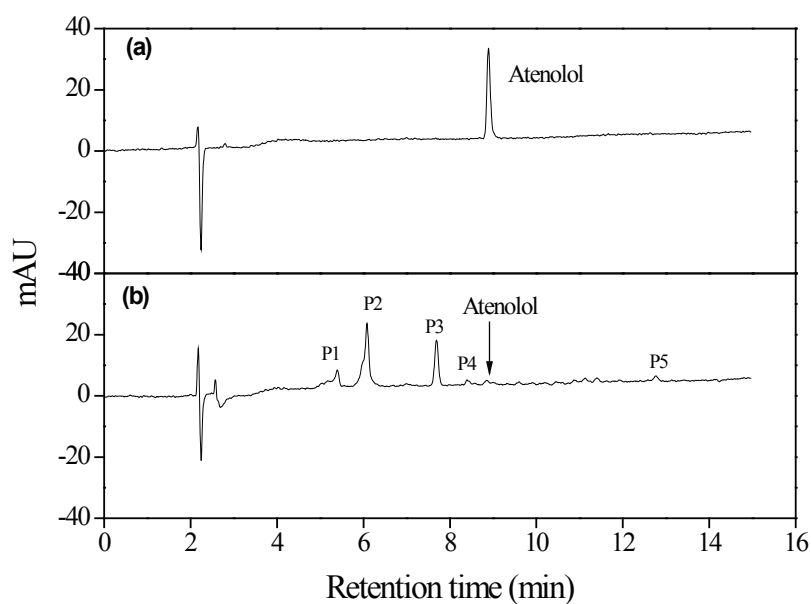
9.2 and 11.3 buffered solutions, suggesting solution pH could not facilitate or suppress ATL direct photolysis under simulated solar irradiation.



**Fig. 3.2. Direct photolysis of atenolol under different irradiation source. [ATL] = 10  $\mu$ M.**

3.1.1.3. Intermediates and degradation pathways of ATL direct photolysis under xenon lamp irradiation.

In order to detect as much photoproducts as possible, 40  $\mu$ M ATL aqueous solution (pH 6.8) was subjected to photolysis under xenon lamp irradiation. After 8 h irradiation, the photolysate (100 mL) was extracted and concentrated by HLB SPE cartridge, and then analyzed by HPLC. Fig. 3.3 displays the HPLC chromatogram of concentrated sample as well as ATL pure solution.

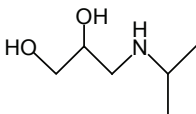
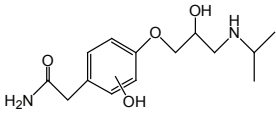
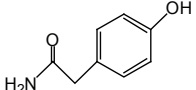
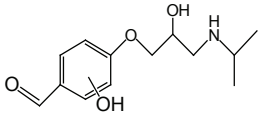


**Fig. 3.3. HPLC chromatogram of (a) 20 $\mu$ M atenolol solution, and (b) 40  $\mu$ M atenolol solution abstracted by**

### SPE after 8 h irradiation.

Compared with the unirradiated sample, five new peaks were observed in irradiated sample, corresponding to the possible intermediates of ATL photodegradation. Among them, four intermediates have a retention time shorter than the mother compound, suggesting their polarity are higher than ATL. Due to the lack of standards for comparison, the identification and elucidation of the intermediates were based on the analysis of the information of LC-MS. According to the total ion chromatogram (TIC) and the MS-MS spectrum, the chemical structures of the intermediates were determined. However, only four of them were elucidated. Their retention time, molecular weight,  $m/z$  of the main mass fragmentation and proposed possible chemical structure are listed in Table 3.1.

**Table 3.1 Proposed degradation products of atenolol by direct photolysis.**

No.	Retention time (min)	Molecular weight	Main mass fragmen ion ( $m/z$ )	Possible structure
I	1.92	133	134 $[M+H]^+$	
			116 $[M+H-H_2O]^+$	
			92 $[M+H-C(CH_3)_2]^+$	
			74 $[M+H-C(CH_3)_2-H_2O]^+$	
II	2.62	282	283 $[M+H]^+$	
			265 $[M+H-H_2O]^+$	
			224 $[M+H-C(CH_3)_2-NH_3]^+$	
			161 $[M+H-C(CH_3)_2-NH_3-H_2O-CO-N]^+$	
III	4.42	151	116 $[M+H-C_8H_9NO_3]^+$	
			152 $[M+H]^+$	
			136 $[M+H-OH-NH]^+$	
IV	7.29	253	126 $[M+H-CH_2CO]^+$	
			254 $[M+H]^+$	
			236 $[M+H-H_2O]^+$	
			212 $[M+H-C(CH_3)_2]^+$	
			177 $[M+H-C(CH_3)_2-NH_2-CHO]^+$	

Based on the intermediates, photodegradation pathways of ATL by xenon lamp irradiation were proposed, as shown in Fig. 3.4.

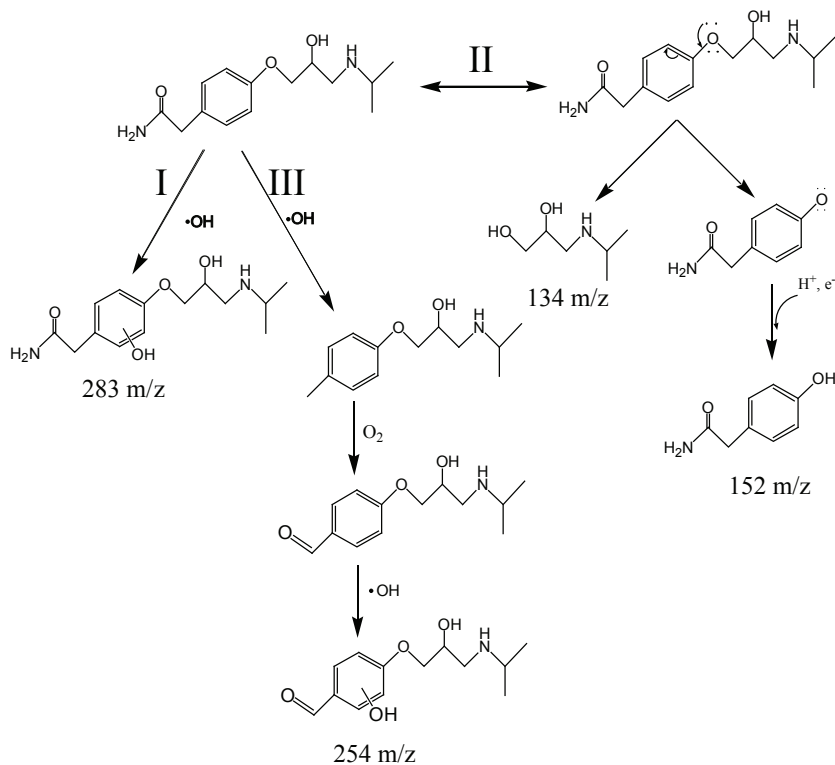


**Fig. 3.4.** Possible photodegradation pathways of atenolol by xenon lamp irradiation.

Pathway I is the hydroxylation of ATL, resulting in the formation of hydroxylated ATL ( $m/z$  283). Due to the big  $\pi$  electronic system of the aromatic ring, as well as the weak electro-donating effect of ether chain, hydroxylation was supposed to be easy on benzyl ring.<sup>21</sup> Pathway II follows *O*-dealkylation mechanism, leading to the generation of 3-(isopropylamino) propane-1,2-diol ( $m/z$  134) and *p*-hydroxyphenylacetamide ( $m/z$  152). It has been proposed that the lone electron-pairs in ether O could easily delocalize to aromatic  $\pi$  electric system, leads to the polarization of the bond between ether O and alkyl-chain C, which was capable of cleavage after absorbing photonic energy. Similar result has been observed by Lam et al. in a study on photodegradation of fluoxetine.<sup>14</sup> Pathway III was in consistent with the pathway proposed by Radjenović et al.<sup>22</sup> Firstly, the acetamide moiety lost amide group under the attack of  $HO\bullet$ , and then formed

benzaldehyde derivative in the presence of dissolved oxygen. Secondly, the benzaldehyde derivative was further transformed to  $m/z$  254 under the attack of  $\text{HO}\cdot$ . The involvement of  $\text{HO}\cdot$  in the ATL photodegradation process was probably due to a self-sensitized mechanism under lamp irradiation. Yang et al. studied the photocatalytic degradation of  $\beta$ -blockers in aqueous suspension of  $\text{TiO}_2$  and found that cleavage of the side chain and the addition of the hydroxyl group to the parent compounds are the two main degradation pathways.<sup>23</sup> Our results are in good agreement with these findings.

### 3.1.2. $\text{NO}_3^-$ induced indirect photolysis of ATL

#### 3.1.2.1. Photolysis kinetics

Preliminary dark control experiments without irradiation were also conducted. No loss of ATL could be observed during the process, indicating hydrolysis was not responsible for the photodegradation efficiency.

##### 3.1.2.1.1. Effect of nitrate concentration

Nitrate is ubiquitously present in natural aquatic environment. The concentration of nitrate may range from  $10^{-5}$  to  $10^{-3}$  M, which is highly related to the geographic location and human agriculture activity.<sup>6,7</sup> In this study, nitrate-induced photodegradation of ATL was carried out in solutions containing 10  $\mu\text{M}$  ATL with different nitrate concentrations upon simulated solar irradiation and the results are shown in Fig. 3.5.

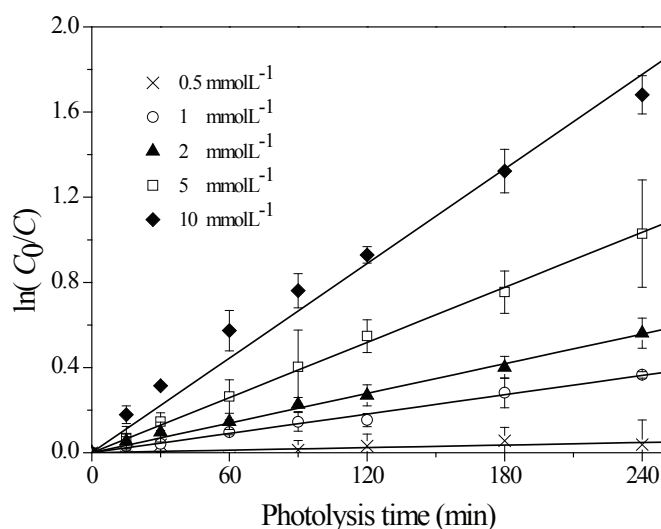


**Fig. 3.5. Photolysis kinetics of atenolol in the presence of nitrate ions with different concentrations (x)0.5 mM, (o)1 mM, (▲)2 mM, (□)5 mM, (◆)10 mM.**

---

As clearly seen, a semi-log plot of concentration of ATL versus irradiation time was linear, indicating overall pseudo-first-order kinetics. Increasing nitrate concentration led to the increase in the kinetic rate constant which were found to be 0.00101, 0.00143, 0.00225, 0.00379 and 0.00716  $\text{min}^{-1}$  at nitrate concentrations 0.5, 1, 2, 5 and 10 mM, respectively (Table S1, Supplementary Material). Previous studies demonstrated that hydroxyl radical's yield amount was correlated well with the nitrate concentration.<sup>24</sup> As a powerful oxidant,  $\cdot\text{OH}$  was capable to unselectively react with most of the aquatic organic compounds with a secondary rate constant of  $10^7$  to  $10^{10} \text{ M}^{-1}\text{s}^{-1}$ .<sup>25</sup> Thus, the obtained result was mainly due to the hydroxyl radicals generated through the irradiation of nitrate solution.

In order to justify  $\cdot\text{OH}$  was involved in the nitrate induced photodegradation of ATL, 100 mM isopropanol, as molecular probe for  $\cdot\text{OH}$  ( $1.9 \times 10^9 \text{ M}^{-1}\text{s}^{-1}$ ), was spiked into the photo reaction solution before irradiation.<sup>26</sup> It was found out that, the rate of decay was completely inhibited after the sample was spiked with isopropanol, suggesting that ATL in nitrate solution was predominantly oxidized by hydroxyl radical. Calculation of competition kinetic equation showed that  $k_{\text{OH,ATL}}$  was determined to be  $(7.49 \pm 0.26) \times 10^9 \text{ M}^{-1}\text{s}^{-1}$  (Fig. S2, Supplementary Material), which was very close to the founding,  $(7.05 \pm 0.27) \times 10^9 \text{ M}^{-1}\text{s}^{-1}$ , reported by Song et al. in  $\gamma$ -irradiation.<sup>21</sup> Such a high second order rate constant allowed the  $\cdot\text{OH}$  oxidation reaction with ATL occurring preferentially than other kind of radical reactions.

#### 3.1.2.1.2. Effect of solution pH

Since the  $pK_a$  of ATL was reported to be 9.16, the variation of solution pH is expected to influence the photolysis.<sup>19</sup> Thus, photodegradation of 10  $\mu\text{M}$  ATL in different pH buffer solutions in the presence of 5 mM nitrate were carried out to study the influence of solution pH on photodegradation kinetics (see Fig. S3, Supplementary Material).

As seen in Fig. S3, increasing the solution pH from 4.8 to 10.4, the photodegradation rate slightly decreased from  $0.00246 \text{ min}^{-1}$  to  $0.00195 \text{ min}^{-1}$ . The effect of solution pH on photodegradation is a complex issue related to the ionization state of organic compound, as well as the formation rate of  $\cdot\text{OH}$  and other ROS in reaction solution.<sup>27</sup> According to Fig. S1, neither the protonated or molecular form of ATL showed absorbance in  $\lambda > 290 \text{ nm}$  range. Since the simulated solar irradiation source used in our experiment was above 290 nm, direct photolysis of ATL was unlikely to occur. Thus, the obtained result was probably due to the influence of solution pH on

nitrate-induced  $\cdot\text{OH}$  formation. Previous report had shown that basification of the solution decrease the generation rate of  $\cdot\text{OH}$  by irradiation nitrate, most likely because of the acid-base equilibrium between  $\text{HOONO}$  and  $\text{ONOO}^-$ .<sup>27</sup>

### 3.1.2.1.3. Effect of bicarbonate concentration

Recent studies have demonstrated that bicarbonate ions were of great importance in organic pollutants depletion in nature sunlit waters.<sup>28</sup> The effect of bicarbonate concentration on  $10\ \mu\text{M}$  ATL photodegradation in  $5\ \text{mM}$  nitrate solution was investigated and the results showed that bicarbonate with different concentration showed inhibitive effect on ATL photodegradation (Fig. 3.6).

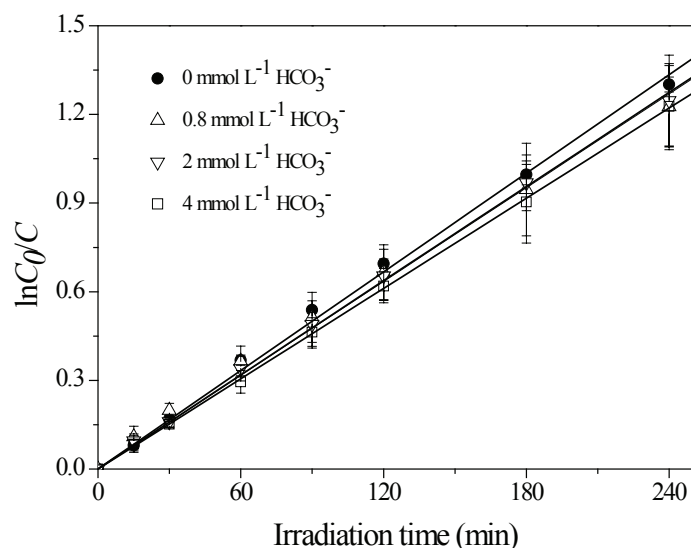
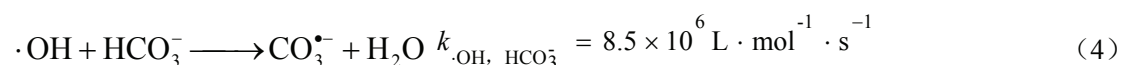
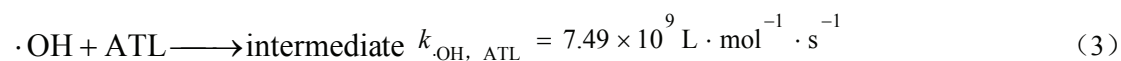


**Fig. 3.6.** Effect of bicarbonate concentration on the nitrate-induced photodegradation of atenolol under simulated solar irradiation ( $[\text{ATL}] = 10\ \mu\text{M}$ ,  $[\text{NO}_3^-] = 5\ \text{mM}$ ).

It was demonstrated that low reactive carbonate radicals can be expectedly generated through the reaction of  $\cdot\text{OH}$  with either carbonate or bicarbonate, with a secondary order reaction constant  $3.9 \times 10^8\ \text{M}^{-1}\text{s}^{-1}$  and  $8.5 \times 10^6\ \text{M}^{-1}\text{s}^{-1}$ , respectively.<sup>27</sup> Considering the coexisting of  $\text{HCO}_3^-$  and ATL in reaction solution, the hydroxyl radical reaction will be partitioned according to the following equations.



Based on the relative rates of these reactions and the concentration of  $\text{HCO}_3^-$  and ATL used in our experiment, the fraction of  $\cdot\text{OH}$  scavenged by  $\text{HCO}_3^-$  was found out to be much less than

by ATL (see Table S2, Supplementary Material). Thus, in Fig. 3.6, the decreased photodegradation rate of ATL after  $\text{HCO}_3^-$  addition maybe primarily due to the pH effect since with more  $\text{HCO}_3^-$  addition, the reaction solution became more basic, which resulted in lower degradation rate constant. This result was also consistent with the founding in 3.2.1.2.. However, it should be pointed out that, at high concentration (4 mM), the scavenging effect of  $\text{HCO}_3^-$  may also played a negative role in ATL photodegradation (31.2%  $\cdot\text{OH}$  scavenged by  $\text{HCO}_3^-$ ), which was presumably responsible for a slightly lower rate constant.

#### 3.1.2.1.4. Effect of humic substance

Humic substance (HS) is the major part of natural dissolved organic matter (DOM) and may accounts for up to 90% of total TOC content. Environmental relevant concentration of DOM may range from  $0.3 \text{ mg L}^{-1}$  to  $30 \text{ mg L}^{-1}$ .<sup>29,30</sup> As a natural photosensitizer, HS could photo-induced organic pollutant degradation through direct electron energy transfer or through indirect oxidation with photo-generated reactive oxygen species.<sup>31-33</sup> Meanwhile, HS may also play a negative role in photodegradation as an inner filter (light attenuator), competing for absorbing the photon with organic contaminants as well as a scavenger for ROS.<sup>14</sup> In this view, the photodegradation of  $10 \mu\text{M}$  ATL was studied at  $5 \text{ mgC L}^{-1}$  different kinds of humic substance in  $5 \text{ mM}$  nitrate solution and the results are shown in Table 3.2.

**Table 3.2 Effect of different humic acid on the photolysis reaction rate of atenolol in aqueous nitrate solution**  
( $[\text{ATL}] = 10 \mu\text{M}$ ,  $[\text{HS}] = 5 \text{ mgC L}^{-1}$ ,  $[\text{NO}_3^-] = 5 \text{ mM}$ ,  $n = 8$ ).

Humic substance	$k_0 \times 10^3$ ( $\text{min}^{-1}$ ) <sup>a</sup>	$S_\lambda$	$k_0 S_\lambda \times 10^3$ ( $\text{min}^{-1}$ )	$k_{\text{app}} \times 10^3$ ( $\text{min}^{-1}$ ) <sup>b</sup>
SRFA	4.3	0.78	3.4	2.5
NOFA	4.3	0.83	3.6	2.6
NOHA	4.3	0.83	3.6	2.4

<sup>a</sup> Pseudo-first-order kinetic rate constant for ATL photodegradation in the presence of nitrate without humic substance

<sup>b</sup> Pseudo-first-order kinetic rate constant for ATL photodegradation in the presence of nitrate and humic substance

As clearly seen, in the presence of SRFA, NOFA and NOHA, pseudo-first-order rate constants  $k_{\text{app}}$  of ATL photodegradation were found to be  $0.0025$ ,  $0.0026$  and  $0.0024 \text{ min}^{-1}$ , respectively. The presence of HS decreased the photolysis rate constant compared with that in

---

absence of HS, implying HS served as an inhibitor rather than a photosensitizer. This result can be explained by HS competing light with nitrate ions, leading less photons available for exciting nitrate, hence, less  $\cdot\text{OH}$  formation. However, after corrected by screening factor, the calculated theory rate constant  $k_0S_\lambda$  was still much larger than  $k_{\text{app}}$ , indicating that radical scavenging effect of HS was also likely to be involving in photodegradation process.<sup>24</sup> It should be emphasized that  $k_0S_\lambda$  value of NOFA and NOHA is the same, which was attributed to their similar absorbance spectrum in the wavelength range of nitrate maximum absorbance (See Fig. S4, Supplementary Material). In the case of SRFA, a much stronger absorbance in the same range can be observed, which was responsible for a slightly lower  $k_0S_\lambda$  value. The absorbance discrepancy of SRFA with NOFA and NOHA was most likely due to its different origin and molecular structure.

### 3.1.2.2. Identification of photoproducts and possible photodegradation pathways

HPLC chromatogram of ATL samples before irradiation and SPE concentrated after 24 h irradiation in the presence of nitrate is displayed in Fig. S5 (Supplementary Material). Four new peaks can be observed from the concentrated irradiation sample, which was probably corresponding to the new photoproducts. Among them, three were appeared quite early than their parent compound in the HPLC chromatogram, indicating that they are more polarized or lower molecular weight than ATL.<sup>22</sup> Because of the lack of standard chemicals for reference, structural identification of the photoproducts was based on the analysis of the total ion chromatogram (TIC) and the corresponding mass spectrum. The overall fragment ion of ATL photoproducts and corresponding proposed molecular structure were summarized in Table S3 (Supplementary Material).

As can be seen, the  $[\text{M}+\text{H}]^+$  molecular ion with  $m/z$  134 was identified as intermediate product (I) 3-(isopropylamino)propane-1, 2-diol, which was proved to be cleavage product of ether side chain.<sup>21,23</sup> The  $m/z$  167 molecular ion was labeled as photo-intermediate product (II) hydroxylated *p*-hydroxylated phenylacetamide. Sirés et al. also identified  $m/z$  167 in electrochemical degradation of ATL.<sup>34</sup> Furthermore, the  $m/z$  254 molecular ion, which was also observed by Radjenović et al.<sup>22</sup> during photocatalysis experiment, was recorded as (III) hydroxylated 4-[2-hydroxy-3-(isopropylamino)propoxy] benzaldehyde. Finally, an additional 16 Da was observed for the molecular ion  $m/z$  283 compared with the  $m/z$  267 of protonated ATL, thus it is likely that  $m/z$  283 represented for the hydroxylated ATL (IV).

---

Based on the structure elucidation of photoproducts, possible photodegradation pathways of ATL in nitrate aqueous solution upon simulated solar irradiation was proposed (Fig. 3.7). As seen, three major pathways were involving in the photodegradation of ATL, both of them linked with  $\cdot\text{OH}$  attack. Pathway I was the formation of hydroxylated ATL (IV) caused by electrophilic  $\cdot\text{OH}$  attacking on the aromatic ring. Song et al.<sup>21</sup> reported the aromatic  $\pi$  electronic system and the electronic donate effect of ether side chain favored hydroxylation. Pathway II obeyed the *ipso* substitution mechanism,<sup>35</sup> namely,  $\cdot\text{OH}$  first attack on the *ipso* carbon, generating hydroxycyclohexadienyl radicals or resonance-stabilized carbon-centered radicals. Subsequent reaction of *O*-dealkylation led cleavage of the ether side chain, resulting in the formation of 3-(isopropylamino)propane-1, 2-diol (I) and *p*-hydroxyphenylacetamide. Further  $\cdot\text{OH}$  electrophilic attack on *p*-hydroxyphenylacetamide formed the hydroxylated *p*-hydroxyphenylacetamide (II). Pathway III starting with the detachment of amide moiety from acetamide side chain under the attack of  $\cdot\text{OH}$ , further oxidation of the alkyl moiety by dissolved oxygen formed benzaldehyde derivative, which was eventually adducted by  $\cdot\text{OH}$  to formed hydroxylated 4-[2-hydroxy-3-(isopropylamino)propoxy] benzaldehyde (III).

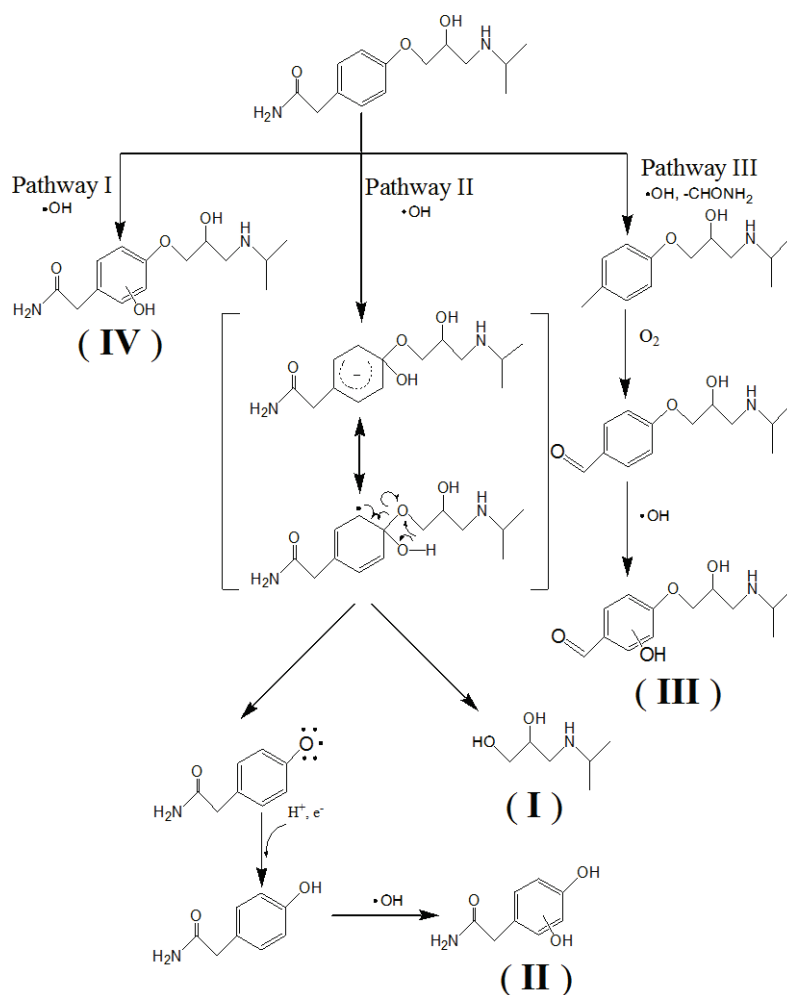


**Fig. 3.7. Possible photodegradation pathways of ATL in nitrate aqueous solution.**

### 3.1.2.3. Mineralization and toxicity

The photolysis of organic pollutants usually leads to the decomposition of structure and eventually to the mineralization of  $\text{CO}_2$  and  $\text{H}_2\text{O}$ . However, complete mineralization of aromatic organic pollutants is always difficult to achieve due to their structure stability. In addition, photo-induced toxicity is usually of great interest because in some case, the photogenerated products are much more toxic than their parent compound.<sup>36</sup> Fig.4 represents the variation of mineralization and toxicity of 40  $\mu\text{M}$  ATL solution in the presence of 5 mM nitrate under 240 min simulated solar irradiation.

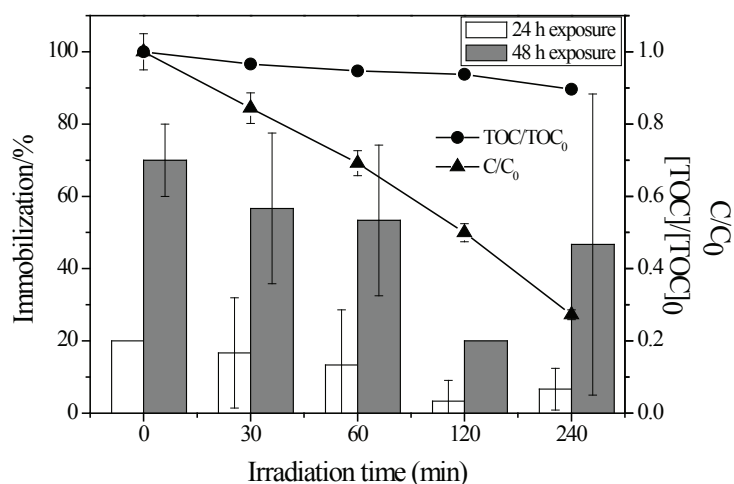


**Fig. 3.8.** Variation of toxicity to *D. magna*, (▲) concentration and (●) TOC of ATL during photodegradation process.

As clearly seen, after 240 min irradiation, approximately 72% transformation rate of ATL can be achieved while only about 10% of the TOC removal rate can be obtained, indicating that a majority of ATL transformed into intermediate products without complete mineralization. However, it is noteworthy that a decreased toxicity to *D. magna* can be observed for both the 24 h and 48 h exposure during the photolysis process, indicating the intermediates appeared to be less ecotoxic to freshwater species. The decreased toxicity was suggested to be a result of structure fragmentation or increasing mineralization of the organic pollutants.<sup>3</sup> In addition, the decreased toxicity may be also evidenced by the fact that no nitration or nitrosation aromatic compounds had been detected in LC-MS, which is generally regarded as potentially toxic and/or mutagenic compound.<sup>36</sup> Similar result was also observed by Hapeshi et al.<sup>19</sup> in photocatalytic degradation on titania suspensions. Therefore, it can be confirmed that photolysis is an important pathway for ATL toxicity reduction in natural environment.

### 3.2. Conclusions

In this paper, ATL photolysis kinetics, toxicity of intermediate products and degradation pathways are investigated in nitrate solution upon simulated solar irradiation. ATL photodegradation obeyed pseudo-first-order kinetics and the rate constant is remarkably enhanced with the increasing concentration of nitrate.  $\cdot\text{OH}$  played an important role in the photolysis process. Increasing the solution pH slightly decreased the photodegradation rate probably due to

---

pH-dependent effect of nitrate-induced  $\cdot\text{OH}$  formation. Bicarbonate decreased the photodegradation of ATL in the presence of nitrate ions mainly through pH effect, while humic substance inhibited the photodegradation as a inner filter as well as a radical scavenger. Upon irradiation, only a minor mineralization of ATL can be achieved, implying a majority of ATL transformed into intermediate products without complete mineralization. The major pathways of ATL photodegradation included hydroxylation and side chain cleavage.

The present study provides important information about ATL photolysis behavior in nature sunlit waters. It should be emphasized that degradation intermediates and products show less toxicity to *D. magna*, suggesting that photo-induced degradation of ATL in natural water is possibly an important way to reduce the toxicity to ecosystem, especially in areas with relatively high concentration of nitrate in waterbody (e.g. agriculture areas with extensive utilization of fertilizers).

### 3.3. Reference

- (1) Daughton, C. G.; Ternes, T. A. Pharmaceuticals and personal products in the environment: agents of subtle change? *Environ. Health Perspect.* **1999**, 107, 907-938.
- (2) Ternes, T.A.; Meisenheimer, M.; Mcdowell, D. Removal of pharmaceuticals during drinking water treatment. *Environ. Sci. Technol.* **2002**, 36, 3855-3863.
- (3) Andreozzi, R.; Raffaele, M.; Nicklas, P. Pharmaceuticals in STP effluents and their solar photodegradation in aquatic environment. *Chemosphere* **2003**, 50, 1319-1330.
- (4) Vieno, N.M.; Härkki, H.; Tuhkanen, T.; Kronberg, L. Occurrence of pharmaceuticals in river water and their elimination in a pilot-scale drinking water treatment plant. *Environ. Sci. Technol.* **2007**, 41, 5077-5084.
- (5) Kolpin, D. W.; Furlong, E. T.; Meyer, M. T.; Thurman, E. M.; Zaugg, S. T.; Barber, L. B.; Buxton, H. T. Pharmaceuticals, hormones, and other organic wastewater contaminants in U.S. streams, 1999-2000: a national reconnaissance. *Environ. Sci. Technol.* **2002**, 36, 1202-1211.
- (6) Zuo. Y.; Wang. C.; Van. T. Simultaneous determination of nitrite and nitrate in dew, rain, snow and lake water samples by ion-pair high-performance liquid chromatography. *Talanta* **2006**, 70, 281-285.
- (7) Zuo. Y.; Zhang. K.; Deng. Y. Occurrence and photochemical degradation of 17 alpha-ethinylestradiol in Acushnet River Estuary. *Chemosphere* **2006**, 63, 1583-1590.

- 
- (8) Borchard, U. Pharmacological properties of beta-adrenoceptor blocking drugs. *J. Clin. Basic. Cardiol.* **1998**, 1, 5-9.
- (9) Alder, A.C.; Schaffner, C.; Majewsky, M.; Klasmeier, J.; Fenner, K. Fate of  $\beta$ -blocker human pharmaceuticals in surface water: comparison of measured and simulated concentrations in the Glatt Valley Watershed, Switzerland. *Water Res.* **2010**, 44, 936-948.
- (10) Huggett, D.B.; Khan, I.A.; Foran, C.M. Determination of beta-adrenergic receptor blocking pharmaceuticals in United States wastewater effluent. *Environ. Pollut.* **2003**, 121, 199-205.
- (11) Cleuvers, M. Initial risk assessment for three  $\beta$ -blockers found in the aquatic environment. *Chemosphere* **2005**, 59, 199-205.
- (12) Doll, T.E.; Frimmel, F.H. Fate of pharmaceuticals: photodegradation by simulated solar UV-light. *Chemosphere* **2003**, 52, 1757-1769.
- (13) Packer, J.L.; Werner, J.J.; Latch, D.E.; McNeill, K.; Arnold, W.A. Photochemical fate of pharmaceuticals in the environment: naproxen, diclofenac, clofibric acid, and ibuprofen. *Aquat. Sci.* **2003**, 65, 342-351.
- (14) Lam, M. W.; Tantuco, K.; Mabury, S. A. Photofate: a new approach in accounting for the contribution of indirect photolysis of pesticides and pharmaceuticals in surface water. *Environ. Sci. Technol.* **2003**, 37, 899-907.
- (15) Vaughan, P.P.; Blough, N. Photochemical formation of hydroxyl radical by constituents of natural waters. *Environ. Sci. Technol.* **1998**, 32, 2947-2953.
- (16) Zhan, M.; Yang, X.; Xian, Q.; Kong, L. Photosensitized degradation of bisphenol A involving reactive oxygen species in the presence of humic substances. *Chemosphere* **2006**, 63, 378-386.
- (17) Zepp, R.G.; Holgne, J.; Bader, H. Nitrate-induced photooxidation of trace organic chemicals in water. *Environ. Sci. Technol.* **1987**, 21, 443-450.
- (18) Liu, Q.-T.; Williams, H. E. Kinetics and degradation products for direct photolysis of  $\beta$ -blockers in water. *Environ. Sci. Technol.* **2007**, 41, 803-810.
- (19) Hapeshi, E.; Achilleos, A.; Vasquez, M. I. Drugs degrading photocatalytically: kinetics and mechanisms of ofloxacin and atenolol removal on titania suspensions. *Water Res.* **2010**, 44, 1737-1746.
- (20) Piram, A.; Salvador, A.; Verne, C.; Herbreteau, B.; Faure, R. Photolysis of  $\beta$ -blockers in environmental waters. *Chemosphere* **2008**, 73, 1265-1271.

- 
- (21) Song, W.; Cooper, W. J.; Mezyk, S. P.; Greaves, J.; Peake, B. M. Free radical destruction of  $\beta$ -blockers in aqueous solution. *Environ. Sci. Technol.* **2008**, *42*, 1256-1261.
- (22) Radjenović, J.; Sirtori, C.; Petrović, M.; Barceló, D.; Malato, S. Solar photocatalytic degradation of persistent pharmaceuticals at pilot-scale: kinetics and characterization of major intermediate products. *Appl. Catal. B: Environ.* **2009**, *89*, 255-264.
- (23) Yang, H.; An, T.; Li, G.; Song, W.; Cooper, W. J.; Luo, H.; Guo, X. Photocatalytic degradation kinetics and mechanism of environmental pharmaceuticals in aqueous suspension of TiO<sub>2</sub>: a case of  $\beta$ -blockers. *J. Hazard. Mater.* **2010**, *179*, 834-839.
- (24) Brezonik, P. L.; Fulkerson-Brekken, J. Nitrate-induced photolysis in natural waters: Controls on concentrations of hydroxyl radical photo-intermediates by natural scavenging agents. *Environ. Sci. Technol.* **1998**, *32*, 3004-3010.
- (25) Buxton, G. V.; Greenstock, C. L.; Helman, W. P. Critical review of rate constants of hydrate electrons, hydrogen atoms and hydroxyl radicals (OH<sup>•</sup>/O<sup>•-</sup>) in aqueous solution. *J. Phys. Chem. Ref. Data.* **1988**, *17*, 513-517.
- (26) Yang, X.; Zhan, M.; Kong, L.; Wang, L. Determination of hydroxyl radicals with salicylic acid in aqueous nitrate and nitrite solutions. *J. Environ. Sci.* **2004**, *16*, 687-689.
- (27) Vione, D.; Khanra, S.; Man, S. C.; Maddigapu, P. R.; Das, R. Inhibition vs. enhancement of the nitrate-induced phototransformation of organic substrates by the  $\cdot$ OH scavengers bicarbonate and carbonate. *Water Res.* **2009**, *43*, 4718-4728.
- (28) Huang, J. P.; Mabury, S. A. Steady-state concentrations of carbonate radicals in field waters. *Environ. Toxicol. Chem.* **2000**, *19*, 2181-2188.
- (29) Corin, N.; Backlund, P.; Kulovaara, M. Degradation products formed during UV-irradiation of humic water. *Chemosphere* **1996**, *33*, 245-255.
- (30) Zuo, Y.; Jones, R. Photochemistry of natural dissolved organic matter in lake and wetland waters: production of carbon monoxide. *Water Res.* **1997**, *31*, 850-858.
- (31) Zepp, R.G.; Schlotzhauer, P. F.; Sink, R. M. Photosensitized transformations involving electronic energy transfer in natural waters: role of humic substances. *Environ. Sci. Technol.* **1985**, *19*, 74-81.
- (32) Richard, C.; Vialation, D.; Aguer, J.-P.; Andreux, F. Transformation of monuron photosensitized by soli extracted humic substances: energy or hydrogen transfer mechanism?. *J.*

---

*Photoch. Photobio. A: Chem.* **1997**, 111, 265-271.

(33) Chen, Y.; Hu, C.; Hu, X.; Qu, J. Indirect photodegradation of amine drugs in aqueous solution under simulated sunlight. *Environ. Sci. Technol.* **2009**, 43, 2760-2765.

(34) Sirés, I.; Oturan, N.; Oturan, M. A. Electrochemical degradation of  $\beta$ -blockers. Studies on single and multicomponent synthetic aqueous solutions. *Water Res.* **2010**, 44, 3109-3120.

(35) Urano, Y.; Higuchi, T.; Hirobe, M. Substrate-dependent changes of the oxidative O-dealkylation mechanism of several chemical and biological oxidizing systems. *J. Chem. Soc. Perkin Trans.* **1996**, 2, 1169-1173.

(36) Suzuki, J.; Okazaki, H.; Sato, T.; Suzuki, S. Formation of mutagens by photochemical reaction of biphenyl in nitrate aqueous solution. *Chemosphere* **1982**, 11, 437-444.

### **3.4. Supplementary Material**

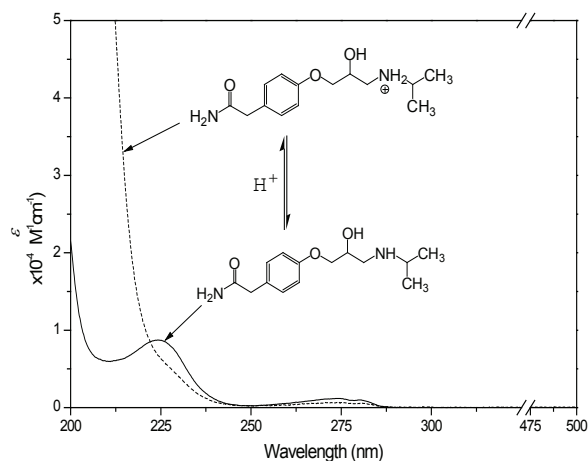


Fig. S1. Chemical structure and UV-vis absorbance spectrum of atenolol (ATL) ( $[ATL]=40 \mu\text{mol L}^{-1}$ ).

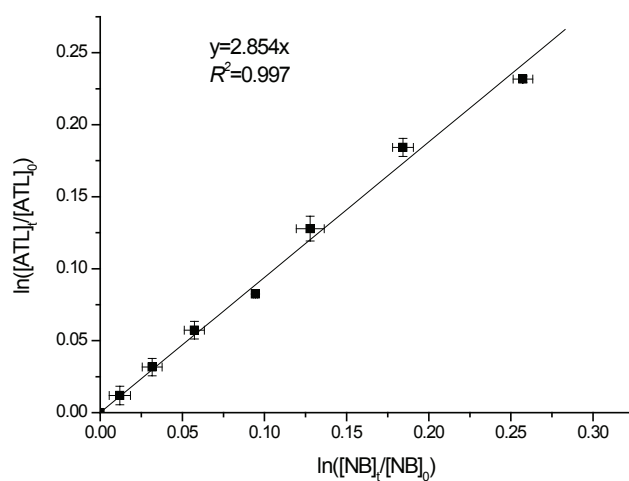


Fig. S2. Linear relationship of  $\ln([ATL]_t/[ATL]_0)$  versus  $\ln([NB]_t/[NB]_0)$  through competition kinetic method ( $[ATL]=10 \mu\text{mol L}^{-1}$ ,  $[NB]=10 \mu\text{mol L}^{-1}$  and  $[NO_3^-]=5 \text{mmol L}^{-1}$ ).

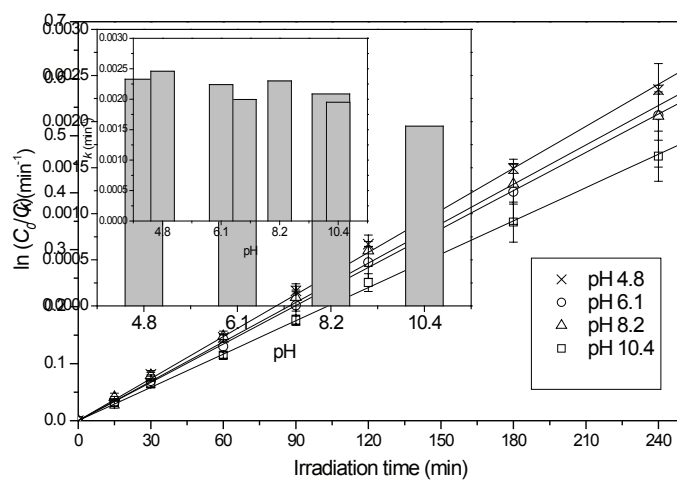
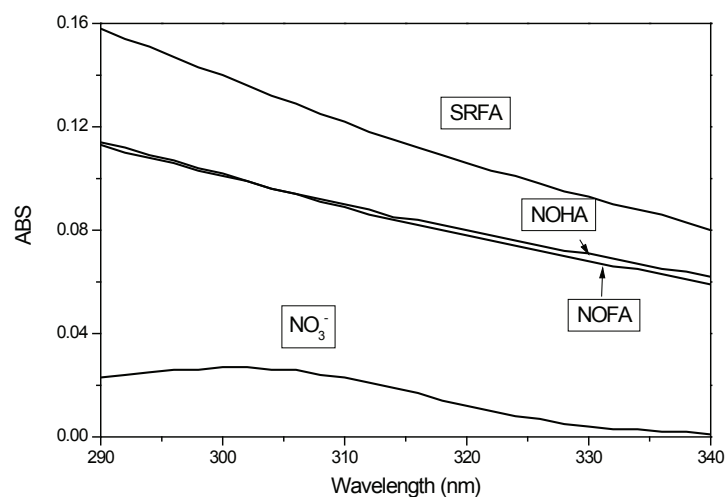
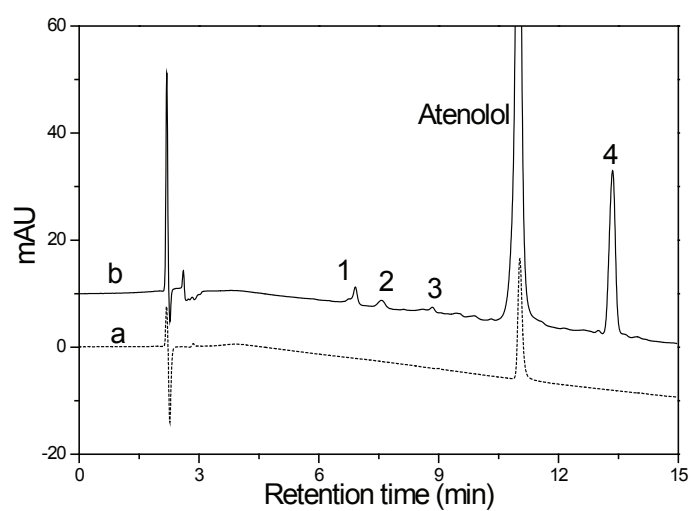


Fig. S3. Effect of solution pH on the atenolol photodegradation kinetics in the presence of nitrate under simulated solar irradiation ( $[ATL]=10 \mu\text{mol L}^{-1}$ ,  $[NO_3^-]=5 \text{mmol L}^{-1}$ ). Inset: the relationship between pseudo-first-order rate constants and different solution pH values.



**Fig. S4. UV-vis absorbance spectrum of SRFA, NOFA, NOHA and NO<sub>3</sub><sup>-</sup> in the range of 290nm–340nm**  
 ([SRFA]=5 mgC L<sup>-1</sup>, [NOFA]=5 mgC L<sup>-1</sup>, [NOHA]=5 mgC L<sup>-1</sup>, [NO<sub>3</sub><sup>-</sup>]=5 mmol L<sup>-1</sup>).



**Fig. S5. HPLC chromatogram of atenolol (...)** 20µM before irradiation, (—) 40µM after 24 h irradiation and concentrated by SPE.

**Table S1 Kinetics of atenolol photolysis induced by nitrate ions under simulated solar irradiation.**

$[\text{NO}_3^-]$ (mmol L <sup>-1</sup> )	$k_{\text{app}} \times 10^3$ (min <sup>-1</sup> ) <sup>a</sup>	$t_{1/2}$ (min)	$R^2$
0.5	1.01±0.15	686	0.998
1	1.43±0.06	485	0.980-0.997
2	2.25±0.37	308	0.998
5	3.79±0.26	183	0.998
10	7.16±0.17	96.7	0.986

<sup>a</sup> The  $k_{\text{app}}$  value was obtained by linear regression after plotting  $\ln([\text{ATL}]_0/[\text{ATL}])=k_{\text{app}}t$ , then  $t_{1/2}=\ln 2/k$ .

**Table S2 The pH and radical scavenging effect of bicarbonate concentration on the atenolol photodegradation kinetics in the presence of nitrate ions under simulated solar irradiation ([ATL]=10 μmol L<sup>-1</sup>, [NO<sub>3</sub>]=5 mmol L<sup>-1</sup>).**

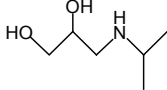
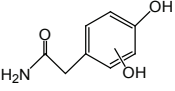
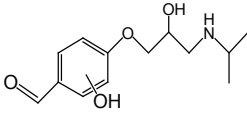
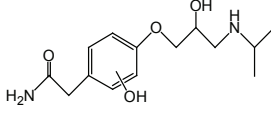
$[\text{HCO}_3^-]$ (mmol L <sup>-1</sup> )	$\eta$ (%) <sup>a</sup>	pH <sup>b</sup>	$k_{\text{app}} \times 10^3$ (min <sup>-1</sup> ) <sup>c</sup>	$R^2$
0	0	6.93	5.56	0.999
0.8	8.3	8.03	5.29	0.999
2	18.5	8.36	5.31	0.999
4	31.2	8.39	5.09	0.999

<sup>a</sup> The fraction of  $\cdot\text{OH}$  scavenged by  $\text{HCO}_3^-$  was calculated according to equation  $\eta = k_{\text{OH}, \text{HCO}_3^-} [\text{HCO}_3^-] / (k_{\text{OH}, \text{HCO}_3^-} [\text{HCO}_3^-] + k_{\text{OH}, \text{ATL}} [\text{ATL}])$ .

<sup>b</sup> The pH value of reaction solution with different  $\text{HCO}_3^-$  concentration was measured under 25 °C.

<sup>c</sup> The  $k_{\text{app}}$  value was obtained by linear regression after plotting  $\ln([\text{ATL}]_0/[\text{ATL}])=k_{\text{app}}t$ .

**Table S3 The main fragment ion of ATL intermediate products and proposed structures.**

No.	Molecular weight <sup>a</sup>	main fragment ion (m/z) <sup>b</sup>	Proposed structure
I	133	134 [M+H] <sup>+</sup>	
		116 [M+H-H <sub>2</sub> O] <sup>+</sup>	
		92 [M+H-C(CH <sub>3</sub> ) <sub>2</sub> ] <sup>+</sup>	
		74 [M+H-C(CH <sub>3</sub> ) <sub>2</sub> -H <sub>2</sub> O] <sup>+</sup>	
II	167	168 [M+H] <sup>+</sup>	
		151 [M+H-OH] <sup>+</sup>	
		136 [M+H-OH-NH] <sup>+</sup>	
		126 [M+H-CH <sub>2</sub> CO] <sup>+</sup>	
III	253	254 [M+H] <sup>+</sup>	
		236 [M+H-H <sub>2</sub> O] <sup>+</sup>	
		212 [M+H-C(CH <sub>3</sub> ) <sub>2</sub> ] <sup>+</sup>	
		177 [M+H-C(CH <sub>3</sub> ) <sub>2</sub> -NH <sub>2</sub> -CHO] <sup>+</sup>	
		116 [M+H-C <sub>7</sub> H <sub>6</sub> O <sub>3</sub> ] <sup>+</sup>	
IV	282	283 [M+H] <sup>+</sup>	
		265 [M+H-H <sub>2</sub> O] <sup>+</sup>	
		224 [M+H-C(CH <sub>3</sub> ) <sub>2</sub> -NH <sub>3</sub> ] <sup>+</sup>	
		161 [M+H-C(CH <sub>3</sub> ) <sub>2</sub> -NH <sub>3</sub> -H <sub>2</sub> O-CH <sub>2</sub> CONH <sub>2</sub> ] <sup>+</sup>	
		116 [M+H-C <sub>8</sub> H <sub>9</sub> NO <sub>3</sub> ] <sup>+</sup>	

<sup>a</sup> Photoproducts molecular weight was tentatively assigned on the basis of the pseudomolecular ions [M+H]<sup>+</sup>

<sup>b</sup> Fragment ion pattern was elucidated by using pseudomolecular [M+H]<sup>+</sup> as precursor ion

---

## Chapter 4 Photocatalytic degradation of atenolol in aqueous titanium dioxide suspensions

As a new kind of micropollutants, pharmaceutical and personal care products (PPCPs) have received growing attention recently due to their potential risk to human beings and ecology systems.<sup>1,2</sup> After being used, most of the PPCPs are released into sewage wastewater treatment system as metabolites as well as unchanged parent molecular. However, the wastewater treatment plant usually failed to remove various groups and huge amounts of PPCPs due to their refractory behavior.<sup>3,4</sup> Consequently, a broad variety of PPCPs were detected in wastewater treatment plant effluents, surface waters, ground waters, even in drinking waters.<sup>5-7</sup>

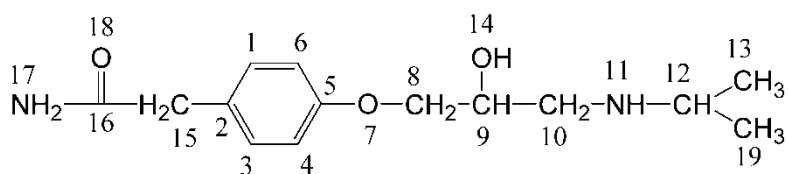


**Fig. 4.1. Chemical structure of atenolol (ATL), C<sub>14</sub>H<sub>22</sub>N<sub>2</sub>O<sub>3</sub>.**

As a selective  $\beta_1$  receptor antagonist, atenolol (ATL), 4-[2-hydroxy-3-[(1-methyl) amino] propoxyl] benzeacetamide (Fig. 4.1) has been used primarily for the treatment of cardiovascular diseases for more than thirty years.<sup>8</sup> Due to its extensive usage and limited human metabolism, ATL was widely detected in sewage effluents and surface waters, usually with a concentration ranging from ng L<sup>-1</sup> to  $\mu\text{g L}^{-1}$ .<sup>9,10</sup> Previous researches have demonstrated that ordinary wastewater treatments such as activated sludge, granular activated carbon filtration and ozonation cannot remove ATL effectively.<sup>4,11</sup> Furthermore, many studies have provided evidence that ATL could inhibit the growth of human embryonic cells and was ecotoxic to freshwater species.<sup>12</sup> Also, chlorination of ATL after the process of wastewater disinfection had phytotoxic activity.<sup>13</sup> Therefore, it is essential to develop advanced treatment technologies for ensuring effective elimination of ATL in wastewaters before release into natural waters.

Heterogeneous photocatalysis is an example of advanced oxidation process (AOPs) capable of achieving complete oxidation of organic and inorganic pollutants, including also pharmaceutical substances.<sup>14,15</sup> Among various photocatalysts, TiO<sub>2</sub> is widely used because it is

---

non-toxic, inexpensive, and relatively biologically and chemically stable. When irradiating with photons of energy equal to or exceeding the band gap energy of TiO<sub>2</sub> (for anatase, 3.2 eV band gap), valence band holes ( $h_{vb}^+$ ) and reductive conduction band electrons ( $e_{cb}^-$ ) are generated. The photogenerated holes can: (i) directly oxidize the adsorbed chemical substance; or (ii) produce adsorbed hydroxyl radical (HO·) via the surface-bound OH<sup>-</sup> and/or the adsorbed water molecules. Thus, the degradation of drugs can be achieved either by oxidative species or by conduction band electron.<sup>16,17</sup>

In practical applications of photocatalysis for organic pollutants treatment, the influence of the water matrix should be taken into consideration since different water constituents may influence the degradation kinetics, and even shift the initial catalytic mechanism.<sup>18,19</sup> In addition, photocatalytic activity is closely related with the properties of photocatalyst and is known to be substrate-specific.<sup>20</sup> However, data about the effect of natural water constituents and different type of photocatalyst on the degradation of ATL are still scarce and the related mechanism is poorly understood up to date. Therefore, the purpose of this study is: (i) to investigate the photocatalytic degradation of ATL and determine the predominant reactive species involved in the photocatalysis process; (ii) to evaluate the effect of two common natural water constituents, humic substance (HS) and bicarbonate ions, on the photocatalysis of ATL and study the difference of photocatalysis in real river water and Milli-Q water; (iii) to compare the degradation efficiency of ATL photocatalysis by using different photocatalysts and (iv) to elucidate the photocatalytic degradation mechanism and propose possible degradation pathways of ATL in aqueous TiO<sub>2</sub> suspensions.

## 4.1. Results and discussion

### 4.1.1. Preliminary experiment

Fig. 4.2 presents the results of a preliminary experiment for the photocatalytic degradation of ATL (with Degussa P25 TiO<sub>2</sub> under irradiation) in comparison to several control runs including hydrolysis (without TiO<sub>2</sub> in dark), photolysis (without TiO<sub>2</sub> under irradiation) and adsorption (with TiO<sub>2</sub> in dark). As seen, hydrolysis, direct photolysis and dark adsorption contributed to negligible decay of ATL. The weak photolysis of ATL was ascribed to the unappreciable overlap of ATL UV-Vis absorbance spectrum with filtered HPK lamp emission spectrum (Fig. S1, Supplementary Material). However, TiO<sub>2</sub>-mediated photocatalysis resulted in a pronounced degradation of ATL

with complete disappearance occurring after 60 min irradiation. Our observation indicates that the loss of ATL was almost exclusively due to photocatalysis process. The extremely appreciable degradation of ATL was most likely due to the formation of highly reactive transient species, such as hydroxyl radical ( $\text{HO}\cdot$ ) and positive valence band holes ( $\text{h}_{\text{vb}}^+$ ), which mediated the oxidation of ATL. Linear relationship of  $\ln(C_{\text{eq}}/C)$  versus irradiation time  $t$  displayed that ATL photocatalytic degradation followed the pseudo-first-order kinetic ( $R^2 = 0.993$ ). The pseudo-first-order rate constant,  $k_p$  ( $\text{min}^{-1}$ ), was determined to be  $0.0570 \text{ min}^{-1}$  from the slope value of the line upon linear regression.

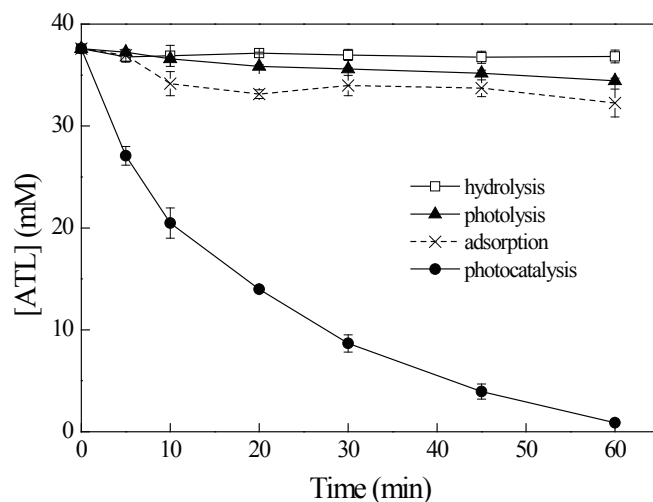


**Fig. 4.2. Comparison of hydrolysis ( $\square$ ), photolysis ( $\blacktriangle$ ), adsorption ( $\times$ ) and photocatalysis degradation ( $\bullet$ ) of atenolol. Experimental conditions: Degussa P25 was used as photocatalyst.  $[\text{TiO}_2] = 2.0 \text{ g L}^{-1}$ ;  $[\text{ATL}] = 37.6 \text{ }\mu\text{M}$ ;  $\text{pH} = 6.8$ . Error bars represent the 95% confidence interval.**

#### 4.1.2. Determination of $\text{HO}\cdot$ as major reactive species

During photocatalysis process, hydroxyl radical ( $\text{HO}\cdot$ ) is usually regarded as the predominant species responsible for the decay of a wide range of organic pollutants due to its non-selective and strong oxidizing power.<sup>21</sup> Second-order reaction rate constants for this oxidant with numerous organic compounds approach diffusion-limited values ( $10^7 - 10^{10} \text{ M}^{-1} \text{ s}^{-1}$ ).<sup>22</sup> The importance of  $\text{HO}\cdot$  for ATL degradation was probed by spiking methanol, a selective  $\text{HO}\cdot$  scavenger ( $k_{\text{HO}\cdot\text{methanol}} = 9.7 \times 10^8 \text{ M}^{-1} \text{ s}^{-1}$ ), into reaction solution (see Fig. 4.3).<sup>23</sup> Methanol was expected to compete mainly for  $\text{HO}\cdot$  because of its low affinity to the  $\text{TiO}_2$  surface.<sup>23</sup>

It was observed that ATL photocatalytic degradation was completely suppressed after methanol was spiked into the reaction solution. This finding provides evidence that  $\text{HO}\cdot$  was the predominant reactive species involved in the ATL photocatalytic degradation process, while other

reactive species, such as  $h_{\text{vb}}^+$ ,  $\text{O}_2^{\cdot-}$  and  $\text{H}_2\text{O}_2$  appeared to be less important. No statistically significant difference was observed by increasing the methanol concentration from 10 mM to 50 mM, suggesting methanol was an effective quencher for  $\text{HO}^\cdot$  in this study. The quantum yield of hole ( $5.7 \times 10^{-2}$ ) during photocatalysis in aqueous solution was estimated to be much higher than  $\text{HO}^\cdot$  ( $7 \times 10^{-5}$ ).<sup>24</sup> However, direct hole oxidation through electron-transfer primarily occurs on  $\text{TiO}_2$  surface where significant adsorption is essential as a prerequisite step.<sup>20</sup> Thus, the weak adsorption of ATL on  $\text{TiO}_2$  may be one reason accounting for the limited importance of  $h_{\text{vb}}^+$ . Conversely,  $\text{HO}^\cdot$  is a mobile photooxidant, which can diffuse into bulk solution and react with the majority of ATL.<sup>20,23</sup>

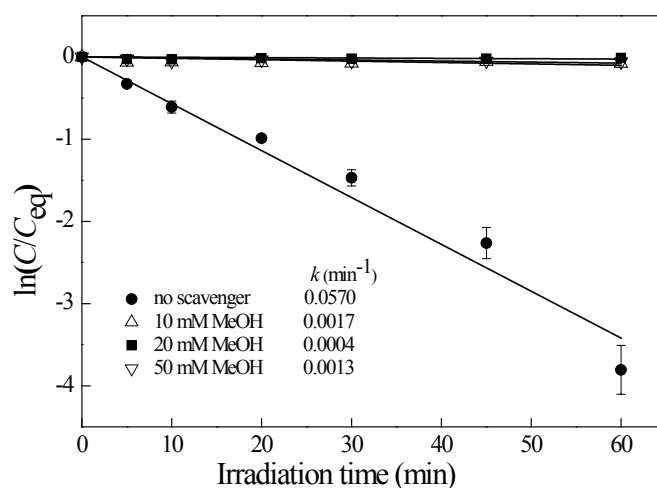


**Fig. 4.3.** Effect of methanol as  $\text{HO}^\cdot$  scavenger on atenolol photocatalysis. Degussa P25 was used as photocatalyst. Experimental conditions:  $[\text{TiO}_2] = 2.0 \text{ g L}^{-1}$ ;  $[\text{ATL}] = 37.6 \text{ }\mu\text{M}$ ;  $[\text{methanol}] = 10\text{-}50 \text{ mM}$ ;  $\text{pH} = 6.8$ .

The importance of  $\text{HO}^\cdot$  was further supported by second order rate constant of ATL reacting with  $\text{HO}^\cdot$ ,  $k_{\text{HO}\cdot\text{ATL}}$ , which was measured by competition kinetics (Eq. (1)) using benzoic acid as a reference compound (Fig. S2, Supplementary Material).

$$\ln\left(\frac{[\text{ATL}]_t}{[\text{ATL}]_0}\right) = \frac{k_{\text{HO}\cdot\text{ATL}}}{k_{\text{HO}\cdot\text{BA}}}\ln\left(\frac{[\text{BA}]_t}{[\text{BA}]_0}\right) \quad (1)$$

Our calculation yielded  $k_{\text{HO}\cdot\text{ATL}} = (5.78 \pm 0.03) \times 10^9 \text{ M}^{-1} \text{ s}^{-1}$  which is comparable to the value  $(7.05 \pm 0.27) \times 10^9 \text{ M}^{-1} \text{ s}^{-1}$  measured previously by Song et al. in  $\gamma$ -irradiation.<sup>25</sup> Such a high second order rate constant means that ATL can be readily oxidized by  $\text{HO}^\cdot$  approaching diffusion-controlled limits. Furthermore, our previous work confirmed that  $\text{HO}^\cdot$  mediated ATL degradation was the principal pathway for ATL elimination in the presence of nitrate under

simulated solar irradiation.<sup>26</sup> Thus, it can be concluded that HO· is the primary reactive species for ATL degradation during the photocatalysis process. This conclusion is also confirmed by intermediates that were identified by LC-MS/MS (discussed later).

#### 4.1.3. Effect of solution pH

Solution pH influences photocatalytic degradation efficiency significantly due to its ability of altering charge state of the photocatalyst as well as the organic compounds (anionic or cationic).<sup>14</sup>

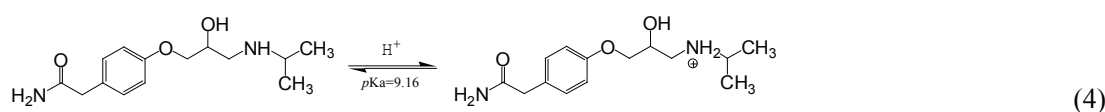


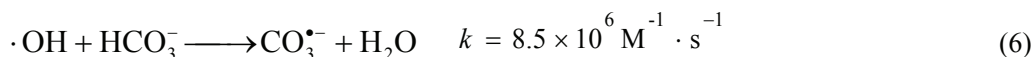
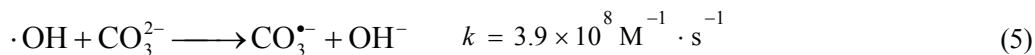
Fig. S3 (Supplementary Material) shows the varying pH from 3.02 to 11.02 remarkably enhances the photocatalytic degradation of ATL. As the zero point charge ( $\text{pH}_{\text{zpc}}$ ) of P25  $\text{TiO}_2$  is reported to be 6.25 and the  $\text{pK}_a$  of ATL is 9.16,<sup>14</sup> electrostatic repulsion occurred between protonated ATL and  $\text{TiOH}_2^+$  at pH 3.02 (Eq. (2) and Eq. (4)), which hindered the photocatalysis. At pH 8.15, electrostatic attraction took place between protonated ATL and  $\text{TiO}^-$  (Eq. (3) and Eq. (4)), which may favor the photocatalytic degradation. The relatively faster degradation at pH 11.02 was likely associated with the pH-dependent effect of  $\text{TiO}_2$ -induced HO· formation since the electrostatic attraction was less because ATL was under neutral molecular form. It is believed that basic solution condition or increasing the solution pH favored  $\text{TiO}_2$  photocatalysis because of a more efficient formation of HO· from  $\text{OH}^-$  than water.<sup>27</sup> However, it is also possible that the better degradation in alkaline pH was due to the fact that the structural orientation of the substrate is favored for the attack of the reactive species under this condition.<sup>28</sup>

#### 4.1.4. Effect of typical natural water constituents and river water matrix

Bicarbonate is one of the most abundant anions present in natural waters with an environmentally relevant concentration ranging from 0.4 to 4 mM.<sup>29-31</sup> The HO· scavenging characteristics make it play a negative role in the degradation of organic compounds in many advanced oxidation processes.<sup>18</sup> We investigated the effect of  $\text{HCO}_3^-$  on photocatalytic degradation of ATL by adjusting solution pH at 8.5 ( $\text{HCO}_3^-$  is the predominant species at pH 8.5 as  $\text{pK}_{a1} = 6.37$  and  $\text{pK}_{a2} = 10.25$ ). Bicarbonate-amendment shows a significant promoting effect on ATL

---

photocatalytic degradation (see Fig. 4.4(a)). The observed enhancement is unexpected since bicarbonate is assumed to reduce photocatalysis efficiency by scavenging HO· according to following reactions.



As a secondary radical, carbonate radical ( $\text{CO}_3^{\bullet-}$ ) is relatively less reactive than HO· and has been shown to be reactive only with electron-rich chemicals such as sulfur-containing compounds and aniline.<sup>30,31</sup> The observed enhancement in ATL degradation can be explained by considering that  $\text{HCO}_3^-$  were present in  $\text{TiO}_2$  suspensions at much higher concentration than ATL and these ions would interact more strongly with Ti(IV) than ATL. As a result,  $\text{HCO}_3^-$  ions might be able to scavenge adsorbed HO· more efficiently than ATL, reducing the fraction of HO· that recombine before reacting with substrates. Since  $\text{CO}_3^{\bullet-}$  is less reactive and has fairly longer life-time, it could reach a much higher steady-state concentration on  $\text{TiO}_2$  surface, which enable them diffusing into the bulk aqueous solution and reacting with ATL. Thus, the higher concentration of  $\text{CO}_3^{\bullet-}$  could offset its lower reactivity and show a promoting effect. Similar  $\text{HCO}_3^-$  promoted photocatalysis efficiency was also reported by Hu et al. in degradation of sulfamethoxazole.<sup>32</sup>

Humic substance (HS) is the major part of natural dissolved organic matter (DOM) and may accounts for up to 90% of total TOC content.<sup>33</sup> Therefore, the presence of HS in the targeted water for  $\text{TiO}_2$  photocatalytic treatment is expected. The effect of HS on ATL photocatalysis was investigated by using commercial Aldrich humic acid and Fluka humic acid as HS analogues. The presence of the two humic acids (HA) showed detrimental impact on ATL photocatalysis (see Fig. 4.4(b) and (c)). In addition, increasing the humic acid concentration drastically decreased degradation efficiency. These observations can be rationalized as follows: (i) blocking active sites on  $\text{TiO}_2$  surface due to adsorption, (ii) attenuating the incident light as an inner filter and (iii) competing with target organic compound for reactive radicals as scavenger.<sup>34-36</sup> Interestingly, at the same concentration level, Fluka HA showed relatively more inhibitive effect than Aldrich HA, which is probably due to the fact that Fluka HA had a slightly higher adsorption on  $\text{TiO}_2$  surface as well as a fairly stronger UV-Vis absorbance (Fig. S4 and Fig. S5. Supplementary Material). It is noteworthy that, the degradation efficiency of ATL in the presence of  $60 \text{ mg L}^{-1}$  Aldrich HA was

slightly higher than that of 30 mg L<sup>-1</sup> Aldrich HA, which can be attributed to the contribution of weak HA-photosensitized degradation (e.g., singlet oxygen, excited triplet state <sup>3</sup>HA\*, etc). However, at high concentration this photosensitized effect became negligible since attenuation effect will be predominant.<sup>37</sup>

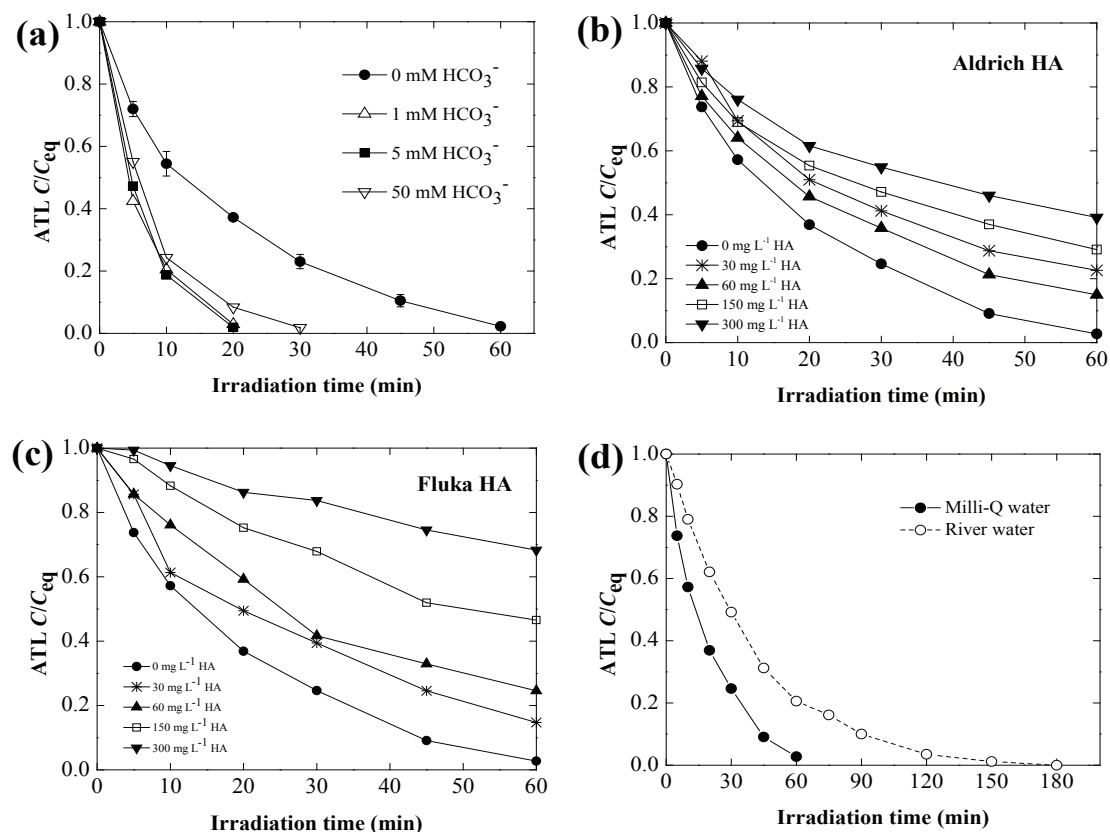


**Fig. 4.4.** Effect of typical natural water constituents and river water matrix on ATL photocatalytic degradation. (a) effect of bicarbonate at pH 8.5; (b) effect of Aldrich humic acid at pH 6.8; (c) effect of Fluka humic acid at pH 6.8; and (d) effect of river water matrix (pH 8.05). Degussa P25 was used as photocatalyst. Experimental conditions: [TiO<sub>2</sub>] = 2.0 g L<sup>-1</sup>; [ATL] = 37.6 μM; pH was adjusted by 0.1 M HCl or 0.1 M NaOH.

To obtain a further insight of water constituents effect on photocatalytic degradation of ATL, field river water taken from Rhône River (France) was employed in photocatalysis to compare with Milli-Q water (see Fig. 4.4(d)). ATL was found to be completely eliminated after 180 min photocatalysis in river water compared to 60 min in Milli-Q water matrix, indicating a detrimental effect of natural water component on ATL photocatalysis. This result can be explained by the following: (i) the competitive adsorption on active sites or the formation of salt layer on TiO<sub>2</sub>

---

surface due to the inorganic ions presented in river water, blocking the accessibility of catalyst and substrate;<sup>38,39</sup> (ii) the presence of natural radical scavengers in river water (e.g.,  $\text{Cl}^-$ ,  $\text{CO}_3^{2-}$ ,  $\text{HCO}_3^-$  and DOM) (see Table S1, Supplementary Material), quenching part of the reactive radicals.<sup>18,19</sup> Interestingly, no dark adsorption of ATL on  $\text{TiO}_2$  surface was found in river water matrix (data not shown), which provided further evidence that active sites on  $\text{TiO}_2$  surface were blocked by inorganic ions.

In addition, the occurrence of phototransformation intermediates was also shown to be highly water matrix-dependent. Fig. S6 (Supplementary Material) shows the evolution of intermediates as a function of irradiation time in both Milli-Q water and river water matrix. In Milli-Q water, intermediates reached their maximum of concentrations around 15 min and then decreased progressively to disappearance after 60 min. However, in river water matrix, intermediates were found to reach maximum later and disappear much more slowly compared to the Milli-Q water matrix. Note that the evolution profiles were only qualitative because there were no authentic standards available of the photoproducts to ensure their quantitative analysis. In addition, some intermediates were undetectable during photocatalysis in river water matrix which were observed in Milli-Q water, indicating no formation of these compounds or that their yield amount was lower than the detection limit of our HPLC-DAD. We deduced that the natural water constituents (e.g., humic substance, bicarbonate ions) which are ubiquitous in river waters could reduce the  $\text{HO}\cdot$  concentration yielded in illuminated suspensions by serving as radical scavengers and/or blocking the  $\text{TiO}_2$  surface, which consequently led to the formation and degradation of intermediates at much slower rate.

#### 4.1.5. Effect of different type of photocatalyst

The photocatalytic activity of  $\text{TiO}_2$  depends on surface and structural semiconductor properties such as crystal composition, surface area, particle size distribution, porosity, band gap and surface hydroxyl density.<sup>20,28</sup> In the present study, we also investigated the photocatalytic activities of other three kinds of commercially available  $\text{TiO}_2$  catalysts (namely Hombikat UV100, Millennium PC500 and Aldrich rutile) on the degradation kinetics of ATL by comparison with Degussa P25. The characteristics of these photocatalysts (i.e., crystallinity, BET surface area and particle size) are summarized in Table S2 (Supplementary Material).

As shown in Fig. 4.5, the photocatalytic degradation of ATL proceeds much more rapidly in

the presence of P25 as compared to other photocatalysts. The efficiency of photocatalysts is found to follow the order: P25 > Aldrich rutile > Millennium PC500  $\approx$  Hombikat UV100.

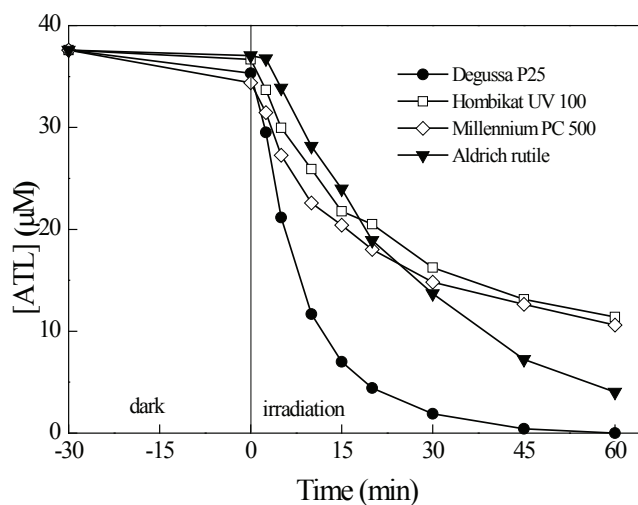


**Fig. 4.5.** Effect of different type of photocatalyst on photocatalytic degradation of atenolol: (●) Degussa P25; (□) Hombikat UV100; (◇) Millennium PC500; (▼) Aldrich rutile. Experimental conditions: [photocatalyst] = 2.0 g L<sup>-1</sup>, [ATL] = 37.6 μM, pH = 6.8.

Our result corroborates with others that P25 is generally more reactive than other commercial photocatalysts.<sup>20,28</sup> The higher photocatalytic activity of P25 has been ascribed to its mixture crystallites with small rutile dispersed into an anatase matrix. Mixed-phase TiO<sub>2</sub> photocatalysts have been reported to have significantly higher activity than single-phase TiO<sub>2</sub>, which has been interpreted as due to electronic interactions between the anatase and rutile phases.<sup>28</sup> It should be noted that although the anatase photocatalysts possess the highest BET surface area, Hombikat UV100 and Millennium PC500 showed no pronounced adsorption of ATL. Indeed, Hombikat UV100 even showed a lower adsorption relative to P25. This observation is most likely due to the high hydrophilicity of ATL ( $K_{ow} = 0.016$ ). The weak adsorption further supports the fact that degradation reaction occurred primarily in bulk solution and was mediated by HO·. Since HO· can diffuse from TiO<sub>2</sub> surface to bulk solution, it could reduce the importance of adsorption.<sup>20,40</sup> Thus, the advantage of anatase photocatalyst with a higher surface area could be diminished. The higher activity of Aldrich rutile compared to the two anatase kind catalysts is not unexpected. Although anatase is widely regarded as more active than rutile because of the higher  $E_{CB}$  of anatase by  $\sim 0.2$  eV (i.e., higher driving force of electron transfer to O<sub>2</sub>), this conclusion cannot be well justified.<sup>20</sup> It has been reported that the photocatalytic activities of anatase and rutile are greatly affected by

the kind of substrates and rutile exhibits higher activity than anatase for some organic compounds such as phenol and 4-chlorophenol.<sup>20</sup> One plausible explanation is that rutile photocatalysts have better crystallinity, fewer defect sites, and consequently longer lifetime of electron-hole pairs.<sup>20</sup>

Different photocatalysts also exhibited different activities for destructing ATL intermediates (Fig. 4.6). As expected, ATL intermediates disappeared much more rapidly in illuminated aqueous P25 TiO<sub>2</sub> suspensions (Fig. 4.6(a)).

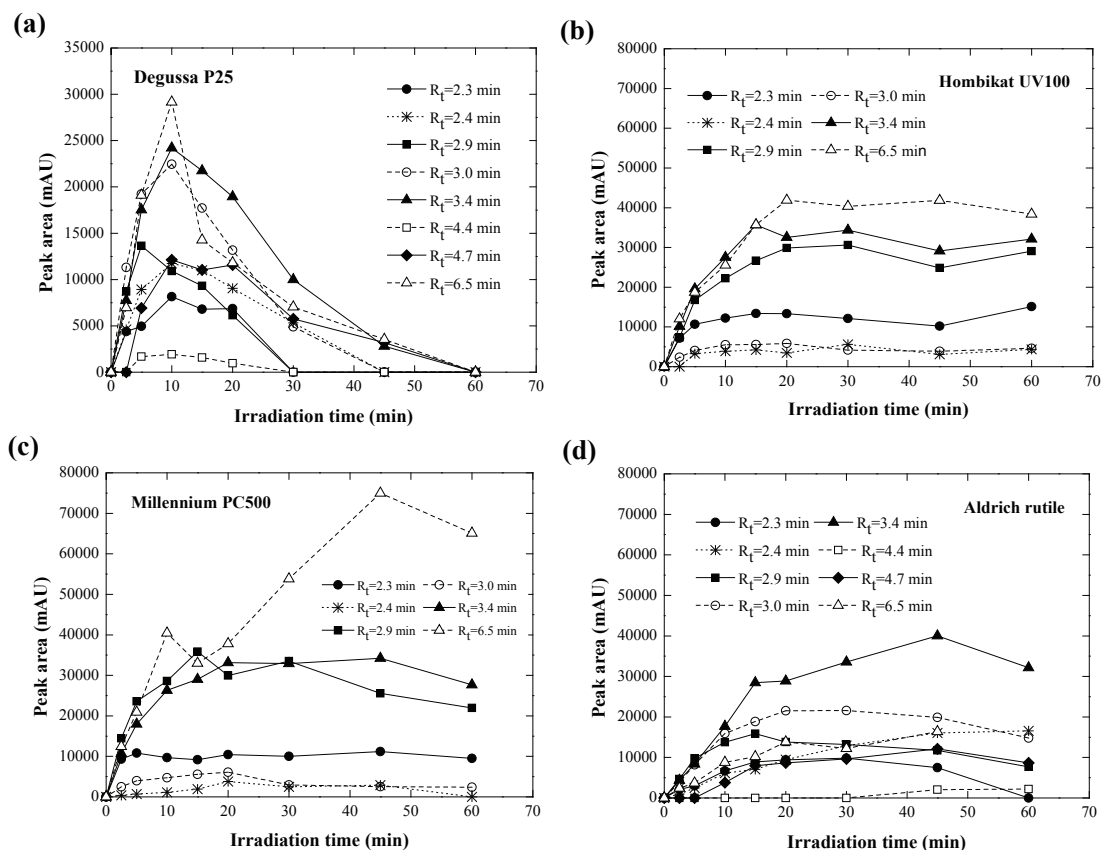


**Fig. 4.6.** Evolution of intermediates over a course of 60 min of photocatalytic degradation of atenolol by using different type of photocatalyst: (a) Degussa P25; (b) Hombikat UV100; (c) Millennium PC500; (d) Aldrich rutile. Experimental conditions: [ATL] = 37.6  $\mu\text{M}$ ; [photocatalyst] = 2.0  $\text{g L}^{-1}$ ; solution pH = 6.8. Peak areas of the intermediates were obtained according to HPLC chromatogram with detection wavelength of their maximum absorbance. Sample separation was performed on a Hypersil C18 column (5  $\mu\text{m}$ , 125 mm  $\times$  4.0 mm, i.d.). The eluent was a mixture of acetonitrile/ $\text{H}_2\text{O}$  (5/95, v/v, pH = 3.0 buffer) with a flow rate of 0.8  $\text{mL min}^{-1}$ .

This finding is especially desirable since P25 could effectively destruct mother compound as well as intermediates. However, when other photocatalysts were used, degradation of intermediates processed very slowly (Fig. 4.6(b) - (d)). Indeed, accumulation of some intermediates during the

---

same time period can be observed, indicating the lower efficiency for these photocatalysts to destroy ATL intermediates. Six intermediates were both found as different TiO<sub>2</sub> photocatalysts were used. However, two intermediates at retention time 4.4 min and 4.7 min, respectively, were not observed in anatase TiO<sub>2</sub> suspensions whereas found in P25 and Aldrich rutile suspensions. Moreover, two intermediates corresponding to retention time 2.4 min and 3.0 min, appeared to have much higher concentration in rutile suspension than in anatase suspension. Further research should be carried out for elucidating such discrepancy.

#### 4.1.6. Identification of organic intermediates

Our HPLC chromatogram of the irradiated sample revealed some new peaks compared to non-irradiated sample, which was indicative of the formation of intermediates. In order to determine as much intermediates as possible, a mixture sample composed of aliquots withdrawn at different irradiation times from photocatalysis process was analyzed by HPLC-MS/MS as described before. At least nine peaks corresponding to intermediates were observed in the total ion chromatogram (TIC). Among them, eight products appeared quite early than mother compound, suggesting most of the intermediates were more hydrophilic than ATL. The overall fragment ions of ATL intermediates, retention time as well as proposed structure are summarized in Table S3 (Supplementary Material). Among these intermediates, *m/z* 134 and *m/z* 152 appeared to be the ether chain cleavage products 3-(isopropylamino)propane-1,2-diol and *p*-hydroxyphenylacetamide, respectively. Intermediate *m/z* 238 was assigned to be 4-[2-hydroxy-3-(isopropylamino)propoxy] benzaldehyde and *m/z* 254 was proposed to be the hydroxylation products of *m/z* 238 due to an excessive 16 amu addition. Assignment of these two intermediates is further supported by the study of photo-Fenton mediated ATL degradation.<sup>41</sup> A series of intermediate peaks corresponding to the molecular weight of oxygenated analogue of ATL (*m/z* 283) in positive ion mode were observed. An additional 16 amu with respect to protonated ATL (*m/z* 267) indicated these compounds likely are the isomers of mono-hydroxylated ATL. Similarly, *m/z* 299 was identified as di-hydroxylated ATL. In order to determine the position of the addition (aromatic or the side chain), ATL mass fragmentation spectra were firstly compared to the photoproducts mass obtained during product ion scan analysis. These compounds exhibited the same loss fragment ion (*m/z* 116) as ATL, which corresponded to the characteristic loss of ether chain  $[\text{CH}_2\text{CH}(\text{OH})\text{CH}_2\text{NHCH}(\text{CH}_3)_2]^+$ . This observation suggests that HO radical addition most likely

occur on benzene ring instead of ether chain.

**Table 4.1 Frontier electron densities on atoms of ATL calculated by using Gaussian 09 program at the B3LYP/6-311+G\* level.**

Atom (number)	$2FED_{HOMO}^2$	$FED_{HOMO+}^2$	Atom (number)	$2FED_{HOMO}^2$	$FED_{HOMO+}^2$
		$FED_{LUMO}^2$			$FED_{LUMO}^2$
1C	0.0582	<b>0.3368</b>	11N	0.0025	0.0023
2C	0.2111	0.1317	12C	0.0025	0.0002
3C	0.0281	<b>0.2522</b>	13C	0.0002	0.0001
4C	0.0846	<b>0.3336</b>	14O	0.0002	0.0013
5C	0.1096	0.0601	15C	0.0943	0.0712
6C	0.0777	<b>0.2617</b>	16C	0.0477	0.0279
7O	0.1968	0.0985	17N	0.0469	0.0287
8C	0.0046	0.0057	18O	0.1894	0.0967
9C	0.0048	0.0067	19C	0.0001	0.0000
10C	0.0037	0.0143			

In order to correctly characterize these mono-hydroxylated compounds (positions of hydroxylation), isolation of each compound using preparative chromatograph followed by  $^1\text{H-NMR}$  analysis is necessary.<sup>42</sup> Another simple and alternative method is theoretical calculations.<sup>43</sup> In the present study, the frontier electron densities (FEDs) of ATL were calculated to predict the reaction sites for  $\text{HO}\cdot$  attack as summarized in Table 4.1. According to Frontier Orbital Theory, positions with higher values of  $2FED_{HOMO}^2$  are more easily subject to electron extraction, while positions with higher value of  $FED_{HOMO+}^2$   $FED_{LUMO}^2$  are more susceptible to  $\text{HO}\cdot$  attack.<sup>44</sup> As shown in Table 4.1, 1C, 4C, 6C and 3C sites have the highest  $FED_{HOMO+}^2$   $FED_{LUMO}^2$  value, which is indicative of the high possibility of mono-hydroxylation formation with  $\text{HO}\cdot$  attack occurring at aromatic ring. Our prediction of the possible sites for hydroxyl addition based on FEDs calculation is in satisfactory agreement with the LC-MS/MS results.

#### 4.1.7. Elucidation of photocatalytic degradation pathways

Based on the proposed molecular structure of photoproducts, possible  $\text{TiO}_2$ -induced

photodegradation pathways of ATL are proposed as illustrated in Fig. 4.7. As can be seen, three major pathways are involved in the photocatalytic degradation of ATL.

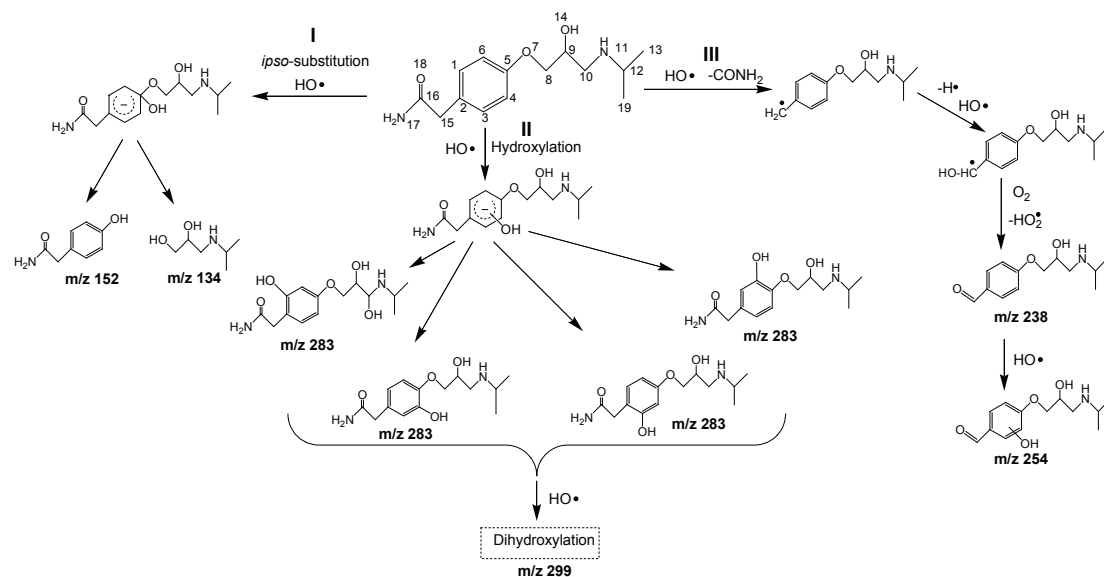


**Fig. 4.7. Possible photocatalytic degradation pathways of atenolol in illuminated aqueous TiO<sub>2</sub> suspensions.**

- (i) Pathway I is initiated by HO• attack on *ipso* aromatic C atom, as so-called *ipso*-substitution, resulting in resonance-stabilized carbon-centered radicals. Subsequent reaction of *O*-dealkylation leads to ether side chain cleavage, giving rise to 3-(isopropylamino)propane-1,2-diol (m/z 134) and *p*-hydroxyphenylacetamide (m/z 152).<sup>25</sup> It is noteworthy that *p*-hydroxyphenylacetamide was also detected in UVA-UVB photolysis,<sup>45</sup>  $\gamma$ -radiolysis,<sup>25</sup> electrochemical degradation,<sup>46</sup> photoelectron-Fenton<sup>47</sup> as well as photocatalysis.<sup>15,48</sup>
- (ii) Pathway II represents the electrophilic adduct reaction with HO• attacking on mother compound, resulting in the formation of mono- and di-hydroxylation products. Our LC-MS/MS analysis and calculated frontier electron densities of ATL on basis of the Frontier Orbital Theory confirmed that aromatic ring is the most likely site for HO• attack. Thus, it is most likely that the mono-hydroxylated compounds are initiated by the addition of HO• to benzene ring, leading to the formation of a hydroxycyclohexadienyl radical. Subsequent O<sub>2</sub> addition to hydroxycyclohexadienyl radical and the elimination of HO<sub>2</sub>• eventually produce these mono-hydroxylated intermediates (m/z 283).<sup>25</sup> Surprisingly, only one di-hydroxylated ATL (m/z 299) was detected, which was most probably due to ring opening and/or side chain cleavage after mono-hydroxylation rather

---

than further hydroxylation, generating low molecular weight intermediates or photoproducts such as aliphatic carboxylic acids.

(iii) Pathway III is initiated by the loss of  $\text{CONH}_2\cdot$  from acetamide function group under  $\text{HO}\cdot$  attack. Further H abstraction and  $\text{HO}\cdot$  addition lead to the formation of a carbon-centered radical, which is finally oxidized by molecular oxygen, producing 4-[2-hydroxy-3-(isopropylamino)propoxy] benzaldehyde ( $m/z$  238). The +2 oxidation state of C in amide group should favor the  $\text{HO}\cdot$  attack at this atom, generating  $\text{CONH}_2\cdot$  radical.<sup>41</sup>  $\text{CONH}_2\cdot$  radical could transfer to carbamic acid, which eventually goes through photo-assisted hydrolysis and nitrogen is released as  $\text{NH}_4^+$ .<sup>41</sup> Radjenović et al. studied the homogeneous photocatalysis of ATL by photo-Fenton and also detected intermediate product  $m/z$  238.<sup>41</sup> The ketone structure of  $m/z$  238 is also evidenced by the fact that strong absorbance at  $\lambda = 300$  nm was observed in HPLC-DAD spectrum due to its chromophore characteristic. Further  $\text{HO}\cdot$  electrophilic attack on  $m/z$  238 resulted in hydroxylated benzaldehyde derivative ( $m/z$  254).<sup>49</sup>

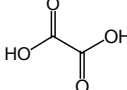
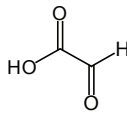
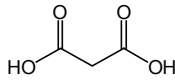
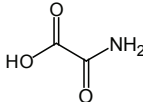
#### 4.1.8. Identification of carboxylic acids

Further oxidation of intermediates and photoproducts during photocatalysis usually lead to ring opening, generating a series of carboxylic acids with lower molecular weight before complete mineralization.<sup>17,42</sup> In present study, the carboxylic acids formed during photocatalysis were identified by ion exchange chromatography by comparison with authentic standards (see Table 4.2).

As depicted in Table 4.2, a total five carboxylic acids, i.e., oxalic, glyoxylic, malonic, oxamic and formic acid, were identified as photoproducts of ATL photocatalytic degradation. The formation of malonic acid is believed to arise from the transformation of malic acid, which is an important intermediate after benzene opening but was not detected in present study<sup>17</sup>. Further destruction of malonic acid led to the generation of lower molecular weight organic acid, such as glyoxylic acid<sup>17</sup>. As discussed above, acetamide group in ATL was subjected to  $\text{CONH}_2\cdot$  loss and  $\text{O}_2$  oxidation, resulting in the formation of ketone moiety, thus, the oxamic acid should originate from the ether chain. It is most likely that further oxidation of 3-(isopropylamino)propane-1,2-diol under  $\text{HO}\cdot$  attack produces oxamic acid. Oxidation of oxamic acid can produce glyoxylic and oxalic acid,<sup>21</sup> which were both confirmed by our HPLC-UV chromatogram. Oxalic acid can be

mineralized to CO<sub>2</sub> either directly by photo-holes oxidation through photo-Kolbe mechanism or indirectly through the formation of formic acid.<sup>17</sup> A tentative mechanism for the formation of carboxylic acids is proposed in Fig. S7 (Supplementary Material).

**Table 4.2 Identification of carboxylic acids arising from photocatalytic degradation of atenolol.**

Retention time (min) <sup>a</sup>	Compounds <sup>b</sup>	Structure
7.4	oxalic	
9.4	glyoxylic	
10.6	malonic	
11.4	oxamic	
13.1	NI <sup>c</sup>	NI
13.8	formic	
14.5	NI	NI

<sup>a</sup> Retention time was recorded according to HPLC-UV chromatogram;

<sup>b</sup> Carboxylic acids were identified by comparing their retention time with those authentic standards;

<sup>c</sup> NI=Not identified.

#### 4.1.9. Mineralization

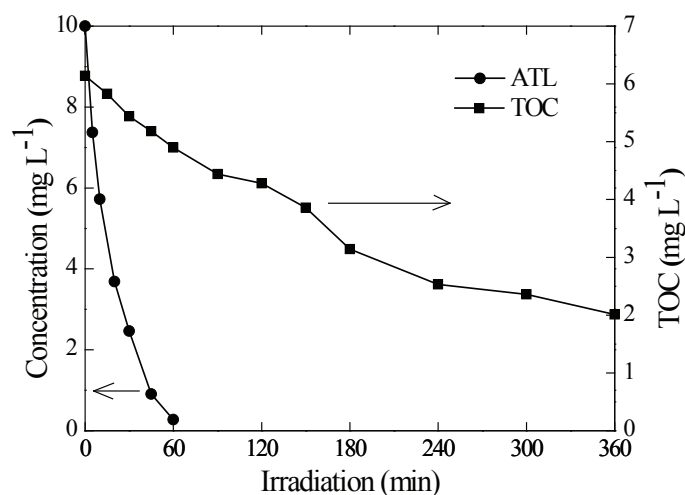


**Fig. 4.8. Variation of concentration (●) and total organic carbon (■) during atenolol photocatalytic degradation. Degussa P25 was used as photocatalyst. Experimental conditions: [TiO<sub>2</sub>] = 2.0 g L<sup>-1</sup>; [ATL] = 10 mg L<sup>-1</sup>; pH = 6.8.**

The photocatalytic degradation of organic pollutants usually leads to the decomposition of

---

structure and eventually to the mineralization to CO<sub>2</sub> and H<sub>2</sub>O, which can be visualized by the decrease of TOC. To assess the extent of mineralization during photocatalytic degradation of ATL, TOC was measured as shown in Fig. 4.8. It was observed that TOC removal processed much more slowly compared to the degradation of ATL. This finding indicates the formation of more stable intermediates toward photo-oxidation.<sup>41</sup> However, approximately 70% TOC was removed after 360 min irradiation, implying complete mineralization could be obtained at a longer time of photocatalysis.

#### 4.2. Conclusions

Photocatalysis was found to be efficient in eliminating ATL in aqueous solution. Disappearance of ATL during photocatalysis using P25 TiO<sub>2</sub> as catalyst followed pseudo-first-order kinetics, as usually found in heterogeneous photocatalysis at low concentration. HO· was determined to be the principal reactive species responsible for a rapid degradation of ATL in illuminated TiO<sub>2</sub> suspensions. Degussa P25 showed the highest photocatalytic activity for oxidizing ATL as well as intermediates compared to Aldrich rutile, Millennium PC500 and Hombikat UV100. TiO<sub>2</sub>-induced ATL photodegradation pathways in Milli-Q water included ether chain cleavage, hydroxylation and the formation of benzaldehyde derivative. Frontier electron densities (FEDs) calculation revealed that mono-hydroxylation was formed with HO· adduct mainly occurring on aromatic ring. Oxalic, glyoxylic, malonic, oxamic and formic acid, were detected during photocatalysis process. TOC decreased much more slowly compared with ATL degradation, but complete mineralization could be obtained with longer irradiation time.

The obtained results in this study not only clearly showed that the presence of constituents in natural waters, e.g., bicarbonate and humic substance, could have a huge impact on the photocatalytic degradation efficiency of the parent compound, but also the change in water composition could result in a variation of transformation products distribution as well as the formation and transformation rate of these organic intermediates (e.g., Milli-Q water vs. river water).

It should be noted that environmentally relevant ATL concentrations are generally lower than those used in the present study. Therefore, extrapolation of the data presented here to a realistic situation should be done with caution, because water matrix effects on photocatalytic degradation of extremely low concentration contaminants remain to be studied. Future research should focus

---

on the reaction pathway difference and toxicological effect of ATL photocatalytic degradation in different water matrix.

### 4.3. Reference

(1) Daughton, C. G.; Ternes, T. A. Pharmaceuticals and personal products in the environment: agents of subtle change? *Environ. Health Perspect.* **1999**, 107, 907-938.

Ternes, T.A.; Meisenheimer, M.; Mcdowell, D. Removal of pharmaceuticals during drinking water treatment. *Environ. Sci. Technol.* **2002**, 36, 3855-3863.

(2) Andreatti, R.; Raffaele, M.; Nicklas, P. Pharmaceuticals in STP effluents and their solar photodegradation in aquatic environment. *Chemosphere* **2003**, 50, 1319-1330.

(3) Vieno, N.M.; Härkki, H.; Tuhkanen, T.; Kronberg, L. Occurrence of pharmaceuticals in river water and their elimination in a pilot-scale drinking water treatment plant. *Environ. Sci. Technol.* **2007**, 41, 5077-5084.

(4) Kolpin, D. W.; Furlong, E. T.; Meyer, M. T.; Thurman, E. M.; Zaugg, S. T.; Barber, L. B.; Buxton, H. T. Pharmaceuticals, hormones, and other organic wastewater contaminants in U.S. streams, 1999-2000: a national reconnaissance. *Environ. Sci. Technol.* **2002**, 36, 1202-1211.

(5) Hilton, M. J.; Thomas, K. V. Determination of selected human pharmaceutical compounds in effluent and surface water samples by high-performance liquid chromatography-electrospray tandem mass spectrometry. *J. Chromatogr. A* **2003**, 1015, 129-141.

(6) Snyder, S. A.; Benotti, M. J.; Trenholm, R. A.; Vanderford, B. J.; Holady, J. C.; Stanford, B. D. Pharmaceuticals and Endocrine Disrupting Compounds in US Drinking Water. *Environ. Sci. Technol.* **2009**, 43, 597-603.

(7) U. Borchard. Pharmacological properties of beta-adrenoceptor blocking drugs. *J. Clin. Basic. Cardiol.* **1998**, 1, 5-9.

(8) Alder, A. C.; Schaffner, C.; Majewsky, M.; Klasmeier, J.; Fenner, K. Fate of  $\beta$ -blocker human pharmaceuticals in surface water: comparison of measured and simulated concentrations in the Glatt Valley Watershed. *Water Res.* **2010**, 44, 936-948.

(9) Huggett, D. B.; Khan, I. A.; Foran, C. M. Determination of beta-adrenergic receptor blocking pharmaceuticals in United States wastewater effluent. *Environ. Pollut.* **2003**, 121, 199-205.

(10) Maurer, M.; Escher, B.I.; Richle, P.; Schaffner, C.; Alder, A.C. Elimination of beta-blockers in sewage treatment plants. *Water Res.* **2007**, 41, 1614-1622.

- 
- (11) Pomati, F.; Castiglioni, S.; Zuccato, E.; Fanelli, R.; Vigetti, D.; Rossetti, C.; Calamari, D. Effects of a complex mixture of therapeutic drugs at environmental levels on human embryonic cells. *Environ. Sci. Technol.* **2006**, *40*, 2442-2447.
- (12) Della-Greca, M.; Iesce, M. R.; Pistillo, P.; Previtera, L.; Temussi, F. Unusual products of the aqueous chlorination of atenolol. *Chemosphere* **2009**, *74*, 730-734.
- (13) Hapeshi, E.; Achilleos, A.; Vasquez, M. I. Drugs degrading photocatalytically: kinetics and mechanisms of ofloxacin and atenolol removal on titania suspensions. *Water Res.* **2010**, *44*, 1737-1746.
- (14) Yang, H.; An, T.; Li, G. Y.; Song, W.; Cooper, W. J.; Luo, H.; Guo, X. Photocatalytic degradation kinetics and mechanism of environmental pharmaceuticals in aqueous suspension of TiO<sub>2</sub>: a case of  $\beta$ -blockers. *J. Hazard. Mater.* **2010**, *179*, 834-839.
- (15) Gaya, U. I.; Abdullah, A. H. Heterogeneous photocatalytic degradation of organic contaminants over titanium dioxide: A review of fundamentals, progress and problems. *J. Photochem. Photobiol. C: Photochem. Rev.* **2008**, *9*, 1-12.
- (16) Herrmann, J.-M. Heterogeneous photocatalysis: fundamentals and applications to the removal of various types of aqueous pollutants. *Catal. Today* **1999**, *53*, 115-129.
- (17) Lair, A.; Ferronato, C.; Chovelon, J.-M.; Herrmann, J.-M. Naphthalene degradation in water by heterogeneous photocatalysis: An investigation of the influence of inorganic anions. *J. Photochem. Photobiol. A: Chem.* **2008**, *193*, 193-203.
- (18) Sirtori, C.; Agüera, A.; Gernjak, W. Effect of water-matrix composition on trimethoprim solar photodegradation kinetics and pathways, *Water Res.* **2010**, *44*, 2735-2744.
- (20) Ryu, J.; Choi, W. Substrate-specific photocatalytic activities of TiO<sub>2</sub> and multiactivity test for water treatment application. *Environ. Sci. and Technol.* **2008**, *42*, 294-300.
- (21) Yang, L.; Yu, L. E.; Ray, M. B. Photocatalytic oxidation of paracetamol : dominant reactants, intermediates, and reaction mechanism. *Environ. Sci. Technol.* **2009**, *43*, 460-465.
- (22) Buxton, G. V.; Greenstock, C. L.; Helman, W. P.; Ross, A. B. Critical review of rate constants of hydrate electrons, hydrogen atoms and hydroxyl radicals (OH $\cdot$ /O $\cdot^-$ ) in aqueous solution. *J. Phys. Chem. Ref. Data* **1988**, *17*, 513-886.
- (23) Chen, Y.; Yang, S.; Wang, K.; Lou, L. Role of primary active species and TiO<sub>2</sub> surface characteristic in UV-illuminated photodegradation of Acid Orange 7. *J. Photochem. Photobiol. A:*

---

*Chem.* **2005**, 172, 47-54.

(24) Ishibashi, K.; Fujishima, A.; Watanabe, T.; Hashimoto, K. Quantum yields of active oxidative species formed on TiO<sub>2</sub> photocatalyst. *J. Photochem. Photobiol. A: Chem.* **2000**, 134, 139-142.

(25) Song, W.; Cooper, W. J.; Mezyk, S. P.; Greaves, J.; Peake, B. M. Free radical destruction of  $\beta$ -blockers in aqueous solution. *Environ. Sci. Technol.* **2008**, 42, 1256-1261.

(26) Ji, Y.; Zeng, C.; Ferronato, C.; Chovelon, J.-M.; Yang, X. Nitrate-induced photodegradation of metenolol in aqueous solution: Kinetics, toxicity and degradation pathways. *Chemosphere* **2012**, 88, 644-649.

(27) (9) Khodja, A. A.; Lavedrine, B.; Richard, C.; Sehili, T. Photocatalytic degradation of metoxuron in aqueous suspensions of TiO<sub>2</sub>. analytical and kinetic studies. *Int. J. Photoenergy* **2002**, 4, 147-151.

(28) Haque, M. M.; Muneer, M.; Bahnemann, D. W. Semiconductor-mediated photocatalyzed degradation of a herbicide derivative, chlorotoluron, in aqueous suspensions. *Environ. Sci. Technol.* **2006**, 40, 4765-4770.

(29) Lam, M. W.; Tantuco, K.; Mabury, S. A. Photofate: a new approach in accounting for the contribution of indirect photolysis of pesticides and pharmaceuticals in surface water. *Environ. Sci. Technol.* **2003**, 37, 899-907.

(30) Huang, J. P.; Mabury, S. A. A new method for measure carbonate radical reactivity toward pesticides. *Environ. Toxicol. Chem.* **2000**, 19, 1501-1507.

(31) Huang, J.; Mabury, S.A.; The role of carbonate radical in limiting the persistence of sulfur-containing chemicals in sunlit natural waters. *Chemosphere* **2000**, 41, 1775-1782.

(32) Hu, L.; Flanders, P. M.; Miller, P. L.; Strathmann, T. J. Oxidation of sulfamethoxazole and related antimicrobial agent by TiO<sub>2</sub> photocatalysis. *Water Res.* **2007**, 41, 2612-2626.

(33) Corin, N.; Backlund, P.; Kulovaara, M. Degradation products formed during UV-irradiation of humic water. *Chemosphere* **1996**, 33, 245-255.

(34) Doll, T. E.; Frimmel, F. H. Photocatalytic degradation of carbamazepine, clofibric acid and iomeprol with P25 and Hombikat UV 100 in the presence of natural organic matter (NOM) and other organic water constituents. *Water Res.* **2005**, 39, 403-411.

(35) Lin, C.; Lin, K.-S. Photocatalytic oxidation of toxic organohalides with TiO<sub>2</sub>/UV: the effects of humic substances and organic mixtures. *Chemosphere* **2007**, 66, 1872-1877.

- 
- (36) Epling, G. A.; Lin, C. Investigation of retardation effects on the titanium dioxide photodegradation system. *Chemosphere* **2002**, 46, 937-944.
- (37) Garbin, J. R.; Milori, D. M. B. P.; Simões, M. L.; Silva, W. T. L.; Neto, L. M. Influence of humic substances on the photolysis of aqueous pesticide residues. *Chemosphere* **2007**, 66, 1692-1698.
- (38) Abdullah, M.; Low, G. K.-C.; Matthews, R. W. Effects of common inorganic anions on rates of photocatalytic oxidation of organic carbon over illuminated titanium dioxide. *J. Phys. Chem.* **1990**, 94, 6820-6825.
- (39) Guillard, C.; Lachheb, H.; Houas, A.; Ksibi, M.; Elaloui, E.; Herrmann, J.-M. Influence of chemical structure of dyes, of pH and of inorganic salts on their photocatalytic degradation by TiO<sub>2</sub> comparison of the efficiency of powder and supported TiO<sub>2</sub>. *J. Photochem. Photobiol. A: Chem.* **2003**, 158, 27-36.
- (40) Enríquez, R.; Agrios, A.G.; Pichat, P. Probing multiple effects of TiO<sub>2</sub> sintering temperature on photocatalytic activity in water by use of a series of organic pollutant molecules. *Catal. Today* **2007**, 120, 196-202.
- (41) Radjenović, J.; Sirtori, C.; Petrović, M.; Barceló, D.; Malato, S. Solar photocatalytic degradation of persistent pharmaceuticals at pilot-scale: kinetics and characterization of major intermediate products. *Appl. Catal. B: Environ.* **2009**, 89, 255-264.
- (42) Sleiman, M.; Conchon, P.; Ferronato, C.; Chovelon, J.-M. Iodosulfuron degradation by TiO<sub>2</sub> photocatalysis: Kinetic and reactional pathway investigations. *Appl. Catal. B: Environ.* **2007**, 71, 279-290.
- (43) Carrier, M.; Guillard, C.; Besson, M.; Bordes, C.; Cheemette, H. Photocatalytic degradation of diuron: Experimental analyses and simulation of HO· radical attacks by density functional theory calculations. *J. Phys. Chem. C* **2009**, 113, 6365-6374.
- (44) An, T.; Yang, H.; Li, G.; Song, W.; Cooper, W. J.; Ne, X. Kinetics and mechanism of advanced oxidation process (AOPs) in degradation of ciprofloxacin in water. *Appl. Catal. B: Environ.* **2010**, 94, 288-294.
- (45) Andrisano, V.; Gotti, R.; Leoni, A.; Cavrini, V. Photodegradation studies on atenolol by liquid chromatography. *J. Pharm. Biomed. Anal.* **1999**, 21, 851-857.
- (46) Sirés, I.; Oturan, N.; Oturan, M. A. Electrochemical degradation of  $\beta$ -blockers. Studies on

---

single and multicomponent synthetic aqueous solutions. *Water Res.* **2010**, 44, 3109-3120.

(47) Isarain-Chávez, E.; Arias, C.; Cabot, P. L.; Centellas, F.; Rodríguez, R. M.; Garrido, J. A.; Brillas, E. Mineralization of the drug  $\beta$ -blocker atenolol by electro-Fenton and photoelectron-Fenton using an air-diffusion cathode for H<sub>2</sub>O<sub>2</sub> electrogeneration combined with a carbon-felt cathode for Fe<sup>2+</sup> regeneration. *Appl. Catal. B: Environ.* **2010**, 96, 361-369.

(48) Medana, C.; Calza, P.; Carbone, F.; Pelizzetti, E.; Hidaka, H.; Baiocchi, C. Characterization of atenolol transformation products on light-activated TiO<sub>2</sub> surface by high-performance liquid chromatography/high-resolution mass spectrometry. *Rapid Commun. Mass Spectrom.* **2008**, 22, 301-303.

(49) Zeng, C.; Ji, Y.; Zhou, L.; Zhang, Y.; Yang, X. The role of dissolved organic matters in the aquatic photodegradation of atenolol. *J. Hazard. Mater.* **2012**, 239-240, 340-347.

#### 4.4. Supplementary Material

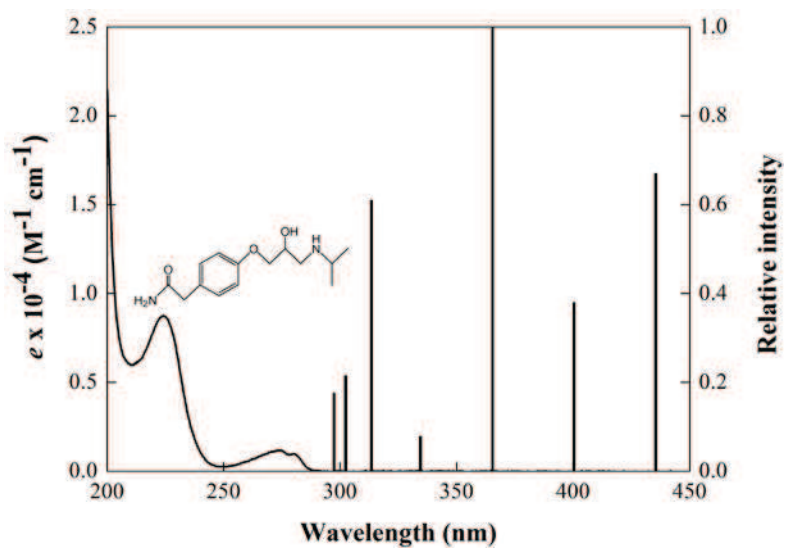


Fig. S1. UV-Vis absorbance spectrum of atenolol and emission spectrum of HPK lamp ( $[\text{ATL}] = 40 \mu\text{M}$ ,  $\text{pH} = 6.8$ ).

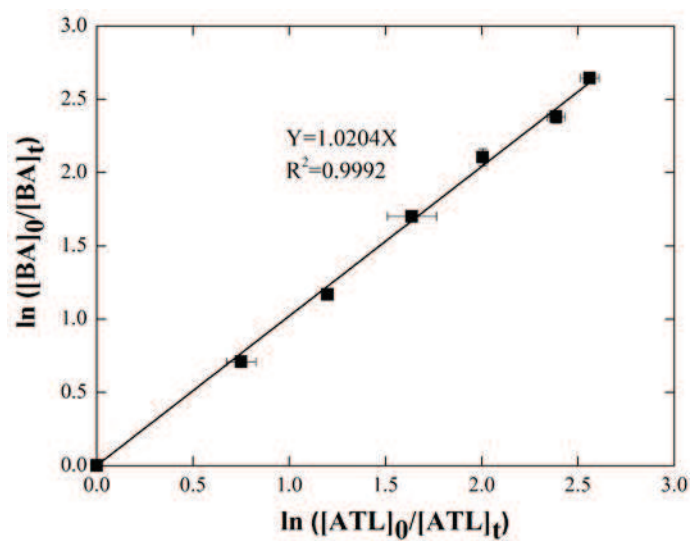


Fig. S2. Determination of second order rate constant of atenolol reacting with  $\text{HO}\cdot$  by competition kinetics.

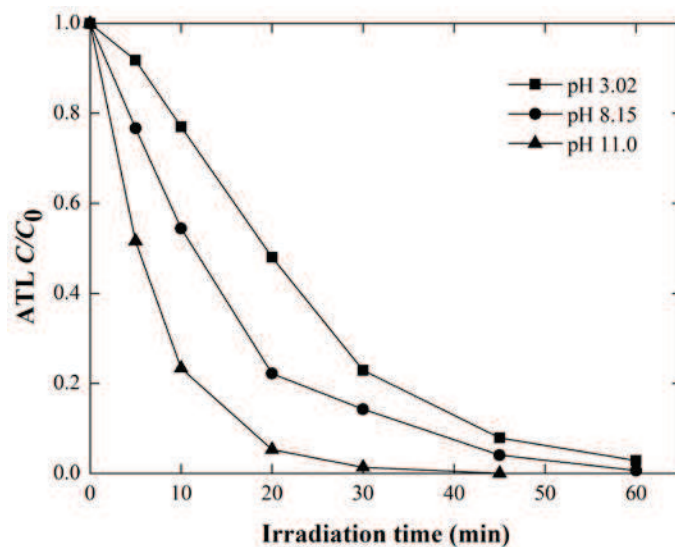


Fig. S3. Effect of solution pH on photocatalytic degradation of atenolol: (■) pH = 3.02; (●) pH = 8.15; (▲) pH = 11.0. Experimental conditions: Degussa P25 was used as photocatalyst;  $[\text{TiO}_2] = 2.0 \text{ g L}^{-1}$ ;  $[\text{ATL}] = 37.6 \text{ }\mu\text{M}$ .

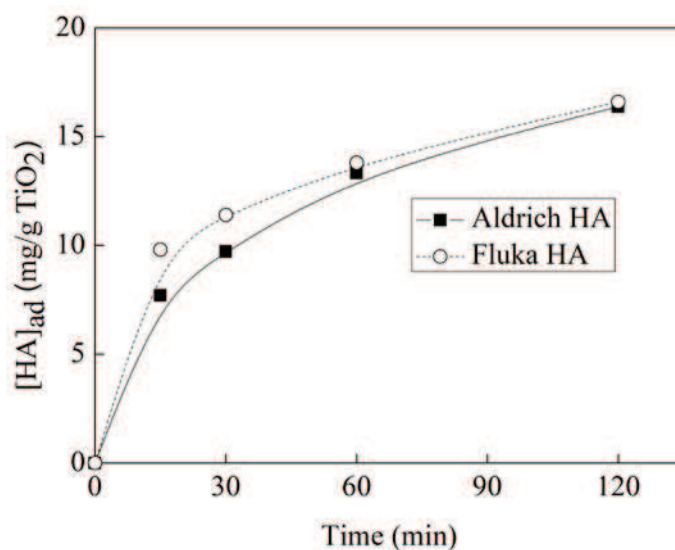


Fig. S4. The adsorption mass (mg / g  $\text{TiO}_2$ ) of humic acid (HA) on  $\text{TiO}_2$  at various time: (■) Aldrich HA; and (○) Fluka HA.  $[\text{HA}]_0 = 60 \text{ mg L}^{-1}$ ,  $[\text{TiO}_2] = 2.0 \text{ g L}^{-1}$ . pH = 6.8. The TOC content of the HAs in solutions with  $\text{TiO}_2$  particle filtered was measured by a SHIMADZU 5050A TOC analyzer. HA concentration ( $\text{mg L}^{-1}$ ) was calculated based on a calibration curve obtained by plotting measured TOC values via standard HA concentrations.

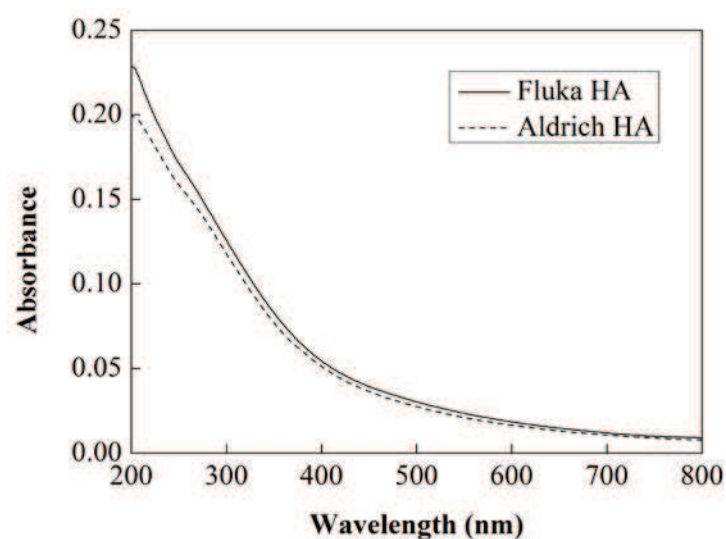


Fig. S5. UV-Visible absorbance spectra of the humic acid solutions: (—) Fluka humic acid; and (---) Aldrich humic acid. [HA] = 6 mg L<sup>-1</sup>.

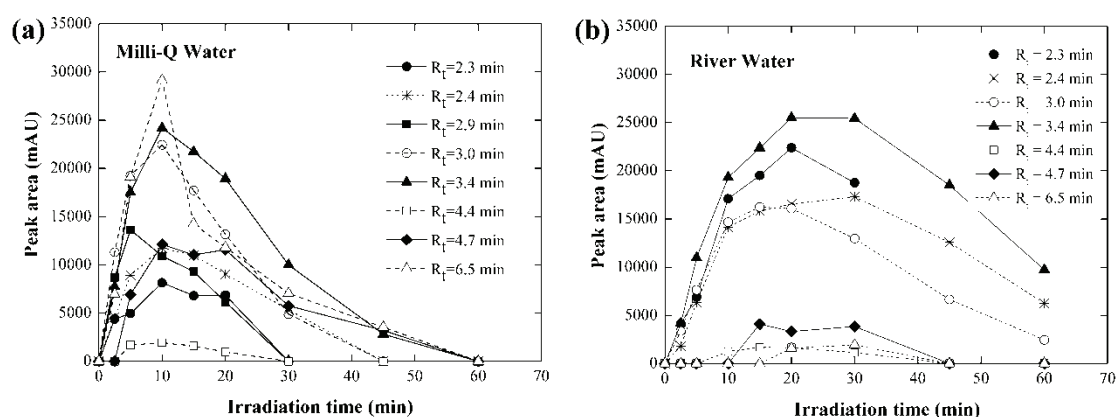


Fig. S6. Evolution of major phototransformation intermediates as a function of irradiation time in Milli-Q water (a) and River water (b). Degussa P25 was used as photocatalyst. Experimental conditions: [ATL] = 37.6  $\mu$ M; [TiO<sub>2</sub>] = 2.0 g L<sup>-1</sup>; Milli-Q water pH = 7.0; River water pH = 8.05. Peak areas of the intermediates were obtained according to HPLC chromatogram with detection wavelength of their maximum absorbance. Sample separation was performed on a Hypersil C18 column (5  $\mu$ m, 125 mm  $\times$  4.0 mm, i.d.). The eluent was a mixture of acetonitrile/H<sub>2</sub>O (5/95, v/v, pH = 3.0 buffer) with a flow rate of 0.8 mL min<sup>-1</sup>.

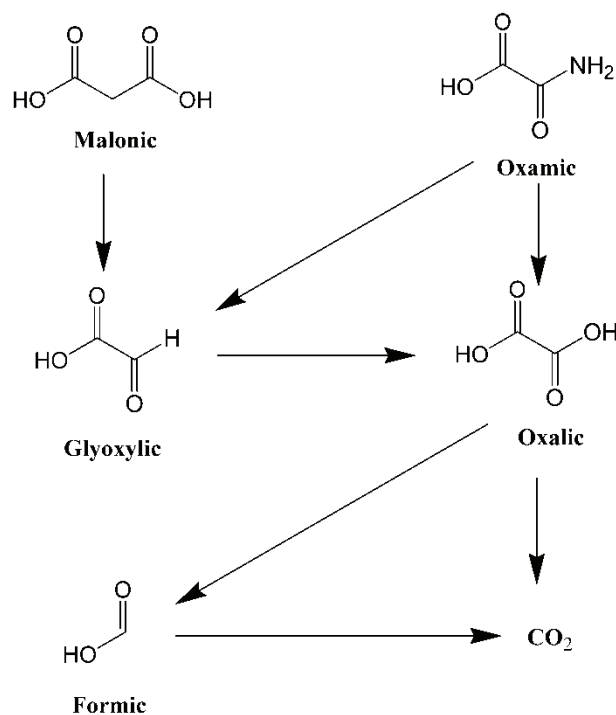


Fig. S7. Proposed scheme for the formation of carboxylic acids.

**Table S1** Composition of Rhône River matrix

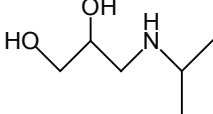
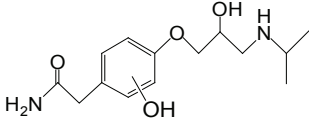
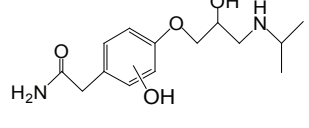
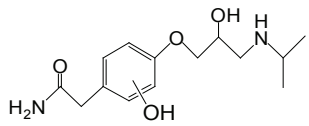
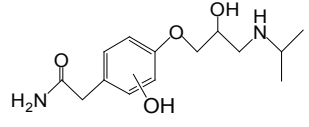
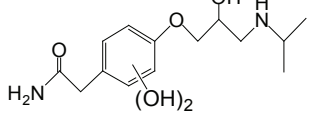
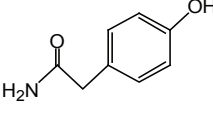
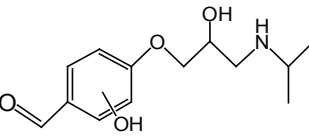
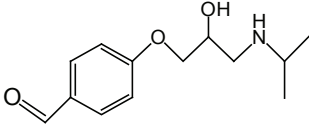
Species <sup>a</sup>	Concentration (mM)
HCO <sub>3</sub> <sup>-</sup>	2.23
Cl <sup>-</sup>	0.29
SO <sub>4</sub> <sup>2-</sup>	0.36
NO <sub>3</sub> <sup>-</sup>	0.08
Na <sup>+</sup>	0.28
K <sup>+</sup>	0.053
Ca <sup>2+</sup>	1.6
Mg <sup>2+</sup>	0.24

<sup>a</sup> Analyzed by ion chromatography

**Table S2** Specification and characteristics of TiO<sub>2</sub> photocatalysts

Photocatalyst	Composition	Specific surface area BET (m <sup>2</sup> /g)	Particle size (nm)
Degussa P25	75% anatase + 25% rutile	50	21
Hombikat UV100	100% anatase	250	5
Millennium PC500	100% anatase	287	5-10
Aldrich rutile	100% rutile	3	750

**Table S3. Mass spectra data and proposed structure of photoproducts by LC-MS/MS analysis for a mixture irradiated sample of atenolol photocatalytic degradation.**

Retention Time (min)	Precursor ion (m/z)	MS/MS	Proposed structure
0.94	134	92, 74, 72	
0.92	283a	265, 116, 74, 72, 58	
1.17	283b	116, 74, 72, 58	
2.74	283c	265, 241, 206, 178, 116, 74, 72, 58	
3.20	283d	266, 116, 74, 56	
1.26	299	238, 161, 73	
3.80	152	107	
4.96	254	236, 177, 116, 105, 74, 72, 56	
8.46	238	196, 161, 149, 133, 74, 72, 56	

---

## Chapter 5 Photochemical degradation of sunscreen agent

### 2-phenylbenzimidazole-5-sulfonic acid in different water matrices

Sunscreens are widely used in personal care products (PCPs) in recent years as a result of growing concern about exposure to sunlight causing burns and skin cancer.<sup>1</sup> After usage, sunscreens are primarily released into the environment through wastewater treatment plant effluents (WWTPs) by washing off from the skin and clothes. Other sources, such as the excretion of human beings after the absorbance of the skin and metabolic activity may also contributed to their occurrence in natural environment.<sup>2,3</sup> Recently, the US Environmental Protection Agency regards sunscreens as environmental emerging contaminants because they are measurable in many aquatic ecosystems.<sup>4</sup> Several studies have demonstrated that organic sunscreens possess estrogenic properties and can behavior as endocrine disrupting chemicals (EDCs) in the environment.<sup>5-7</sup> Furthermore, phototransformation products of some kinds of sunscreens upon natural solar irradiation are shown to be even more toxic than their parent species, which can be a further danger to the biota in environment.<sup>7,8</sup> Therefore, the long-term and extensive use of sunscreens may cause irreversible adversity on the ecology system.

The sunscreen agent 2-phenylbenzimidazole-5-sulfonic acid (PBSA) is widely used in sunscreen formulations and cosmetics because of its strong absorption in the UVB region (see Fig. 1). It has also been approved by the U.S. Food and Drug Administration as an effective sunscreen ingredient based on its ability to prevent erythema.<sup>1</sup> The environmentally relevant level of PBSA has been reported to be 109 to 2679 ng L<sup>-1</sup>.<sup>9</sup> Recent studies have demonstrated that PBSA is capable of photo-generating reactive oxygen species (i.e., <sup>1</sup>O<sub>2</sub> and O<sub>2</sub><sup>•-</sup>) under UV irradiation and causing DNA damage.<sup>10</sup> For instance, Johnson Inbaraj et al. (2002) studied the photophysical and photochemical properties of PBSA and demonstrated that UV irradiation of PBSA generates a variety of free radicals and active oxygen species that may be involved in the photodamage of DNA.<sup>11</sup> Zhang et al. (2010) developed a computational method based on the density functional theory (DFT) to predict and evaluate the photodegradation behavior of PBSA and found that energy and electron transfer reactions of excited state PBSA (PBSA<sup>\*</sup>) could photogenerate <sup>1</sup>O<sub>2</sub> and O<sub>2</sub><sup>•-</sup>.<sup>12</sup> However, up to date, transformation and fate of this sunscreen in the environment is still largely unknown.

---

Photochemical degradation is believed to be an important factor influencing the environmental fate of aquatic contaminants. As sunscreens are designed to absorb solar energy, many of them are expected to be susceptible to photodegradation in sunlit surface waters.<sup>13</sup> Photodegradation of sunscreens can be catalogued as direct photolysis when their absorption spectra overlap with the solar emitting spectrum and indirect photolysis by reaction with reactive oxygen species, e.g. singlet oxygen ( $^1\text{O}_2$ ) and hydroxyl radical ( $\text{HO}\cdot$ ) from photosensitizers (i.e., nitrate, dissolved organic matter (DOM)). Direct photolysis is expected to be the dominant loss pathways for sunscreens degradation in natural surface waters. However, in extremely DOM- or nitrate-enriched waters where direct photolysis is retarded and large concentrations of reactive species (e.g.,  $^*\text{DOM}^3$ ,  $^1\text{O}_2$  and  $\text{HO}\cdot$ ) are formed, indirect photolysis could out-compete direct photolysis and be responsible for the major loss of sunscreens. Since the underlying mechanism of direct and indirect photolysis is disparate, it is possible that the related photodegradation products and pathways could also be different. However, little is known about the difference in photodegradation of PBSA caused by direct and indirect photolysis although direct photolysis pathways of PBSA have been proposed by Zhang et al. recently.<sup>12</sup>

In this work, we reported the photochemical degradation of PBSA in different water matrices. Especially, laser flash photolysis (LFP) experiments were performed to verify the involvement of transient species during direct photolysis. The second order rate constant for reaction of PBSA and  $\text{HO}\cdot$  and quantum yield of PBSA direct photolysis were determined to predict the photochemical fate of PBSA in the natural waters. Major degradation products arising from direct (i.e., in Milli-Q water) and indirect photolysis (i.e., in Milli-Q water in the presence of  $\text{NO}_3^-$ ) of PBSA were identified by liquid chromatography-mass spectrometry (LC-MS) analysis. Based on the above analysis, we proposed the possible degradation pathways of PBSA in aqueous solutions caused by direct and indirect photolysis. In particular, this study demonstrates that indirect photolysis of PBSA mediated by  $\text{HO}\cdot$  may occur through different pathways as compared to direct photolysis.

## 5.1. Results and discussion

### 5.1.1. Protonation states of PBSA and UV-vis absorption spectra

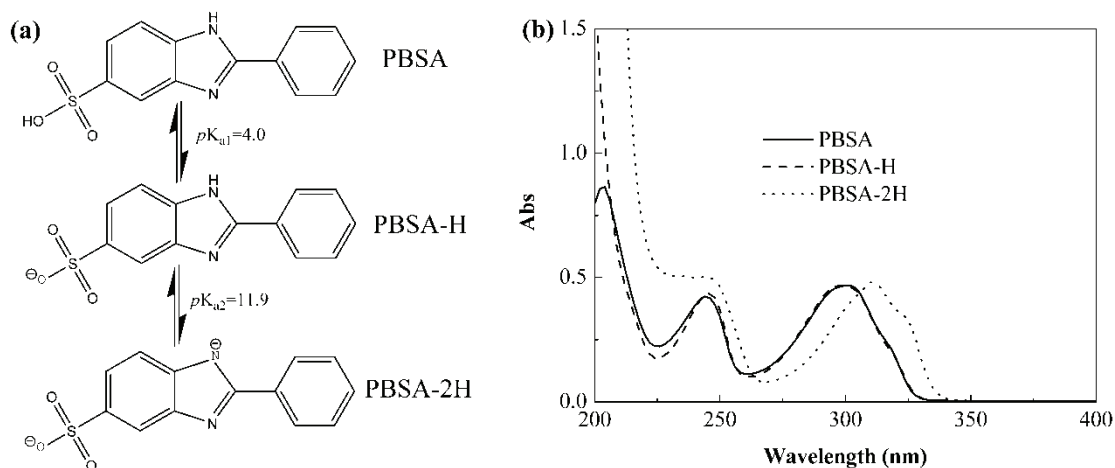


**Fig. 5.1. (a) Protonation states of PBSA and (b) UV-vis absorption spectrum of each PBSA species. [PBSA] = 10  $\mu$ M; PBSA = neutral form; PBSA-H = monoionic form; and PBSA-2H = dianionic form.**

PBSA possesses two  $pK_a$  (i.e.,  $pK_{a1} = 4.0$  and  $pK_{a2} = 11.9$ ) and thus the molecule is able to undergo two acid-base processes (Fig. 5.1(a)). Molecular form PBSA can only be expected to be dominant species in highly acidic aqueous solutions. Since the environmentally relevant pH normally ranges from 6 to 9, sulfonate monoanion form (PBSA-H) appears to be the primary species in most of the natural surface waters. PBSA and PBSA-H show similar UV-vis absorption spectrum and both of them exhibit a strong absorption band near 300 nm. In highly basic solution, this absorption is redshifted because of the dissociation of the imino group to form the dianion (PBSA-2H) (Fig. 5.1(b)).<sup>11</sup> PBSA have been shown to photochemically degrade in previous studies.<sup>12,14</sup> The redshift of PBSA-2H provides evidence that imidazole ring is the chromophore of PBSA that has a strong absorption near 300 nm and is responsible for the photochemistry of this compound.

### 5.1.2. LFP experiments to measure transient species of PBSA

The LFP experiments were carried out using a water solution of PBSA of 100 $\mu$ M. In Fig. 5.2, we report the time-dependence decay of the transient spectrum at different time scale after the laser pulse. A comparison of the decay rate of the two transients at 380 and 480 nm shows that the same specie is present at the two wavelengths. Moreover, LFP of argon saturated solution shows no differences with that in aerated medium. Supplementary experiments using acrylamide as triplet state quencher show a quite low dependence on the quencher concentration and a second order rate constant of  $(4.0 \pm 2.8) \times 10^7 \text{ M}^{-1} \text{ s}^{-1}$  was estimated. However, when NaI was used as radical cation quencher, the second order rate constant of transient at 380 nm was determined to be

$(1.5 \pm 0.1) \times 10^8 \text{ M}^{-1} \text{ s}^{-1}$  (inset in Fig. 5.2). Our LFP results showed that PBSA radical cation ( $\text{PBSA}^{+\bullet}$ ) was produced during PBSA excitation at 266 nm.  $\text{PBSA}^{+\bullet}$  was known to be generated through excited state of PBSA ( $\text{PBSA}^*$ ) based on previous reports.<sup>11,12</sup> Moreover, the broad absorbance of the transient at 750 nm was assigned to be solvated electron ( $e_{\text{aq}}^-$ ), which is consistent with previous reports.<sup>15,16</sup> The  $e_{\text{aq}}^-$  was most probably formed by excited singlet state of PBSA ( $^1\text{PBSA}^*$ ) via electron ejection process.<sup>15,16</sup> The presence of the transient signal at 380 nm ( $\text{PBSA}^{+\bullet}$ ) and at 750 nm ( $e_{\text{aq}}^-$ ) using high acrylamide concentration further confirmed that the formation of  $\text{PBSA}^{+\bullet}$  arising from  $^1\text{PBSA}^*$  after electron ejection. This conclusion was in line with a previous report of LFP study on phototransformation of carbaryl.<sup>15</sup>

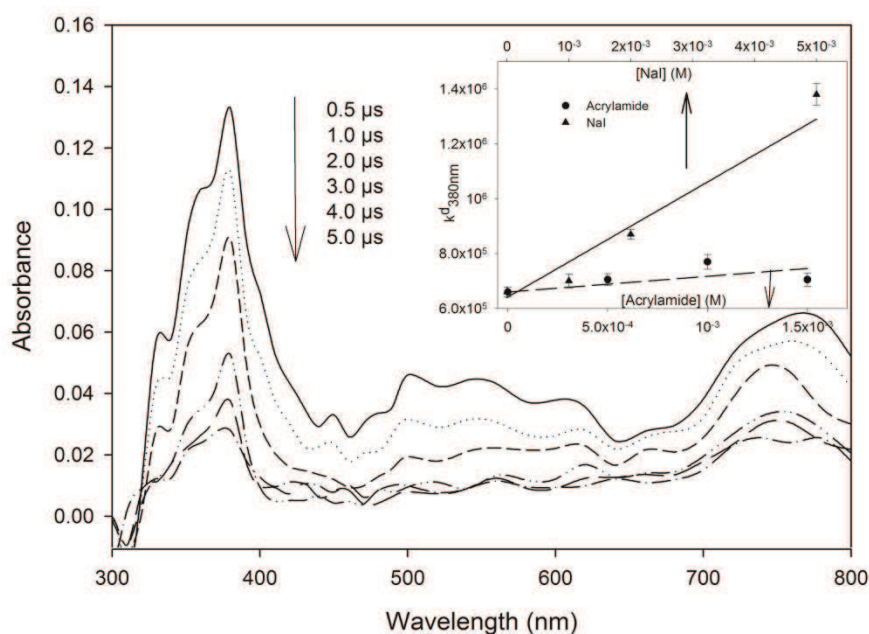


**Fig. 5.2.** Transient absorption spectra of PBSA (100  $\mu\text{M}$ ) in water produced by LFP (266 nm, 30 mJ) at various delay times. The insert shows the dependence on the ( $\bullet$ ) acrylamide and ( $\blacktriangle$ ) NaI concentrations of the pseudo-first order decay of transient signal at 380 nm. The error bars represent 95% confidence intervals.

### 5.1.3. Direct photolysis of PBSA at various pH values

Dark control experiment revealed no decay of PBSA over a period of 30 d laboratory study (data not shown). Thus, hydrolytic or microbial degradation were not responsible for PBSA elimination in the present study. A pronounced degradation of PBSA was observed for the samples under irradiation, implying photochemical reaction appeared to be important for limiting the

persistence of PBSA in aqueous solution by direct or indirect pathways.

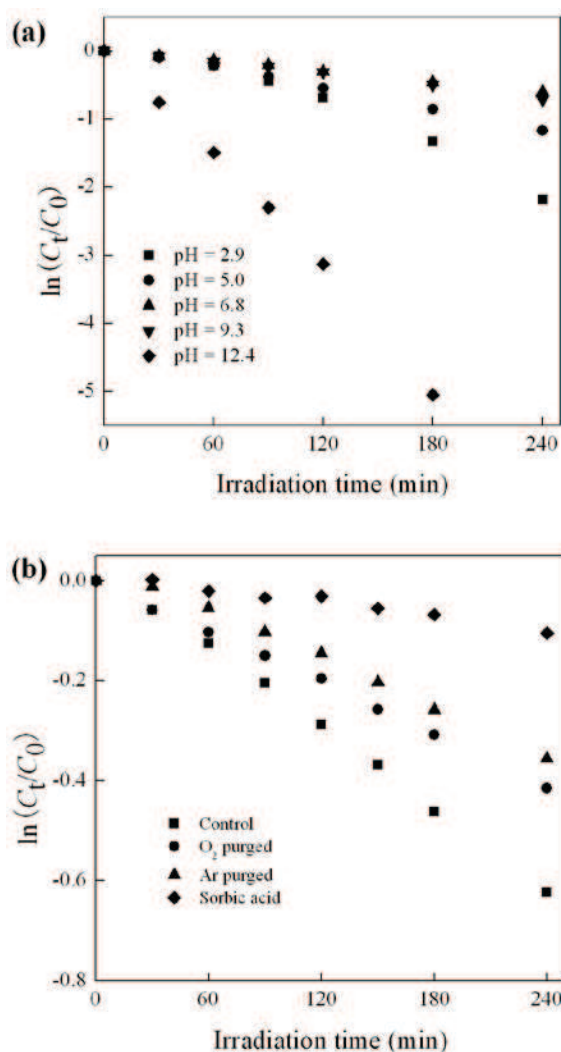


Fig. 5.3. (a) Effect of solution pH on direct photolysis of PBSA in Milli-Q water. (■) pH 2.9; (●) pH 5.0; (▲) pH 6.8; (▼) pH 9.3; and (◆) pH 12.4. Reaction solutions were prepared by 10 mM phosphate buffer or 10 mM borate buffer except pH 12.4 was adjusted by 0.1 M NaOH. (b) Effect of dissolved oxygen on direct photolysis of PBSA in Milli-Q water. (■) non-purged (control run); (●) under oxygen-purged condition (aeration); (▲) under argon-purged condition (deoxygenation); (◆) in the presence of triplet quencher sorbic acid. Reaction solutions were prepared by pH 8.0 buffers (10 mM phosphate). Experimental condition: [PBSA] = 10  $\mu$ M; [sorbic acid] = 2.5  $\mu$ M; V = 50 mL; irradiation was provided by a Pyrex filtered high Hg lamp ( $\lambda \geq 290$  nm).

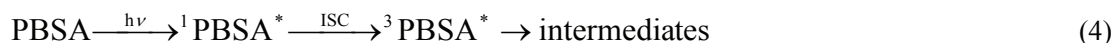
**Table 5.1. Pseudo-first-order rate constants, half-lives and quantum yields for PBSA direct photolysis in Milli-Q water under different conditions.**

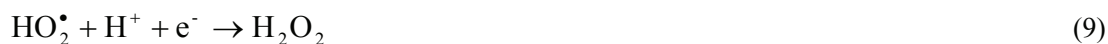
Solution <sup>a</sup>	Degradation rate constant ( $k_{\text{obs}}$ , $\text{h}^{-1}$ )	Half-live ( $t_{1/2}$ , h)	Quantum yield ( $\Phi_{\text{p}}$ , $\times 10^{-4}$ ) <sup>b</sup>
pH 2.9	0.563	1.23	9.74
pH 6.8	0.152	4.55	2.70
pH 12.4	1.690	0.41	20.5
pH 8.0	0.158	4.38	2.80
pH 8.0, O <sub>2</sub> -purged	1.023	6.75	-
pH 8.0, Ar-purged	0.093	7.45	-

<sup>a</sup> Reaction solutions were prepared by 10 mM phosphate or 10 mM borate buffer, except that pH 12.4 was adjusted by NaOH. Experimental condition: [PBSA] = 10  $\mu\text{M}$ ; V = 50 mL; irradiation was provided by a Pyrex filtered high Hg lamp ( $\lambda \geq 290$  nm).

<sup>b</sup> The quantum yield was calculated by *p*-nitroanisole (PNA)/pyridine (pyr) method.

Fig. 5.3(a) compares the direct photolysis of 10  $\mu\text{M}$  PBSA at various pH values upon irradiation of filtered HPK lamp. The quantum yield of PBSA direct photolysis at different pH values are shown in Table 5.1. It is evident that direct photolysis of PBSA is highly pH-dependent. For example, the observed quantum yield in acidic or basic condition was much higher than that in neutral pH (e.g.,  $\Phi_{\text{p,pH}2.9} / \Phi_{\text{p,pH}6.8} = 3.6$  and  $\Phi_{\text{p,pH}12.4} / \Phi_{\text{p,pH}6.8} = 7.6$ ). This finding was consistent with previous studies by Zhang et al.<sup>2</sup> PBSA has been known to undergo direct photolysis and O<sub>2</sub><sup>•-</sup> mediated self-sensitized degradation ((Eqs. (4) and (7)).<sup>11,12</sup> O<sub>2</sub><sup>•-</sup> can be generated via the reaction of e<sub>aq</sub><sup>-</sup> in the presence of oxygen ((Eq. (6)). It is known that at acidic pH, O<sub>2</sub><sup>•-</sup> undergoes rapid protonation to produce H<sub>2</sub>O<sub>2</sub> through the intermediate hydroperoxyl radical (HO<sub>2</sub><sup>•</sup>), which is capable of forming stronger oxidant HO• upon irradiation (Eqs. (8)-(10)).





Therefore, the observed enhancement in PBSA photolysis at acidic pH may be attributed to an alternative degradation pathway caused by HO• mediated oxidation reaction. To support this conclusion, further experiment of PBSA photolysis at pH 2.9 in the presence of HO• scavenger (1% 2-propanol, v/v) was carried out. As expected, the enhancement in PBSA photolysis was suppressed upon addition of 2-propanol used as hydroxyl radical scavenger, suggesting the involvement of HO• in PBSA photolysis at acid pH (Fig. S1, Supplementary Data).

During self-sensitized photodegradation, PBSA<sup>•+</sup> could be produced through <sup>1</sup>PBSA\* after electron ejection (Eq. (5)). Zhang et al. have also proposed that PBSA<sup>•+</sup> could be produced from autoionization, which was proved to be possible from PBSA\*/PBSA-H\*/PBSA-2H\* based on DFT calculation.<sup>12</sup> The involvement of PBSA<sup>•+</sup> during direct photolysis of PBSA was confirmed by our LFP results. PBSA<sup>•+</sup> was believed to be the critical transient species initiating the further reactions. Johnson Inbaraj et al. used electron paramagnetic resonance (EPR) and the EPR-spin trapping technique to characterize the photochemical free-radical pathways of PBSA.<sup>11</sup> These authors observed signal of DMPO/•H adduct that is formed by reaction of 5,5-dimethyl-1-pyrroline *N*-oxide (DMPO) with e<sub>aq</sub><sup>-</sup> followed by protonation in pH 12 solution rather than pH 7.4 solution, which they argued that PBSA-2H undergoes photoionization much more readily than monoionic form (PBSA-H) or neutral form PBSA. Therefore, we assume that the additional pathway for generating PBSA<sup>•+</sup> at basic pH partly contributed to an increased degradation rate. On the other hand, a redshift of PBSA-2H can be observed in UV-vis spectrum (Fig. 1(b)), indicating a larger spectral overlap integral with emission spectrum of HPK lamp, which may also account for an enhancement in degradation rate at basic pH.

The involvement of <sup>3</sup>PBSA\* in steady-state direct photolysis was also confirmed by addition of triplet quencher sorbic acid in reaction solution (Fig. 5.3(b)). In our previous report, the presence of sorbic acid decreased the photolysis of *p*-aminobenzoic acid (PABA), another kind of sunscreen agent, which is indicative of the energy transfer from <sup>3</sup>PABA\* to sorbic acid.<sup>18</sup> A similar result was observed in the present study, in which the presence of sorbic acid was found to retard the direct

photolysis of PBSA. This result indicates that  $^3\text{PBSA}^*$  was involved in direct photolysis of PBSA. The  $^3\text{PBSA}^*$  should be formed through an intersystem crossing (ISC) process from  $^1\text{PBSA}^*$ . However,  $^3\text{PBSA}^*$  was not found in our LFP study.

Both the elimination (Ar purged) and addition ( $\text{O}_2$  purged) of dissolved oxygen in solution retarded the direct photolysis of PBSA (Fig. 5.3(b)), implying  $\text{O}_2$  played a dual role in PBSA direct photolysis.  $\text{O}_2$  could inhibit PBSA photodegradation by serving as  $^3\text{PBSA}^*$  quencher, which may suppress the direct photolysis. However, the presence of  $\text{O}_2$  is essential for the formation of  $\text{O}_2^{\bullet-}$  (Eq. (6)), which could facilitate self-sensitized degradation of PBSA. On the other hand, the elimination of oxygen increased the lifetime of  $^3\text{PBSA}^*$ , allowing a great fraction of  $^3\text{PBSA}^*$  to be transformed.<sup>19</sup> However, the lower formation of  $\text{O}_2^{\bullet-}$  due to the absence of  $\text{O}_2$  may inhibit the self-sensitized degradation pathway.

#### 5.1.4. Indirect photolysis of PBSA in the presence of nitrate

Indirect photolysis of PBSA was performed in the presence of nitrate ( $\text{NO}_3^-$ ) at environmentally relevant level (0.08 to 2 mM) to investigate if indirect photodegradation (i.e., mediated by  $\text{HO}\bullet$ ) contribute significantly to the overall PBSA transformation.  $\text{NO}_3^-$  is known to be ubiquitous in natural aquatic environment with a concentration ranging from  $10^{-5}$  to  $10^{-3}$  M, which is highly related to the geographic location and human agriculture activity.<sup>20</sup> Previous studies have demonstrated that  $\text{NO}_3^-$  is the key source of  $\text{HO}\bullet$  in natural waters.<sup>21,22</sup> Upon the solar irradiation,  $\text{NO}_3^-$  could mediated indirect degradation of pollutants by reaction with photogenerated reactive radicals (i.e.,  $\text{HO}\bullet$  and  $\text{NO}_2^{\bullet}$ ) (Eqs. (11)-(13)).<sup>23,24</sup>



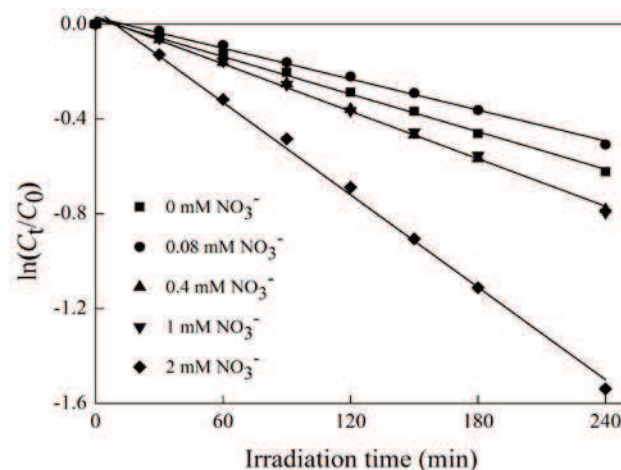


**Fig. 5.4.** The effect of nitrate on photodegradation of PBSA. (■) 0 mM NO<sub>3</sub><sup>-</sup>; (●) 0.08 mM NO<sub>3</sub><sup>-</sup>; (▲) 0.4 mM NO<sub>3</sub><sup>-</sup>; (▼) 1 mM NO<sub>3</sub><sup>-</sup>; (◆) 2 mM NO<sub>3</sub><sup>-</sup>. Experimental condition: [PBSA] = 10 μM; V = 50 mL; pH = 6.8 (10 mM phosphate buffered solution); irradiation was provided by a Pyrex filtered high Hg lamp (λ ≥ 290 nm).

As seen from Fig. 5.4, an increase in photodegradation rate of PBSA was observed in the presence of NO<sub>3</sub><sup>-</sup>, especially at higher concentration (e.g., 2 mM). However, such enhancement in photodegradation rate was not found when NO<sub>3</sub><sup>-</sup> concentration was low. Indeed, in the presence of 0.08 mM NO<sub>3</sub><sup>-</sup>, a slightly reduced PBSA photodegradation was observed compared to that in the absence of NO<sub>3</sub><sup>-</sup>. The concentration-dependent effect of NO<sub>3</sub><sup>-</sup> on PBSA photodegradation can be explained by the competition for light between NO<sub>3</sub><sup>-</sup> and PBSA and the formation of HO• by photo-excited NO<sub>3</sub><sup>-</sup>. The reaction with HO• could promote PBSA degradation, on the other hand, the reduced fraction of light due to NO<sub>3</sub><sup>-</sup> absorption may suppress PBSA direct photolysis. Therefore, considering the light screening effect, observed degradation rate constant of PBSA photolysis in the presence of NO<sub>3</sub><sup>-</sup>,  $k_{obs}$ , is the sum of the contributions from both direct photolysis and indirect photolysis (Eq. (14)).

$$k_{obs} = k_{dp} + k_{ip} = k_{Milli-Q} S_{\Sigma\lambda} + k_{ip} \quad (14)$$

where  $k_{dp}$  is the direct photodegradation rate constant of PBSA in the presence of NO<sub>3</sub><sup>-</sup>,  $k_{ip}$  is the indirect photodegradation rate constant of PBSA caused by the photosensitized effect of NO<sub>3</sub><sup>-</sup>,  $k_{Milli-Q}$  corresponds to the direct photolysis rate constant of PBSA in Milli-Q water alone. The direct photolysis rate constant in the presence of NO<sub>3</sub><sup>-</sup> was predicted from equation  $k_{dp} = k_{Milli-Q} \times S_{\Sigma\lambda}$ . Based on Eq. (14), application of the light screening factor allow the calculation of relative contribution to  $k_{obs}$  from the direct and indirect process for a given samples (Table 5.2). As seen,

direct photolysis is the major loss pathway for PBSA transformation, and HO• mediated indirect photolysis out-compete direct photolysis only at higher concentration of NO<sub>3</sub><sup>-</sup> (e.g., 2 mM).

**Table 5.2. Observed pseudo-first order photodegradation rate constants ( $k_{\text{obs}}$ ) and predicted contributions from the direct and indirect photolysis of PBSA in the presence of NO<sub>3</sub><sup>-</sup>. [PBSA]=10 μM; [NO<sub>3</sub><sup>-</sup>] = 0-2 mM; pH=6.8.**

[NO <sub>3</sub> <sup>-</sup> ] (mM)	<sup>a</sup> $k_{\text{obs}} \times 10^3$ (min <sup>-1</sup> )	<sup>b</sup> $S_{\Sigma\lambda 290-340}$	<sup>c</sup> $k_{\text{dp}} \times 10^3$ (min <sup>-1</sup> )	<sup>d</sup> $k_{\text{ip}} \times 10^3$ (min <sup>-1</sup> )	%DP <sup>e</sup>	%IP <sup>f</sup>
0	2.51	1.000	2.51	0	100	0
0.08	2.00	0.959	2.41	-0.41	120	-20
0.4	3.13	0.956	2.40	0.73	76.7	23.3
1	3.14	0.948	2.38	0.76	75.8	24.2
2	6.13	0.936	2.35	3.78	38.3	61.7

<sup>a</sup>  $k_{\text{obs}}$  represents the observed pseudo-first-order rate constant of PBSA photodegradation in the presence or absence of NO<sub>3</sub><sup>-</sup>.

<sup>b</sup>  $S_{\Sigma\lambda 290-340}$  represents the light screening factor applied to evaluate light attenuation effect of NO<sub>3</sub><sup>-</sup> on PBSA direct photolysis in the wavelength range 290-340 nm.

<sup>c</sup>  $k_{\text{dp}}$  represents the predicted rate constant of direct photolysis in the presence of NO<sub>3</sub><sup>-</sup>, which was calculated by the rate constant in Milli-Q water multiplied by light screening factor  $S_{\Sigma\lambda 290-340}$ .

<sup>d</sup>  $k_{\text{ip}}$  represents the rate constant caused by the indirect photolysis in the presence of NO<sub>3</sub><sup>-</sup>.

<sup>e</sup> DP represents the percentage contribution of direct photolysis to the overall photolysis degradation rate constant.

<sup>f</sup> IP represents the percentage contribution of indirect photolysis to the overall photolysis degradation rate constant.

Because of the high reactivity and nonselectivity, HO• reacts with most of the aquatic organic compounds with a second order rate constant of 10<sup>7</sup> to 10<sup>10</sup> M<sup>-1</sup> s<sup>-1</sup>.<sup>25</sup> In the present study, competition kinetics was used to determine the second order rate constant for reaction of PBSA with HO• as described in *Materials and Methods* section. The second order rate constant was measured to be 5.8 × 10<sup>9</sup> M<sup>-1</sup> s<sup>-1</sup> based on the slope value of the line which was obtained by plotting of ln([PBSA]<sub>t</sub>/[PBSA]<sub>0</sub>) versus ln([BA]<sub>t</sub>/[BA]<sub>0</sub>) (Fig. S2, Supplementary Data). It is apparent that the measured second order rate constant is high and approaches diffusion-controlled limit. However, reaction with HO• is not expected to be a significant decay process for PBSA in

natural waters due to the extremely low steady-state concentration of HO• ( $[\text{HO}\cdot]_{\text{ss}}$ ). For example, at a typical, upper-range value of  $10^{-16}$  M for HO•, ca. 1.39% of the transformation can be attributed to hydroxyl radical based on the second-order rate constant determined for PBSA. Due to the fact that  $[\text{HO}\cdot]_{\text{ss}}$  in natural waters ranged from  $10^{-18}$  M for pristine waters to  $10^{-16}$  M for agriculturally impacted waters,<sup>25</sup> HO•-mediated indirect photolysis appears to play an insignificant role in the transformation of PBSA in natural sunlit surface waters compared to direct photolysis (see Table S1, Supplementary Data). Thus, the presence of photosensitizers producing HO• in natural waters does not appear to impact the photolytic degradation of PBSA and direct photolysis of PBSA is the dominant photochemical loss process in most of the natural surface waters.

#### 5.1.5. Photolysis of PBSA in different water matrices

To obtain a further insight into how water constituents influence photodegradation, photolysis of PBSA were carried out in different water matrices. As shown in Fig. 5.5, no significant difference of PBSA photodegradation was observed in the presence of 0.2 M NaCl in comparison to that in Milli-Q water (▼ versus ■). Although chlorinated products of sunscreens formed in aquatic solutions containing Cl<sup>-</sup> (e.g., swimming-pool water) have been widely reported,<sup>26</sup> we observed neither enhancement in photodegradation rate nor chlorination by-products of PBSA in this work. Our observation also implies that photolysis of PBSA in marine waters is likely identical to that in fresh waters since Cl<sup>-</sup> played a negligible role in PBSA degradation.

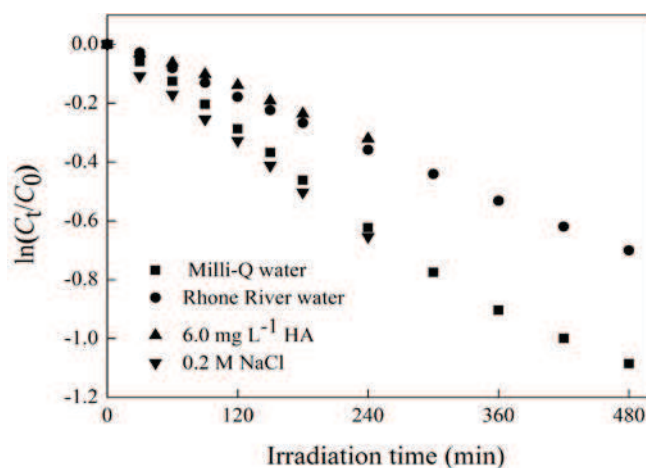


Fig. 5.5. Photolysis of PBSA in (■) Milli-Q water; (●) Rhône River water; (▲) Milli-Q water in the presence of 6.0 mg L<sup>-1</sup> Fluka humic acid; and (▼) Milli-Q water in the presence of 0.2 M NaCl. Experimental condition: [PBSA] = 10 μM; V = 50 mL; pH = 8.0; irradiation was provided by a Pyrex filtered high Hg lamp ( $\lambda \geq 290$  nm).

---

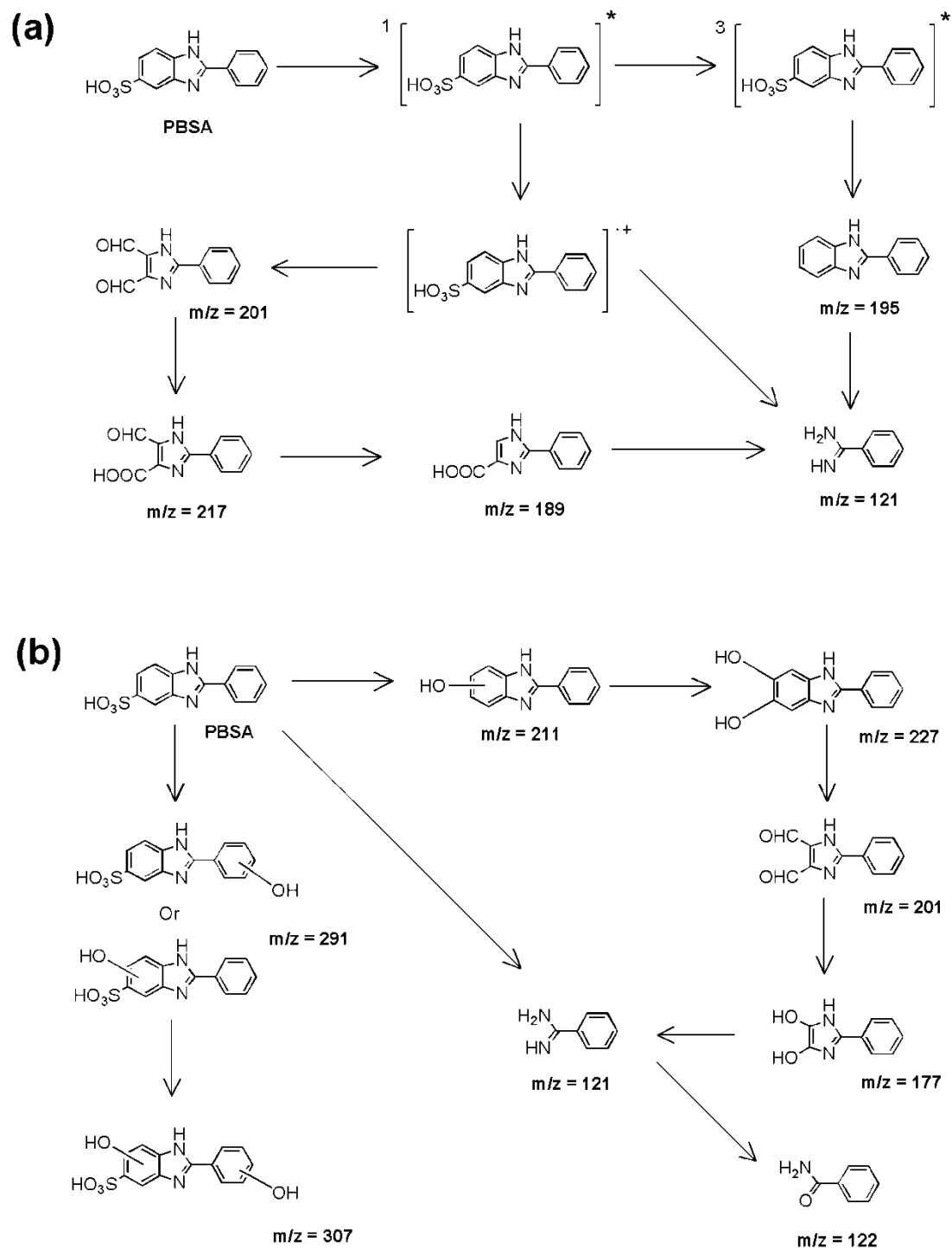
The presence of humic acid showed a detrimental effect on PBSA photolysis (▲ in Fig. 5.5). Dissolved organic matter (DOM) is another well-known photosensitizer widely presented in natural surface waters.<sup>22,27</sup> Humic acid is the major part of DOM which can account for up to 90% of the total carbon content.<sup>28</sup> DOM-mediated indirect photodegradation of organic pollutants through reactions with photogenerated reactive oxygen species (e.g.,  $^1\text{O}_2$  and  $\text{HO}\cdot$ ) as well as excited triplet state  $^3\text{DOM}^*$  has been well documented.<sup>18,27,29</sup>  $^1\text{O}_2$  is an electrophilic species and electron-rich compounds react at higher rate with  $^1\text{O}_2$ . Imidazole model compound has been shown to be reactive toward  $^1\text{O}_2$  with a bimolecular rate constant of approximately  $10^8 \text{ M}^{-1} \text{ s}^{-1}$ .<sup>30</sup> However, PBSA was found to be unreactive to  $^1\text{O}_2$  as previously reported by Zhang et al.<sup>12</sup> Indeed, PBSA could generate  $^1\text{O}_2$  by itself upon irradiation with a yield amount of 0.05.<sup>11</sup> On the other hand,  $^3\text{DOM}^*$ -induced degradation of PBSA was also shown to be highly unlikely through either energy transfer or electron transfer photosensitization.<sup>14</sup> Furthermore, DOM competed for light absorption and  $\text{O}_2$  with PBSA, and scavenged  $^3\text{PBSA}^*$ , which retarded the direct/self-sensitized photolysis of PBSA.<sup>14</sup> Therefore, DOM is expected to play a negative role in photodegradation of PBSA in natural sunlit surface waters and the indirect photolysis of PBSA in the presence of DOM is most likely induced by  $\text{HO}\cdot$ .<sup>14</sup>

Photolysis of PBSA in Rhône River water processed much more slowly than that in Milli-Q water (● versus ■). Interestingly, we observed very little variability in PBSA photodegradation in Rhône River water compared with that in the presence of  $6.0 \text{ mg L}^{-1}$  humic acid (● and ▲). Since  $\text{HO}\cdot$  plays an insignificant role in PBSA degradation in natural environment as discussed above, the influence of natural  $\text{HO}\cdot$  scavengers such as  $\text{HCO}_3^-$ ,  $\text{Cl}^-$  in river water matrix is expected to be minimal. Given that direct photolysis is of importance, we speculate that the presence of DOM in the river water was responsible for the decreased photodegradation of PBSA due to its light screening effect (see Table S2 for the composition of Rhône River water, Supplementary Data).

#### 5.1.6. Photodegradation products and pathways

In order to further study the mechanism of PBSA photodegradation in different water matrices, we have attempted to identify products formed in the photo-mediated PBSA reactions using SPE-LC-MS technique. The product molecular weight was assigned on the basis of the pseudomolecular ions  $[\text{M}+\text{H}]^+$ . The structural assignments of all detected intermediates were based on both analysis of the molecular ions peaks and their corresponding fragmentation pattern

(Table S3 and S4 in Supplementary Data). On the basis of the elucidated photodegradation intermediates and products, pathways of PBSA direct and indirect photolysis ( $\text{NO}_3^-$  mediated) were temporarily proposed as presented in Scheme 5.1.



**Scheme 5.1. Possible photodegradation pathways of PBSA: (a) direct photolysis in Milli-Q water, and (b) indirect photolysis in Milli-Q water in the presence of nitrate,  $[\text{NO}_3^-] = 2 \text{ mM}$ .**

---

As shown in Scheme 5.1(a), direct photolysis of PBSA results in the formation of excited triplet state of PBSA ( $^3\text{PBSA}^*$ ), as evidenced by our quenching experiment, most probably undergoes intersystem crossing (ISC) after excitation. The formation of desulfonated product, 2-phenyl-1H-benzimidazole (PBI) ( $m/z$  195), can be ascribed to the loss of sulfonic moiety from  $^3\text{PBSA}^*$ . As an important intermediate, radical cation ( $\text{PBSA}^{+\bullet}$ ) can be produced via electron ejection from  $^1\text{PBSA}^*$  to  $\text{O}_2$  as mentioned above. Bond cleavage of  $\text{PBSA}^{+\bullet}$  produces intermediate products, and the intermediate products further react with  $\text{O}_2^{\bullet-}$  and  $\text{H}_2\text{O}$ , leading to the final products.<sup>12</sup> For example,  $m/z$  201, 217 and 189 can be rationalized by the cleavage of the benzene ring adjacent to the imidazole ring, oxidation of aldehyde group to be carboxyl group and decarboxylation. 2-phenyl-imidazole-4, 5-dicarboxylic acid was not found in the current investigation, which was reported by Zhang et al. in direct photolysis of PBSA,<sup>12</sup> presumably because of a rapid decarboxylation process. Similarly, the formation of benzamidine ( $m/z$  121) is likely to be attributed to the imidazole ring cleavage of  $\text{PBSA}^{+\bullet}$ ,  $m/z$  195 or  $m/z$  189. Benzamidine has been known to further transform to benzamide in direct photolysis of PBSA.<sup>12</sup> However, the latter compound was also undetectable in the current study.

Considering indirect photodegradation pathways, the major difference in comparison to direct photolysis is that mono- and di-hydroxylation products ( $m/z$  291 and 307) are produced under successive attack of  $\text{HO}\cdot$  (left, Scheme 5.1 (b)). This result provides further evidence that  $\text{NO}_3^-$ -induced indirect photolysis of PBSA upon irradiation is primarily initiated by reaction with  $\text{HO}\cdot$ . Hydroxylation is generally regarded as the first step in  $\text{HO}\cdot$  mediated oxidation of organic compounds, which further undergo ring opening and/or chain cleavage and eventually mineralization to  $\text{CO}_2$  and  $\text{H}_2\text{O}$ . The cleavage of benzimidazole ring also occurs in indirect photolysis process through  $\text{HO}\cdot$  successive attack (right, Scheme 5.1 (b)). Firstly, 2-phenyl-1H-benzimidazole (PBI) is likely produced via sulfonic moiety cleavage under  $\text{HO}\cdot$  attack. Subsequently, PBI is subject to  $\text{HO}\cdot$  electrophilic attack at the left benzene ring, leading to the formation of mono- and di-hydroxylated PBI ( $m/z$  211 and  $m/z$  227, respectively). It is noteworthy that PBI was not detected in the indirect photolysis experiment, which might be due to the rapid hydroxylation process. Di-hydroxylated PBI further undergoes ring opening, producing 2-phenyl-imidazole-4, 5-dialdehyde ( $m/z$  201). Similar pathway has been reported previously in  $\text{TiO}_2$  photocatalytic degradation of thiabendazole, one kind of benzimidazole derivative fungicide

---

which has similar structure with PBI.<sup>31</sup> The aldehyde groups in m/z 201 can be converted to carboxylic groups by HO• oxidation followed by decarboxylation and HO• attack, resulting in the generation of m/z 177. It is proposed that imidazole ring of m/z 177 is cleaved under HO• attack due to the free electron-pairs in N atoms,<sup>32</sup> giving rise to benzamidine (m/z 121). Benzamidine is further oxidized by HO• to be benzamide (m/z 122). It is also possible that benzamidine arises from the initial reaction between PBSA and HO• with imidazole ring opening. It should be pointed out that NO<sub>3</sub><sup>-</sup>-induced phototransformation of organic compounds in some cases lead to nitration or nitrosation and therefore generate carcinogenic or mutagenic compounds.<sup>33</sup> However, no nitration or nitrosation products were observed in the present study on NO<sub>3</sub><sup>-</sup>-induced photodegradation of PBSA.

## 5.2. Conclusions

Overall, photochemical transformation via direct photolysis is expected to be an important degradation pathway, compared to other processes such as sorption or biological degradation, in the environmental fate of the 2-phenylbenzimidazole-5-sulfonic acid. Even through the bimolecular rate constants of PBSA with HO• are near the diffusion-controlled limit, the environmental fate of the PBSA is likely not controlled by reaction with HO•, except possibly in high nitrate-containing waters ([NO<sub>3</sub><sup>-</sup>] > 2 mM). Similarly, <sup>1</sup>O<sub>2</sub> and <sup>3</sup>DOM\* play a minor role in phototransformation of PBSA in sunlit natural waters. The photodegradation rates may be largely influenced by the season and latitude as well as limited photic zone and overcast condition. Although it is clear that rapid phototransformation of PBSA will occur, further environment monitoring studies should focus on the photoproducts as the parent half-lives will be short. An investigation focus on the toxicity test of these photoproducts from photodegradation is in progress.

## 5.3. Reference

- (1) Gasparro, F.P. Sunscreens, skin photobiology, and skin cancer: the need for UV protection and evaluation of efficacy. *Environ. Health Perspect.* **2000**, 108, 71-78.
- (2) Poiger, T.; Buser, H.R.; Balmer, M.E.; Bergqvist, P.A.; Müller, M.D. Occurrence of UV filter compounds from sunscreens in surface waters: regional mass balance in two Swiss lakes. *Chemosphere* **2004**, 55, 951-963.
- (3) Plagellat, C.; Kupper, T.; Furrer, R.; Felipe de Alencastro, L.; Grandjean, D.; Tarradellas, J. Concentrations and specific loads of UV filters in sewage sludge originating from a monitoring

- 
- network in Switzerland. *Chemosphere* **2006**, 62, 915- 925.
- (4) Schwarzenbach, R.P.; Escher, B.I.; Fenner, K.; Hofstetter, T.B.; Annette Johnson, C.; von Gunten, U; Wehrli, B. The challenge of micropollutants in aquatic systems. *Science* **2006**, 313, 1072-1077.
- (5) Schlumpf, M.; Schmid, P.; Durrer, S.; Conscience, M.; Maerkel, K.; Henseler, M.; Gruetter, M.; Herzog, I.; Reolon, S.; Ceccatelli, R.; Faass, O.; Stutz, E.; Jarry, H.; Wuttke, W.; Lichtensteiger, W. Endocrine activity and developmental toxicity of cosmetic UV filters-an update. *Toxicology* **2004**, 205, 113-122.
- (6) Di'az-Cruz, S.M.; Llorca, M.; Barceló, D. Organic UV filters and their photodegradates, metabolites and disinfection by-products in the aquatic environment. *Trend. Anal. Chem.* **2008**, 27, 873-887.
- (7) Di'az-Cruz, S.M.; Barceló, D. Chemical analysis and ecotoxicological effects of organic UV-absorbing compounds in aquatic ecosystems. *Trend. Anal. Chem.* **2009**, 28, 708-717.
- (8) Daughton, C.G.; Ternes, T.A. Pharmaceuticals and personal care products in the environment: agents of subtle change?. *Environ. Health Perspect.* **1999**, 107, 907-938.
- (9) Rodil, R.; Quintana, J.B.; López-Mahía, P.; Muniategui-Lorenzo, S.; Prada-Rodríguez, D. Multiclass determination of sunscreen chemicals in water samples by liquid chromatography-tandem mass spectrometry. *Anal. Chem.* **2008**, 80, 1307-1315.
- (10) Stevenson, C.; Davies, R.J.H. Photosensitization of guanine-specific DNA damage by 2-phenylbenzimidazole and the sunscreen agent 2-phenylbenzimidazole-5-sulfonic acid. *Chem. Res. Toxicol.* **1999**, 12, 38-45.
- (11) Johnson Inbaraj, J.; Bilski, P.; Chignell, C. F. Photophysical and photochemical studies of 2-phenylbenzimidazole and UVB sunscreen 2-phenylbenzimidazole-5-sulfonic acid. *Photochem. Photobiol.* **2002**, 75, 107-116.
- (12) Zhang, S.; Chen, J.; Qiao, X.; Ge, L.; Cai, X.; Na, G. Quantum chemical investigation and experimental verification on the aquatic photochemistry of the sunscreen 2-phenylbenzimidazole-5-sulfonic acid. *Environ. Sci. Technol.* **2010**, 44, 7484-7490.
- (13) Santos, A.J.M.; Miranda, M.S.; Esteves da Silva, J.C.G. The degradation products of UV filters in aqueous and chlorinated aqueous solutions. *Water Res.* **2012**, 46, 3167-3176.
- (14) Zhang, S.; Chen, J.; Wang, Y.; Wei, X. Humic acids decrease the photodegradation of the sunscreen UV filter 2-phenylbenzimidazole-5-sulfonic acid. *Environ. Chem. Lett.* **2012**, 10, 389-394.
- (15) Brahmia, O.; Richard, C. Phototransformation of carbaryl in aqueous solution Laser-flash photolysis and steady-state studies. *J. Photochem. Photobiol. A: Chem.* **2003**, 156, 9-14.

- 
- (16) Yuan, H.; Pan, H.; Wu, Y.; Zhao, J.; Dong, W. Laser flash photolysis mechanism of pyrenetetrasulfonate in aqueous solution. *Acta Phys.-Chim. Sin.* **2012**, *28*, 957-962.
- (17) Power, J. F.; Sharma, K.; Langford, C. H.; Bonneau, R.; Jousset-Dubien, J. Photophysics of a well characterized humic substance. *Photochem. Photobiol.* **1986**, *44*, 11-13.
- (18) Zhou, L.; Ji, Y.; Zeng, C.; Zhang, Y.; Wang, Z.; Yang, X. Aquatic photodegradation of sunscreen agent p-aminobenzoic acid in the presence of dissolved organic matter. *Water Res.* **2013**, *47*, 153-162.
- (19) Ryan, C. C.; Tan, D. T.; Arnold, W. A. Direct and indirect photolysis of sulfamethoxazole and trimethoprim in wastewater treatment plant effluent. *Water Res.* **2011**, *45*, 1280-1286.
- (20) Zuo, Y.; Wang, C.; Van, T. Simultaneous determination of nitrite and nitrate in dew, rain, snow and lake water samples by ion-pair high-performance liquid chromatography. *Talanta* **2006**, *70*, 281-285.
- (21) Brezonik, P. L.; Fulkerson-Brekken, J. Nitrate-induced photolysis in natural waters: Controls on concentrations of hydroxyl radical photo-intermediates by natural scavenging agents. *Environ. Sci. Technol.* **1998**, *32*, 3004-3010.
- (22) Vione, D.; Falletti, G.; Maurino, V.; Minero, C.; Pelizzetti, E.; Malandrino, M.; Ajassa, R.; Olariu, R. I.; Arsene, C. Sources and sinks of hydroxyl radicals upon irradiation of natural water samples. *Environ. Sci. Technol.* **2006**, *40*, 3775-3781.
- (23) Zepp, R. G.; Hoigne, J.; Bader, H. Nitrate-induced photooxidation of trace organic chemicals in water. *Environ. Sci. Technol.* **1987**, *21*, 443-450.
- (24) Warneck, P.; Wurzinger, C. Product quantum yields for the 305-nm photodegradation of nitrate in aqueous solution. *J. Phys. Chem.* **1988**, *92*, 6278-6283.
- (25) Buxton, G. V.; Greenstock, C. L.; Helman, W. P.; Ross, A. B. Critical review of rate constants for reactions of hydrate electrons, hydrogen atoms and hydroxyl radicals (OH·/O·) in aqueous solution. *J. Phys. Chem. Ref. Data.* **1988**, *17*, 513-517.
- (26) Sakkas, V. A.; Giokas, D. L.; Lambropoulou, D. A.; Albanis, T. A. Aqueous photolysis of the sunscreen agent octyl-dimethyl-p-aminobenzoic acid: Formation of disinfection byproducts in chlorinated swimming pool water. *J. Chromatogr. A.* **2003**, *1016*, 211-222.
- (27) Chin, Y. P.; Miller, P. L.; Zeng, L.; Cawley, K.; Weavers, L. K. Photosensitized degradation of bisphenol A by dissolved organic matter. *Environ. Sci. Technol.* **2004**, *38*, 5888-5894.
- (28) Corin, N.; Backlund, P.; Kulovaara, M. Degradation products formed during UV-irradiation of humic water. *Chemosphere* **1996**, *33*, 245-255.

- 
- (29) Guerard, J. J.; Miller, P. L.; Trouts, T. D.; Chin, Y. P. The role of fulvic acid composition in the photosensitized degradation of aquatic contaminants. *Aquat. Sci.* **2009**, 71, 160-169.
- (30) Latch, D. E.; Stender, B. L.; Packer, J. L.; Arnold, W. A.; McNeill, K. Photochemical fate of pharmaceuticals in the environment: cimetidine and ranitidine. *Environ. Sci. Technol.* **2003**, 37, 3342-3350.
- (31) Calza, P.; Baudino, S.; Aigotti, R.; Baiocchi, C.; Pelizzetti, E. Ion trap tandem mass spectrometric identification of thiabendazole phototransformation products on titanium dioxide. *J. Chromatogr. A.* **2003**, 984, 59-66.
- (32) Pelizzetti, E.; Calza, P.; Mariella, G.; Maurino, V.; Minero, C.; Hidaka, H. Different photocatalytic fate of amido nitrogen in formamide and urea. *Chem. Commun.* **2004**, 13, 1504-1505.
- (33) Chiron, S.; Comoretto, L.; Rinaldi, E.; Maurino, V.; Minero, C.; Vione, D. Pesticide by-products in the Rhône delta (Southern France). The case of 4-chloro-2-methylphenol and of its nitroderivative. *Chemosphere* **2009**, 74, 599-604.

#### 5.4. Supplementary Material

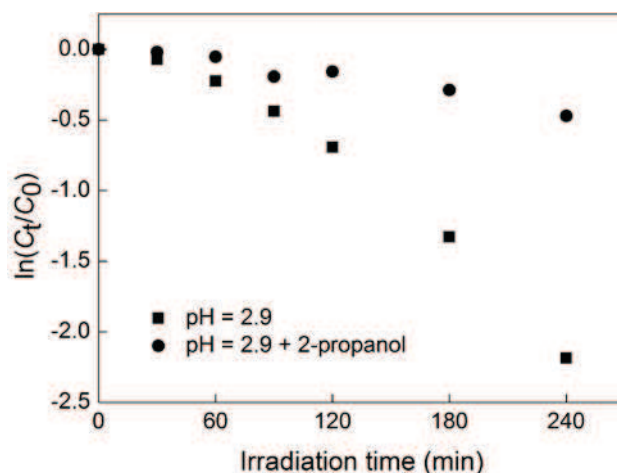


Fig. S1. Direct photolysis of PBSA in Milli-Q water at (■) pH = 2.9 and (●) pH = 2.9 with 2-propanol as HO<sup>•</sup> scavenger. Experimental condition: [PBSA] = 10 μM; 2-propanol = 0.5 mL; V = 50 mL; irradiation was provided by a Pyrex filtered high Hg lamp ( $\lambda \geq 290$  nm).

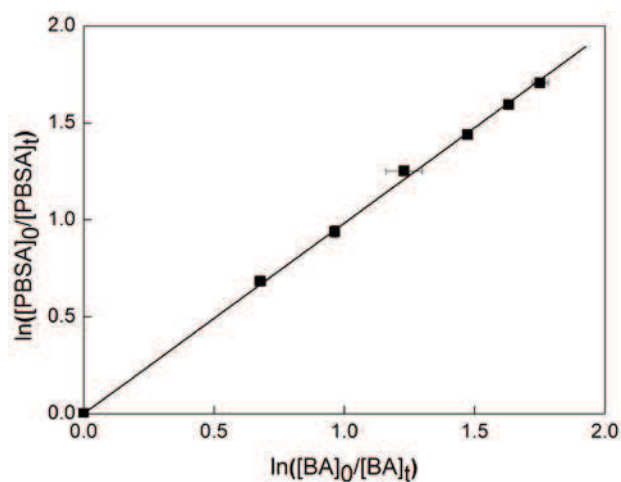


Fig. S2. Competitive oxidation of PBSA versus the reference compound benzoic acid (BA) by hydroxyl radicals generated using Fenton's reagent. Experiment condition: The reactions were carried out in foil-wrapped vessel. The initial solution contained 60 μM BA, 60 μM PBSA, 0.2 mM FeSO<sub>4</sub>·H<sub>2</sub>O and 0.5 mM H<sub>2</sub>O<sub>2</sub> at pH 3.5 (adjusted by sulfuric acid). Samples (0.5 mL) were withdrawn and quenched with methanol (0.5 mL). The slopes were shown with their 95% confidence intervals.

**Table S1 Predicted  $\cdot\text{OH}$ -mediated rate constants and environmental half lives of PBSA based on hydroxyl radical concentrations.**

$[\text{HO}\cdot]_{\text{ss}}$ (M)	$k_{\text{HO}\cdot}$ ( $\text{min}^{-1}$ ) <sup>a</sup>	$t_{1/2}$ (d) <sup>b</sup>
$10^{-15}$	$3.48 \times 10^{-4}$	2.78
$10^{-16}$	$3.48 \times 10^{-5}$	27.8
$10^{-17}$	$3.48 \times 10^{-6}$	278
$10^{-18}$	$3.48 \times 10^{-7}$	2775

<sup>a</sup>  $k_{\text{HO}\cdot} = k_{\text{HO}\cdot, \text{PBSA}}[\text{OH}\cdot]_{\text{ss}}$ , where  $k_{\text{HO}\cdot, \text{PBSA}} = 5.8 \times 10^9 \text{ M}^{-1} \text{ s}^{-1}$  by competition kinetic method.

<sup>b</sup> The half-life corresponding to hydroxyl radical concentration,  $t_{1/2} = \ln 2 / k_{\text{HO}\cdot}$ .

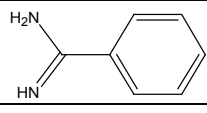
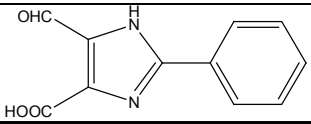
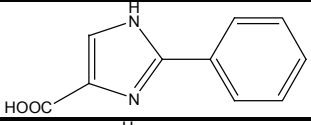
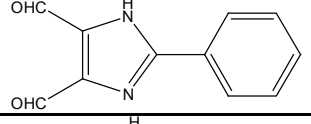
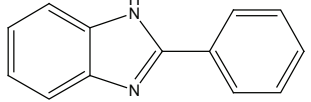
**Table S2 Composition of Rhône River matrix**

TOC <sup>a</sup>	0.167 mgC L <sup>-1</sup>
pH	8.45
Inorganic ions <sup>b</sup>	Concentration (mM)
HCO <sub>3</sub> <sup>-</sup>	2.23
Cl <sup>-</sup>	0.29
SO <sub>4</sub> <sup>2-</sup>	0.36
NO <sub>3</sub> <sup>-</sup>	0.08
Na <sup>+</sup>	0.28
K <sup>+</sup>	0.053
Ca <sup>2+</sup>	1.6
Mg <sup>2+</sup>	0.24

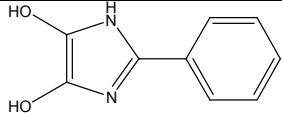
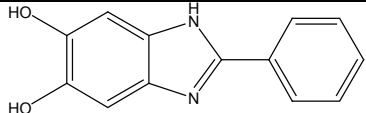
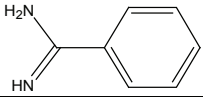
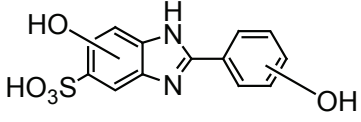
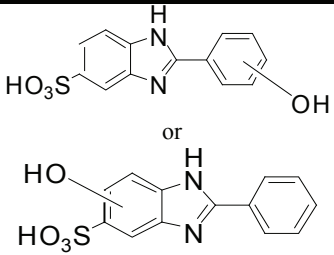
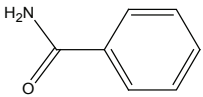
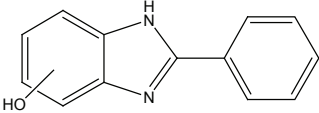
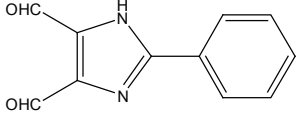
<sup>a</sup> Analyzed by a TOC-5050A analyzer.

<sup>b</sup> Analyzed by ion chromatography.

**Table S3 Retention time, mass spectra and proposed molecular structure of main photoproducts of PBSA photolyzed in Milli-Q water.**

Retention time (min)	Mass (m/z)	Compounds
1.54	121 [M+H] <sup>+</sup> 104 [M+H-NH <sub>3</sub> ] <sup>+</sup> 77 [C <sub>6</sub> H <sub>5</sub> ] <sup>+</sup>	
2.58	217 [M+H] <sup>+</sup> 199 [M+H-H <sub>2</sub> O] <sup>+</sup> 171 [M+H-COOH-H] <sup>+</sup> 153 [M+H-H <sub>2</sub> O-COOH-H] <sup>+</sup>	
3.52	189 [M+H] <sup>+</sup> 171 [M+H-H <sub>2</sub> O] <sup>+</sup> 143 [M+H-COOH-H] <sup>+</sup>	
9.18	201 [M+H] <sup>+</sup> 183 [M+H-H <sub>2</sub> O] <sup>+</sup> 171 [M+H-CHO-H] <sup>+</sup> 141 [M+H-2CHO-2H] <sup>+</sup>	
17.72	195 [M+H] <sup>+</sup> 77 [C <sub>6</sub> H <sub>5</sub> ] <sup>+</sup> 117 [C <sub>7</sub> H <sub>5</sub> N <sub>2</sub> ] <sup>+</sup>	

**Table S4 Retention time, mass spectra and proposed molecular structure of main photoproducts of PBSA photolyzed in aqueous solution containing nitrate.**

Retention time (min)	Mass (m/z)	Compounds
0.74	177 [M+H] <sup>+</sup> 141 [M+H-2H <sub>2</sub> O] <sup>+</sup>	
0.79	227 [M+H] <sup>+</sup> 191 [M+H-2H <sub>2</sub> O] <sup>+</sup> 77 [C <sub>6</sub> H <sub>5</sub> ] <sup>+</sup>	
1.53	121 [M+H] <sup>+</sup> 104 [M+H-NH <sub>3</sub> ] <sup>+</sup> 77 [C <sub>6</sub> H <sub>5</sub> ] <sup>+</sup>	
4.12	307 [M+H] <sup>+</sup> 271 [M+H-2H <sub>2</sub> O] <sup>+</sup>	
4.55, 5.15, 6.48, 7.58	291 [M+H] <sup>+</sup> 273 [M+H-H <sub>2</sub> O] <sup>+</sup>	
5.45	122 [M+H] <sup>+</sup> 105 [M+H-NH <sub>3</sub> ] <sup>+</sup> 77 [C <sub>6</sub> H <sub>5</sub> ] <sup>+</sup>	
8.53	211 [M+H] <sup>+</sup> 193 [M+H-H <sub>2</sub> O] <sup>+</sup> 77 [C <sub>6</sub> H <sub>5</sub> ] <sup>+</sup>	
9.18	201 [M+H] <sup>+</sup> 183 [M+H-H <sub>2</sub> O] <sup>+</sup> 171 [M+H-CHO-H] <sup>+</sup> 141 [M+H-2CHO-2H] <sup>+</sup>	

---

## Chapter 6 Degradation of sunscreen agent

### 2-phenylbenzimidazole-5-sulfonic acid by TiO<sub>2</sub> photocatalysis

Sunscreens are widely used in personal care products (PCPs) in recent years due to the public awareness of protection against ultraviolet (UV) irradiation and skin cancer.<sup>1</sup> Sunscreens enter the aquatic environment directly as consequence of recreational water activities (e.g., bathing and swimming) or indirectly via wastewater treatment plants (WWTPs) as result of the use of cosmetics, showering, washing, rubbing off and excretion after dermal application.<sup>2,3</sup> The extensive use of sunscreens already led to frequent detection in many aquatic ecosystems with a considerably high concentration.<sup>2-4</sup> Indeed, sunscreens are regarded as a new kind of environmental contaminants according to US Environmental Protection Agency.<sup>5</sup> Recent studies have provided evidence that organic sunscreens possess estrogenic properties and behavior as endocrine disrupting chemicals (EDCs) in the environment.<sup>6-11</sup> Furthermore, photo-induced transformation products of some kinds of sunscreens under natural solar irradiation were found to be more toxic than their parent species, which could be a further danger to the biota in environment.<sup>9</sup> Therefore, the long-term and extensive use of sunscreens may cause irreversible adversity on the ecology system.

2-phenylbenzimidazole-5-sulfonic acid (PBSA), as one kind of sunscreens, is widely used in sunscreen formulations and cosmetics because of its strong absorption in the UVB region (see Fig. 1). It has also been approved by the U.S. Food and Drug Administration as an effective sunscreen ingredient based on its ability to prevent erythema.<sup>1</sup> Due to its high polarity and continued input into the environment through personal care applications and incomplete elimination during wastewater treatment, PBSA was frequently detected in natural surface waters with a concentration ranging from 109 to 2679 ng L<sup>-1</sup>.<sup>10</sup> PBSA has been known to photochemically generate reactive oxygen species (i.e., <sup>1</sup>O<sub>2</sub> and O<sub>2</sub>•<sup>-</sup>) under UV irradiation and cause DNA damage. For example, Johnson Inbaraj et al. reported that PBSA showed strong oxidizing properties when UV irradiated in neutral aqueous solution in the presence of cysteine, glutathione and azide.<sup>12</sup> Zhang et al. developed a computational method based on the density functional theory (DFT) to predict and evaluate the photodegradation behavior of PBSA and found that energy and electron transfer reactions of excited state PBSA (PBSA\*) could photogenerate <sup>1</sup>O<sub>2</sub> and O<sub>2</sub>•<sup>-</sup>.<sup>13</sup> Therefore,

it is essential to develop advanced treatment technologies for eliminating PBSA in aqueous solutions for the sake of reducing potential risk to ecological system.

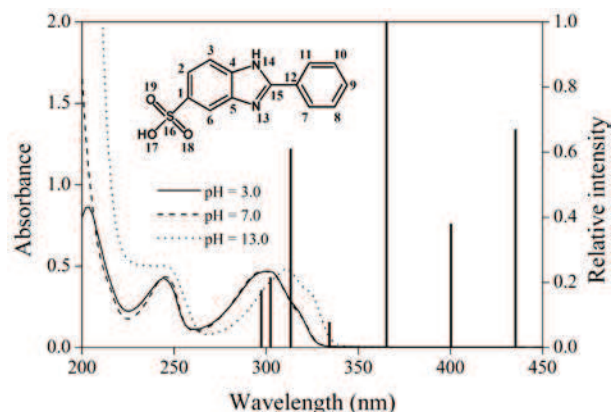


**Fig. 6.1.** UV-vis absorption spectra of 2-phenylbenzimidazole-5-sulfonic acid (PBSA) at different pH values and emission spectrum of HPK lamp. [PBSA] = 45  $\mu$ M. Note that wavelength with  $\lambda < 340$  nm was filtered by a 340 nm cut-off filter (0-52 Corning) to avoid direct photolysis of PBSA. The insert figure shows the chemical structure of PBSA,  $C_{13}H_{10}O_3N_2S$ . The atoms in PBSA molecular were labeled with numbers for the purpose of frontier electron density (FED) calculation.

During the past years, various advanced oxidation processes (AOPs) have been reported for the decomposition of organic pollutants in aqueous matrices. Among them, heterogeneous semiconductor photocatalysis using  $TiO_2$  as the photocatalyst has been found to be a promising treatment technology for eliminating organic pollutants, including sunscreens and other PCPs. When irradiating with photons of energy equal to or exceeding the band gap energy of  $TiO_2$  (for anatase, 3.2 eV band gap), valence band holes ( $h_{vb}^+$ ) and reductive conduction band electrons ( $e_{cb}^-$ ) are generated.<sup>14</sup> The photogenerated holes can: (i) directly oxidize the adsorbed chemical substance; or (ii) produce adsorbed hydroxyl radical ( $HO\bullet$ ) via the surface-bound  $OH^-$  and/or the adsorbed water molecules. As a highly reactive oxidant,  $HO\bullet$  is capable of unselectively reacting with most recalcitrant organic contaminants at near-diffusion-controlled rates in water ( $10^8 - 10^{10} M^{-1} s^{-1}$ ). Therefore,  $TiO_2$  is considered to be the most suitable semiconductor for widespread environmental photocatalytic applications because it is photoactive, non-toxic, inexpensive, and relatively biologically and chemically stable.<sup>15,16</sup>

This study reports on the photocatalytic degradation of PBSA in aqueous suspensions of  $TiO_2$ . The main purpose of this study is to (i) study the influence of process condition and water matrix on photocatalytic degradation; (ii) clarify the dominant reactive species involved in photocatalysis

process; (iii) characterize intermediates and photoproducts; (iv) elucidate the mechanism and transformation pathways leading to PBSA mineralization; (v) compare with structurally related compounds in photocatalytic degradation. To the authors' knowledge, this is the first study which includes a systematic exploration of kinetics, intermediates and degradation pathways of PBSA photocatalytic degradation.

## 6.1. Results and discussion

### 6.1.1. Preliminary experiments of PBSA photocatalytic degradation

Preliminary experiments of hydrolysis (without TiO<sub>2</sub> in dark), direct photolysis (without TiO<sub>2</sub> under irradiation) and adsorption (with TiO<sub>2</sub> in dark) were carried out to assess their contribution to photocatalytic degradation of PBSA by Degussa P25 TiO<sub>2</sub> as presented in Fig. 6.2A. As seen, no loss of PBSA was observed due to hydrolysis, suggesting PBSA was stable in Milli-Q water under dark condition. Dark controls also indicated that PBSA was stable in aqueous solution with pH ranging from 3 to 13 without light. Direct photolysis of PBSA in Milli-Q water contributed to a negligible degradation of PBSA (less than 5%), which can be attributed to an unappreciable overlap of PBSA UV-vis absorption spectrum ( $\lambda < 340$  nm) and the emitting spectrum (340-800 nm) of the filtered HPK lamp used as irradiation source in our study (see Fig. 6.1). Adsorption of PBSA on TiO<sub>2</sub> was also found to be marginal probably due to the relatively high hydrophilicity of PBSA (solubility 0.26 g L<sup>-1</sup>). Therefore, hydrolysis, direct photolysis and adsorption contributed insignificantly to the decay of PBSA in comparison to photocatalysis.

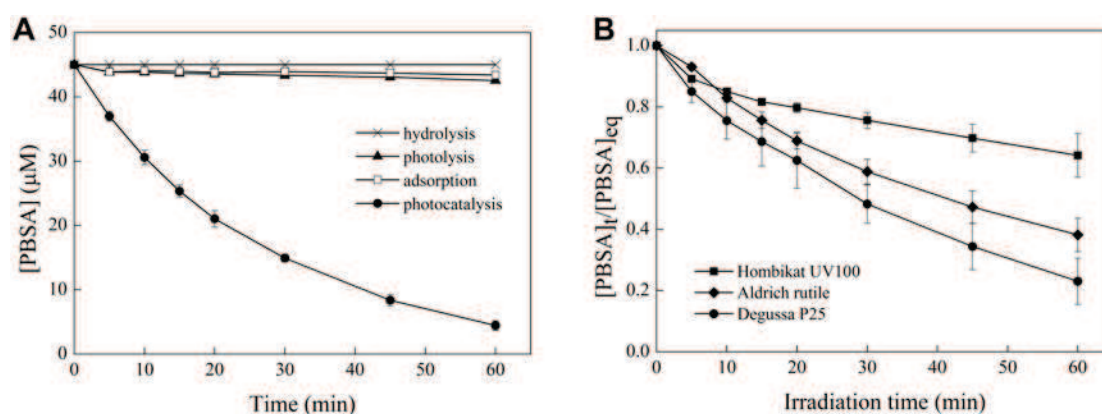


Fig. 6.2. (A) Comparison of hydrolysis, photolysis, adsorption and photocatalysis of PBSA in aqueous solutions. Degussa P25 TiO<sub>2</sub> was used as photocatalyst. [TiO<sub>2</sub>] = 1.0 g L<sup>-1</sup>; [PBSA] = 45  $\mu\text{M}$ ; pH = 7.0. (B) Effect of different photocatalysts on PBSA photocatalytic degradation. [TiO<sub>2</sub>] = 1.0 g L<sup>-1</sup>; [PBSA] = 45  $\mu\text{M}$ ; pH = 4.5. Error bars represent 95% confidence intervals.

---

In order to choose the most suitable catalyst for PBSA photocatalytic degradation, experiments using different kinds of catalysts (i.e., Degussa P25, Aldrich rutile and Hombikat UV100) were carried out (Fig. 6.2B). As seen, photocatalytic degradation of PBSA proceeded much more rapidly in the presence of P25 relative to other photocatalysts. The photoreactivities of these catalysts followed the order Degussa P25 > Aldrich rutile > Hombikat UV100. The substantially higher activity of P25 is not unexpected since similar results were observed by other authors.<sup>15,16</sup> The low re-combination rate of photogenerated electrons and holes due to a mixture crystal structure of P25 compared to other pure crystal catalyst is believed to be responsible for a significantly higher photoactivity.<sup>16</sup> However, it should be noted that the photocatalytic activity of TiO<sub>2</sub> depends on various parameters in a complex way (e.g., crystallinity, surface, particle size, defect sites, surface charge).<sup>17</sup> Recent studies also have shown that the photocatalytic activity of TiO<sub>2</sub> is highly substrate-specific.<sup>18</sup> Concerning the preliminary experiment result, our subsequent runs were carried out using P25 as photocatalyst.

#### 6.1.2. Determination of major reactive species

Preliminary experiment demonstrated that TiO<sub>2</sub> mediated photocatalysis was responsible for an appreciable degradation of PBSA. During photocatalysis process, photo-excited separation of valence band holes ( $h_{vb}^+$ ) and reductive conduction band electrons ( $e_{cb}^-$ ) occurs when TiO<sub>2</sub> absorbs photons with energy larger than band gap. The highly oxidative  $h_{vb}^+$  can be transferred to the surface-adsorbed water or hydroxyl groups (i.e., titanol group) to form the surface-bound hydroxyl radical ( $HO\bullet_{surf}$ ) or free hydroxyl radical ( $HO\bullet_{free}$ ) after desorption from the surface. On the other hand,  $e_{cb}^-$  transfers to dissolved oxygen, leading to the production of superoxide radical anion ( $O_2\bullet^-$ ) and hydroperoxyl radical ( $HO_2\bullet$ ) and its further reduction to hydrogen peroxide ( $H_2O_2$ )<sup>19-21</sup>. Among them,  $HO\bullet$  (either adsorbed or free) are often assumed to be the major species responsible for the photocatalytic oxidation, based on the evidences including detection of hydroxylated intermediates, distribution of the hydroxylation products, and spin trapping with subsequent ESR detection.<sup>20</sup> On the other hand, direct hole oxidation through electron transfer is also feasible since the oxidation potentials of most organic compounds lie below that of  $h_{vb}^+$ . For example, carboxylic acids, lacking abstractable hydrogens or C-C unsaturation, are believed to be oxidized primarily by  $h_{vb}^+$  via a photo-Kolbe process.<sup>22</sup>

In order to verify the photocatalysis mechanism and distinguish the contribution of these

reactive species, radical scavengers are usually employed as diagnostic tools to investigate the importance of certain kind of radicals since these scavengers selectively react with radicals to form stable or persistent intermediates.<sup>22-25</sup> For example, alcohols such as isopropanol, methanol and *tert*-butanol, have been commonly used to estimate HO• mediated mechanism.<sup>22,23</sup> The direct oxidation of these alcohols by  $h_{\nu b}^+$  is believed to be negligible because they have a very low affinity to TiO<sub>2</sub> surface in aqueous solution.<sup>23</sup> Iodide ion is an excellent scavenger which reacts with  $h_{\nu b}^+$  and adsorbed HO• because  $h_{\nu b}^+$  can be easily captured by I<sup>-</sup> (an electron donor) and oxidation of I<sup>-</sup> by surficial HO• is also possible.<sup>24,25</sup>

In this study, *tert*-butanol, as a scavenger of HO• ( $5.0 \times 10^8 \text{ M}^{-1} \text{ s}^{-1}$ ),<sup>19</sup> and potassium iodide (KI), as a scavenger of both  $h_{\nu b}^+$  and HO• ( $1.2 \times 10^{10} \text{ M}^{-1} \text{ s}^{-1}$ )<sup>24</sup> were used and the results are shown in Fig. 3. It was observed that PBSA photocatalysis reactions with or without radical scavengers all followed pseudo-first-order kinetics. The obtained pseudo-first-order rate constants as well as corresponding linear correlation coefficient are presented in Table S2 (Supplementary Data).

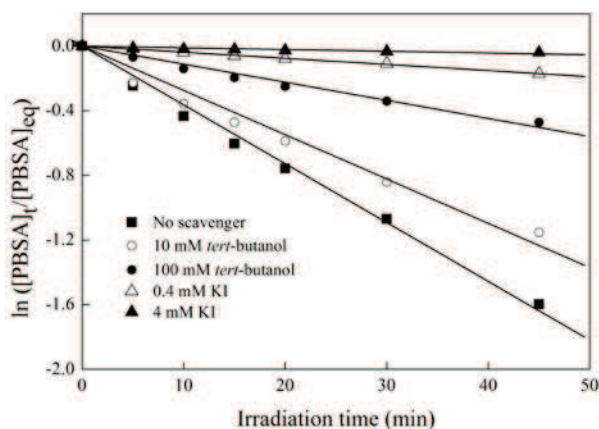


**Fig. 6.3.** Effect of radical scavengers on PBSA photocatalytic degradation. The *tert*-butanol was used as a scavenger of HO• while KI was used as a scavenger of both  $h_{\nu b}^+$  and HO•. Experimental conditions: Degussa P25 TiO<sub>2</sub> was used as photocatalyst; [TiO<sub>2</sub>] = 2.0 g L<sup>-1</sup>; [PBSA] = 37.9 μM; pH = 4.5.

In Fig. 6.3, the control run (no scavenger) exhibited a degradation rate constant of 0.0486 min<sup>-1</sup>, resulting from combined effects of all the possible radicals. However, the degradation rate constant decreased more than 92% and 97% in the presence of 0.4 mM and 4 mM KI, respectively. This suggests that both HO• and  $h_{\nu b}^+$  together were responsible for the major degradation of PBSA, while other radicals such as O<sub>2</sub><sup>•-</sup>, HO<sub>2</sub><sup>•</sup> and H<sub>2</sub>O<sub>2</sub> contributed insignificantly to PBSA degradation.

To determine the relative contribution between HO• and  $h_{vb}^+$ , further runs using *tert*-butanol as HO• scavenger were carried out. In Fig. 3, the addition of 10 mM and 100 mM *tert*-butanol resulted in a degradation rate constant of 0.0274 min<sup>-1</sup> and 0.0112 min<sup>-1</sup>, respectively, which decreased 43% and 77% compared with control run. Hence, HO• was likely to be the most important radical during PBSA photocatalytic degradation. It is believed that reaction with holes is more important for hydrophobic compounds that are repelled from the aqueous solution and are thus more likely to undergo adsorption on the photocatalyst surface.<sup>18</sup> Therefore, the relatively higher hydrophilicity of PBSA and lower adsorption may be one reason accounting for the less importance of  $h_{vb}^+$ . Since HO• is highly electrophilic, we speculate that the rich  $\pi$  electron system of benzimidazole and phenyl moiety of PBSA molecular favor HO• attack, which in turn enable HO• playing a more important role than other radicals. This hypothesis is further verified by the intermediates that were identified by LC-MS.

Second-order rate constant of PBSA-HO• reaction was determined by competition kinetic method as described in Experimental section according to the following equation.<sup>25</sup>

$$\ln\left(\frac{[PBSA]_t}{[PBSA]_0}\right) = \frac{k_{HO\cdot, PBSA}}{k_{HO\cdot, BA}} \ln\left(\frac{[BA]_t}{[BA]_0}\right) \quad (1)$$

Where BA is the reference compound, benzoic acid, with a known rate constant of reaction with HO• ( $k_{HO\cdot, BA} = 5.9 \times 10^9 \text{ M}^{-1} \text{ s}^{-1}$ ).<sup>25</sup> From Eq. 1, the second-order rate constant of PBSA-HO• reaction was calculated to be  $5.8 \times 10^9 \text{ M}^{-1} \text{ s}^{-1}$  by plotting of  $\ln([PBSA]_t/[PBSA]_0)$  versus  $\ln([BA]_t/[BA]_0)$  (see Fig. S1, Supplementary Data). Such a high second order rate constant suggests that PBSA could readily react with HO• near the diffusion-controlled limit. This observation further supports the result of radical scavenging experiment, that, HO• is the most important radical involved in PBSA photocatalysis.

### 6.1.3. Effect of process conditions and water matrices on PBSA photocatalytic degradation

Further batch experiments under different process condition (i.e., catalyst loading, initial substrate concentration and solution pH) were performed for the purpose of a systematic study and the obtained overall results are summarized in Table 6.1. Our results reveal that photocatalytic degradation of PBSA under different operation conditions all followed pseudo-first-order kinetics.

**Table 6.1. Results of batch experiments for degradation of PBSA by TiO<sub>2</sub> photocatalysis.**

Photocatalyst	TiO <sub>2</sub> (g L <sup>-1</sup> )	C <sub>0</sub> (μM) <sup>a</sup>	pH <sup>b</sup>	HCO <sub>3</sub> <sup>-</sup> (mM)	HA <sup>c</sup> (mg L <sup>-1</sup> )	k <sub>p</sub> (min <sup>-1</sup> ) <sup>d</sup>	r <sub>0</sub> (μM min <sup>-1</sup> ) <sup>e</sup>	R <sup>2f</sup>
1. Effect of photocatalyst type								
Aldrich rutile	1.0	45	4.5	0	0	0.0184	-	0.999
Hombikat	1.0	45	4.5	0	0	0.0095	-	0.969
UV100								
Degussa P25	1.0	45	4.5	0	0	0.0285	-	0.998
2. Effect of photocatalyst loading								
Degussa P25	0.25	37.9	4.5	0	0	-	1.14	-
Degussa P25	0.5	37.9	4.5	0	0	-	1.47	-
Degussa P25	1.0	37.9	4.5	0	0	-	1.61	-
Degussa P25	1.5	37.9	4.5	0	0	-	2.20	-
Degussa P25	2.0	37.9	4.5	0	0	-	2.36	-
Degussa P25	3.0	37.9	4.5	0	0	-	0.94	-
3. Effect of substrate concentration								
Degussa P25	2.0	8.85	4.5	0	0	-	1.57	-
Degussa P25	2.0	22.1	4.5	0	0	-	1.63	-
Degussa P25	2.0	37.9	4.5	0	0	-	2.36	-
Degussa P25	2.0	44.3	4.5	0	0	-	2.06	-
Degussa P25	2.0	61.7	4.5	0	0	-	1.54	-
4. Effect of solution pH								
Degussa P25	2.0	37.9	2.5	0	0	0.0203	-	0.998
Degussa P25	2.0	37.9	4.5	0	0	0.0486	-	0.991
Degussa P25	2.0	37.9	8.5	0	0	0.0521	-	0.999
Degussa P25	2.0	37.9	10.9	0	0	0.0466	-	0.999
Degussa P25	2.0	37.9	11.3	0	0	0.0163	-	0.997
5. Effect of bicarbonate ion								
Degussa P25	2.0	37.9	8.5	1	0	0.0383	-	0.999

Degussa P25	2.0	37.9	8.5	10	0	0.0310	-	0.999
Degussa P25	2.0	37.9	8.5	100	0	0.0062	-	0.999
6. Effect of humic acid								
Degussa P25	2.0	37.9	5.5	0	6	0.0417	-	0.990
Degussa P25	2.0	37.9	5.5	0	18	0.0220	-	0.999
Degussa P25	2.0	37.9	5.5	0	60	0.0028	-	0.931

<sup>a</sup> The initial concentration of PBSA.

<sup>b</sup> The pH of the solutions was adjusted by 0.1 M HClO<sub>4</sub> or 0.1 M NaOH.

<sup>c</sup> HA represents humic acid.

<sup>d</sup>  $k_p$  is the pseudo-first-order rate constant.

<sup>e</sup>  $r_0$  is the initial reaction rate which was calculated from the slope value of PBSA degradation curve over the first 5 min of reaction.  $r_0$  was calculated instead of  $k_p$  for investigating the effect of catalyst loading and initial organic substrate on photodegradation efficiency.

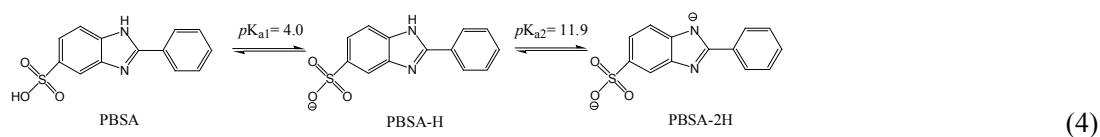
<sup>f</sup>  $R^2$  is the linear correlation coefficient.

For the TiO<sub>2</sub> loading, the initial reaction rate  $r_0$ , which was calculated over the course of first 5 min of irradiation, increased with increasing catalyst loading up to a certain value, while further increasing the catalyst loading significantly reduced  $r_0$  (Table 6.1). It is proposed that with TiO<sub>2</sub> dosage increasing, more photons are expected to be absorbed by TiO<sub>2</sub>, which consequently lead to higher amount of reactive species.<sup>26</sup> The enhanced concentrations of reactive species are generally responsible for a much faster degradation. However, when TiO<sub>2</sub> loading was higher than 2.0 g L<sup>-1</sup>, a decreased  $r_0$  was observed which can be explained by screening effect of excess particles, masking part of the photosensitive surface, as well as scattering or reflecting the amount of photons needed for exciting the catalyst.<sup>27,28</sup> In addition, a higher TiO<sub>2</sub> loading usually leads to aggregation of the photocatalyst particles that decreases the contact surface area between reactant and photocatalyst, consequently, reduces the number of active sites and lowers the rate of photodegradation.<sup>29</sup>

Previous studies have reported the dependency of the TiO<sub>2</sub> photocatalytic reaction rate on the concentration of the organic substrate.<sup>16,27,28</sup> Table 6.1 also illustrates the effect of different initial concentration of PBSA on the initial reaction rate  $r_0$ . As seen,  $r_0$  increased as the concentration of PBSA increased up to a maximum value, while further elevating the concentration led to a

decreased reaction rate. The enhancement of  $r_0$  with increasing PBSA concentration could be explained by the scavenging of reactive species by the substrate. The reaction of PBSA with  $\text{HO}\cdot$  and  $h_{\text{vb}}^+$  on the surface of  $\text{TiO}_2$  is in competition with the thermal recombination process  $\text{HO}\cdot/e_{\text{cb}}^-$  and  $h_{\text{vb}}^+/e_{\text{cb}}^-$ . An excessive concentration of PBSA could completely inhibit the unfavorable recombination, thus, the initial reaction rate of PBSA can be expected to reach a maximum value equivalent to the trapping rate of  $\text{HO}\cdot$  and  $h_{\text{vb}}^+$  on  $\text{TiO}_2$  surface. During photocatalysis process, organic compounds generally transform to radical transient at first step by reacting with  $h_{\text{vb}}^+$  and  $\text{HO}\cdot$  (e.g.,  $\text{HO}\cdot$  adduct or H-abstract). These partially oxidized radical transient could either undergo further oxidation to a non-radical stable intermediate or react with an electron to return back to the initial substrate. The so-called back or recombination reaction will become dominant when the substrate concentration is high enough, which negatively contribute to a decreased initial reaction rate.<sup>30</sup> Considering the elevated initial concentration of PBSA, a larger yield amount of intermediates can also be expected, which are capable of poisoning the  $\text{TiO}_2$  active sites and/or competing for photons with the catalyst, leading to a decreased transformation rate of mother compound.<sup>30</sup>

The effect of solution pH on photocatalytic degradation is a complex issue related to the ionization states of organic compounds and the surface charge of catalyst as well as the formation rate of  $\text{HO}\cdot$  and other active radicals in the reaction solution.<sup>26,27</sup> The solution pH also alters the  $\text{TiO}_2$  energy levels according to the Nernstian behavior (-59 mV/pH) due to the pH-dependent surface charge.<sup>21</sup> Since the point of zero charge ( $\text{pH}_{\text{pzc}}$ ) of Degussa P25 is widely reported to be 6.25 and PBSA has two  $\text{pK}_a$  (i.e.,  $\text{pK}_{a1} = 4.0$  and  $\text{pK}_{a2} = 11.9$ ) due to the presence of sulfonic and imidazole moiety in PBSA molecular,<sup>12</sup> the predominant existing speciation of  $\text{TiO}_2$  and PBSA in different pH solutions are according to the following equations.

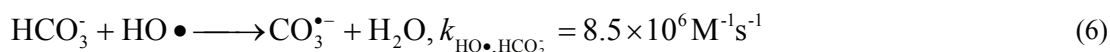
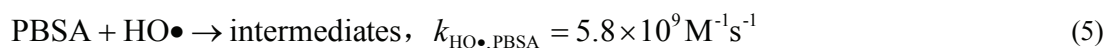


As shown in Table 6.1, photocatalytic degradation of PBSA is highly pH-dependent. At pH

2.5, the relatively low photodegradation rate constant was most likely due to the lack of electrostatic attraction between  $\text{TiOH}_2^+$  and PBSA. Accordingly, the comparatively high rate constant at pH 4.5 can be attributed to the electrostatic attraction between  $\text{TiOH}_2^+$  and PBSA-H, which facilitates the adsorption of PBSA on  $\text{TiO}_2$  surface. However, the high rate constant at pH 8.5 was unexpected since electrostatic repulsion was expected to take place between  $\text{TiO}^-$  and PBSA-H. Therefore, the pH-dependent effect of  $\text{HO}\bullet$  formation rate was likely responsible for such phenomenon because previous literatures have demonstrated that alkaline condition could promote photogeneration of hydroxyl radicals.<sup>15,31,32</sup> Nevertheless, at extremely high pH (pH = 13.0), the electrostatic repulsion between  $\text{TiO}^-$  and PBSA-2H would become much stronger, which out-competed the positive effect of  $\text{HO}\bullet$  formation, consequently decreased the degradation rate constant.

Water matrix plays an important role in photocatalytic degradation of organic compounds because some constituents which are ubiquitous in natural waters (e.g., bicarbonate ions, dissolved organic matter (DOM)) may serve as  $\text{HO}\bullet$  scavengers.<sup>33,34</sup> From this viewpoint, bicarbonate ( $\text{HCO}_3^-$ ) and humic acid (HA) were chosen to investigate their effect on the photocatalysis degradation of PBSA since they are not only well-known  $\text{HO}\bullet$  scavengers but also widely present in natural waters. Experiments were conducted in aqueous 37.9  $\mu\text{M}$  PBSA solutions with a  $\text{HCO}_3^-$  concentration range of 0-100 mM or a HA concentration range of 0-60  $\text{mg L}^{-1}$ . Note that, in the case of  $\text{HCO}_3^-$ , solution pH was maintained at 8.5 to ensure  $\text{HCO}_3^-$  was the dominant species ( $\text{p}K_{a1} = 6.37$  and  $\text{p}K_{a2} = 10.25$ ) in the reaction solution.

It is evident that the presence of  $\text{HCO}_3^-$  or HA suppressed the photocatalytic degradation of PBSA (Table 6.1 and Fig. 6.4). For example, PBSA transformation ratio was found to be only 24% and 12.2% after 45 min irradiation in the presence of 100 mM  $\text{HCO}_3^-$  or 60  $\text{mg L}^{-1}$  HA, respectively, compared to 92.4% and 85.5% in absence of  $\text{HCO}_3^-$  (pH = 8.5) or HA (pH = 5.5), respectively. The inhibition can be ascribed to the competition for  $\text{HO}\bullet$  by  $\text{HCO}_3^-$  and HA. It is assumed that if the PBSA coexist with  $\text{HCO}_3^-$  or HA in reaction solution, the  $\text{HO}\bullet$  will be partitioned according to the following equations.<sup>35,36</sup>



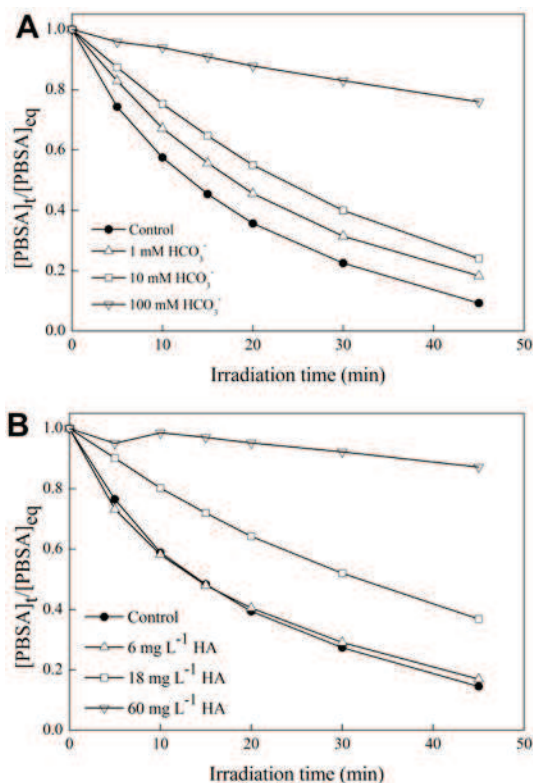


**Fig. 6.4.** Effect of (A) bicarbonate ion (pH = 8.5), and (B) humic acid (pH = 5.5) on PBSA photocatalytic degradation. Experimental conditions: Degussa P25 TiO<sub>2</sub> was used as photocatalyst; [TiO<sub>2</sub>] = 2.0 g L<sup>-1</sup>; [PBSA] = 37.9 μM; [HCO<sub>3</sub><sup>-</sup>] = 0-100 mM; [HA] = 0-60 mM.

Therefore, a fraction of HO• will be quenched by HCO<sub>3</sub><sup>-</sup> or HA. If we assume that HO• yield amount remained constant during photocatalysis, the increase in the concentration of HCO<sub>3</sub><sup>-</sup> or HA would lower the amount of HO•, leading less HO• available for reacting with PBSA. For HA at higher concentration, competitive adsorption on TiO<sub>2</sub> active sites and light attenuating may also occur simultaneously (see Fig. S2, the adsorption mass (mg/g TiO<sub>2</sub>) of HA on TiO<sub>2</sub> versus time and Fig. S3, the UV-vis absorption spectra of HA at different concentration, Supplementary Data).<sup>37</sup> These factors may take together to retard PBSA photocatalytic degradation. Nevertheless, at lower concentration (e.g., 1 mM HCO<sub>3</sub><sup>-</sup> or 6 mg L<sup>-1</sup> HA), the presence of HCO<sub>3</sub><sup>-</sup> or HA showed slight inhibition on PBSA photocatalysis. Since the environmentally relevant concentration of HCO<sub>3</sub><sup>-</sup> and HA are reported to be 0.4-4 mM and 0.3-30 mg L<sup>-1</sup>, respectively,<sup>35,38</sup> this observation is particularly interesting because of the feasibility of applying TiO<sub>2</sub> photocatalysis for treating

---

PBSA micropollutant in environmentally realistic water matrix. It is worthy noting that quenching of HO• by HCO<sub>3</sub><sup>-</sup> yields carbonate radical (CO<sub>3</sub><sup>•-</sup>) (Eq. 6), and CO<sub>3</sub><sup>•-</sup> may react with PBSA due to its electron rich nature. However, no enhancement in photocatalytic degradation of PBSA was observed in this study as the HCO<sub>3</sub><sup>-</sup> concentration increased. Given that CO<sub>3</sub><sup>•-</sup> is generally less reactive than HO• (second-order rate constant for reaction of CO<sub>3</sub><sup>•-</sup> with organic compound is normally 2 - 3 magnitude order lower than that of HO•),<sup>35,36</sup> it is possible that CO<sub>3</sub><sup>•-</sup>-mediated PBSA oxidation was negligible in the present study.

#### 6.1.4. Identification of photodegradation intermediates and products

##### 6.1.4.1. Evolution of organic intermediates

Advanced oxidation processes often yield various degradation intermediates and products due to the non-selective reaction of HO• with organic pollutants. In this work, we have attempted to identify photodegradation intermediates using LC-MS technique. A mixture sample composed of aliquots withdrawn at different irradiation time was analyzed for the purpose of identifying as more intermediates as possible. Structural identification of these intermediates was based on the analysis of the total ion chromatogram (TIC) and the corresponding mass spectrum (Fig. S4 and Table S3, Supplementary Data). Major intermediates included hydroxylation products (mono-, di- and tri-hydroxylated PBSA), imidazole ring cleavage products (e.g., benzamide), and hydroxylated 2-phenyl-1H-benzimidazole as well as phenylimidazolecarboxylic derivatives.

In order to correctly characterize mono-hydroxylated compounds (positions of hydroxylation), the frontier electron densities (FEDs) of PBSA (as PBSA-H form) were calculated to predict the reaction sites for HO• attacking, and the obtained results are summarized in Table 6.2. In the Frontier Orbital Theory, the preferential HO• addition probably take place on the atom with the highest  $FED_{HOMO}^2 + FED_{LUMO}^2$  value,<sup>39</sup> which has been proved to be reasonable by the published work.<sup>40</sup> As shown in Table 6.2, 9C, 11C, 7C and 8C sites in phenyl ring and 2C in benzimidazole have the highest  $FED_{HOMO}^2 + FED_{LUMO}^2$  value, implying both the two benzenes are likely to be attacked by HO•, resulting in the formation of mono-hydroxylation products. However, it should be noted that the possibility for HO• addition to phenyl moiety is much higher than addition to benzyl moiety which is adjacent to imidazole. Although the 12C has a much higher  $FED_{HOMO}^2 + FED_{LUMO}^2$  value, we speculate that the HO• unlikely attack on this site due to steric hindering effect.

**Table 6.2.  $FED^2_{HOMO} + FED^2_{LUMO}$  values of PBSA (PBSA-H form) atoms calculated by using Gaussian 09 program at the B3LYP/6-311+G\* level.**

Number (atom) <sup>a</sup>	$FED^2_{HOMO} + FED^2_{LUMO}$	Number (atom)	$FED^2_{HOMO} + FED^2_{LUMO}$
1C	0.0054	<b>11C</b>	<b>0.0927</b>
<b>2C<sup>b</sup></b>	<b>0.0339</b>	12C	0.1916
3C	0.0151	13N	0.0722
4C	0.0130	14N	0.0451
5C	0.0021	15C	0.0438
6C	0.0280	16S	0.0001
<b>7C</b>	<b>0.0701</b>	17O	0.1793
<b>8C</b>	<b>0.0474</b>	18O	0.1996
<b>9C</b>	<b>0.2112</b>	19O	0.1877
10C	0.0306		

<sup>a</sup> See Fig. 1 for atom numbering.

<sup>b</sup> Atoms in bold means these atoms have the highest  $FED^2_{HOMO} + FED^2_{LUMO}$  values, thus are more likely to be attacked by hydroxyl radical.

Fig. 6.5A describes the evolution profiles of five major intermediates of PBSA (i.e., mono-hydroxylated benzamidine (OH-BZMD); three isomers of mono-hydroxylated PBSA (OH-PBSA, A, C and E, respectively); and mono-hydroxylated 2-phenyl-1H-benzimidazole (OH-PBI)) during photocatalytic degradation. As seen, all the intermediates quickly reached to maximum concentration during 10 min to 20 min followed by a gradually decay, indicating the formation and transformation of these intermediates were accompanied with the degradation of PBSA. Complete disappearance of these intermediates was observed after 90 min, suggesting TiO<sub>2</sub> photocatalysis is a promising technique for PBSA removal as well as intermediates elimination. The disappearance of the intermediates is also a reflection of further oxidation to low molecular weight organic compounds (e.g., carboxylic acids) or mineralization to inorganic ions.

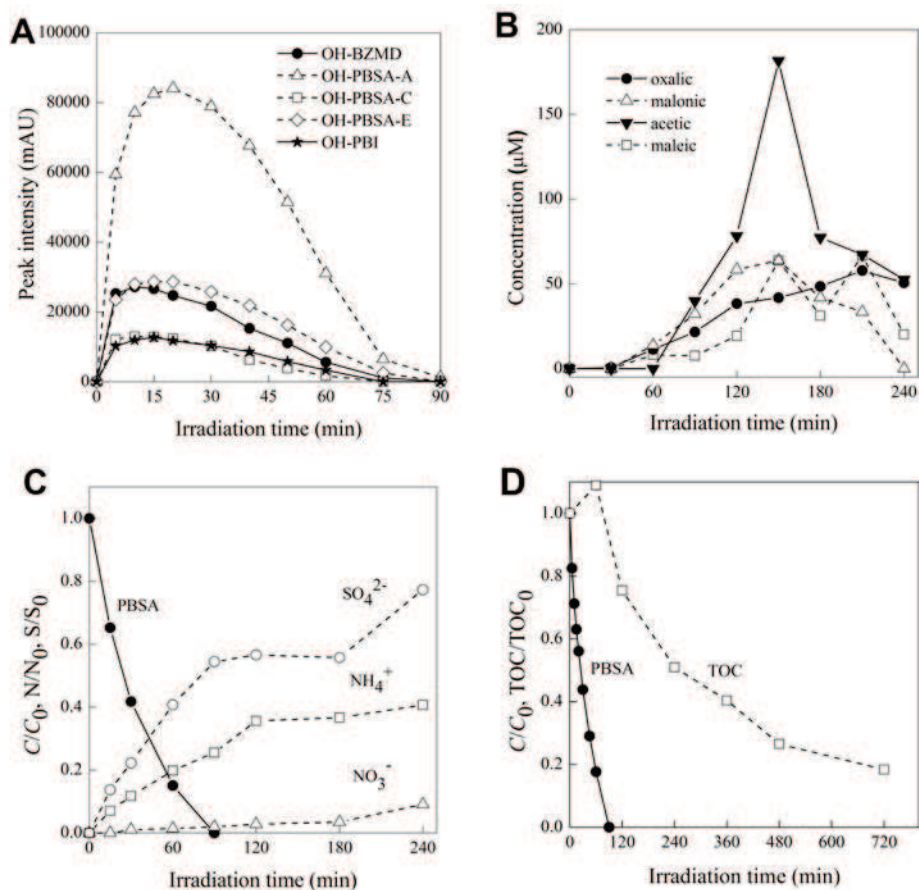


Fig. 6.5. Evolution of (A) organic intermediates, (B) carboxylic acids, (C) inorganic ions and (D) the variation of TOC during photocatalytic degradation of PBSA. Peak intensity was recorded according to HPLC-DAD spectrum. The detection wavelength was  $\lambda = 300$  nm. OH-BZMD = mono-hydroxylated benzimidine; OH-PBSA = mono-hydroxylated PBSA; OH-PBI = mono-hydroxylated 2-phenyl-1H-benzimidazole. Experimental conditions: Degussa P25  $\text{TiO}_2$  was used as photocatalyst;  $[\text{TiO}_2] = 2.0 \text{ g L}^{-1}$ ;  $[\text{PBSA}] = 45 \mu\text{M}$ ;  $\text{pH} = 4.5$ .

#### 6.1.4.2. Evolution of carboxylic acids

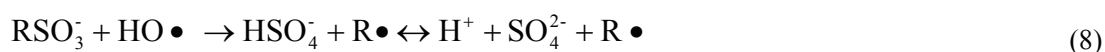
It is well-known that further oxidation of intermediates during photocatalysis usually leads to ring opening, generating a series of carboxylic acids with lower molecular weight before complete mineralization.<sup>14,28,32</sup> In this work, four major acids (i.e., oxalic, malonic, acetic and maleic acid) were identified by ion exchange chromatography by comparison with standards. Fig. 6.5B shows the evolution of these carboxylic acids as a function of irradiation time.

As seen, oxalic acid appeared as early as 30 min, and then gradually accumulated up to 57.8  $\mu\text{M}$  at 210 min followed by a slow disappearance. The formation of oxalic acid can be explained either by the benzene ring opening or by dimerization of  $\text{HCO}_2$  radicals as reported by previous

studies.<sup>28</sup> Oxalic could be oxidized to two molecular of CO<sub>2</sub> by photo-holes through photo-Kolbe mechanism.<sup>14</sup> Since maleic acid has been known to be an important intermediate after ring opening,<sup>14</sup> its detection in the present study was not unexpected. Malonic acid appeared at 60 min, reached a maximum (63.8 μM) at 150 min, and then gradually disappeared. Acetic acid was not observed until 90 min later and reached to maximum (181.6 μM) at 150 min, followed by a notable decrease. Note that the concentration of acetic was the highest among the four carboxylic acids. Therefore, acetic acid was presumably resulted from the transformation of other carboxylic acids such as malonic and maleic acid.<sup>14</sup> Based on the above analysis, a description of the formation and transformation of carboxylic acids is presented in solid line box in Fig. 6.6.

#### 6.1.4.3. Evolution of inorganic ions

Complete mineralization is the ultimate step in photocatalytic degradation of organic compounds. Thus, it is essential to investigate not only the disappearance of the initial pollutant but also its mineralization to CO<sub>2</sub> and inorganic ions. The evolution of inorganic ions during PBSA photocatalysis process is depicted in Fig. 6.5C. As clearly seen, sulfonic moiety in PBSA was converted to sulfate ions (SO<sub>4</sub><sup>2-</sup>) while nitrogen atoms in imidazole structure were released as ammonium (NH<sub>4</sub><sup>+</sup>) and nitrate (NO<sub>3</sub><sup>-</sup>). At 90 min, 45 μM PBSA was completely degraded, while only 25.5% and 1.9% of the nitrogen and 54.5% of sulfur were released as NH<sub>4</sub><sup>+</sup>, NO<sub>3</sub><sup>-</sup> and SO<sub>4</sub><sup>2-</sup>, respectively. It is interesting to note that a majority of N was converted to NH<sub>4</sub><sup>+</sup> while only a minor amount of N was transformed to NO<sub>3</sub><sup>-</sup>. This observation is consistent with previous reports that nitrogen in heterocyclic aromatic rings can be transformed to both NH<sub>4</sub><sup>+</sup> and NO<sub>3</sub><sup>-</sup> species, while secondary, tertiary and quaternary nitrogen atoms are photo-converted predominantly to ammonium ions.<sup>41,42</sup> Increasing the irradiation time favors the releasing of inorganic species. At 240 min, 40.7% and 9.1% of the N and 77.3% of S were released as NH<sub>4</sub><sup>+</sup>, NO<sub>3</sub><sup>-</sup> and SO<sub>4</sub><sup>2-</sup>, respectively. It is evident that less than 50% of total N was mineralized, indicating a significant amount of nitrogenated transformation products at the end of the treatment. Therefore, 240 min irradiation seemed to be not enough to yield a full mineralization. Unlike nitrogen, sulfur is expected to be quickly converted to SO<sub>4</sub><sup>2-</sup> under the attack of HO• as the following equation describes.<sup>43</sup>



---

The reason for 77.3% S transformation ratio can be rationalized by the following: (i) complete mineralization of S containing organic intermediates was not obtained after 240 min irradiation, (ii) S atom was initially released as HS<sup>-</sup> or SO<sub>3</sub><sup>2-</sup> rather than directly oxidation to SO<sub>4</sub><sup>2-</sup>,<sup>41</sup> (iii) SO<sub>4</sub><sup>2-</sup> was probably strongly adsorbed on TiO<sub>2</sub> active sites which led the detection amount below the stoichiometric value.<sup>44</sup>

#### 6.1.4.4. Mineralization

The photocatalytic degradation of organic pollutants usually leads to the decomposition of structure and eventually the mineralization to CO<sub>2</sub> and H<sub>2</sub>O, which can be visualized by the decrease of TOC.<sup>45</sup> Fig. 6.5D shows the variation of TOC during photocatalytic degradation of PBSA. It was observed that TOC reduction processed much more slowly compared to the degradation of PBSA. This finding indicates the formation of more stable intermediates toward photo-oxidation.<sup>31</sup> However, approximately 80% TOC was removed after 720 min irradiation. Therefore, we can expect to have a mineralization at a very long irradiation time.

#### 6.1.5. Elucidation of photocatalytic degradation pathways

Based on the elucidated molecular structure of photoproducts, possible TiO<sub>2</sub>-induced photodegradation pathways of PBSA are proposed as illustrated in Fig. 6.6. As can be seen, three major pathways, namely, successive hydroxylation of mother compound (Pathway I), imidazole ring cleavage (Pathway II) and de-sulfonic as well as further hydroxylation and oxidation (Pathway III), are involved in the photocatalytic degradation of PBSA.

- (I) The successive addition of HO• to mother compound leads to the formation of mono-, di-, and tri-hydroxylated PBSA. A total five mono-hydroxylation, three di-hydroxylation and one tri-hydroxylation products were detected according to LC-MS spectrum. Since HO• is known to be electrophilic, the rich electron density of benzimidazole and phenyl ring may facilitate its addition. The calculated frontier electron densities revealed that both the two benzene moiety in PBSA molecular appeared to be susceptible to the electrophilic attack of the HO•, resulting in the formation of mono-hydroxylation. It is well accepted that hydroxylation is usually the first step, but also the most important step during photocatalysis. Hydroxylated organic compounds further undergo structure decomposition, such as ring opening and chain cleavage, which eventually lead to complete mineralization.<sup>46</sup>

- 
- (II) The two N atoms in imidazole group have been reported to be the sites most likely attacked by HO• due to their much higher electron density.<sup>47</sup> The substrate molecular will break at these points, forming some precursor intermediates toward formation of NH<sub>4</sub><sup>+</sup> such as an amide.<sup>48</sup> In this work, the corresponding C-N bonds cleavage leads to the formation of benzamidine (BZMD) after imidazole ring opening. Further attack of HO• could either oxidize BZMD to benzamide or form hydroxylated benzamidine (OH-BZMD). Note that two isomers of OH-BZMD were detected according to LC-MS analysis, possibly resulted from *para*- and *ortho*- addition because of the electron donating effect of amidine moiety. *Para*-hydroxyl benzamidine has been known to absorb appreciably at 300 nm,<sup>49</sup> which was confirmed in our HPLC-DAD chromatogram. It is also possible that OH-BZMD arose from the C-N bonds rupture of mono-hydroxylated PBSA. BZMD has been observed previously in PBSA photolysis as an important intermediate.<sup>13</sup> However, it was not detected in this work, probably due to a rapid transformation under HO• attack. During TiO<sub>2</sub> photocatalysis process, benzamide could further transform to 4-hydroxyl benzamide and hydroquinone followed by ring opening.<sup>50</sup>
- (III) Pathway III is initiated by the detachment of sulfonic moiety in benzimidazole group, which consequently converts to sulfate. The detection of sulfate ions by ion chromatography (IC) verified the feasibility of such process. The de-sulfonic product 2-phenyl-1H-benzimidazole (PBI) further undergoes hydroxylation under the successive HO• attack. The hydroxylated PBI (OH-PBI) is supposed to generate 2-phenyl-4-carboxyl-5-aldehyde imidazole via benzene ring opening under further HO• attack. Similar benzene ring opening has been previously observed during photocatalytic degradation of thiabendazole, one kind of benzimidazole derivative fungicide which has similar structure with PBI.<sup>51</sup> Further oxidation of aldehyde group generate 2-phenyl-4, 5-imidazolecarboxylic acid, which subsequently lost one carboxyl group through photo-Kolbe mechanism to form two isomers of 2-phenyl-imidazole carboxylic acid. It should be emphasized that some intermediate products (i.e., phenylimidazolecarboxylic derivatives and benzamide) were also observed by Zhang et al. in direct photolysis of PBSA,<sup>13</sup> suggesting the similar

degradation pathways are possibly involved in photolysis and photocatalysis.

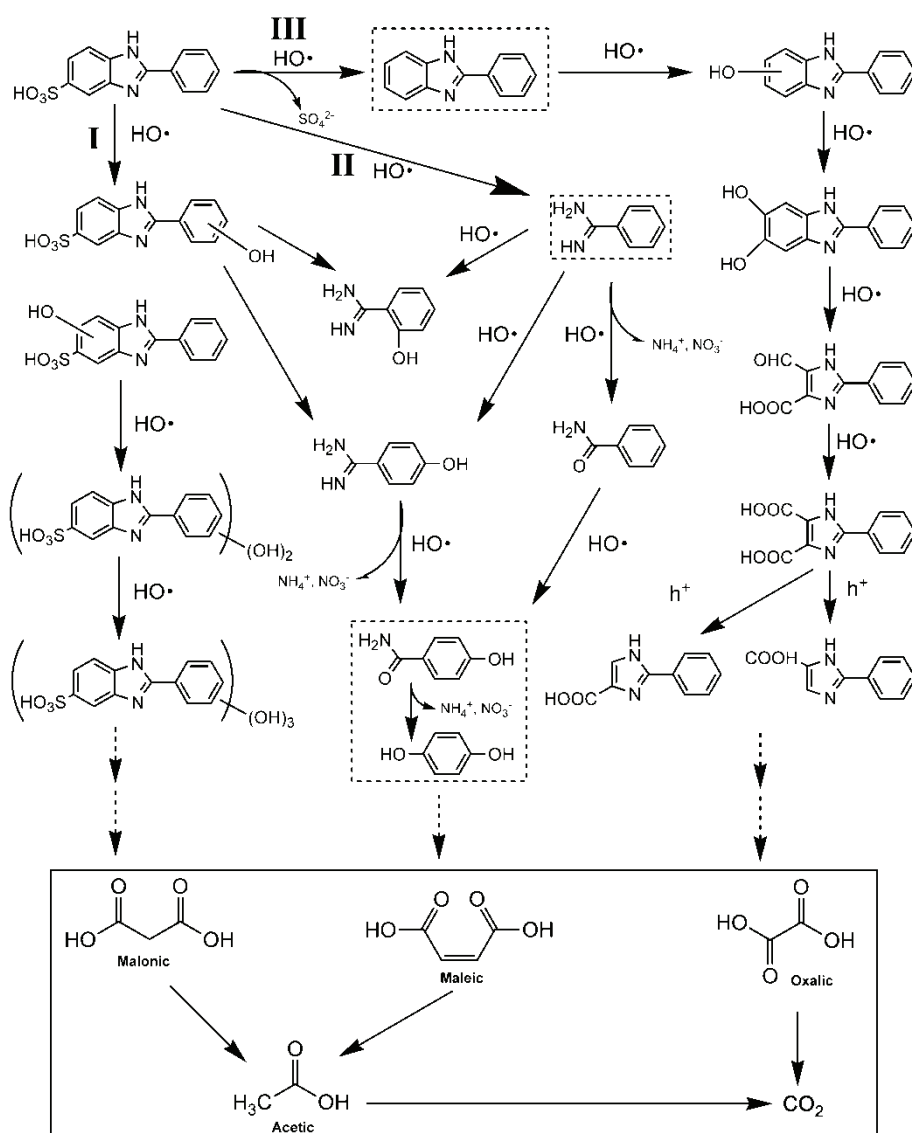


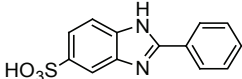
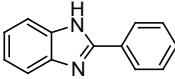
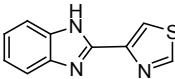
**Fig. 6.6.** Possible photocatalytic degradation pathways of PBSA in illuminated aqueous TiO<sub>2</sub> suspensions. Chemicals in dash line box were not detected in this work by using LC-MS but were previously reported [14,52]. Possible formation and transformation pathways of carboxylic acids were also elucidated as proposed in solid line box.

### 6.1.6. Comparison to structurally related compounds

To obtain a further insight into the mechanism of photocatalysis, PBSA was compared to benzimidazole (BI), 2-phenyl-1H-benzimidazole (PBI) and 2-(4-thiazolyl)-1H-benzimidazole (thiabenzazole) in photocatalytic degradation because these compounds have a benzimidazole ring in common. Table 3 compares the experimental results of photocatalytic degradation of these benzimidazole analogs under identical conditions. PBI has the same molecular structure as PBSA

except that the latter has a sulfonic moiety linking to the benzimidazole ring. Due to the electron-withdraw effect, the lack of sulfonic moiety in PBI was expected to facilitate its photocatalytic degradation via HO• attack. However, no enhancement in photocatalytic degradation rate of PBI was observed in comparison to PBSA (Table 6.3), suggesting 5-sulfonic moiety in PBSA had negligible effect on the photocatalysis of PBI. Previous studies have demonstrated that the two compounds actually have very similar photophysical and photochemical properties.<sup>12</sup> This result was also supported by the fact that the possibility of HO• attacking on 2-phenyl group is much higher than benzyl group in PBSA as illustrated by FEDs calculation. PBI has also known to be a product of PBSA upon photolysis, however, it was not detected by LC-MS in this work. BI photocatalytically degraded at a rate constant approximately 1.6 times faster than PBSA and PBI (Table 6.3). This result was unexpected and interesting. Due to the 2-phenyl substitution in PBSA and PBI, and the electrophilic and nonselective nature of HO•, we postulated that the photocatalytic degradation of PBSA and PBI would have processed much more rapidly than BI because 2-phenyl provided additional sites for HO• attack. However, BI was found to be more susceptible to photocatalytic destruction. It is possible that 2-phenyl substitution enabled BI molecular being more resistant to photocatalytic degradation.

**Table 6.3. Photocatalytic degradation of PBSA and structurally related compounds.**

Compounds	Molecular structure	Degradation rate constant (min <sup>-1</sup> ) <sup>a</sup>	Linear correlation coefficient (R <sup>2</sup> )
2-phenylbenzimidazole-5-sulfonic acid (PBSA)		0.0381 ± 0.0026	0.999
Benzimidazole (BI)		0.0591 ± 0.0064	0.980
2-phenyl-1H-benzimidazole (PBI)		0.0352 ± 0.0022	0.996-0.999
2-(4-thiazolyl)-1H-benzimidazole (thiabenzazole) <sup>b</sup>		NA <sup>c</sup>	NA

<sup>a</sup> Experimental conditions: Degussa P25 TiO<sub>2</sub> was used as photocatalyst; [substrate] = 45 μM; [TiO<sub>2</sub>] = 1.0 g L<sup>-1</sup>; pH = 7.0. Errors are 95% confidence intervals.

<sup>b</sup> Photocatalytic degradation pathways of thiabenzazole was compared to PBSA according to reference [55].

<sup>c</sup> NA = not available. No kinetic data of thiabenzazole photocatalysis was available in reference [55].

---

A noticeable peak corresponding to the photoproduct was found in the HPLC-DAD chromatogram of the irradiated PBI sample. Although further LC-MS analysis is necessary for the accurate identification of this photoproduct, its nearly identical UV-vis spectrum relative to the mother compound as well as the early retention time implied that this photoproduct was most likely to be the hydroxylated product. This result was consistent with the pathway III proposed in Fig. 6.6. A similar peak was also observed in the case of BI. The evolution of the photoproducts of PBI and BI during photocatalysis process was also depicted in Fig. S5 (Supplementary Data). Note that the evolution profiles were only qualitative because there were no standards available of the photoproducts to ensure their quantitative analysis.

On the other hand, thiabendazole, a widely used fungicide, has a thiazole ring adjacent to benzimidazole ring instead of a phenyl ring in PBI. A previous study on identification of thiabendazole phototransformation products on  $\text{TiO}_2$  by Calza et al. showed that there are two different parallel pathways: (i) the hydroxylation of the molecular on the aromatic ring, a further oxidation leads to ring opening and to the formation of aldehydic and alcoholic structure; (ii) the cleavage of a C-C bond and the formation of benzimidazole.<sup>51</sup> It is apparent that pathway (i) was identical to the pathway III as we proposed in photocatalytic degradation of PBSA in this work (Fig. 6.6). However, the cleavage of the bond between benzimidazole and phenyl ring was not observed in the present study, which differed from thiabendazole in photocatalytic degradation. This finding can be explained by the strong  $\pi$ - $\pi$  conjugation of benzimidazole and phenyl ring, resulting in the bond being stable. Similar result has been observed previously by a study on photolysis of various 2-substituted benzimidazoles.<sup>52</sup> It has been proposed that 2-phenyl group stabilizes the benzimidazole ring system to photolysis as does the 2-thiazolyl group; however, the latter suffers thiazole ring cleavage.<sup>52</sup> This finding also supported the above result that BI was substantially more susceptible to photocatalytic degradation compared to PBSA and PBI.

## 6.2. Conclusions

The aqueous photocatalytic degradation of sunscreen agent 2-phenylbenzimidazole-5-sulfonic acid (PBSA) has been studied in illuminated  $\text{TiO}_2$  suspensions.  $\text{TiO}_2$ -induced photocatalysis resulted in a pronounced degradation of PBSA. Photocatalytic reactions followed pseudo-first-order kinetics. Radical scavenger experiments indicated that  $\text{HO}\cdot$  was the predominant radical responsible for an appreciable degradation of PBSA. Secondary order

---

rate constant of PBSA-HO• reaction was determined to be  $5.8 \times 10^9 \text{ M}^{-1} \text{ s}^{-1}$  by competition kinetics method, suggesting HO•-mediated PBSA oxidation is near the diffusion-controlled limit. Organic intermediates were identified by LC-MS analysis, and the major photoproducts included hydroxylated products, imidazole ring cleavage compounds and phenylimidazolecarboxylic derivatives. Frontier electron densities (FEDs) calculation predicted that both the two benzenes in PBSA are likely to be attacked by HO•, resulting in the formation of mono-hydroxylation products. Four carboxylic acids, oxalic, malonic, acetic and maleic acids were detected during PBSA photocatalysis. Sulfonic moiety of PBSA was primarily released as sulfate ion while nitrogen atoms were converted predominantly to ammonium and a less extent to nitrate. Approximately 80% TOC was removed after 720 min irradiation, implying mineralization can be expected to obtain after a very long irradiation time. A comparative study on photocatalytic degradation of PBSA and structurally related compounds revealed that the 5-sulfonic moiety had negligible effect on the photocatalysis while 2-phenyl substituent stabilized the benzimidazole ring system to photocatalytic degradation.

Although results from the present study suggest that TiO<sub>2</sub> photocatalysis is a promising treatment technology for sunscreen agent PBSA, a thorough evaluation of the toxicity of intermediates is essential in order to optimize photocatalytic treatment and evaluate the potential risks to the ecology system before the technology is applied for water purification.

### 6.3. Reference

- (1) Gasparro, F.P. Sunscreens, skin photobiology, and skin cancer: the need for UVA protection and evaluation of efficacy. *Environ. Health Perspect.* **2000**, 108, 71-78.
- (2) Poiger, T.; Buser, H.R.; Balmer, M.E.; Bergqvist, P.A.; Müller, M.D. Occurrence of UV filter compounds from sunscreens in surface waters: regional mass balance in two Swiss lakes. *Chemosphere* **2004**, 55, 951-963.
- (3) Plagellat, C.; Kupper, T.; Furrer, R.; Felipe de Alencastro, L.; Grandjean, D.; Tarradellas, J. Concentrations and specific loads of UV filters in sewage sludge originating from a monitoring network in Switzerland. *Chemosphere* **2006**, 62, 915- 925.
- (4) P. Gago-Ferrero, M. Silvia Díaz-Cruz, D. Barceló. Liquid chromatography-tandem mass spectrometry for the multi-residue analysis of organic UV-filters and their transformation products in the aquatic environment. *Anal. Methods* **2013**, 5, 355-366.
- (5) Schwarzenbach, R.P.; Escher, B.I.; Fenner, K.; Hofstetter, T.B.; Annette Johnson, C.; von Gunten, U; Wehrli, B. The challenge of micropollutants in aquatic systems. *Science* **2006**, 313,

---

1072-1077.

(6) Schlumpf, M.; Schmid, P.; Durrer, S.; Conscience, M.; Maerker, K.; Henseler, M.; Gruetter, M.; Herzog, I.; Reolon, S.; Ceccatelli, R.; Faass, O.; Stutz, E.; Jarry, H.; Wuttke, W.; Lichtensteiger, W. Endocrine activity and developmental toxicity of cosmetic UV filters-an update. *Toxicology* **2004**, 205, 113-122.

(7) Dí'az-Cruz, S.M.; Llorca, M.; Barceló, D. Organic UV filters and their photodegradates, metabolites and disinfection by-products in the aquatic environment. *Trend. Anal. Chem.* **2008**, 27, 873-887.

(8) Dí'az-Cruz, S.M.; Barceló, D. Chemical analysis and ecotoxicological effects of organic UV-absorbing compounds in aquatic ecosystems. *Trend. Anal. Chem.* **2009**, 28, 708-717.

(9) Daughton, C.G.; Ternes, T.A. Pharmaceuticals and personal care products in the environment: agents of subtle change?. *Environ. Health Perspect.* **1999**, 107, 907-938.

(10) Rodil, R.; Quintana, J.B.; López-Mahía, P.; Muniategui-Lorenzo, S.; Prada-Rodríguez, D. Multiclass determination of sunscreen chemicals in water samples by liquid chromatography-tandem mass spectrometry. *Anal. Chem.* **2008**, 80, 1307-1315.

(11) Gilbert, E.; Pirot, F.; Bertholle, V.; Roussel, L.; Falson, F.; Padois, K. Commonly used UV filter toxicity on biological functions: review of last decade studies. *Int. J. Cosmet. Sci.* **2012**, 1-12.

(12) Johnson Inbaraj, J.; Bilski, P.; Chignell, C. F. Photophysical and photochemical Studies of 2-phenylbenzimidazole and UVB sunscreen 2-phenylbenzimidazole-5-sulfonic acid. *Photochem. Photobiol.* **2002**, 75, 107-116.

(13) Zhang, S.; Chen, J.; Qiao, X.; Ge, L.; Cai, X.; Na, G. Quantum chemical investigation and experimental verification on the aquatic photochemistry of the sunscreen 2-phenylbenzimidazole-5-sulfonic acid. *Environ. Sci. Technol.* **2010**, 44, 7484-7490.

(14) Herrmann, J.-M. Heterogeneous photocatalysis: fundamentals and applications to the removal of various types of aqueous pollutants. *Catal. Today* **1999**, 53, 115-129.

(15) Khodja, A. A.; Lavedrine, B.; Richard, C.; Sehili, T. Photocatalytic degradation of metoxuron in aqueous suspensions of TiO<sub>2</sub>. analytical and kinetic studies. *Int. J. Photoenergy* **2002**, 4, 147-151.

(16) Haque, M. M.; Muneer, M.; Bahnemann, D. W. Semiconductor-mediated photocatalyzed degradation of a herbicide derivative, chlorotoluron, in aqueous suspensions. *Environ. Sci. Technol.* **2006**, 40, 4765-4770.

(17) Hurum, D. C.; Agrios, A. G.; Gray, K. A. Explaining the enhanced photocatalytic activity of

- 
- Degussa P25 mixed-phase TiO<sub>2</sub> using EPR. *J. Phys. Chem. B* **2003**, 107, 4545-4549.
- (18) Ryu, J.; Choi, W. Substrate-specific photocatalytic activities of TiO<sub>2</sub> and multiactivity test for water treatment application. *Environ. Sci. and Technol.* **2008**, 42, 294-300.
- (19) Rao, Y. F.; Chu, W. Reaction mechanism of linuron degradation in TiO<sub>2</sub> suspension under visible light irradiation with the assistance of H<sub>2</sub>O<sub>2</sub>. *Environ. Sci. Technol.* **2009**, 43, 6183-6189.
- (20) Kim, J. ; Lee, C.W. ; Choi, W. Platinized WO<sub>3</sub> as an environmental photocatalyst that generates OH radicals under visible light. *Environ. Sci. Technol.* **2010**, 44, 6849-6854.
- (21) Park, H.; Park, Y. ; Kim, W.; Choi, W. Surface modification of TiO<sub>2</sub> photocatalyst for environmental application. *J. Photochem. Photobiol. C : Photochem. Rev.*  
<http://dx.doi.org/10.1016/j.jphotochemrev.2012.10.001>.
- (22) Sun, Y.; Pignatello, J. J. Evidence for a surface dual hole-radical mechanism in the titanium dioxide photocatalytic oxidation of 2,4-D. *Environ. Sci. Technol.* **1995**, 29, 2065-2072.
- (23) Chen, Y.; Yang, S.; Wang, K.; Lou, L. Role of primary active species and TiO<sub>2</sub> surface characteristic in UV-illuminated photodegradation of Acid Orange 7. *J. Photochem. Photobiol. A: Chem.* **2005**, 172, 47-54.
- (24) Martin, S. T.; Lee, A. T.; Hoffmann, M. R. Chemical mechanism of inorganic oxidants in the TiO<sub>2</sub>/UV process: increased rates of degradation of chlorinated hydrocarbons. *Environ. Sci. Technol.* **1995**, 29, 2567-2573.
- (25) Yang, L.; Yu, L. E.; Ray, M. B. Photocatalytic oxidation of paracetamol : dominant reactants, intermediates, and reaction mechanism. *Environ. Sci. Technol.* **2009**, 43, 460-465.
- (26) Nan Chong, M.; Jin, B.; Chow, C. W. K.; Saint, C. Recent developments in photocatalytic water treatment technology: A review. *Water Res.* **2010**, 44, 2997-3027.
- (27) Hapeshi, E.; Achilleos, A.; Vasquez, M. I. Drugs degrading photocatalytically: kinetics and mechanisms of ofloxacin and atenolol removal on titania suspensions. *Water Res.* **2010**, 44, 1737-1746.
- (28) Sleiman, M.; Conchon, P.; Ferronato, C.; Chovelon, J.-M. Iodosulfuron degradation by TiO<sub>2</sub> photocatalysis: Kinetic and reactional pathway investigations. *Appl. Catal. B: Environ.* **2007**, 71, 279-290.
- (29) Ahmed, S.; Rasul, M. G.; Brown, R.; Hashib, M. A. Influence of parameters on the heterogeneous photocatalytic degradation of pesticides and phenolic contaminants in wastewater:

- 
- a short review. *J. Environ. Manag.* **2011**, 92, 311-330.
- (30) Abramović, B.; Šojić, D.; Despotović, V.; Vione, D.; Pazzi, M.; Csanádi, J. A comparative study of the activity of TiO<sub>2</sub> Wackherr and Degussa P25 in the photocatalytic degradation of picloram. *Appl. Catal. B: Environ.* **2011**, 105, 191-198.
- (31) Lin, X.; Ferronato, C.; Deng, N.; Wu, F.; Chovelon, J.-M. Photocatalytic degradation of methylparaben by TiO<sub>2</sub>: Multivariable experimental design and mechanism. *Appl. Catal. B: Environ.* **2009**, 88, 32-41.
- (32) Lagunas-Allué, L.; Martínez-Soria, M.-T.; Sanz-Asensio, J.; Salvador, A.; Ferronato, C.; Chovelon, J.-M. Photocatalytic degradation of boscalid in aqueous titanium dioxide suspension: Identification of intermediates and degradation pathways. *Appl. Catal. B: Environ.* **2010**, 98, 122-131.
- (33) Radjenović, J.; Sirtori, C.; Petrović, M.; Barceló, D.; Malato, S. Solar photocatalytic degradation of persistent pharmaceuticals at pilot-scale: kinetics and characterization of major intermediate products. *Appl. Catal. B: Environ.* **2009**, 89, 255-264.
- (34) Sirtori, C.; Agüera, A.; Gernjak, W. Effect of water-matrix composition on trimethoprim solar photodegradation kinetics and pathways. *Water Res.* **2010**, 44, 2735-2744.
- (35) Huang, J. P.; Mabury, S. A. A new method for measure carbonate radical reactivity toward pesticides. *Environ. Toxicol. Chem.* **2000**, 19, 1501-1507.
- (36) Brezonik, P. L.; Fulkerson-Brekken, J. Nitrate-induced photolysis in natural waters: Controls on concentrations of hydroxyl radical photo-intermediates by natural scavenging agents. *Environ. Sci. Technol.* **1998**, 32, 3004-3010.
- (37) Hu, L.; Flanders, P. M.; Miller, P. L.; Strathmann, T. J. Oxidation of sulfamethoxazole and related antimicrobial agent by TiO<sub>2</sub> photocatalysis. *Water Res.* **2007**, 41, 2612-2626.
- (38) Corin, N.; Backlund, P.; Kulovaara, M. Degradation products formed during UV-irradiation of humic water. *Chemosphere* **1996**, 33, 245-255.
- (39) An, T.; Yang, H.; Li, G.; Song, W.; Cooper, W. J.; Nie, X. Kinetics and mechanism of advanced oxidation processes (AOPs) in degradation of ciprofloxacin in water. *Appl. Catal. B: Environ.* **2010**, 94, 288-294.
- (40) Ohko, Y.; Iuchi, K.; Niwa, C.; Tatsuma, T.; Nakashima, T.; Iguchi, T.; Kubota, Y.; Fujishima, A. 17 $\beta$ -Estradiol degradation by TiO<sub>2</sub> photocatalysis as a means of reducing estrogenic activity.

---

*Environ. Sci. Technol.* **2002**, 36, 4175-4181.

- (41) Calza, P.; Medana, C.; Baiocchi, C.; Pelizzetti, E. Thioureas methyl-derivatives photo-induced transformation on titanium dioxide. *J. Photochem. Photobiol. A: Chem.* **2007**, 189, 380-386.
- (42) Yang, H.; Li, G.; An, T.; Gao, Y.; Fu, J. Photocatalytic degradation kinetics and mechanism of environmental pharmaceuticals in aqueous suspension of TiO<sub>2</sub>: A case of sulfa drugs. *Catal. Today* **2010**, 153, 200-207.
- (43) Szabó-Bárdos, E.; Markovics, O.; Horváth, O.; Törő, N.; Kiss, G. Photocatalytic degradation of benzenesulfonate on colloidal titanium dioxide. *Water Res.* **2011**, 45, 1617-1628.
- (44) Sleiman, M.; Vildoza, D.; Ferronato, C.; Chovelon, J.-M. Photocatalytic degradation of azo dye Metanil Yellow: optimization and kinetic modeling using a chemometric approach. *Appl. Catal. B: Environ.* **2007**, 77, 1-11.
- (45) Lagunas-Allué, L.; Martínez-Soria, M.-T.; Sanz-Asensio, J.; Salvador, A.; Ferronato, C.; Chovelon, J.-M. Degradation intermediates and reaction pathway of pyraclostrobin with TiO<sub>2</sub> photocatalysis. *Appl. Catal. B: Environ.* **2012**, 115-116, 285-293.
- (46) Méndez-Arriaga, F.; Esplugas, S.; Giménez, J. Photocatalytic degradation of non-steroidal anti-inflammatory drugs with TiO<sub>2</sub> and simulated solar irradiation. *Water Res.* **2008**, 42, 585-594.
- (47) Hidaka, H.; García-López, E.; Palmisano, L.; Serpone, N. Photoassisted mineralization of aromatic and aliphatic N-heterocycles in aqueous titanium dioxide suspensions and the fate of the nitrogen heteroatoms. *Appl. Catal. B: Environ.* **2008**, 78, 139-150.
- (48) Pelizzetti, E.; Calza, P.; Mariella, G.; Maurino, V.; Minero, C.; Hidaka, H. Different photocatalytic fate of amido nitrogen in formamide and urea. *Chem. Commun.* **2004**, 13, 1504-1505.
- (49) Rogana, E.; Nelson, D. L.; Mares-Guia, M. Characterization of the ultraviolet absorption spectra of p-substituted derivatives of benzamidine. *J. Am. Chem. Soc.* **1975**, 97, 6844-6848.
- (50) Piscopo, A.; Robert, D.; Weber, J. V. Comparison between the reactivity of commercial and synthetic TiO<sub>2</sub> photocatalysts. *J. Photochem. Photobiol. A: Chem.* **2001**, 139, 253-256.
- (51) Calza, P.; Baudino, S.; Aigotti, R.; Baiocchi, C.; Pelizzetti, E. Ion trap tandem mass spectrometric identification of thiabendazole phototransformation products on titanium dioxide. *J. Chromatogr. A.* **2003**, 984, 59-66.

---

(52) Crank, G.; Mursyidi, A. Photochemistry of heterocyclics. III. Photolysis of various 2-substituted benzimidazoles. *Aust. J. Chem.* **1982**, *35*, 775-784.

#### 6.4. Supplementary Material

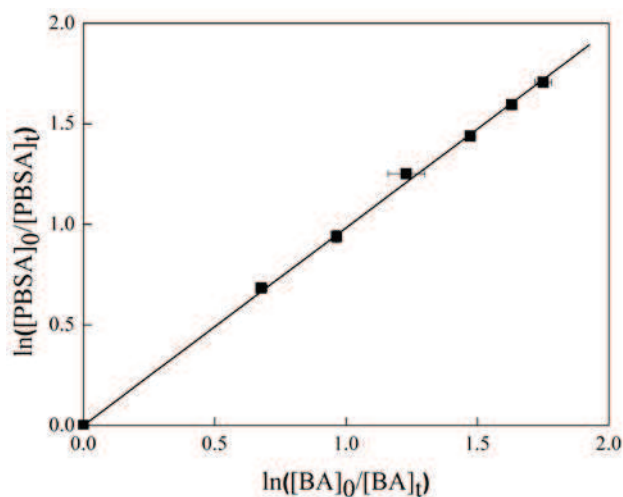


Fig. S1. Determination of second-order rate constant for reaction of PBSA with HO• by competition kinetics method. [PBSA] = 60  $\mu\text{M}$ ; [BA] = 60  $\mu\text{M}$ ;  $[\text{Fe}^{2+}] = 0.2 \text{ mM}$ ;  $[\text{H}_2\text{O}_2] = 0.5 \text{ mM}$ ; pH = 3.5.

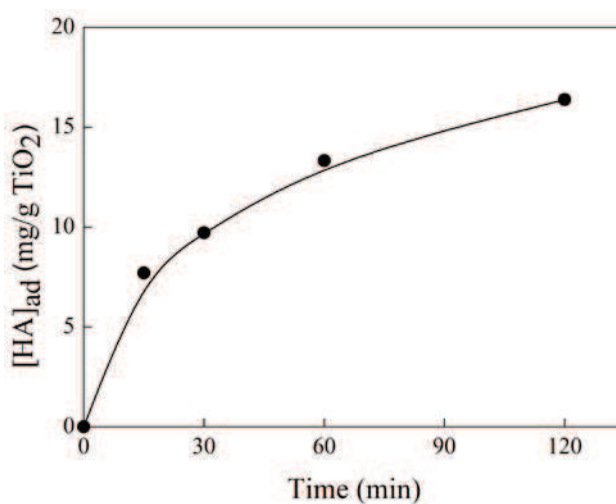


Fig. S2. The adsorption mass (mg/g TiO<sub>2</sub>) of humic acid (HA) on TiO<sub>2</sub> at various time.  $[\text{HA}]_0 = 60 \text{ mg L}^{-1}$ ,  $[\text{TiO}_2] = 2.0 \text{ g L}^{-1}$ . The TOC content of the HA solution with TiO<sub>2</sub> particle filtered was measured by a SHIMADZU 5050A TOC analyzer. HA concentration ( $\text{mg L}^{-1}$ ) was calculated based on a calibration curve obtained by plotting measured TOC values via standard HA concentrations.

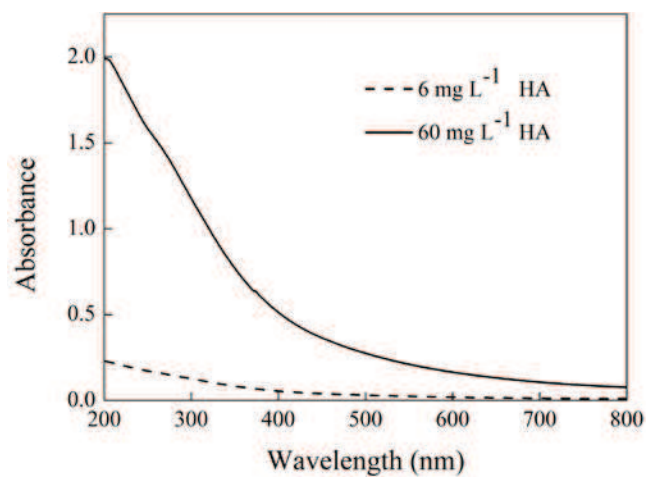


Fig. S3. UV-visible absorption spectra of the humic acid (HA) solutions: (...) 6 mg L<sup>-1</sup> HA; (—) 60 mg L<sup>-1</sup> HA.

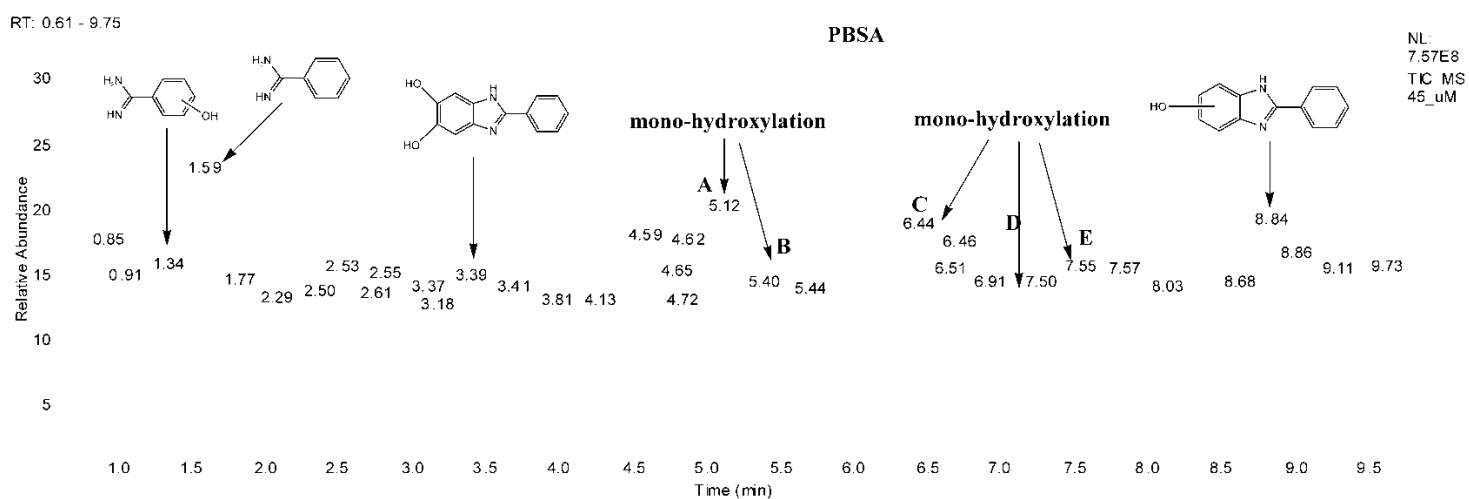


Fig. S4. Total ion chromatogram (TIC) obtained in TSI(+) MS of PBSA photocatalytic degradation sample.

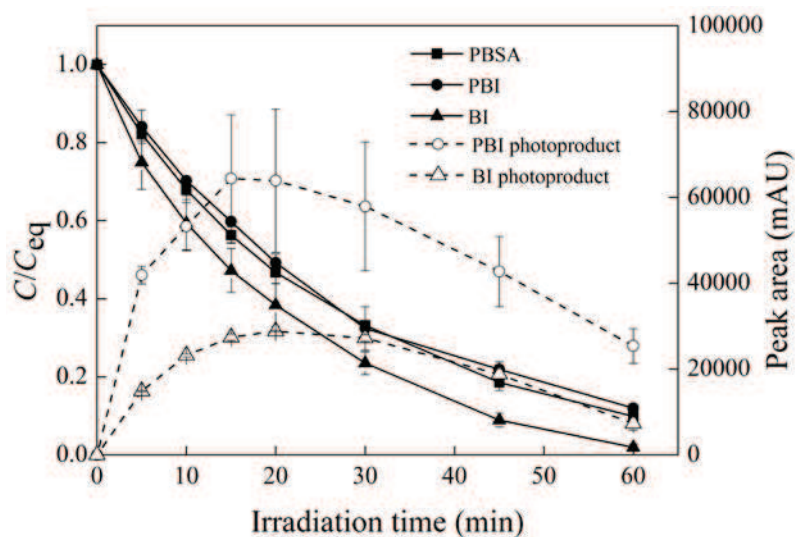


Fig. S5. Photocatalytic degradation of PBSA and structurally related compounds and the formation of photoproducts as a function of the irradiation time: (■) 2-phenylbenzimidazole-5-sulfonic acid (PBSA), (●) 2-phenyl-1H-benzimidazole (PBI), (▲) benzimidazole (BI), and (○) the photoproduct of PBI, (△) the photoproduct of BI. Degussa P25 TiO<sub>2</sub> was used as photocatalyst. Experimental condition: [substrate] = 45 μM; [TiO<sub>2</sub>] = 1.0 g L<sup>-1</sup>; pH = 7.0. Peak areas of the photoproducts were recorded according to the HPLC-DAD chromatogram. The detection wavelength was 300 nm and 266 nm for the photoproduct of PBI and BI, respectively. Error bars represent the 95% confidence intervals.

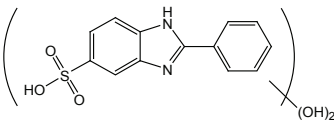
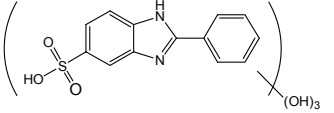
**Table S1. Reaction rate constant and linear correlation coefficient of photocatalytic degradation of PBSA with or without radical scavengers.**

Scavenger <sup>a</sup>	Reactive species	$k_p$ (min <sup>-1</sup> )	$R^2$
	quenched		
no scavenger	-	0.0486	0.991
0.4 mM KI	$h_{vb}^+$ and $HO\bullet$	0.0038	0.998
4 mM KI	$h_{vb}^+$ and $HO\bullet$	0.0011	0.940
10 mM <i>tert</i> -butanol	$HO\bullet$	0.0274	0.994
100 mM <i>tert</i> -butanol	$HO\bullet$	0.0112	0.994

<sup>a</sup> Degussa P25 TiO<sub>2</sub> was used as photocatalyst. Experimental condition: [TiO<sub>2</sub>] = 2.0 g L<sup>-1</sup>; [PBSA] = 37.9 μM, pH = 4.5.

**Table S2. Identified intermediates of PBSA photocatalytic degradation.**

Retention time (min)	Nomenclature	[M+H] <sup>+</sup> (m/z)	UV-Vis absorbance ( $\lambda_{\max}$ , nm) <sup>a</sup>	Molecular structure <sup>b</sup>
6.0	PBSA	275	205, 247, 300	
8.84	hydroxylated 2-phenyl-1H-benzimidazole	211	205, 225, 296	
3.39	di-hydroxylated 2-phenyl-1H-benzimidazole	227	–	
10.96	2-phenyl-4-carboxyl-5-aldehyde imidazole	217	–	
6.60	2-phenyl-4, 5-imidazoledicarboxylic acid	233	–	
5.72, 7.76	2-phenyl-imidazole carboxylic acid	189	–	
1.32, 1.17	hydroxylated benzamidine	137	300	
1.59	benzamide	122	–	
5.13(A), 5.39(B), 6.43(C), 6.85(D), 7.55(E)	mono-hydroxylation <sup>c</sup>	291	215, 260, 315(A), 205, 247, 300(C), 252, 300, 325(D)	

5.46, 6.68, 7.88	di-hydroxylation <sup>d</sup>	307	205, 256, 296	
3.81	tri-hydroxylation	323	–	

<sup>a</sup> UV-vis absorption spectra of the photoproducts was recorded according to the HPLC-DAD spectrum.

<sup>b</sup> Intermediates molecular weight and structure was tentatively elucidated on the basis of the pseudomolecular ions  $[M+H]^+$  and corresponding mass spectrum.

<sup>c</sup> Five isomers of mono-hydroxylation were detected.

<sup>d</sup> Three isomers of di- hydroxylation were detected.

---

## Chapter 7 General conclusions and prospects

In this thesis, the photochemical and photocatalytic degradation of atenolol(ATL) and 2-phenylbenzimidazole-5-sulfonic acid (PBSA) have been investigated in aqueous solutions.

Our results show that direct photolysis of ATL is weak because ATL has an unappreciable absorbance over the wavelength of 290 nm, thus the indirect photolysis, e.g., induced by photosensitizers such as nitrate, may contributed to its major loss process in natural sunlit waters. In the case of PBSA, direct photolysis is found to be important while the indirect photolysis may play a less important role in its elimination in natural surface waters. The photolytic reactions (either direct or indirect) generally obey pseudo-first-order kinetics and can be influence by the solution pH, the co-existence of other water constituents such as dissolved organic matter (DOM) and bicarbonate ion ( $\text{HCO}_3^-$ ). The photolytic degradation lead to a variety of intermediates and products. However, the reduction in TOC of the photolyte is usually found to be insignificant compared to the disappearance of the mother compound. Nevertheless, the observed decrease in toxicity toward fresh water species *D. magna* in nitrate-induced photodegradation of ATL implies indirect photolysis of ATL is possibly an important way to reduce the toxicity to ecosystem. It should be noted that direct and indirect photodegradation may process through different pathways and mechanism as observed in the photolysis of PBSA in this work. Since the direct photolysis of PBSA is more important than indirect photolysis, the degradation rate of PBSA may be largely influenced by the season and latitude as well as limited photic zone and overcast condition. Further environment monitoring studies should focus on the photoproducts since the parent half-lives will be short.

Photocatalytic oxidation of ATL and PBSA were carried out in illuminated aqueous  $\text{TiO}_2$  suspensions. Photocatalytic reactions normally follow pseudo-first-order kinetics. The kinetics are strongly affected by the photocatalyst type, the photocatalyst dosage, the solution pH value and the substrate concentration. Hydroxyl radical ( $\text{HO}\cdot$ ) was determined to be the major reactive specie responsible for the remarkable degradation of mother compounds. The degradation efficiency is largely influenced by the water matrices as well as the formation and transformation of intermediates. It should be noted that Degussa P25 showed the highest photocatalytic activity for oxidizing ATL and PBSA compared to pure anatase or rutile catalyst such as Hombikat UV

---

100, Millennium PC 500 and Aldrich rutile, which is in line with previous reports. The photocatalytic degradation of mother compounds results in the formation of various intermediates (e.g., hydroxylation, side chain cleavage, benzyl ring opening), carboxylic acids (e.g., formic, oxalic, malonic acid) and inorganic ions (e.g.,  $\text{NH}_4^+$ ,  $\text{NO}_3^-$ ,  $\text{SO}_4^{2-}$ ). TOC decreases much more slowly as compared to the disappearance of the mother compounds, however, complete mineralization could be obtained with longer irradiation time.

The present study showed that photocatalysis by using  $\text{TiO}_2$  as catalyst is a promising treatment technology for elimination of PPCPs in waters. However, using this technology should be with caution in real water matrix such as wastewater treatment plants effluents (WWTPs) since the water constituents ( $\text{HCO}_3^-$ , DOM) may scavenge  $\text{HO}\bullet$ , reducing the transformation efficiency. A thorough evaluation of the toxicity of the intermediates is also essential in order to optimized photocatalytic treatment and evaluate the potential risks to the ecology before the technology is applied for water purification.

---

## Acknowledgement

This scientific work was accomplished at the School of the Environment, Nanjing University (China) and the Institut de recherches sur la catalyse et l'environnement de Lyon (IRCELYON), Université Claude Bernard-Lyon 1 in Lyon (France).

Firstly, my thanks should be given to the China Scholarship Council (CSC) for financial support for me to pursue my studies at IRCELYON, Université Claude Bernard-Lyon 1 as a joint Ph.D student from November 2011 to October 2013.

Secondly, I cordially express my thanks to my supervisors Prof. Xi Yang, Prof. Shixiang Gao and Prof. Jean-Marc Chovelon. I would like to say without their guidance and encouragement, I could not obtain my scientific achievement. Their deep knowledge and huge enthusiasm in scientific research strongly influence me and will accompany with me in my following life and research activities.

I would like to thank IRCELYON and State Key Laboratory of Pollution Control and Resource Reuse, Nanjing University for providing resources and facilities for my research.

My thanks to Corinne Ferronato, Ludovic Fine, Gilles Mailhot, Marcello Brigante, Cui Meng, Chao Zeng, Lei Zhou, Ya Zhang, and Lianhong Wang for experimental collaborations. I also express my thanks to those who gave me various recommendations and technical supports during my research.

My special thanks should be given to my wife Lihua Shen for her deep love, silent support and tremendous sacrifice during these years of my studies. Finally, I would like to thank my parents for their support and love.

---

## Appendix

### Appendix I List of published papers related to this work

- (1) Meng C, **Ji YF**, Zeng C, Yang X. Photodegradation of UV filter PABA in nitrate solution. *Huan Jing Ke Xue*. **2011**, 32(9), 2549-2553.
- (2) **Ji YF**, C. Zeng C, Meng C, Yang X, Gao SX. Photodegradation of atenolol in aqueous nitrate solution. *Huan Jing Ke Xue*. **2012**, 33(2), 481-487.
- (3) **Ji YF**, Zeng C, Zhou L, Yang X, Gao SX. Photodegradation of atenolol under simulated solar irradiation. *Acta Scientiae Circumstantiae*. **2012**, 32 (6), 1357-1363. (in Chinese)
- (4) **Ji, Y.**, Zeng, C., Ferronato, C., Chovelon, J.-M., Yang, X. Nitrate-induced photodegradation of atenolol in aqueous solution: Kinetics, toxicity and degradation pathways. *Chemosphere* **2012**, 88, 644-649. (IF=3.137)
- (5) **Ji, Y.**, Zhou, L., Ferronato, C., Yang, X., Salvador, A., Zeng, C., Chovelon, J.-M. Photocatalytic degradation of atenolol in aqueous titanium dioxide suspensions: Kinetics, intermediates and degradation pathways. *Journal of Photochemistry and Photobiology A: Chemistry* **2013**, 254, 35-44. (IF=2.416)
- (6) **Ji, Y.**, Zhou, L., Ferronato, C., Salvador, A., Yang, X., Chovelon, J.-M. Degradation of sunscreen agent 2-phenylbenzimidazole-5-sulfonic acid by TiO<sub>2</sub> photocatalysis: Kinetics, photoproducts and comparison to structurally related compounds. *Applied Catalysis B: Environmental* **2013**, 140-141, 457-467. (IF=5.825)
- (7) **Ji, Y.**, Zhou, L., Zhang, Y., Ferronato, C., Brigante, M., Mailhot, G., Yang, X., Chovelon, J.-M. Photochemical degradation of sunscreen agent 2-phenylbenzimidazole-5-sulfonic acid in different water matrices. *Water Research* **2013**, 47 (15), 5865-5875. (IF=4.655)
- (8) **Ji, Y.**, Ferronato, C., Salvador, A., Yang, X., Chovelon, J.-M. Degradation of ciprofloxacin and sulfamethoxazole by ferrous-activated persulfate: Implications for remediation of groundwater contaminated by antibiotics. *Science of the Total Environment*, **2014**, 800-808. (IF=3.258)
- (9) Zeng, C., **Ji, Y.**, Zhou, L., Zhang, Y., Yang, X. The role of dissolved organic matters in the aquatic photodegradation of atenolol. *Journal of Hazardous Materials* **2012**, 239-240, 340-347. (IF=3.925)
- (10) Zhou, L., **Ji, Y.**, Zeng, C., Zhang, Y., Wang, Z., Yang, X. Aquatic photodegradation of

---

sunscreen agent p-amimobenzoic acid in the presence of dissolved organic matter. *Water Research* **2013**, 47, 153-162. (IF=4.655)

(11) Zhang, Y., Zhou, L., Zeng, C., Wang, Q., Wang, Z., Gao, S., **Ji, Y.**, Yang, X. Photoreactivity of hydroxylated multi-walled carbon nanotubes and its effects on the photodegradation of atenolol in water. *Chemosphere* **2013**, 93 (9), 1747-1754. (IF=3.137)

(12) Zhou, L., Zheng, W., **Ji, Y.**, Zhang, J., Zeng, C., Zhang, Y., Wang, Q., Yang, X. Ferrous-activated persulfate oxidation of arsenic (III) and diuron in aquatic system. *Journal of Hazardous Materials* **2013**, 263, 422-430. (IF=3.925).

**Dégradation photochimique et photocatalytique en solutions aqueuses de composés pharmaceutiques et de soins personnels (PPSP). Application à l'atenolol et au 2-phenylbenzimidazole-5-sulfonique acide.**

**I/ Introduction**

La présence sans cesse croissante dans les eaux de surface de micro-polluants organiques telles que les produits pharmaceutiques et de soins personnels (PPSP), suscite un intérêt croissant de la part de la communauté scientifique mais aussi du public, en raison du risque potentiel élevé que présente ces substances, d'une part sur la santé des êtres humains et d'autre part sur la qualité de notre environnement. De plus, le devenir de ces substances dans l'environnement est à ce jour mal compris et des études comme leur transport, leurs transformations biotique ou abiotique ne sont pas suffisamment développées. Parmi les dégradations abiotiques, les dégradations photochimiques sont connues comme pouvant être une voie de transformation importante pour les composés organiques. Ces réactions photochimiques peuvent se diviser en deux catégories, à savoir la photolyse directe et la photolyse indirecte. Dans la photolyse directe, le produit se dégrade lorsque son spectre d'absorption recouvre le spectre d'émission du soleil. Dans les eaux naturelles, cette transformation ne se fait qu'en surface, dans une zone appelée zone photique où les photons d'origine solaire sont absorbés. Dans la photolyse indirecte, la photo-transformation induite, indirecte ou sensibilisée provient de l'absorption des radiations lumineuses par un composé présent dans le milieu aquatique autre que le polluant dont on suit la dégradation.

---

Dans les milieux aquatiques naturels, la photo-dégradation sensibilisée implique donc diverses substances intermédiaires telles que les matières organiques naturelles (acides humique et fulvique) ou certains composés minéraux tels que les ions nitrates, nitrites, fer (III) etc. Ces substances, après absorption de la lumière, passent de l'état excité à un autre état de plus faible énergie sans ré-émission de photons. Elles peuvent ensuite transmettre l'énergie reçues au polluant qui passera à son tour dans un état excité qui va pouvoir évoluer vers une transformation chimique. En outre elles peuvent également subir des réactions de photolyse et générer des électrons aqueux ou d'autres espèces oxydantes réactives ( $^1\text{O}_2$ ,  $\text{HO}^\circ$ ,  $\text{HO}_2^\circ$ ,  $\text{O}_2^{\circ-}$  etc). Pour les composés organiques qui ne peuvent pas subir de photolyse directe, la photolyse indirecte peut devenir une voie de dégradation naturelle non négligeable, mais pas forcément suffisante pour les éliminer complètement de notre environnement

En fait la question que l'on peut se poser concerne l'origine des ces PPSPs dans les eaux de surface ou dans les nappes phréatiques ?

Pour répondre à cette question, il faut se rappeler que la plupart de ces PPSP sont biologiquement actifs, c'est-à-dire qu'ils ne seront pas ou peu biodégradés dans les usines de traitement des eaux usées (STEP) classiques. Tout se passe alors comme si les eaux usées représentaient une source ponctuelle importante de génération de ces micro-polluants. Dans ce contexte, afin de réduire la présence de ces micro-polluants dans les eaux de rejets, des solutions consistant à rajouter un traitement tertiaire à la filière font de plus en plus l'objet d'investigations. Parmi ces traitement tertiaires, les processus d'oxydation avancée (ozone, ozone/ $\text{H}_2\text{O}_2$ , UV/ $\text{H}_2\text{O}_2$ , Fenton, photo-Fenton etc) dans lequel des radicaux hydroxyles hautement réactifs sont générés présentent un intérêt tout particulier de par leur efficacité élevée, leurs coûts relativement faibles et leur respect de l'environnement.

La photocatalyse hétérogène utilisant le dioxyde de titane ( $\text{TiO}_2$ ) comme photocatalyseur fait partie de ces processus d'oxydation avancée et reste une voie prometteuse pour la dégradation des polluants organiques, notamment les PPSP.

La dégradation photocatalytique exploite les radiations lumineuses comme source d'énergie capable de générer des trous dans la bande de valence ( $h^+_{\text{VB}}$ ) et des

électrons dans la bande de conduction ( $e^-_{BC}$ ) du semi-conducteur (le catalyseur) après que ce dernier ait été excité par des photons dont l'énergie était égale ou supérieure à l'énergie de la bande interdite. Les trous ainsi photo-générés peuvent oxyder directement les composés organiques adsorbés à la surface du  $TiO_2$  ou produire des radicaux hydroxyles ( $HO^\circ$ ) par oxydation de  $OH^-$  et / ou des molécules d'eaux adsorbée à la surface du catalyseur. Un certain nombre d'espèces oxydantes réactives sont ainsi générées, la photocatalyse étant un précédé de photolyse indirecte.

C'est dans ce contexte que s'inscrit ce travail de thèse au cours duquel les dégradations photochimique et photocatalytique de l'atenolol (ATL) et du 2-phenylbenzimidazole-5-sulfonique acide (PBSA) (cf figure 1) ont été systématiquement étudiées dans des solutions aqueuses dans le but premier d'évaluer leur devenir dans l'environnement mais aussi pour étudier leur « traitabilité » par photocatalyse.

L'ATL et le PBSA ont été choisis comme deux composés modèles de PPSP, leur présence étant souvent signalée dans les milieux aquatiques naturels. L'ATL est utilisé pour le traitement des maladies cardiovasculaires depuis plus de trente ans. Des études ont montré qu'il pouvait inhiber la croissance des cellules embryonnaires humaines et qu'il était écotoxique en phase aqueuse. Quant au PBSA utilisé dans les crèmes solaires il a été montré qu'il pouvait photo-générer en phase aqueuse des espèces réactives telles que  $^1O_2$  et  $O_2^\circ$ , ces dernières pouvant endommager l'ADN

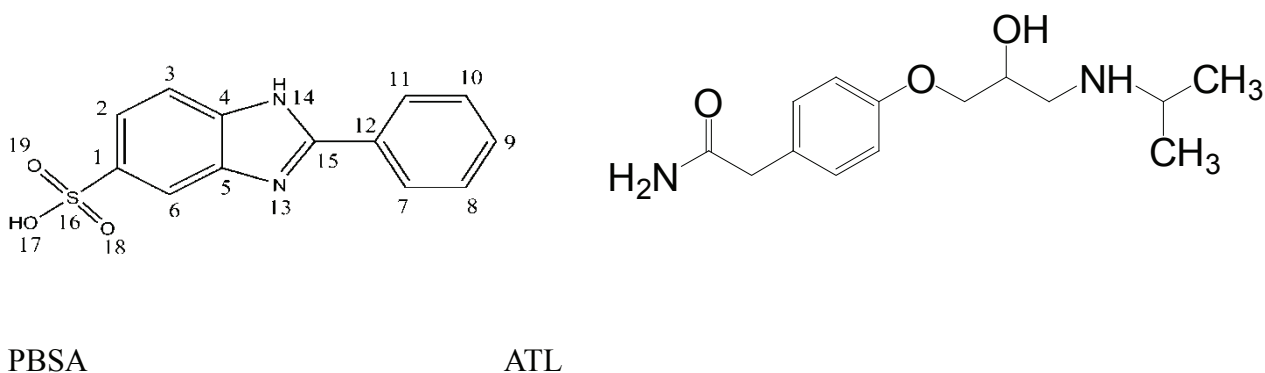


*Figure 1 : structure chimique des deux PPSP choisis pour cette étude*

---

Dans le premier chapitre de cette thèse, une étude bibliographique a été réalisée afin de faire le point sur l'origine des PPSP dans les eaux de surface, leur effet sur l'environnement et leur devenir aussi bien biotique (biodégradation) que abiotique (adsorption, transformation photochimique directe et induite). Enfin ce chapitre se termine en faisant le point sur l'utilisation de la photocatalyse pour le traitement des PPSP.

Le chapitre 2, introduit les différentes méthodes et outils qui ont été utilisés durant ce travail. Sont ainsi détaillées les systèmes d'irradiation photochimique (dont la photolyse flash laser) et les techniques d'analyses utilisées telles que l'HPLC-DAD, la LC-MS-MS, le COTmètre, la spectrométrie UV/visible.

Les chapitres de 3 à 7 correspondent aux résultats expérimentaux obtenus, et ont fait l'objet de publications dans des revues internationales de rang A.

## II/ Résultats expérimentaux

### Chapitre 3 : Transformation photochimique en phase aqueuse de l'atenolol induite par les ions nitrates : cinétiques, toxicité et mécanisme de dégradation.



#### Nitrate-induced photodegradation of atenolol in aqueous solution: Kinetics, toxicity and degradation pathways

Yuefei Ji<sup>a,b</sup>, Chao Zeng<sup>a</sup>, Corinne Ferronato<sup>b</sup>, Jean-Marc Chovelon<sup>b</sup>, Xi Yang<sup>a,\*</sup>

<sup>a</sup> State Key Laboratory of Pollution Control and Resource Reuse, School of the Environment, Nanjing University, Nanjing 210046, PR China

<sup>b</sup> Université Lyon 1, UMR CNRS 5256, Institut de recherches sur la catalyse et l'environnement de Lyon (IRCELYON), 2 Avenue Albert Einstein, F-69626 Villeurbanne, France

Les principales conclusions sont les suivantes :

1/ Les résultats ont montré que la photolyse directe de l'ATL est faible, l'ATL présentant une faible absorbance pour les longueurs d'onde supérieures à 290 nm. La photodégradation de l'atenolol a alors été étudiée de façon indirecte *via* l'intervention des ions nitrate. Nous avons montré que la dégradation photo-induite par les ions nitrate suit une cinétique de premier ordre. Cette photo-dégradation s'est avérée être

dépendante de la concentration (cf figure 2) en ions nitrates et augmente quand la concentration en nitrate passe de 0,5 mmol L<sup>-1</sup> à 10 mmol L<sup>-1</sup> ( $k = 0,00101 \text{ min}^{-1}$  à  $0,00716 \text{ min}^{-1}$ , respectivement).

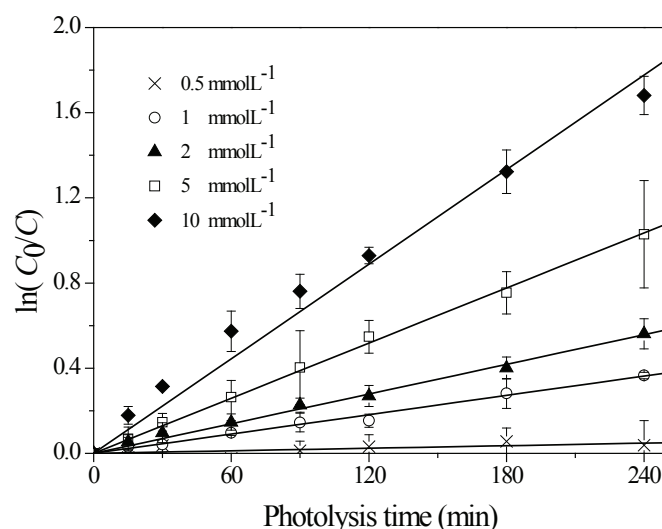


Figure 2 Photodégradation de l'atenolol en présence de différentes concentrations en ions nitrates (x) 0,5 mM, (o) 1 mM, (▲) 2 mM, (□) 5 mM, (◆) 10 mM.

2/ L'utilisation de l'isopropanol comme inhibiteur des radicaux hydroxyles ( $k=1,9 \times 10^9 \text{ M}^{-1} \text{ s}^{-1}$ ) a montré que ces derniers jouaient un rôle primordial au cours de la dégradation. En effet l'ajout de 100 mM d'isopropanol à la solution a complètement inhibé la photodégradation de l'atenolol en présence de nitrate. La détermination de la constante de vitesse absolue entre le radical hydroxyle et l'ATL en utilisant une méthode de cinétique de compétition a permis d'obtenir la valeur de  $k_{\text{OH,ATL}} = 7,49 \pm 0,26 \times 10^9 \text{ M}^{-1} \text{ s}^{-1}$ , valeur élevée en accord avec un mécanisme de dégradation se faisant principalement *via* les radicaux hydroxyles.

De même, l'identification par SPE-LC-MS des produits de dégradation de l'ATL en présence des ions nitrates confirme encore le rôle des radicaux OH° dans la dégradation (cf le mécanisme de dégradation de l'ATL proposé dans la figure 3).

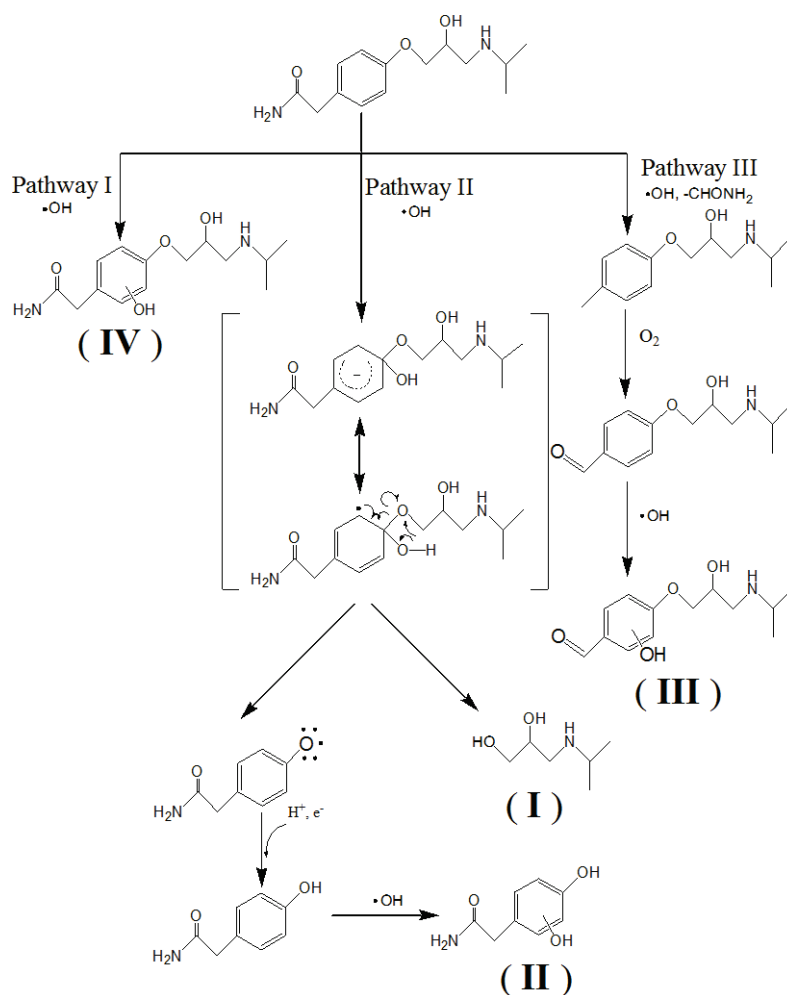


Figure 3 : Proposition d'un mécanisme de dégradation de l'ATL en phase aqueuse en présence des ions nitrate déterminé d'après identification des intermédiaires.

3/ En solution réelle, la présence d'ions bicarbonates diminue la vitesse de photodégradation de l'ATL en présence des ions nitrates (cf Figure 4). Cette diminution est due à la fois à l'inhibition des radicaux hydroxyles par les ions bicarbonates et aux variations de pH.

De même, il a été montré que les substances humiques inhibent la photodégradation d'une part par inhibition des radicaux OH et d'autre part par atténuation de la lumière.

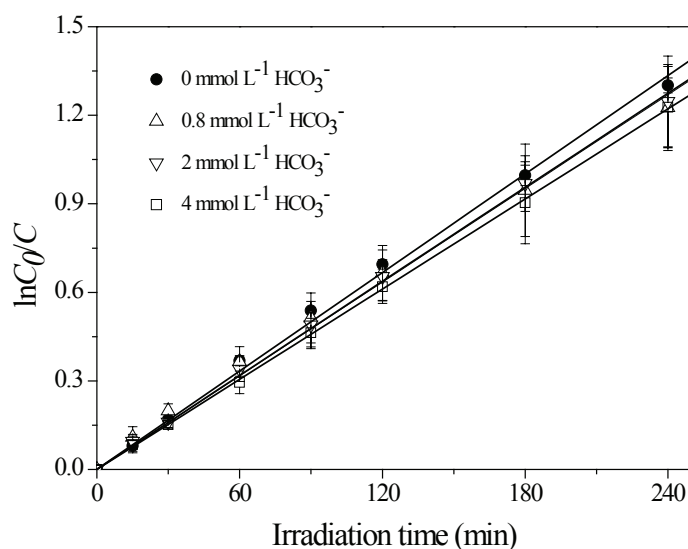
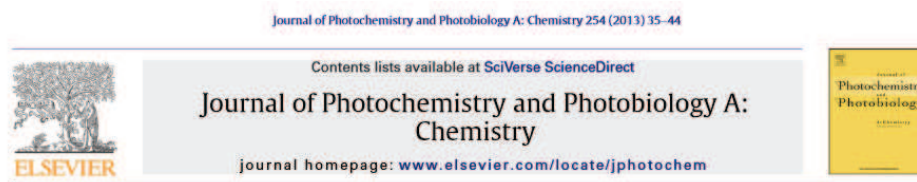


Figure 4 : Effet des ions bicarbonates sur la photodégradation de l'ATL en présence des ions nitrates.

3/ Après 240 min d'irradiation en présence des ions nitrates, le carbone organique total (COT) n'a diminué seulement que de 10% alors que le taux de transformation de l'ATL est de 72%. Ce résultat implique qu'une quantité importante de produits intermédiaires est générée (cf figure 3) avant la minéralisation.

La toxicité des produits de phototransformation a été par ailleurs évaluée en utilisant les espèces aquatiques *Daphnia magna* et les résultats montrent qu'au cours de la photodégradation de l'ATL dans les eaux naturelles, la toxicité de l'ATL décroît.

#### Chapitre 4 : Dégradation photocatalytique de l'atenolol en solution aqueuse : cinétiques, intermédiaires de réactions et mécanismes de la dégradation.



Photocatalytic degradation of atenolol in aqueous titanium dioxide suspensions: Kinetics, intermediates and degradation pathways

Yuefei Ji<sup>a,b</sup>, Lei Zhou<sup>a</sup>, Corinne Ferronato<sup>b</sup>, Xi Yang<sup>a,\*</sup>, Arnaud Salvador<sup>c</sup>, Chao Zeng<sup>a</sup>, Jean-Marc Chovelon<sup>b,\*\*</sup>

<sup>a</sup> State Key Laboratory of Pollution Control and Resource Reuse, School of the Environment, Nanjing University, Nanjing 210046, PR China

<sup>b</sup> Université Lyon 1, UMR CNRS 5256, Institut de recherches sur la catalyse et l'environnement de Lyon (IRCELYON), 2 Avenue Albert Einstein, F-69626 Villeurbanne, France

<sup>c</sup> Laboratoire des Sciences Analytiques, Université Lyon 1, UMR 5180, Batiment CPE, 43, Boulevard du 11 novembre 1918, F-69622 Villeurbanne, France

1/ La dégradation photocatalytique de l'aténolol (ATL) en solution aqueuse a été étudiée en utilisant du  $\text{TiO}_2$  en suspension comme photocatalyseur. Une dégradation complète de  $37,6 \mu\text{M}$  d'ATL a été obtenue après 60 minutes d'irradiation à pH 6,8 (eau Milli-Q) en présence de  $2,0 \text{ g L}^{-1}$  de  $\text{TiO}_2$  (Degussa P25), cinétique bien plus rapide que celle correspondant à la photodégradation par voie directe (cf Figure 5). Les résultats montrent également que la dégradation suit une cinétique de pseudo-premier ordre.

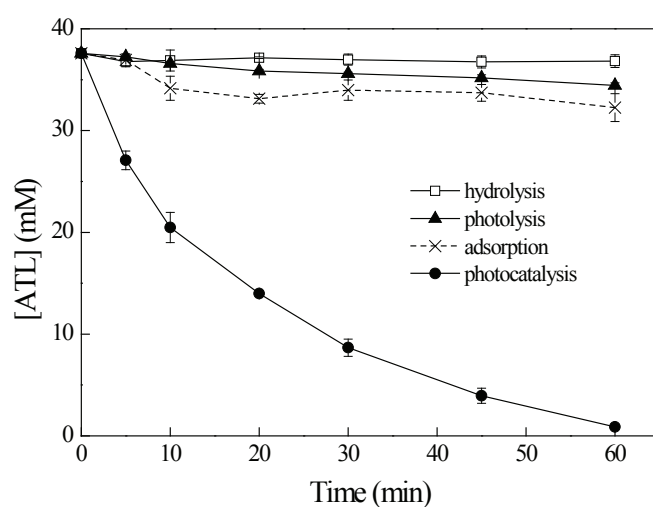


Figure 5: Atténuation de l'ATL en phase aqueuse par hydrolyse (□), photolyse (▲), adsorption (×) et photocatalyse (●). Conditions expérimentales:  $[\text{TiO}_2] = 2,0 \text{ g L}^{-1}$ ;  $[\text{ATL}] = 37,6 \mu\text{M}$ ;  $\text{pH} = 6,8$ . La barre d'erreur représente 95% de l'intervalle de confiance.

2/ Il a été montré ici également que le radical hydroxyle agissait comme étant l'espèce réactive prédominante au cours de la dégradation photocatalytique. Pour ce faire l'utilisation du méthanol comme sonde radicalaire a été utilisée ( $k_{\text{HO-methanol}} = 9,7 \times 10^8 \text{ M}^{-1} \text{ s}^{-1}$ ).

3/ L'identification des principaux produits de transformation par chromatographe liquide haute performance – couplée à la spectrométrie de masse ( HPLC-MS/MS ) a permis de proposer comme intermédiaires le 3-(isopropylamino)-propane-1,2-diol et le p- hydroxyphénylacétamide obtenus par clivage de la chaîne étherée, ou encore

après l'hydroxylation de l'ATL, la formation du 4-[2-hydroxy-3-(isopropylamino)propoxy] benzaldéhyde.

Par ailleurs, l'utilisation des calculs de densité (DFT) a confirmé que la formation des produits mono hydroxylés *via* le radical hydroxyle se faisait principalement sur le noyau benzénique, en accord avec l'analyse LC-MS/MS.

Cinq acides carboxyliques ont par ailleurs été identifiés par chromatographie liquide par comparaison avec des standards authentiques, à savoir, les acides oxalique, glyoxylique, malonique, oxamique et formique

D'après les données expérimentales obtenues ci-dessus, nous avons proposé un mécanisme de dégradation (Figure 6).

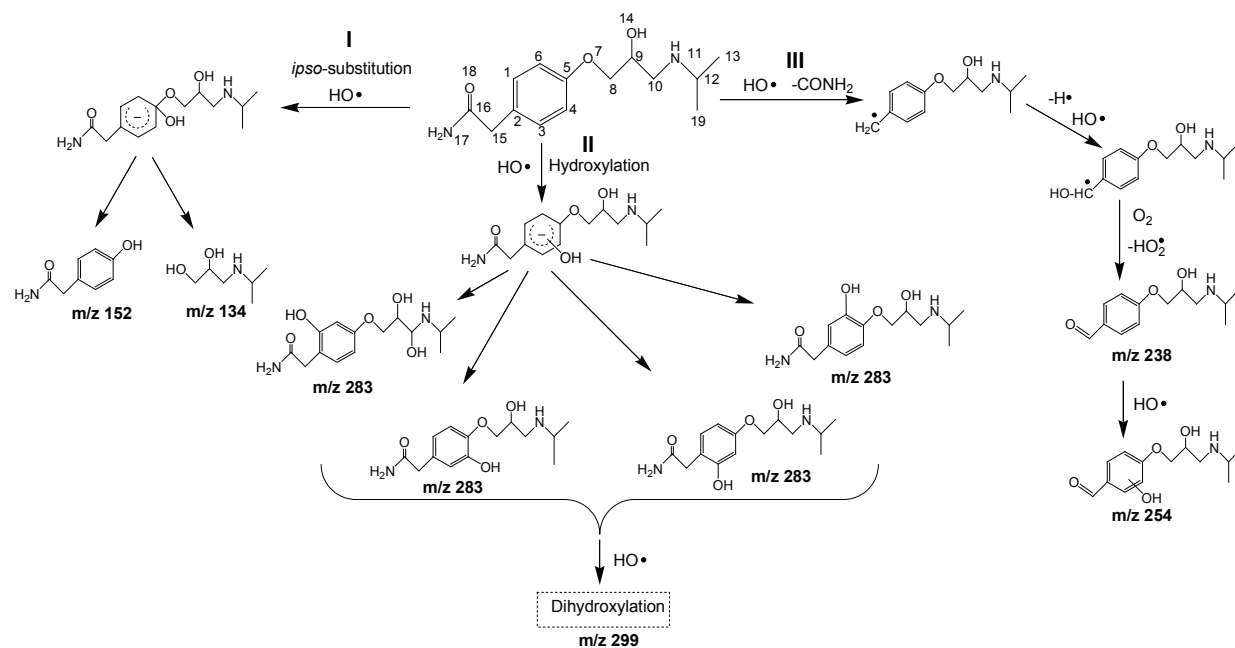
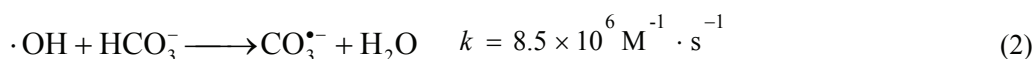
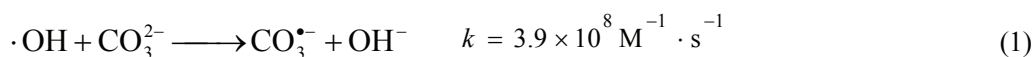


Figure 6 : Proposition d'un mécanisme de dégradation photocatalytique de l'ATL en phase aqueuse.

4/ Nous avons montré que l'efficacité photocatalytique de l'ATL était fortement dépendante des propriétés de la matrice de l'eau (cf Figure 7). Par exemple le pH, la présence d'espèces organiques et/ou inorganiques (substances humiques,  $\text{HCO}_3^-$ ) influent fortement les cinétiques de dégradation. Le résultat le plus intéressant et

surprenant a certainement été une augmentation de la vitesse de dégradation de l'ATL en présence des ions carbonate/hydrogénocarbonates (cf Figure 7a). En effet dans le système avec les ions nitrates (cf Chapitre 3) nous avons montré que les ions carbonates/hydrogénocarbonates ralentissaient les cinétiques de dégradation alors qu'ici les vitesses sont accélérées. Le rôle de l'oxyde de titane semble donc être évident. Les explications à ce stade ne sont pas évidentes, mais nous pouvons supposer que les ions hydrogénocarbonates doivent s'adsorber à la surface du TiO<sub>2</sub> à la place de l'ATL (pH = 8,5) et se transformer en radical hydrogénocarbonate, d'une part par les trous, et d'autre part par inhibition des radicaux hydroxyles (réactions 1 et 2). Ces radicaux hydrogénocarbonates sont certes moins efficaces par rapport aux radicaux hydroxyles, mais sont plus nombreux car moins sélectifs que les radicaux hydroxyles. Ils peuvent donc s'accumuler à la surface du TiO<sub>2</sub> et se déplacer plus aisément sur une distance plus importante que les radicaux hydroxyles au sein de la solution. Ceci pourrait expliquer l'augmentation des cinétiques de dégradation.



Sinon, quelque soit l'origine des acides humiques utilisés, une atténuation de la vitesse de dégradation a toujours été obtenue (Figure 7b et 7c).

Enfin, même si les ions hydrogénocarbonates augmentent les cinétiques de dégradation de l'ATL, c'est une diminution de l'efficacité photocatalytique qui est observée quand on utilise de l'eau de rivière (eau du Rhône) au lieu de l'eau de qualité milli-Q (Figure 7 d).

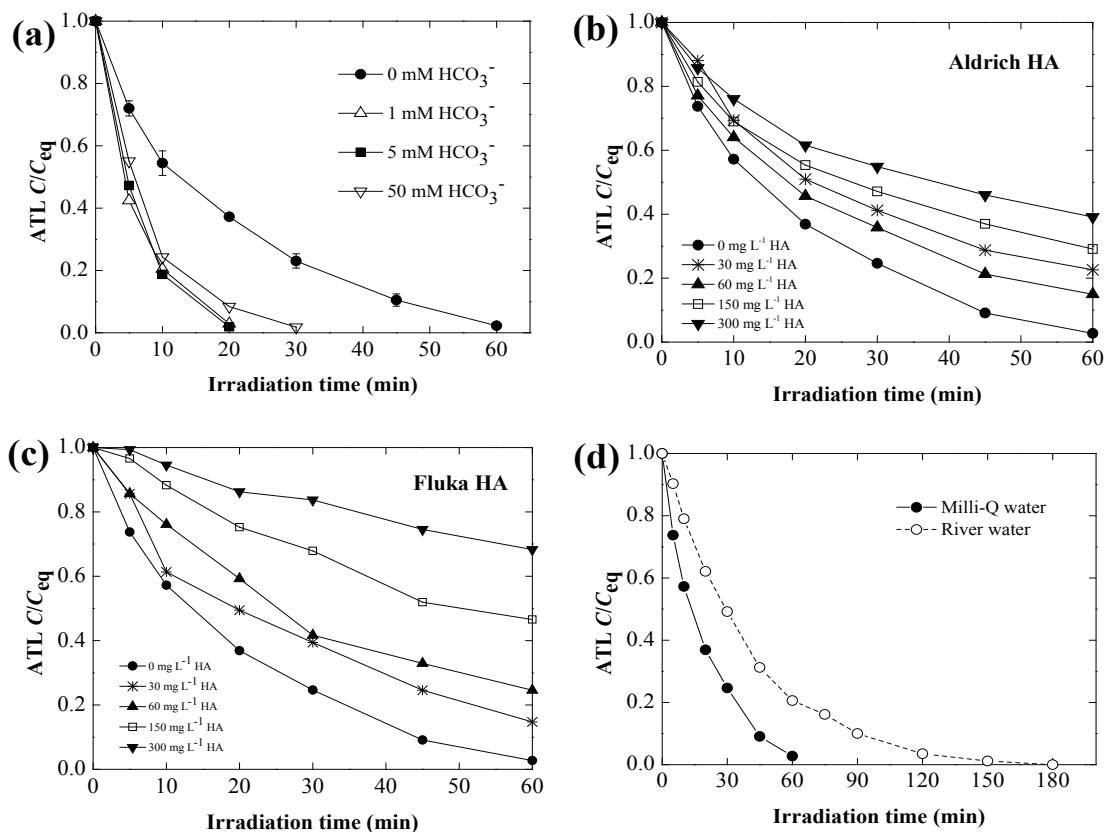


Figure 7 Effets de certains constituants de l'eau et de l'eau de rivière (eau du Rhône) sur l'efficacité photocatalytique de l'ATL. (a) effet du bicarbonate à pH 8.5; (b) effet des acides humiques de type Aldrich et (c) Fluka à pH 6.8; et (d) effet of l'eau de rivière (pH 8,05).  $[TiO_2] = 2.0 \text{ g L}^{-1}$ ;  $[ATL] = 37,6 \mu\text{M}$ ; pH.

5/ Nous avons testé différents photocatalyseurs et montré que le  $TiO_2$  Degussa P25 présentait l'activité photocatalytique d'oxydation de l'ATL ainsi que des intermédiaires le plus élevée par rapport à du  $TiO_2$  d'Aldrich (100 % rutile) de Millennium (PC500) et de Hombikat (UV100).

**Chapitre 5 Dégradation photochimique du 2-phenylbenzimidazole-5-sulfonique acid utilisé dans les crèmes solaires, dans différentes matrices aqueuses.**



## Photochemical degradation of sunscreen agent 2-phenylbenzimidazole-5-sulfonic acid in different water matrices



Yuefei Ji<sup>a,b</sup>, Lei Zhou<sup>a</sup>, Ya Zhang<sup>a</sup>, Corinne Ferronato<sup>b</sup>, Marcello Brigante<sup>c</sup>, Gilles Mailhot<sup>c</sup>, Xi Yang<sup>a,\*</sup>, Jean-Marc Chovelon<sup>b,\*\*</sup>

<sup>a</sup> State Key Laboratory of Pollution Control and Resource Reuse, School of the Environment, Nanjing University, Nanjing 210023, PR China

<sup>b</sup> Université Lyon 1, UMR CNRS 5256, Institut de recherches sur la catalyse et l'environnement de Lyon (IRCELYON), 2 Avenue Albert Einstein, F-69626 Villeurbanne, France

<sup>c</sup> Clermont Université, Université Blaise Pascal-ENSCCF, Institut de Chimie de Clermont-Ferrand (ICCF), F-63000 Clermont-Ferrand, France

1/ Nous avons commencé ce travail par une étude de cinétique rapide en utilisant la photolyse flash laser (PFL) afin de déterminer la nature des espèces transitoires. Ces études ont permis de montrer que durant l'excitation du PBSA à 266 nm, le radical cation  $\text{PBSA}^{\circ+}$  était produit à partir de l'état excité du PBSA. De plus, une large bande d'absorption transitoire à 750 nm a été attribuée à la présence de l'électron solvaté. Cet électron solvaté a probablement été généré à partir de l'état excité singulet du PBSA *via* un processus d'éjection. En effet, le signal transitoire à 380 nm ( $\text{PBSA}^{++}$ ) et celui de l'électron solvaté à 750 nm ( $e_{\text{aq}}^-$ ) en présence d'une forte concentration en acrylamide (inhibiteur de l'état triplet) confirme que  $\text{PBSA}^{++}$  provient de l'état excité singulet  $^1\text{PBSA}^*$  et de l'éjection de l'électron.

2/ Photolyse directe du PBSA à différents pH.

La figure 9, représente la photodégradation de 10  $\mu\text{M}$  de PBSA sous photolyse directe à différents pH. Les calculs de rendement quantique à ces pH ont été réalisés et les valeurs sont consignées dans le tableau 1.

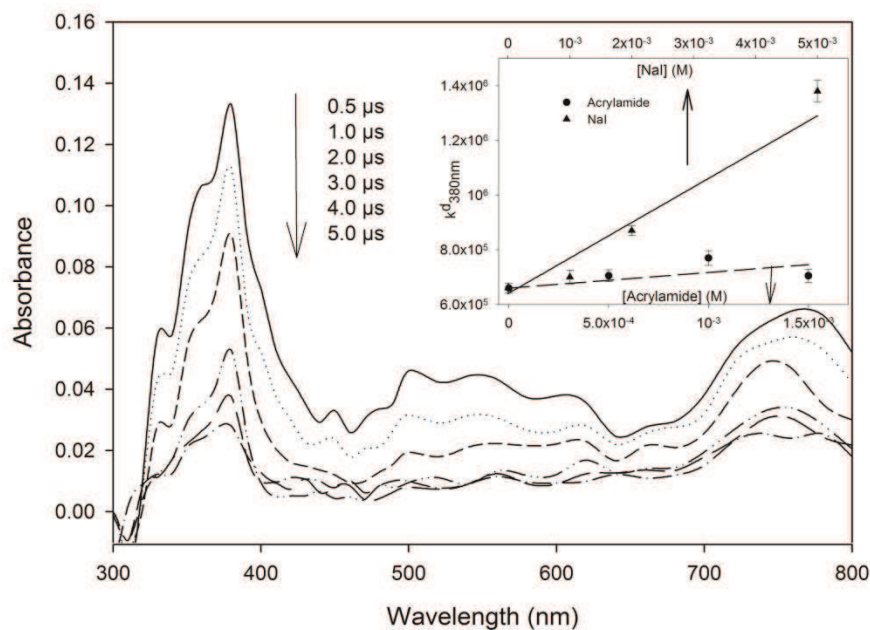


Figure 8 Spectre d'absorption transitoire du PBSA (100  $\mu$ M) dans l'eau produit par PFL (266 nm, 30 mJ) pour différents temps. L'encart montre l'influence de (●) l'acrylamide et de (▲) NaI sur l'atténuation du signal à 380 nm.

Table 1 : Constantes de vitesse apparentes, temps de demi-réaction et rendements quantiques de la dégradation photochimique du PBSA en phase aqueuse pour différents pH.

Solution	Constant de vitesse ( $k_{\text{obs}}$ , $\text{h}^{-1}$ )	Temps de demi-réaction ( $t_{1/2}$ , h)	Rendement quantique ( $\Phi_p$ , $\times 10^{-4}$ ) <sup>a</sup>
pH 2,9	0.563	1,23	9,74
pH 6,8	0.152	4,55	2,70
pH 12,4	1.690	0,41	20,5
pH 8,0	0.158	4,38	2,80
pH 8,0 sous O <sub>2</sub> .	1.023	6,75	-
pH 8,0, sous Ar-	0.093	7,45	-

<sup>a</sup> Le rendement quantique a été déterminé par la méthode au p-nitroanisole (PNA)/pyridine (pyr).

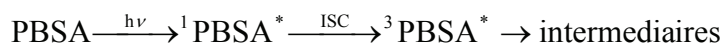
Les valeurs montrent clairement une influence du pH sur le rendement quantique

puisque à pH acide ou basique des valeurs bien plus élevées qu'à pH neutre sont obtenues ( $\Phi_{pH2,9} / \Phi_{pH6,8} = 3,6$  et  $\Phi_{pH12,4} / \Phi_{pH6,8} = 7,6$ ).

Pour interpréter les résultats à pH acide, on suppose dans un premier temps que PBSA a réagi avec l'anion superoxyde  $O_2^{\bullet-}$  générée à partir de l'électron solvaté et de l'oxygène (cf réaction 5).

A pH acide  $O_2^{\bullet-}$  se protone rapidement en  $HO_2^{\bullet}$  et peut conduire au peroxyde d'hydrogène  $H_2O_2$  (équation 8). Ce dernier peut alors après photolyse générer  $HO^{\bullet}$  (réaction 9).

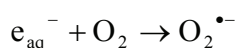
D'où, l'augmentation du rendement quantique de PBSA à pH acide, serait due à un mécanisme alternatif faisant intervenir  $OH^{\bullet}$ . Pour vérifier cette hypothèse, nous avons utilisé pendant la dégradation à pH 2,9 de l'isopropanol connu pour être un inhibiteur efficace des radicaux hydroxyles. Dans ce cas, les résultats ont montré une inhibition de la réaction confirmant ainsi notre hypothèse.



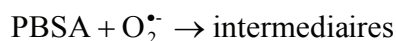
(3)



(4)



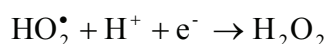
(5)



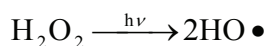
(6)



(7)



(8)



(9)

Par ailleurs, nous avons montré par PFL que  $\text{PBSA}^{*+}$  et un électron solvaté étaient produits à partir de  $^1\text{PBSA}^*$ . Or dans la littérature il a été observé par la technique RPE (Electron Paramagnetic Resonance) qu'un signal correspondant à l'adduit  $\text{DMPO}/\bullet\text{H}$  était formé suite à la réaction du 5,5-diméthyl-1-pyrroline *N*-oxide (DMPO) avec l'électron solvaté, cette observation se faisant surtout avec PBSA-2H (pH basique), un peu moins avec la forme mono-ionique PBSA-H et encore moins avec PBSA (cf figure 10).

Nous avons donc supposé qu'à pH basique  $\text{PBSA}^{*+}$  et l'électron solvaté se formait plus facilement qu'à pH neutre. Par ailleurs, le spectre UV-visible (cf figure 10) indique qu'à pH basique, le spectre d'absorption de PBSA-2H était décalé vers les plus grandes longueurs d'onde, permettant ainsi une plus grande quantité de photons d'être absorbés.

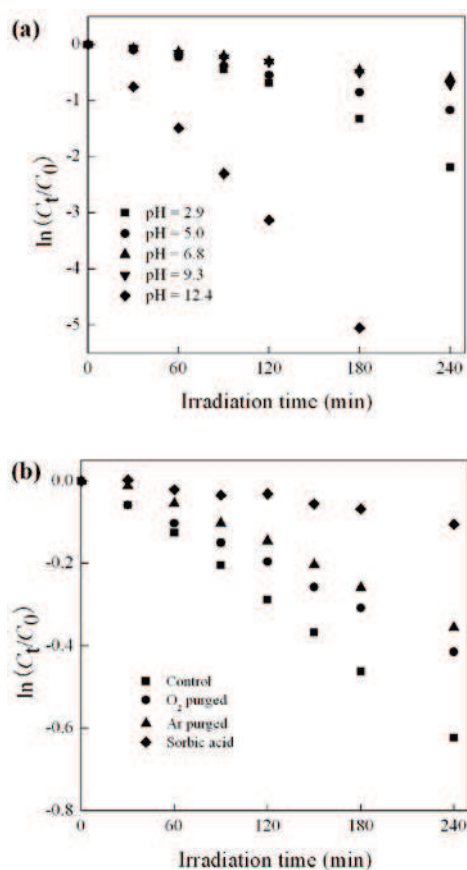


Figure 9a: Effet du pH sur la dégradation photochimique du PBSA en phase aqueuse (eau de

qualité Milli-Q). (■) pH 2,9; (●) pH 5,0; (▲) pH 6,8; (▼) pH 9,3; and (◆) pH 12,4.

**Figure 9b**: Effet de l'oxygène dissout sur la photolyse directe du PBSA en phase aqueuse

(Milli-Q). (■) solution non purgée (●) saturée en oxygène (▲) sous argon

(de-oxygénation)(◆) en présence d'acide sorbique (inhibiteur de l'état triplet). [PBSA] = 10

μM; [acide sorbique] = 2.5 μM;

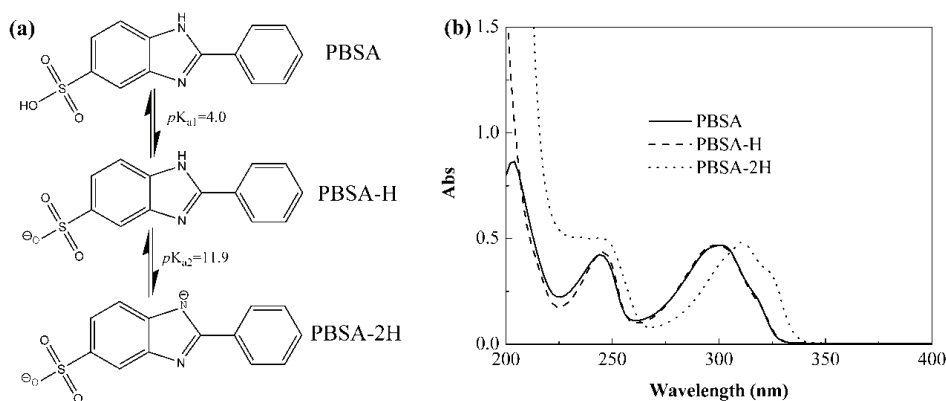


**Figure 10** Spectres UV-Visible du PBSA à différent pH

Enfin l'implication d'un état triplet  $^3\text{PBSA}^*$  a été confirmé par irradiation directe en présence d'un inhibiteur de l'état triplet (l'acide sorbique).

Les différentes étapes de la dégradation photochimiques du PBSA sont résumées par les équations 3-9.

Par ailleurs des expériences de photo dégradation indirecte en présence des ions nitrate ont été réalisés et comme avec l'atenolol, il a été observé une augmentation de la vitesse de dégradation quand la concentration en nitrate augmentait (augmentation du nombre de radicaux hydroxyles). A partir de cette étude, deux mécanismes de dégradation ont été proposés suite à l'identification par LC/MS/MS des produits de dégradation : un correspondant à la photochimie directe et l'autre photo-induite par les ions nitrate.

## Chapitre 6 : Dégradation photocatalytique du PBSA : Cinétique, photo-produits

et comparaison avec des composés structurellement proches.

Applied Catalysis B: Environmental 140–141 (2013) 457–467



Contents lists available at SciVerse ScienceDirect

Applied Catalysis B: Environmental

journal homepage: [www.elsevier.com/locate/apcatb](http://www.elsevier.com/locate/apcatb)



Degradation of sunscreen agent 2-phenylbenzimidazole-5-sulfonic acid by TiO<sub>2</sub> photocatalysis: Kinetics, photoproducts and comparison to structurally related compounds



Yuefei Ji<sup>a,b</sup>, Lei Zhou<sup>a</sup>, Corinne Ferronato<sup>b</sup>, Arnaud Salvador<sup>c</sup>, Xi Yang<sup>a,\*</sup>, Jean-Marc Chovelon<sup>b,\*\*</sup>

<sup>a</sup> State Key Laboratory of Pollution Control and Resource Reuse, School of the Environment, Nanjing University, Nanjing 210023, PR China

<sup>b</sup> Université Lyon 1, UMR CNRS 5256, Institut de recherches sur la catalyse et l'environnement de Lyon (IRCELYON), 2 Avenue Albert Einstein, F-69626 Villeurbanne, France

<sup>c</sup> Laboratoire des Sciences Analytiques, Université Lyon 1, UMR 5180, Batiment CPE, 43, Boulevard du 11 novembre 1918, F-69622 Villeurbanne, France

1/ La cinétique de dégradation photocatalytique du PBSA a été déterminée comme étant de pseudo-ordre 1. Afin de vérifier quelles étaient les principales espèces réactives responsables de la dégradation, des inhibiteurs des radicaux hydroxyles (*ter*-butanol) et de trous (KI) ont été rajoutés dans les solutions et nous avons montré que le radical OH° jouait un rôle fondamental dans la dégradation. Ces observations ont été corrélées par des expériences de cinétiques compétitives *via* l'acide benzoïque pris comme référence et des valeurs élevées proche des constante de diffusion ont été obtenues, confirmant ainsi nos résultats précédents ( $k_{\text{PBSA-HO}\cdot} = 5,8 \times 10^9 \text{ M}^{-1} \text{ s}^{-1}$ ). De même l'identification par LC/MS des principaux produits de dégradation a montré qu'ils résultaient principalement d'une hydroxylation (cf Figure 11).

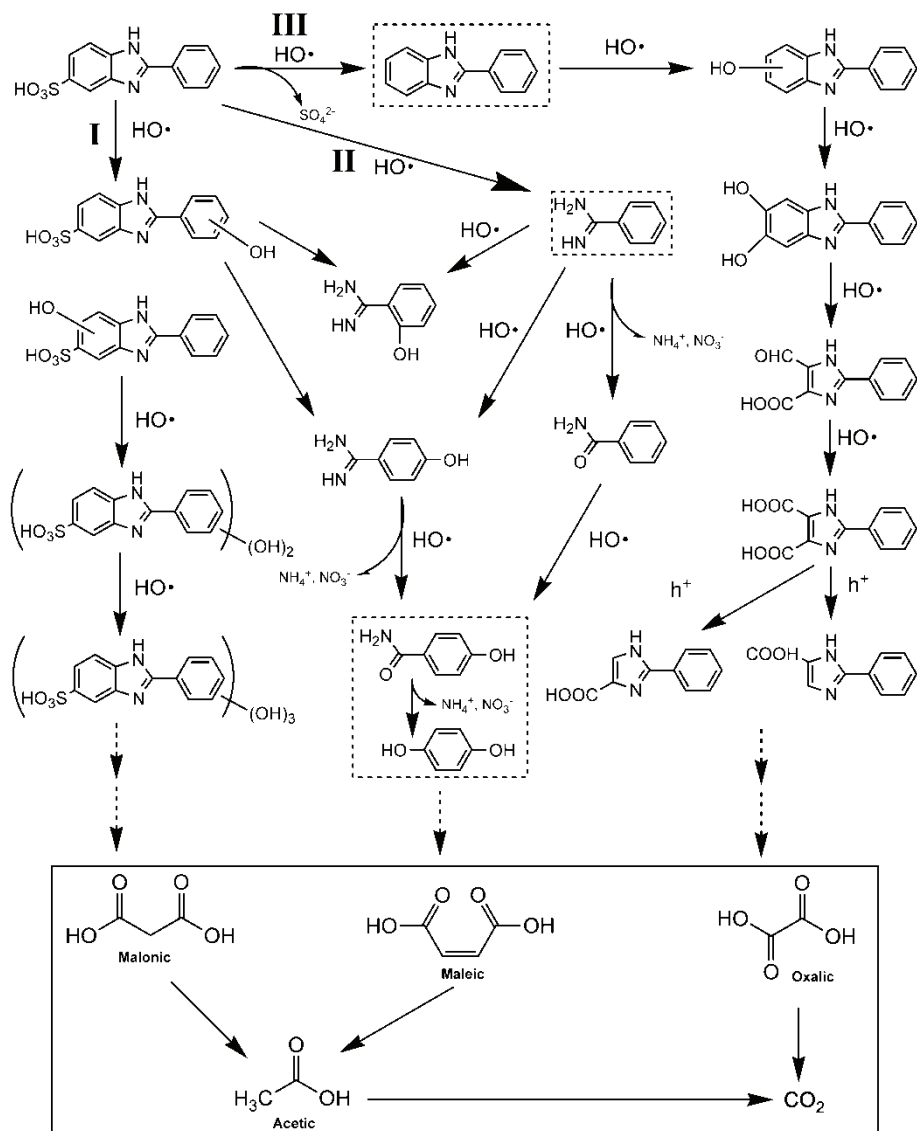


Figure 11: Proposition d'un mécanisme de dégradation photocatalytique du PBSA. Les produits en pointillés n'ont pas été identifiés dans cette étude mais ont été signalés dans la littérature.

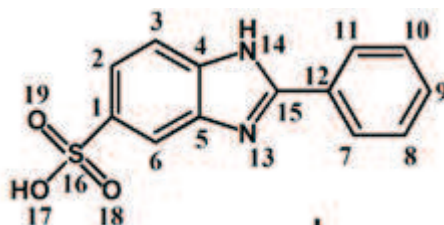
En outre, quatre acides carboxyliques (oxalique, malonique, acétique et maléique) ont été détectés par HPLC – UV et la chromatographie ionique (CI) nous a permis de suivre l'évolution des ions sulfate, ammonium, nitrate (faibles concentrations par rapport aux ions ammonium). L'ensemble de ces résultats nous a permis de proposer un mécanisme de dégradation (Figure 11)

2/ Une approche plus théorique utilisant la FED (Frontier Electron Densities) nous a

par ailleurs permis de localiser les sites de réaction des radicaux hydroxyles sur la molécule, OH° réagissant sur l'atome ayant la plus forte valeur de  $FED^2_{HOMO+}$   $FED^2_{LUMO}$  (cf Table 2). Le tableau montre clairement que les sites d'attaques correspondent surtout aux positions des atomes 9C, 11C, 7C et 8C du cycle benzénique et le 2C du benzimidazole.

Table 2. Valeurs de  $FED^2_{HOMO+}$   $FED^2_{LUMO}$  des atomes de PBSA (PBSA-H) déterminées en utilisant le programme Gaussian 09.

Number (atom) <sup>a</sup>	$FED^2_{HOMO+}$ $FED^2_{LUMO}$	Number (atom)	$FED^2_{HOMO+}+FED^2_{LUMO}$
1C	0.0054	<b>11C</b>	<b>0.0927</b>
<b>2C<sup>b</sup></b>	<b>0.0339</b>	12C	0.1916
3C	0.0151	13N	0.0722
4C	0.0130	14N	0.0451
5C	0.0021	15C	0.0438
6C	0.0280	16S	0.0001
<b>7C</b>	<b>0.0701</b>	17O	0.1793
<b>8C</b>	<b>0.0474</b>	18O	0.1996
<b>9C</b>	<b>0.2112</b>	19O	0.1877
10C	0.0306		



3/ Il est connu que la matrice de l'eau joue un rôle important dans la dégradation photocatalytique des composés organiques, certains constituants omniprésents dans les eaux naturelles comme les ions bicarbonate, phosphate, sulfate ou la matière

organique dissoute (MOD) pouvant inhiber les radicaux HO°. Dans ce contexte, nous avons étudié l'influence du bicarbonate (HCO<sub>3</sub><sup>-</sup>) et de l'acide humique (HA) sur la dégradation photocatalytique du PBSA.

Des expériences ont donc été menées dans des solutions aqueuses de PBSA (37,9 µM) en présence de différentes concentrations en ions bicarbonate (de 0 à 100 mM) ou d'acide humique (de 0 à 60 mg L<sup>-1</sup>).

Les figures 12a et 12b montrent clairement que ces deux espèces ralentissent les cinétiques de dégradation du PBSA

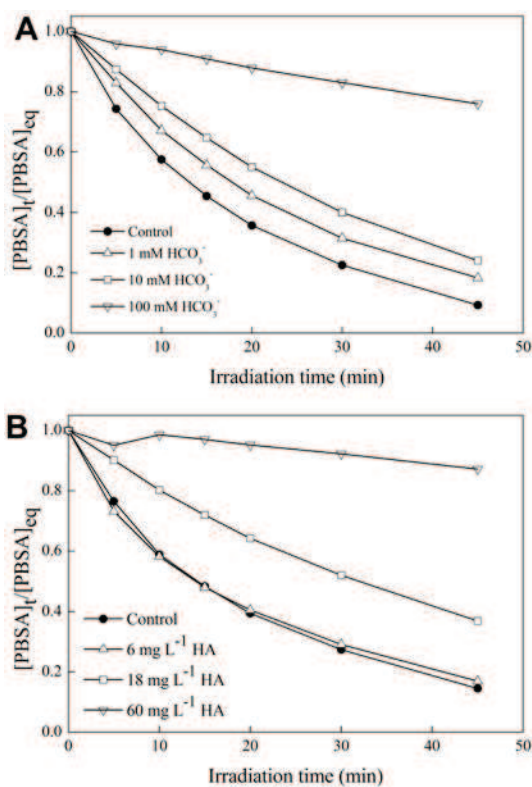
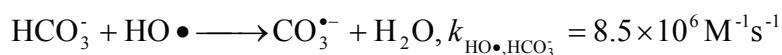
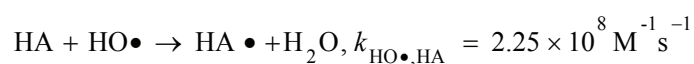


Figure 12a et 12b : Effet des ions bicarbonates (A) (pH = 8,5), et de l'acide humique (B) (pH = 5,5) sur la dégradation photocatalytique du PBSA : [TiO<sub>2</sub>] = 2,0 g L<sup>-1</sup>; [PBSA] = 37,9 µM; [HCO<sub>3</sub><sup>-</sup>] = 0-100 mM; [HA] = 0-60 mM.

Ce ralentissement est attribué aux réactions entre HO° et HCO<sup>-</sup> d'une part et HO° et HA d'autre part (cf réaction 10 et 11)



(10)



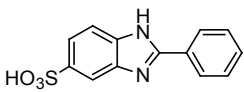
(11)

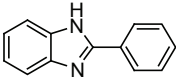
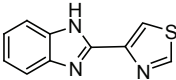
Une comparaison de la dégradation photocatalytique du PBSA avec des composés de structures apparentées comme le benzimidazole (BI), le 2- phényl- 1H -benzimidazole (PBI) et le 2 - (4- thiazolyl) -1H- benzyimidazole (thiabendazole ) a été réalisée et les résultats figurent dans le tableau 3.

Ces résultats montrent que le PBI qui ne diffère du PBSA que par la présence d'un groupement sulfonique, a les mêmes vitesses de dégradation que le PBSA, signifiant que ce groupement n'influence pas la cinétique de dégradation, et ce malgré son effet électro-attracteur. Ce résultat a été également confirmé par le fait que HO° réagit beaucoup plus facilement avec le groupe 2-phényle que sur le groupe benzyle du PBSA comme il a été montré par les calculs FED ci-dessus.

Par contre, la constante de vitesse de dégradation de BI a été estimée à environ 1,6 fois plus rapide que celle du PBSA. Ce résultat inattendu et intéressant nous a permis de conclure que la présence du groupement 2-phenyl stabilisé le cycle benzimidazole vis-à-vis de la photocatalyse.

*Table 3. Dégradation photocatalytique du PBSA et de composés structurellement proches*

Composés	Structure moléculaire	Constant de vitesse de dégradation (min <sup>-1</sup> ) <sup>a</sup>	coefficient de régression linéaire (R <sup>2</sup> )
2-phenylbenzimidazole-5-sulfonic acid (PBSA)		0,0381 ± 0,0026	0,999
Benzimidazole (BI)		0,0591 ± 0,0064	0,980

2-phenyl-1H-benzimidazole (PBI)		0,0352 ± 0,0022	0,996-0.999
2-(4-thiazolyl)-1H-benzimidazole (thiabendazole)		ND <sup>c</sup>	ND

<sup>a</sup> Conditions expérimentales: Degussa P25 TiO<sub>2</sub> [composés] = 45 μM; [TiO<sub>2</sub>] = 1.0 g L<sup>-1</sup>; pH = 7.0.

<sup>b</sup> NA = non disponible.

### Conclusions générales

Dans ce travail, nous avons étudié la dégradation photochimique et photocatalytique de l'aténolol (ATL) et du 2-phénylbenzimidazole-5-sulfonique acide (PBSA) soit dans des solutions aqueuses de qualité milli-Q dopée ou non avec des espèces présentes dans les eaux naturelles (ions bicarbonate, nitrate, substances humiques) soit dans de l'eau naturelle (eau du Rhône).

Nos résultats ont montré que la photolyse directe de l'ATL est faible, l'ATL présentant une faible absorbance pour les longueurs d'onde supérieures à 290 nm. C'est donc la photolyse induite par exemple par des photo-sensibilisateurs tels que le nitrate qui peuvent contribuer à son processus de dégradation dans les eaux naturelles ensoleillées.

En revanche, dans le cas du PBSA, la photolyse directe a été jugée importante alors que la photolyse indirecte jouerait un rôle moindre dans les eaux de surface naturelles, cette dégradation étant fortement inhibé par la présence des ions hydrogénocarbonates. Dans les deux cas, les réactions de photolyse (directs ou indirects) obéissent généralement à des cinétiques de pseudo- premier ordre et peuvent être influencées par le pH de la solution, la coexistence d'autres constituants de l'eau tels que la matière organique dissoute (MOD) et de l'ion bicarbonate (HCO<sub>3</sub><sup>-</sup>).

L'oxydation photocatalytique de l'ATL et du PBSA ont également été étudiés dans des solutions aqueuses de TiO<sub>2</sub> en suspension. Nous avons montré que les cinétiques étaient fortement dépendantes du type et de la concentration en photocatalyseur, du

---

pH de la solution et de la concentration en substrat . Dans les deux cas, le radical hydroxyle serait la principale espèce réactive responsable de la dégradation de ces composés. Ici aussi, l'efficacité de la dégradation est largement influencée par les constituants de la matrice de l'eau. Il convient de noter que le TiO<sub>2</sub> Degussa P25 a montré l'activité photocatalytique la plus élevée par rapport aux autres catalyseurs de type Hombikat UV 100, le PC 500 de millennium et le rutile d'Aldrich.

La présente étude a également montré que la photocatalyse représentait une technologie de traitement prometteuse pour l'élimination des PPSP en phase aqueuse. Cependant, l'utilisation de cette technologie doit être utilisée avec prudence dans les eaux réelles telles que les eaux de rejets des usines de traitement des eaux des stations d'épuration (STEP) contenant des espèces (bicarbonates, DOM ) susceptibles de piéger les radicaux hydroxyles, réduisant ainsi l'efficacité de la dégradation. Une évaluation approfondie de la toxicité des produits intermédiaires est également essentielle pour optimiser le traitement photocatalytique et évaluer les risques potentiels pour l'écologie avant que la technologie ne soit appliquée pour la purification de l'eau.